Uranium-Lead dating of hominid fossil sites in South Africa

Joanne Walker

Submitted in accordance with the requirements for the degree of
Doctor of Philosophy

The University of Leeds
School of Earth & Environment

September 2005

Abstract

Discoveries of hominid, or apeman, fossils in the twentieth century have brought human evolution into the scientific spotlight. It is important that ages are assigned to such hominids so that their place in human evolution can be established. South African hominids are found in cave sites that are complex in terms of their stratigraphy. Dating methods previously applied at the caves include faunal, palaeomagnetic, electron-spin resonance and cosmogenic isotope methods. These have been unable to give conclusive ages to the fossils. South African hominids are therefore poorly dated in comparison to their East African counterparts, which lie in volcanic deposits that are more simply stratified and more simply dated.

U-Pb dating is a radiogenic method proven to be applicable to carbonate deposits. More recently it has been applied to young speleothem deposits with sufficiently high concentrations of U and low levels of common Pb. In this study U-Pb dating is applied to speleothem deposits in stratigraphic context with the South African hominid fossils.

Samples were taken from the Silberberg Grotto at Sterkfontein. The hominid fossil, StW 573, was found here in 1998. Three layers of flowstone were sampled, two from above the skeleton and one from below. The combined results indicate an age for StW 573 of $\approx$ 2.2Ma. This is considerably younger than previous age estimates have inferred. Samples from three other caves were analysed - Kromdraai, Swartkrans and the Limeworks - but these did not produce reliable ages.

Within the samples both U and Pb were found to vary spatially over small scales in quantity, and Pb in composition too. Published studies in the area have revealed a major ^{234}U excess in groundwater and speleothem. Where conventional age calculations are used this effect could result in an age much greater than the

true age. After the sample analyses presented here, ^{234}U excess analyses of some samples became available and these were used to calculate corrected ages. Variations in initial Pb composition introduced scatter on the age plots but this was not investigated further here.

The results are presented firstly as maximum ages and following correction for ^{234}U excess, as best estimates. The flowstone layers immediately above - layer 2C - and below - layer 2B - StW 573 gave maximum ages of 3.04 ± 0.08Ma (SK3 result) and 2.97 ± 0.13Ma respectively. Layer 2C was corrected for disequilibrium and gave a best estimate age of 2.17 ± 0.17Ma using a weighted average of three results. The corrected age for Layer 2B was $2.24 + 0.09/-0.07$.

There are important implications for the U-Pb age of StW 573. Firstly it provides evidence as to the age and formation of the Sterkfontein cave and therefore other hominid bearing caves with comparable faunal assemblages. The cave sediments exhibit complex stratigraphic relationships that render chronostratigraphy uncertain. More importantly it lends further information on how South African hominids fit into the family tree. At 2.2Ma StW 573 may come under the classification of *Australopithecus africanus* and be contemporaneous with the fossil Sts 5, also from Sterkfontein, which had previously been considered to postdate StW 573. It also confirms that the South African branch of this genus is probably not as ancient as the East African and that these hominids were not widespread in Africa at 4Ma. With the first evidence for the genus *Homo* at $\approx$ 2.5Ma, StW 573 is unlikely to be a direct ancestor of modern humans.

Beyond their implications for human evolution, these results confirm the applicability of U-Pb dating to carbonates, and more specifically to young carbonates.

Acknowledgements

I wouldn't have been able to complete this research without the continued support of my primary supervisor Bob Cliff. Over the last four years Bob has been reassuringly reliable and has remained patient despite my continued lack of mathematical skills. For all this I am eternally grateful. In the field and at the Geoscience Africa conference I was aided by my second supervisor Alf Latham. As well as providing entertainment and sticking up for me in the turbulent world of palaeoanthropology Alf has to be given credit for putting the wheels of this project in motion.

There are a lot of people I need to thank in South Africa, firstly for allowing me into this exciting area of science but also for helping me whenever possible. Tim Partridge, Kevin Kuykendall, Francis Thackeray, Lee Berger, Andre Keyser, and Ron Clarke gave me access to sample at the sites and Mary Leslie from SAHRA assisted with permits to remove the samples from the country. I would like to thank Tim and Francis in particular for their help and continued support, and Kevin for allowing me to join in the Makapansgat field school and giving me a floor to sleep on, on several occasions. I also need to thank Jan Kramers in Bern for allowing us to take advantage of their machine for the purpose of age corrections. Lastly, huge thanks go to my two partners in crime in South Africa. Phil - I couldn't have spent four weeks in such close proximity with many other people. Thanks for being a fab and very funny field partner, and only swearing at me once over the month. Robyn - I can't think of anyone better suited to continuing the U-Pb work in South Africa. You made the conference an enjoyable experience rather than a painful one.

I was lucky enough to not have to fight for lab time in either the clean lab or on the mass spec, but I was even luckier to share these work spaces with such friendly helpful people. I am indebted to Christine for all the cleaning and prep she did for

me, and the non-control-freak way in which she did it. I already miss our clean lab gossips. Massimo was a genius in both the clean lab and on the machine and was always there to provide scientific advice when I needed it. as well as teaching me to swear in Italian, cook Italian and read Italian literature. Outside of the lab I was confined to an office with a load of bonkers people who have made my life all the more richer; Steve, Jennie, Jane, Mat, Ransome, Rachel, Anika. Rachael and Dexta. Not forgetting Emma K - my demo partner - thanks for taking Pedro on board. I would like to thank you all for the continued friendship, support and PhD-related wisdom that you have given me. There several other people in the department who I would like to thank for their various skills and advice, those that I have remembered are Phil Murphy, Nick Barber, Neil Cundall, Joe Cann, Eric Condliffe, Quentin Fisher and Rob Mortimer.

Despite lacking (in most cases) any knowledge of U-Pb dating my friends and family have been just as important as my supervisors during my PhD. I have to mention Catherine first as she has asked me every week for the last couple of months whether I have written this yet, and also because she has been in my life since I can remember in spite of continued attempts to get rid of her - only joking! How will we cope without our weekly grumbles over lunch in the ES coffee room? Secondly I must thank Sonia. Thanks for flying 3000 miles to travel across South Africa with me on a train with inadequate amenities. The cup incident will haunt me forever. Truly, you two have given me support and helped me to take life not so seriously when the PhD has been hard. I could go on and thank loads of other friends but I have been writing now for a very long time so I hope you will forgive me if your name isn't down - I thought of you. Mum, dad and Richard, I would like to thank you for all your support over the years. Mum, I haven't forgotten all the lunches and coffees I owe you, and will probably always owe you. Dad, thanks for your never ending interest and enthusiasm in my work - long may it continue. And yes, I owe you a tenner.

Lastly Ransome, my best office mate, best friend and best mathematician. I wouldn't have wanted to do any of it without you. Especially not those Bateman equations.

Contents

List of Figures

List of Tables

Nomenclature

Chemistry

Al	aluminium
Ba	barium
Be	beryllium
Br	bromine
C	carbon
Ca	calcium
Fe	iron
K	potassium
Mg	magnesium
Na	sodium
O_2	oxygen
Pa	protactinium
Pb	lead
Ra	radium
Re	rhenium
Rn	radon
Th	thorium
Ti	titanium
U	uranium

BaFBr	barium fluorobromide
$CaCO_3$	calcium carbonate
CaF_2	calcium fluoride

$Ca_{10}(PO_4)_6(OH)_2$	hydroxyapatite
CO_2	carbon dioxide
CPHBr	column-passed hydrobromic acid
H_3PO_4	phosphoric acid
HBr	hydrobromic acid
HCl	hydrochloric acid
HF	hydrofluoric acid
HNO_3	nitric acid
UO_2^{2+}	uranium oxide

Units

μl	microlitres
A	amps
cm	centimetres
g	grammes
ka	thousands of years old
ky	thousands of years
M	molarity
m	metres
Ma	millions of years old
mA	milliamps
mg	milligrams
ml	millilitres
mm	millimetres
mV	millivolts
my	millions of years
ng	nanograms
nM	nanomoles
pA	picoamps
pM	picomoles

ppb	parts per billion
ppm	parts per million
ppt	parts per trillion
rpm	revolutions per minute
y	years

Acronyms

EP	Error Propogation
ESR	Electron Spin Resonance
EU	Early Uptake
GPTS	Global Polarity Timescale
LU	Linear Uptake
MSWD	Mean Square of Weighted Deviates
OAE	Original Ancient Entrance
SEM	Secondary Electron Multiplier
S.E.M	Scanning Electron Microprobe
TIMS	Thermal Ionisation Mass Spectrometry
UpA	Ultra purity Acid

Roman variables

b	bias in ratio
m-s	ratio of $^{238}U/^{235}U$, measured minus spike
c	bias corrected ratio
mu	ratio of $^{238}U/^{204}Pb$
mu_{208}	ratio of $^{238}U/^{208}Pb$
m	measured value
n	normalised ratio
nat	ratio in nature

r	re-normalised ratio
s	value in spike
$\overline{x}$	mean
C_i	ith constant of integration
D	total daughters at time t
D_0	D at $t = 0$
D^*	stable daughters produced by radioactive decay of parent where $N_0 = 0$ at $t = 0$
N	number of parent atoms at time t
N_0	N at $t = 0$
N_i	$i = 1, 2, 3, ...n$, where subscript 1 denotes parent in decay chain, $2, 3, ..$ are radiogenic daughters, and n denotes stable end daughter
N_i^0	abundance of N_i at $t = 0$
t	time
$t_{1/2}$	half-life

Greek variables

λ	decay constant
λ_i	decay constant of N_i
σ	absolute standard deviation
ϕ(Phi)	U fractionation factor
Ω	ohms (where MΩ is mega ohms)

Miscellaneous

%	percent
‰	permil
1σ	confidence level of 68%
2σ	confidence level of 95%

Chapter 1

Introduction

1.1 Background to the study

At some point in the hugely varied and interesting history of the human lineage, *Homo sapiens*, or modern humans, shared a common ancestor with today's pygmy and common chimpanzees. This ancestor has not as yet been identified but it is thought to have existed no earlier than 8 Ma (Johanson and Edgar, 2001). At this time, changes in climate had already led to the divergence of gorillas from the flourishing ape lineage that had been established in Africa. What remained of the lineage then split further into two evolutionary groups. One half comprised the species that went on to become pygmy and common chimpanzees, the other led to modern humans (McKie, 2000).

Long before African hominid discoveries were first made, Darwin predicted the origins of modern man lay in Africa in his book *The Descent of Man*, 1871. However at the beginning of the 20th century, fossil remains and popular opinion had led scientists to believe that humans had originated in Asia (Tobias, 2000). At the same time, South Africa was in the grip of the gold rush. Essential to the processing of the raw material was lime. Limemining was a lucrative industry and the huge limestone deposits that cover the Transvaal area of South Africa attracted the miners. In 1924 limeworkers blasting on a site called Taung, Figure (1.1), on the edge of the Kalahari discovered the skull of a small apelike creature. The skull found its way into the hands of skilled anatomist Raymond Dart, who recognised

the significance of the discovery. It became known as the Taung Child, see Figure (1.2). This find was the beginning of an exciting time in the story of human evolution. What unfolded in the next 75 years was the wide and varied story of our origins across the African continent. In addition to the excavation of many South African hominid sites a wealth of fossil evidence confirming Africa is indeed the cradle of humankind was accumulated from Malawi, Tanzania, Kenya, Ethiopia and the Chad Republic (Tobias, 2000). Fossils such as Sts 5 (Figure (1.3)) - also known as Mrs Ples - A.L. 288-1, more often known as Lucy and most recently, StW 573 (Figure (1.4)) - or Little Foot - have helped to paint a picture of the human family tree. In turn this has helped us to find out more about who we are and why we are here.

1.1.1 Timeline of hominid discoveries in South Africa

Figure (1.1) shows the South African sites relevant to this study and the following timeline.

1920's

In 1925 Raymond Dart announced the discovery of the Taung Child, see Figure (1.2). It possessed small canine teeth and the shape of the skull suggested that this creature was bipedal (walked on two legs), although the brain was ape size (McKie, 2000). It was thought by many scientists at the time to be a related to a chimpanzee or a gorilla (Leakey, 1981).

After the announcement of the Taung Child, W.I. Eitzman a schoolteacher from Pietersburg sent Dart some specimens from a mine in what was the Northern Province, called the Limeworks (Tobias, 2000). These samples prompted him to describe the site as a "site of early human occupation".

1930's

The scientific community would have continued to look at the Taung Child with derision had it not been for the discovery of an adult hominid in South Africa in

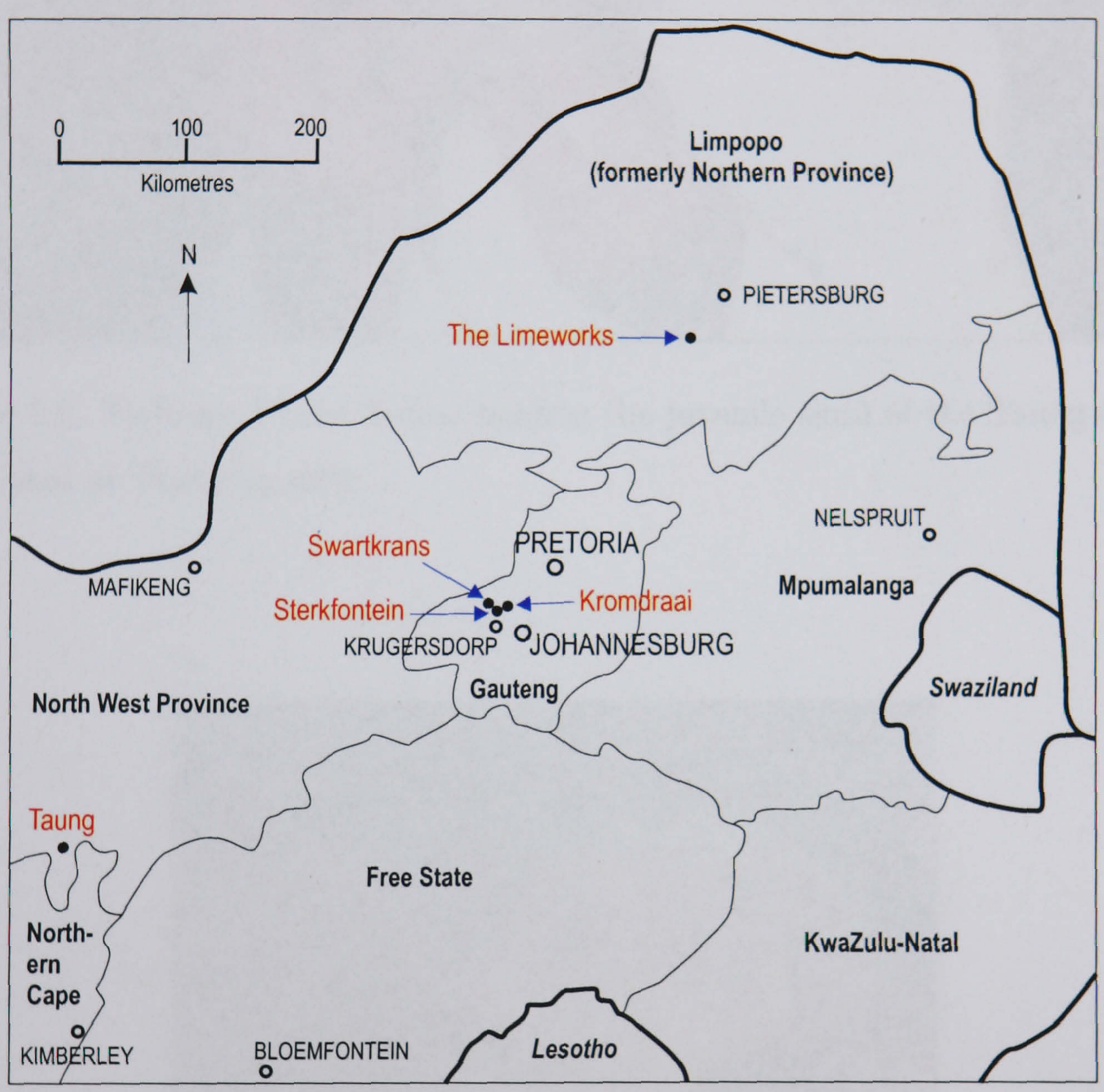

Figure 1.1: Map showing positioning of hominid cave sites in South Africa relevant to this study. After Partridge (2000a).

Figure 1.2: Professor Philip Tobias holding the juvenile skull of the Taung Child, discovered at Taung in 1924.

Figure 1.3: Photograph of adult Sts 5, Mrs Ples, an adult *Australopithecus africanus* cranium found at Sterkfontein in 1947.

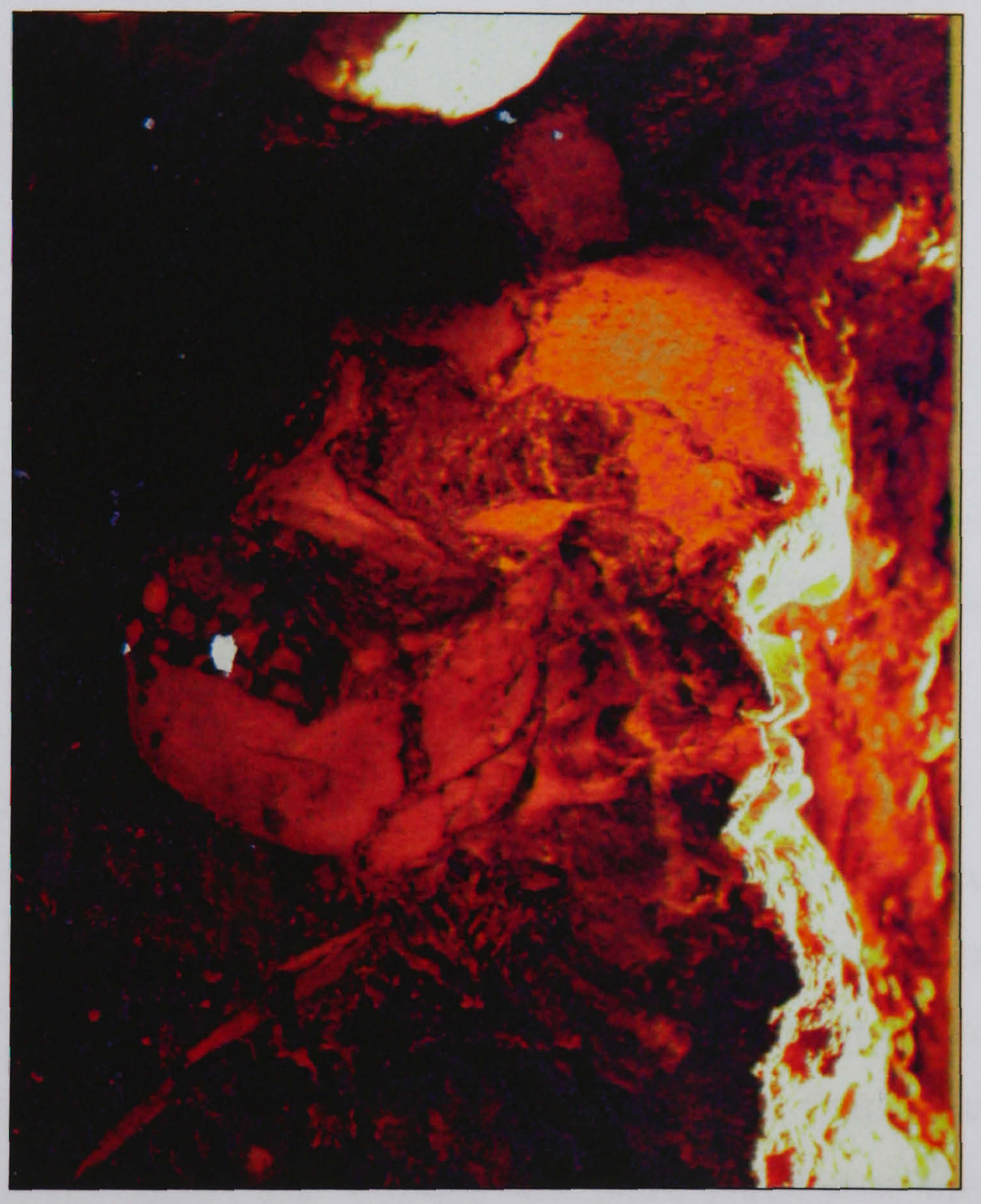

Figure 1.4: Photograph of StW 573, Little foot, found at Sterkfontein in 1998. P. Myburgh Film Pty Ltd., 2001 Palaeo series.

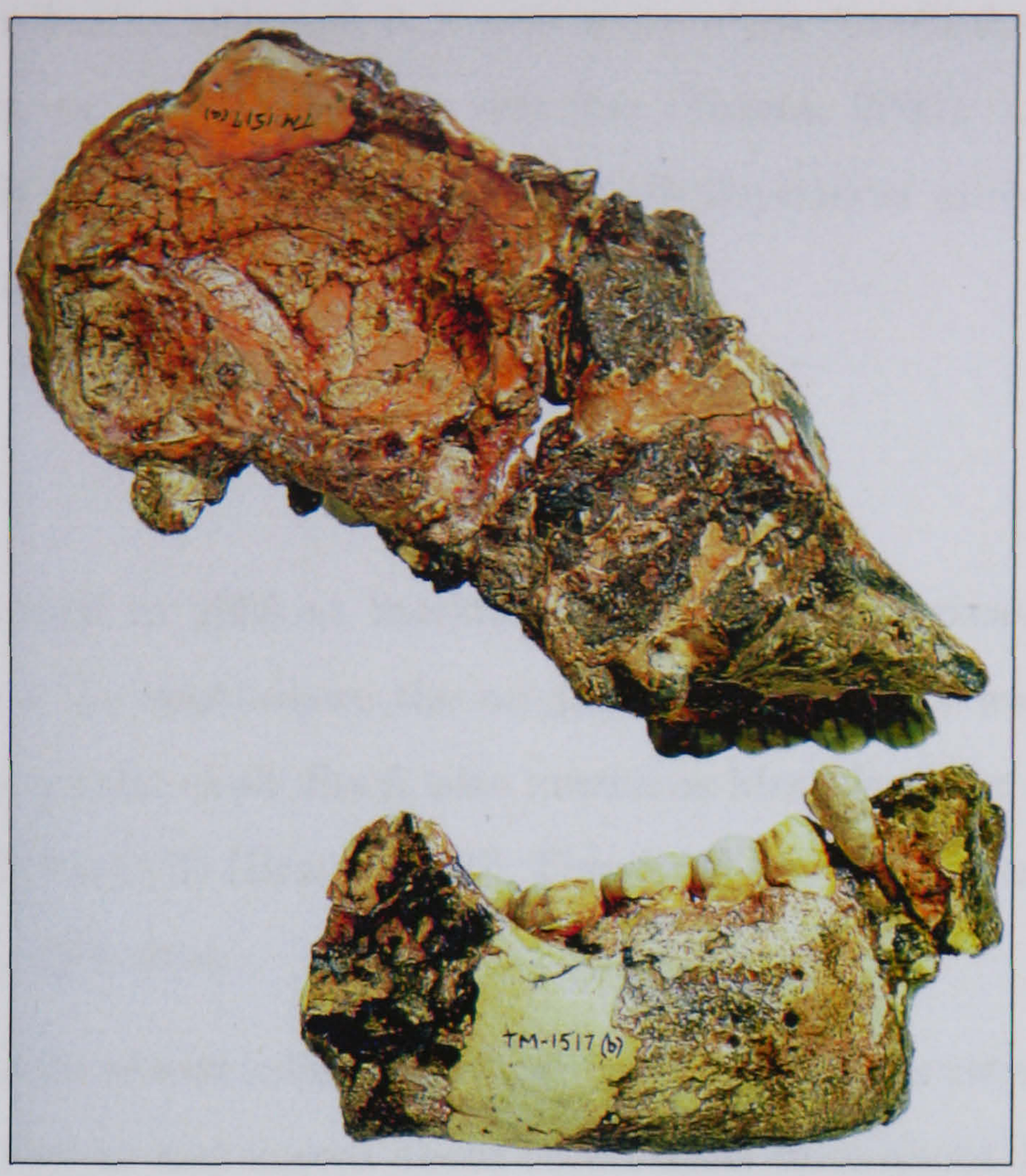

Figure 1.5: Photograph of TM 1517, the adult partial cranium and mandible of an *Australopithecus robustus* found at Kromdraai in 1938. Photographed by J. Reader, Science Source/Photo Researchers, from Johanson (2001).

1936. Limemining in the late 19th century led to the discovery of the bone rich breccias of a site called Sterkfontein just west of Johannesburg. During the next 40 years small amounts of bones were collected here by several interested parties, but it wasn't until 1936 that palaeontologist Robert Broom obtained the part skull and endocranial cast of an adult australopithecine that excavations began in earnest (Tobias, 2000). The remains that were found over the next 3 years were originally classified as *Australopithecus transvaalensis* then *Plesianthropus transvaalensis* (Tobias, 2000; Brain, 1958). Eventually these along with the Taung Child were classified as *Australopithecus africanus* meaning southern ape of Africa.

Schoolboy Gert Terblanche was the first to discover hominid remains at a neighbouring site, Kromdraai, in 1938. Broom was working just down the road at Sterkfontein and he bought an initial fragment of this specimen from the limeworks manager there (Brain, 1958). Broom recognised that the fossil fragments belonged to an individual that differed somewhat from the *Australopithecus africanus* remains at Sterkfontein. The new find, TM 1517 (Figure (1.5)), was classified as

Plesianthropus robustus although it is now more often classified under the genus *Australopithecus*, as *Australopithecus robustus* (Tobias, 2000). *Australopithecus Robustus* is believed to have evolved from *Australopithecus africanus* (Johanson and Edgar, 2001).

1940's

Limemining stopped in 1939 at Sterkfontein, and in 1946 excavations were resumed. Close to the spot where the original *Plesianthropus* was found Broom unearthed a spectacular skull, Sts 5, also known as Mrs Ples after its original classification, see Figure (1.3) (Brain, 1958). This fossil was subsequently classified as *Australopithecus africanus.*

A mile across the Bloubank valley from Sterkfontein was the as yet unexcavated site of Swartkrans. Broom had known about Swartkrans since about 1936 when work began at Sterkfontein, but excavation was not started there until late 1948 (Tobias, 2000). Swartkrans was immediately a fruitful site, producing a hominid molar within the first blast, and a mandible within the first week (Brain, 1958; Brain and Watson, 1992). More remains were quickly revealed and Broom recognised these as the same genus as specimen TM 1517 from Kromdraai. The Swartkrans robust hominids were originally classified as *Paranthropus crassidens*, and although some researchers still believe them to differ from the robust hominids of Kromdraai they are usually classified as the same, that is *Australopithecus robustus* (Johanson and Edgar, 2001). Sterkfontein at this point was closed down so that Broom and his student, John T. Robinson, could concentrate on Swartkrans (Tobias, 2000). During this period remains of what was later reassigned as *Homo erectus* were unearthed at Swartkrans. Thus, Swartkrans was the first site to produce evidence of the coexistence of two types of hominids (Tobias, 2000). By the end of 1949 the project hit financial problems although the continued blasting had revealed a thick layer of very pure basal speleothem. Since this was commercially valuable, excavation was forced to cease as limemining took precedence.

It was 22 years after Dart examined fossil evidence from the Northern Province site of the Limeworks before the first pre-hominid and then hominid remains were excavated there. In 1947 J. Kitching, sent by Dart, recovered part of a hominid skull cap

(Tobias, 2000). During the following year hominid discoveries surfaced in the old limeminers dumps along with a large collection of associated fauna (Brain, 1958). The Limeworks hominids were primarily classified as *Australopithecus prometheus* by Raymond Dart, after their black colouration, which he attributed to burning. They are now under the heading of *Australopithecus africanus* (Tobias, 2000).

1950's

At the end of 1951 scientific investigations began again at Swartkrans (Brain, 1958). After the death of Broom in 1951, Robinson continued working there until 1953, after which the site was left unworked for 12 years (Brain and Watson, 1992).

At Sterkfontein work undertaken by C. K. Brain in 1956 produced stone artifacts from some of the younger deposits. In 1976 a skull of the proposed maker of the tools found at Sterkfontein, *Homo* c.f. *habilis*, was removed (Tobias, 2000).

1960's

In 1965, after a 12 year interval in work, a new excavation was undertaken by C. K. Brain at Swartkrans. This ran for 21 years (Brain and Watson, 1992). Swartkrans had been extensively mined during the 1930's and a lot of the excavations done under the supervision of Brain involved sorting through the miners dumps.

Today's picture

Nearly 75 years after the discovery of the Taung Child the most complete hominid fossil skeleton ever found was revealed at Sterkfontein. The foot bones of StW 573, Little Foot (Figure (1.4)), were originally found in 1980 but were not recognised as belonging to a hominid (Tobias, 2000; Clarke and Tobias, 1995). The bones were rediscovered in 1994 and a subsequent excavation revealed the in situ skeleton in 1998 (Clarke, 1998). This included the skull, complete arm and hand bones and the most complete hominid foot. The completeness of this fossil is what makes it such an important discovery. For the first time osteomorphic parameters such as the ratio of arm length to leg length can be compared, which may be used to determine degree of adaptation to bipedalism (Clarke, 1998; Clarke, 2002a).

1.1.2 Summary

The australopithecines were a group of early hominids found in both Southern and Eastern Africa between roughly 1 and 4 Ma (Johanson and Edgar. 2001). Following the discovery of the Taung Child, hundreds of hominid fossils have been recovered from several cave sites in South Africa including Sterkfontein, Kromdraai, Swartkrans and the Limeworks. There are at least 120 *Australopithecus africanus* individuals known from Sterkfontein, as well as the Taung child and several from the Limeworks (Johanson and Edgar, 2001). Additionally Swartkrans has produced the remains of a minimium of 85 *Australopithecus robustus* and 6 *Homo* individuals (Johanson and Edgar, 2001). These are an incredibly important group of archaeological sites as recognised by UNESCO who has made "The Fossil Hominid sites of Sterkfontein, Swartkrans, Kromdraai and the Environs" a World Heritage Site. Sterkfontein alone is the "richest single fossil hominid site in the world" (Tobias, 2000).

1.1.3 Dating hominids

One of the major differences between the South African and the East African hominids is the geological context of the fossils. In East Africa the fossils lie in volcanic deposits. The ^{40}K-^{40}Ar technique, which was developed in the 1950s has been applied throughout the East African hominid deposits as a dating method. This technique was refined and now uses ^{40}Ar and ^{39}Ar, an artificial isotope created to serve as a proxy indicator of the amount of ^{40}K (Johanson and Edgar, 2001). As a consequence of this the East African hominids are extremely well dated. In contrast the South African hominids are cemented in cave deposits and a direct dating method has not yet been successfully applied. Dating techniques previously attempted on these sediments have been able to provide a good estimate of the chronology at some of the sites, but multiple tests are required to secure greater accuracy. It is vital that these fossils are dated as accurately as possible in order to place them within the hominid phylogeny, and to gain a greater understanding of how and why we evolved the way we did.

1.2 Aims of this project

The three main aims of this project are:

1. U-Pb dating of hominid fossils. This was to be achieved by dating speleothem deposits at the South African hominid sites of Sterkfontein, Kromdraai, Swartkrans, and the Limeworks, that were associated with the hominid fossil discoveries made at these sites. Ages were to be assigned where there were clear stratigraphic relationships between the fossils and the cave deposits being dated.

2. Assess the implications of any new ages in terms of, (i) what they mean for the position of South African hominids in the human family tree, and how this position affects the overall picture of human evolution, and (ii) what they mean for the formation and evolution of the caves in which they are found.

3. Further test the feasibility of U-Pb dating on young carbonate deposits. Application of U-Pb dating to these kinds of deposits is a technique still in its infancy. The objective was to gain further knowledge about applying this technique, and to get a greater understanding of the issues arising from the use of U-Pb in this context and how these issues can be approached.

1.3 Thesis structure

1.3.1 Chapter 2

On the geology of cave formation and deposits in karst landscapes, but in particular on the South African hominid bearing caves.

This chapter covers the basic geology of the area in which the caves are found and then goes on to describe each site individually. The individual descriptions include how the cave formed and its depositional history. This is important, as a grasp of the stratigraphic relationships was necessary for any U-Pb dates to be assigned to the fossils themselves. The description of the type of deposits in the caves also

comprises a section on speleothem, the deposit to which the dating technique was applied.

1.3.2 Chapter 3

On the other dating techniques that have been applied at the South African hominid cave sites as a precursor to this study.

This chapter provides a breakdown of four dating techniques which have been used at the hominid sites and their results. It also examines the limitations of these techniques, and some of the contrasting interpretations of the evidence these techniques have provided.

1.3.3 Chapter 4

On U-Pb dating theory and contextual issues.

This chapter charts the history of the mathematical theory behind radiogenic dating, before looking at U-series and U-Pb dating. The chapter examines their application in dating both hominid remains and speleothem deposits. Lastly concentrating on the method specific to this study, U-Pb, the issues concerned with the application of this technique to the South African cave deposits are reviewed in detail.

1.3.4 Chapter 5

On the methodology of U-Pb dating the South African hominid sites.

This chapter firstly introduces the sampling methodology in the field specific to each site, and the sampling methodology in the lab, specific to each hand sample. It goes on to describe the important aspects of the experimental procedure including chemistry theory, lab techniques, mass spectrometric analysis, data processing, and handling of standards and blanks. The final section of this chapter deals with the issues taken into consideration for data evaluation.

1.3.5 Chapter 6

On the results of U-Pb dating of South African hominid sites.

This chapter covers the results for all four of the sites studied but concentrates mainly on Sterkfontein. The individual hand samples and sub-samples are critically assessed along with any graphs plotted and ages deduced from these. Where hand samples are linked stratigraphically, results are compared and further evaluated. Section (6.3) deals with the issue of initial U-series disequilibrium and how to apply a correction to the original ages calculated. Original ages and best estimate ages are reported for the StW 573 fossil from Sterkfontein. Further samples and results are reported from the Limeworks, Kromdraai and Swartkrans.

1.3.6 Chapter 7

On the interpretation of the Sterkfontein results, their concordance with other methods and the application of U-Pb dating to young carbonate deposits.

The Sterkfontein results are first considered in terms of their meaning for hominid phylogeny and for the formation of the Sterkfontein cave site. The results for the dating techniques previously used on these deposits are then critically reviewed in view of the U-Pb results and reinterpreted where possible. Further possible work in South Africa is then briefly appraised. This is followed by an exploration of the wider issues for the U-Pb method. Important lessons that have been highlighted by this study and what they mean for further investigations of this nature are discussed. A re-examination of the original aims and objectives precedes the concluding statement for the study.

Chapter 2

Geology

2.1 Cave formation and deposits

Caves are natural underground openings in rock that originate through the dissolution of limestone by phreatic and vadose waters. Caves develop initially in the phreatic region, where cave sizes and shapes are determined. As the water table lowers the cave enters into the vadose region which is characterised by a period of sediment deposition. Throughout its lifetime a cave will collect large amounts of sediment. The arrangement of such sediments is seldom simple, in that the law of superposition does not always apply. Deposits accumulated in the interior of the cave can be divided into clastic, organic and precipitated. These can be further classified according to where they originated from; allogenic for sediments formed outside the cave and transported in, authigenic for for those created within the cave (Ford and Williams, 1989).

Speleothem

The main precipitated material in caves is speleothem. Water passing through the soil may pick up significant quantities of CO_2 forming carbonic acid. This dissolves carbonate rocks forming a solution of Ca and Mg carbonates (Brain, 1958). Higher levels of soil CO_2 will result in a more aggressive dissolution of the rock. Speleothem forms wherever such seepage water enters a cave and becomes supersaturated with respect to $CaCO_3$. This may be the result of outgassing of soil

derived CO_2 and/or evaporation, although evaporation is usually only important in low humidity environments (Latham and Schwarcz, 1992).

Differences in fluid flow and water chemistry result in the formation of a wide variety of speleothems in caves. These include subaerial forms like stalagmites, stalactites, and flowstones, and subaqueous forms, such as rimstone pools and mammillary calcite (Richards and Dorale, 2003). Flowstones are uniform flows of speleothem that run parallel to the host surface (Ford and Williams, 1989). In karst regions flowstones are the main precipitated deposits, where they can occur in thicknesses of tens of metres.

Calcite is the main speleothem mineral in caves (Ford and Williams, 1989). Aragonite is often the second most abundant, originating from Mg-rich waters that typically inhibit calcite growth. Elevated Mg is found in waters which percolate through dolomite bedrock, such as that in the Transvaal (Frisia, 1996). The instability of aragonite means any formed usually recrystallises to calcite, especially in an environment where water is always present (Frisia, 1996). Despite the dolomite host rock, in the caves of the Transvaal calcite prevails. Many of the caves contain exceptionally pure speleothem (Brain, 1958).

Speleothems can be used in many ways to explore the past history of a cave. They are often used for environmental reconstruction and for dating purposes. The presence or absence of speleothem is often the most telling palaeoclimatic indicator. Flowstone deposition rates can vary widely depending on environmental conditions and the form of the cave. Growth is dependent on a continuous flow of water. Growth stops with the cessation of this flow, allowing thin layers of detrital sediment to accumulate on the speleothem (Latham and Schwarcz, 1992). Deposition rates are therefore greatly affected by seasonality, and the production of flowstone in many caves appears to be periodic or even cyclic. Rates have been observed to double when summer soil water reaches a speleothem during autumn. Temperature also affects speleothem formation. Higher temperatures result in greater exsolution of CO_2 and increased formation of speleothems (Brain, 1958).

Mineralogy and fabric are indicative of the suitability of speleothems for chronological analysis. Primary or unaltered samples must be sought (Richards and Dorale, 2003). Inclusion free calcites and aragonites are colourless and translucent, whereas

inclusions give the material a white, opaque appearance. Most speleothem formed in the inner parts of caves is free of clastic detritus (Latham and Schwarcz, 1992). Discrete black, grey, brown and red layers may be attributable to mud, although it has been found that most colour in speleothems is the result of humic and fulvic acids (Ford and Williams, 1989). Crystals in flowstones typically grow perpendicular to the growth surface and form columnar or fibrous fabric. These types of fabrics are associated with constant flow (Frisia *et al.*, 2000). Speleothems are usually composed of massive, non-porous calcite so the problems associated with diagenetic modification are rare (Latham and Schwarcz, 1992; Frisia, 1996).

Clastic sediments

Clastic sediments are classified according to clast size. Ford and Williams (1989) divide clastic cave sediments into three types; gravel to boulder sized material from the surrounding area (typical in hilly karst regions); sand (sandstones are often found in the same basins as limestone); and silts and clays (most widespread clastic deposits in caves). In-cave weathering or winnowing of existing deposits may produce authigenic versions of these.

An important clastic sediment in the South African caves is breccia. This is a diamictite of cemented angular material, which can be grain or matrix supported.

2.2 South African hominid bearing cave sites

2.2.1 Geology of the area

The deposits which accommodate the hominid remains are the infillings of karst caverns and fissures (Partridge, 2000). The caves are located in the Malmani Dolomite which crops out extensively in this area. The Malmani Subgroup is part of the Chuniespoort Group and the Transvaal Supergroup and lies conformably on the Black Reef Series (Wilkinson, 1973). Figure (2.1) shows the stratigraphy of the Chuniespoort Group.

The Malmani Subgroup is formed of massive blue-grey dolomitic limestones. The

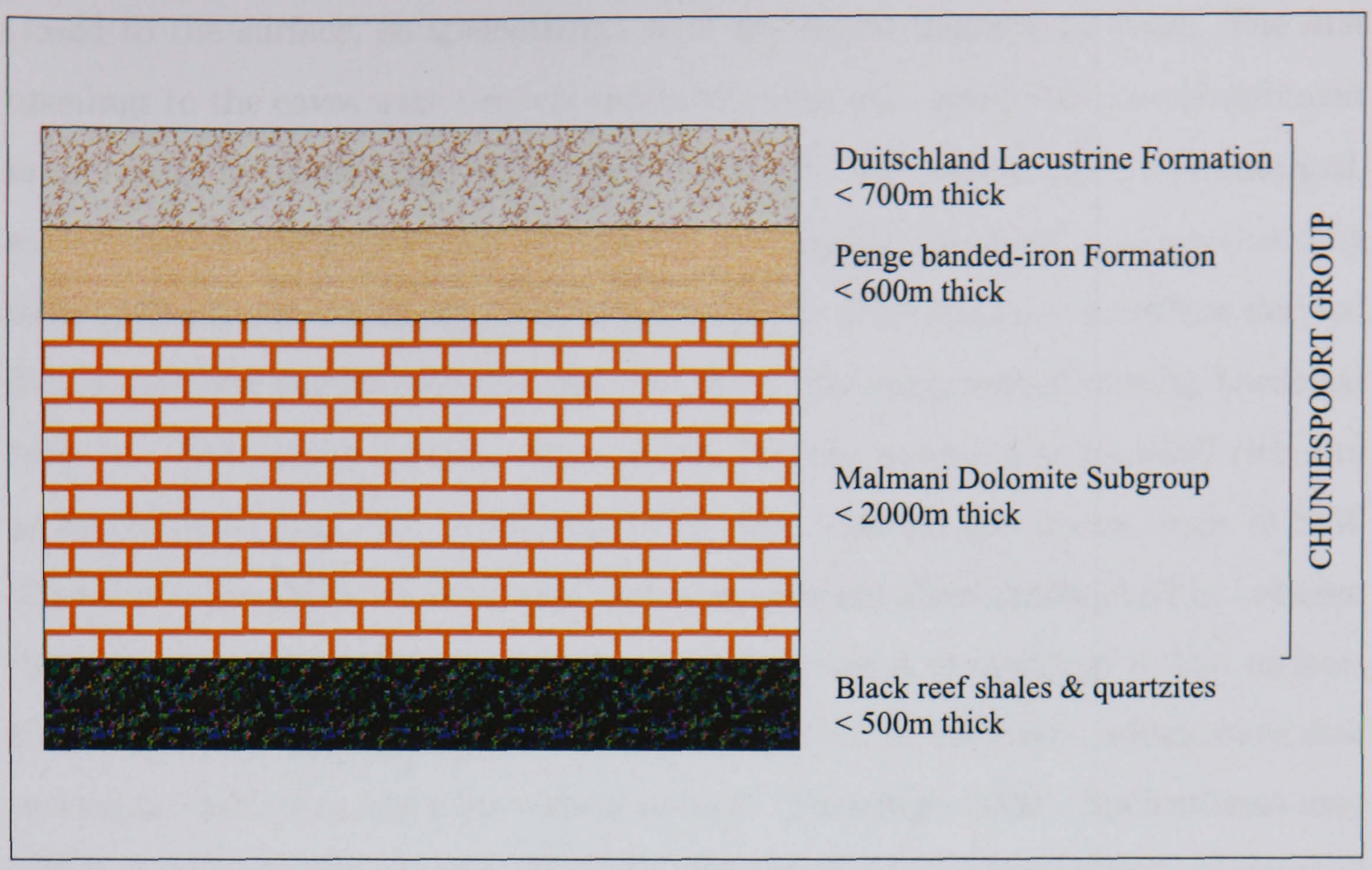

Figure 2.1: Stratigraphic relationships within the Chuniespoort Group of the Transvaal Supergroup - After Catuneanu and Eriksson (1999) and Tankard et al., (1982). Not to scale.

base of the sequence is characterised by narrow but abundant chert bands (Brain, 1958). These insoluble bands contribute to the cave earth deposits which accumulate at the hominid sites (Partridge, 2000). The dolomite is Pre-Cambrian in age and evidence in the form of stromatolites and algal features suggest that this deposit formed in a shallow sea (Wilkinson, 1973; Brain, 1958).

2.2.2 Cave formation in the Transvaal dolomite

The following description of cave formation in this region is taken from Brain (1958) unless otherwise specified.

Like other karst cave systems, the caves in the Transvaal originated in a water-filled zone where caverns and passages were dissolved out of the dolomite bedrock. Water tables in the truest sense do not exist in carbonate rocks such as these since the porosity is too low. Instead, water flows via linked, totally water filled or partially air-filled conduits, which form along weak points in the rock (Latham *et al.*, 1999; Latham *et al.*, 2003). When the caves are brought out of the water-filled zones, deposits begin forming. At this stage the Transvaal caves were still essentially

closed to the surface, so speleothems were the major deposits to form. The first openings to the caves were vertical shafts allowing only small amounts of sediment in or acting as death traps (Partridge, 2000). As openings in the caves enlarged, surface derived debris entered, mixing with authigenic cave earth and interbedding with speleothems which also continued to form. The mixture of surface derived debris and cave earths were cemented by the percolating waters forming hardened breccias. This slowly accumulating breccia had the potential to be fossil rich and at Sterkfontein gave rise to the more complete hominid specimens, such as StW 573 (Partridge, 2000). These fossil rich breccias were often sandwiched in between flowstone formations. With the increased enlargement of openings to the surface, large quantities of allogenic material were admitted to the caves, which were now serving as shelters or traps for various animals (Partridge, 2000). Speleothems may still have been forming at this stage but were subject to contamination. Continued enlargement of cave openings eventually resulted in roof collapse and the caves became almost completely filled with deposits. After this erosion slowly began to destroy the cave formations. Most of the caves which house the australopithecine fossils have suffered severely from erosion, which has removed the majority of the original roofs and left the cave infilling exposed to further weathering and erosion (Brain, 1958).

In the following cave descriptions the formation and member notation are from (Partridge, 1978); the unit notation from (Partridge, 2000).

2.2.3 Sterkfontein

Sterkfontein is found on the southern side of the Bloubank river valley, to the north west of Krugersdorp, see Figure (1.1) and Figure (2.2). The Sterkfontein formation, after (Partridge, 1978), measures $\approx$ 75x15m at the surface, is $\approx$ 30m in depth below the the current surface, and is marked by a dolomite floor (Partridge, 1978; Partridge and Watt, 1991). Figure (2.3) shows the the extent of the underground and exposed cave system. Over time the cave sediments have been subject to alteration through subsidence into lower cavities, collapse of cave walls and roofs, and through the percolation of calcium carbonate rich waters (Partridge, 1978). It is thought that there are extensive hiatuses in the clastic deposits, some of which

Figure 2.2: View of southern side of Bloubank river valley from Swartkrans (Sterkfontein and Kromdraai not visible).

are associated with calcite deposition. This indicates periods of deposition where the influx of clastic material was severely reduced (Partridge, 1978). Development of subsequent caves below the formation has caused some subsidence allowing allogenic material to infiltrate the caves below the hominid bearing deposits (Partridge and Watt, 1991).

The Sterkfontein formation is split into six members, after Partridge (1978), which occur in a "continuous succession" (Partridge and Watt, 1991). Partridge (1978) seems to suggest that member 5 is the only unconsolidated one. Figures (2.4) and (2.5) show these members as represented in the Silberberg Grotto.

The following descriptions of the deposits are taken from Partridge (1978) and Partridge (2000) unless indicated otherwise.

Member 1

In terms of volume this is the second largest member (Partridge and Watt, 1991). It can be found above the dolomite floor in the Silberberg Grotto and is 0.5-2.0m thick. It is formed of white and brown banded recrystallised calcite. This was deposited during a time when the cave was being enlarged by erosion. It contains very little in the way of bones or allogenic material (Clarke, 1994; Partridge, 2000).

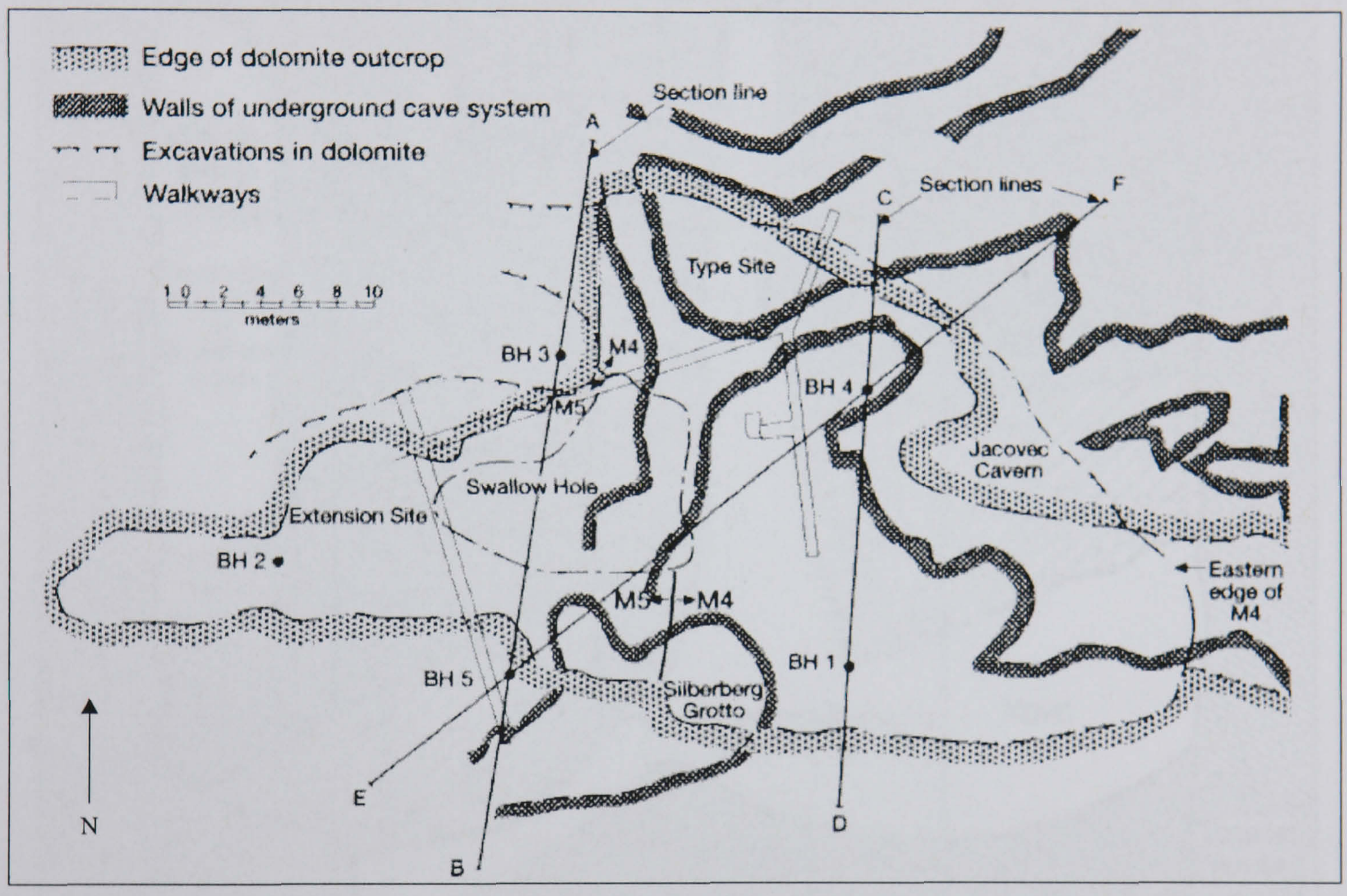

Figure 2.3: Plan of Sterkfontein showing extent of cave system. BH = bore holes (cores of sediment taken for stratigraphic analyses). M4 = member 4, etc. Section lines refer to cross-sections in Figures (2.4) and (2.5). From Partridge (2000), after Partridge and Watt (1991).

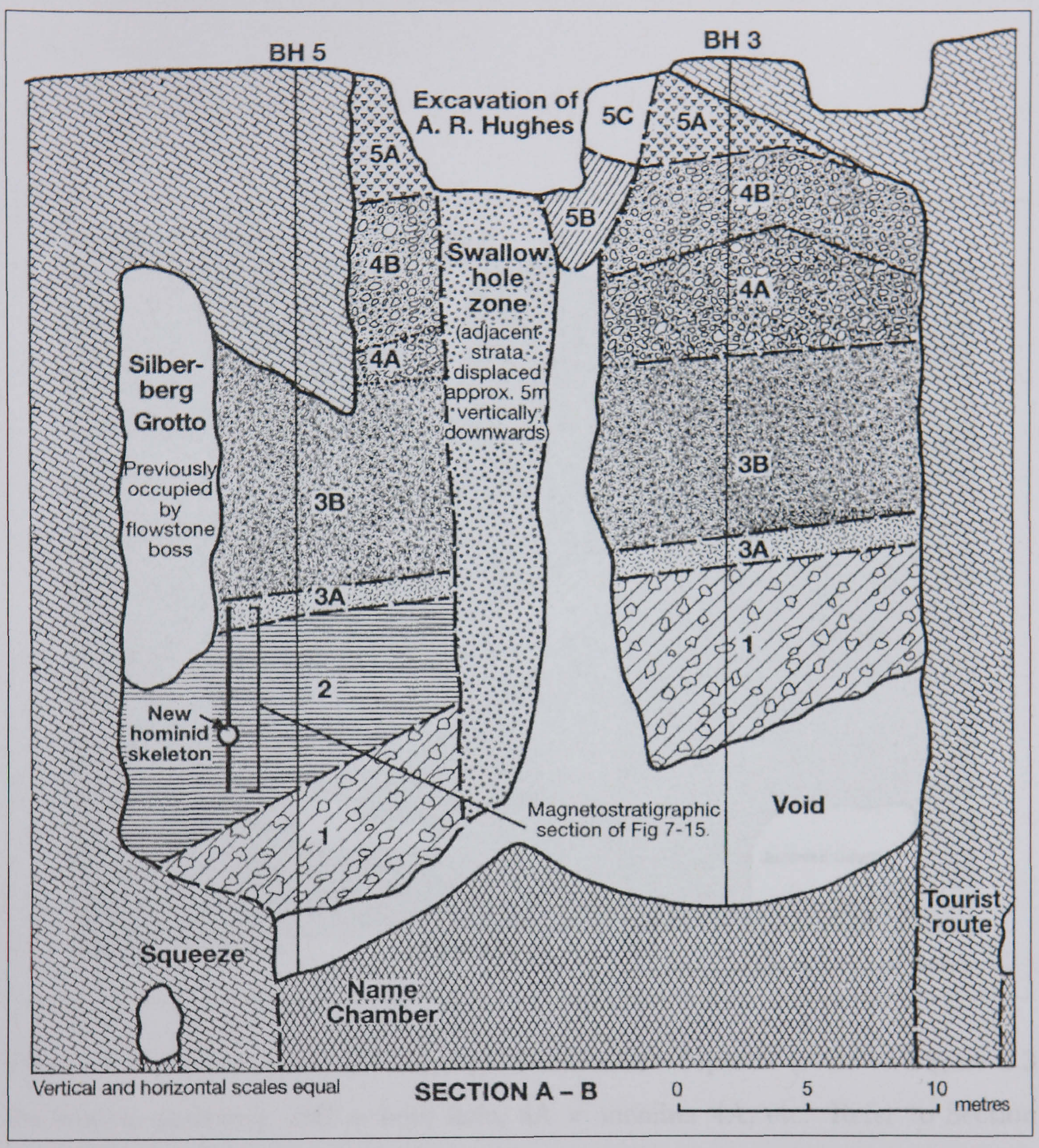

Figure 2.4: Cross-section A-B through Sterkfontein deposits (refer to Figure 2.3 for section position). BH = bore hole, 4A = member 4A, etc. Refer to Section (2.2.3) for full descriptions of each member deposit. New hominid skeleton is that of StW 573. Magnetostratigraphic section shown in Figure (3.4), interpretation A. From Partridge (2000), after Partridge and Watt (1991).

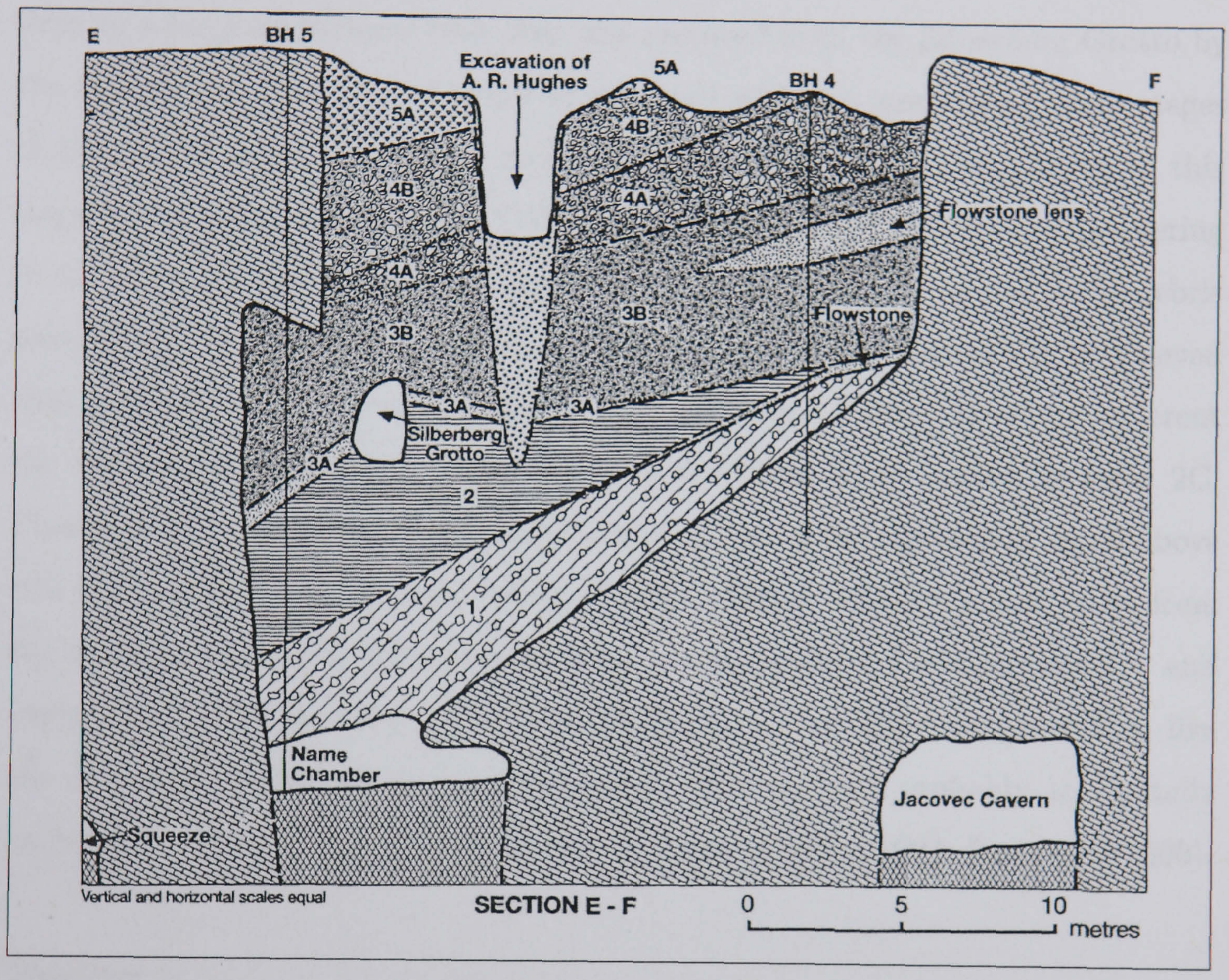

Figure 2.5: Cross-section E-F through Sterkfontein deposits (refer to Figure 2.3 for section position). BH = bore hole, 4A = member 4A, etc. Refer to Section (2.2.3) for full descriptions of each member deposit. From Partridge (2000), after Partridge and Watt (1991).

Member 2

Member 2 is found in the Silberberg Grotto and yielded the hominid skeleton, StW 573, Figure (1.4) and Figure (2.6). The sediments are up to 8.0m thick of breccia with broken speleothems and abundant bone near the base. Most of this deposit is on the southern face of the cave but it forms a westward sloping debris cone in the western end of the grotto. The breccia was deposited at the same time as a large speleothem boss that was removed from the Silberberg Grotto by the limeminers. The boss is found interlayered with the numerous growth stages of the debris cone, which also includes various mudflows. The growth of this large speleothem sealed in the StW 573 hominid on the debris cone (Pickering *et al.*, 2004). Sediment positions are indicative of a shaft opening above the debris cone. Soon after deposition of the breccia containing the skeleton it is believed that part of the breccia collapsed into a cavity which formed as water undercut the talus cone. Following this collapse, a flowstone layer, known as layer 2C, Figure (2.6), formed. Because of the collapse, some of the skeleton is found above this layer whilst some is found below (Clarke, 2002a). Fossil remains apart from the hominid StW 573, include a hunting hyena, skulls of Cercopithecidae[1], and various cats (Clarke, 1994). The way the fossils are arranged suggests they, like the sediments, fell in through an opening in the cave roof, probably accidentally as indicated by the completeness of the skeletons (Clarke, 1994; Partridge, 2000).

Member 3

Member 3 is the largest of the six deposits. It is divided into units A and B and reaches a thickness of $\approx$ 9m. The base of member 3 is a 1.2m thick flowstone (A) which is topped by 8m of red-brown breccia with scattered large clasts and flowstone lenses (B). Member 3 remained unexcavated when Partridge (2000) was published.

[1]Old world monkeys

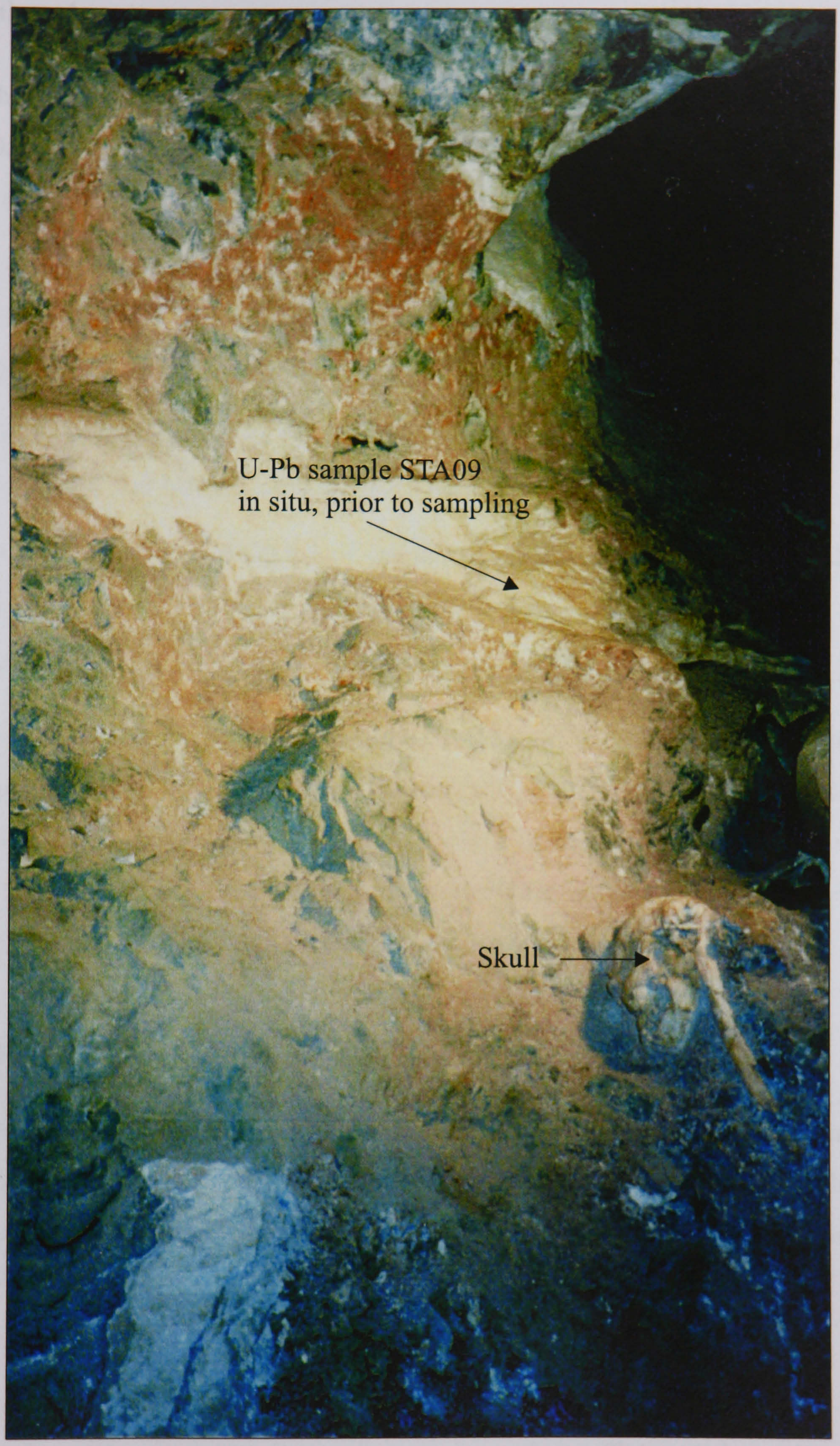

Figure 2.6: Photograph showing the member 2 deposits. The skull of StW 573 can be seen in the lower right of the picture, and a layer of flowstone (layer 2C) can be seen running through the deposit above and in the lower left of the picture. The position of the U-Pb sample STA09 in flowstone 2C is also shown. For further information on the stratigraphic relationships in this deposit see Figure (5.1) and Figure (6.1).

Member 4

Member 4 is subdivided into units A,B C and D and is found in an area of the cave known as the type site. The type site area can be seen in Figures (2.3) and (2.7) and has very little associated speleothem according to Brain (1958).

Unit A is 1-5m of red-brown breccia with chert and dolomite clasts, containing occasional bone fragments. It is believed that this resulted from a series of roof collapses.

Unit B is composed of up to 6.0m of mainly red-brown breccia with an abundance of large clasts and infrequent bone fragments.

Unit C is composed of 0.5-2.0m of yellow-red breccia containing occasional large clasts and bone fragments. It is found in pockets around unit B.

Unit D comprises horizontal white-brown laminations of recrystallised calcite lenses.

Member 4 has produced the majority of the faunal remains at Sterkfontein, including the hominid Mrs Ples, Sts 5, Figure (1.3). It is thought to be a debris cone that formed beneath a vertical shaft into which big cats dropped the bones from their kills as they ate them in the trees above (Clarke, 1994). Figure (2.7) shows the member 4 deposits from which Sts 5 was excavated.

Member 5

This member has been subject to several periods of collapse, erosion and infilling resulting in some vertical movement of the deposits (Clarke, 1994). The largest movements occurred in what is known as the swallow hole. Downwards movement of the sediments in this area is estimated at 5m. Despite this the sequence of layers has remained almost intact (Partridge and Watt, 1991).

Member 5 is divided into three units, A, B and C. Unit A is formed of 1-5m of red-brown calcite-veined breccia with many large clasts. This unit housed the skull of a *Homo habilis* (Clarke, 1994; Partridge, 2000).

Unit B is composed of dark red-brown poorly calcified breccia which is part of the swallow hole deposit. It has yielded numerous Oldowan artifacts and teeth of an

Figure 2.7: Photograph of Ron Clarke standing on the member 4 deposits in the type site area at Sterkfontein. The plaque in the background shows where the Sts 5 skull was recovered from.

Australopithecus robustus (Clarke, 1994; Partridge, 2000).

Yellow-red, well calcified breccia, makes up unit C. This unit produced a stone tool assemblage accepted to be Early Acheulean. The fragmentary hominid remains in unit C are thought to be those of *Homo ergaster* (Clarke, 1994).

Member 6

There is very little of this member remaining except for a few isolated pockets in solutional cavities in member 5 (Clarke, 1994; Partridge, 2000). Member 6 is subdivided into units A and B. Unit A comprises 25cm of contaminated, recrystallised basal calcite, with odd bone fragments. Unit B is a dark red-brown breccia with infrequent large clasts and some bone. The artifacts and faunal remains are believed to be Middle Stone Age.

2.2.4 Kromdraai B

Kromdraai is located on the southern side of the Bloubank valley about 1.5km east of Sterkfontein, see Figure (1.1) and Figure (2.2) (Partridge, 2000). It formed in an east-west orientated joint $\approx$ 46m long, in the Malmani Dolomite (Partridge, 1982; Partridge, 2000).

Kromdraai is spilt into two separate sites - Kromdraai A and Kromdraai B. Kromdraai A has so far produced only faunal remains, so was not analysed in this study. Kromdraai B, however, has produced hominid fossils along with an associated fauna.

The deposits of Kromdraai B take the form of a debris cone which formed beneath a shaft opening, around 12m from the eastern end of the cave (Partridge, 1982; Partridge, 2000). The height of the roof at that time is thought to have been at least 12m above the present surface elevation (Partridge, 1982; Partridge, 2000). Kromdraai B itself is further subdivided into the Kromdraai and Kromdraai West formations. The Kromdraai formation, from which the hominid remains were derived, is subdivided into 5 members. Figure (2.8) shows the two different formations and the member division. The following member descriptions apply to the

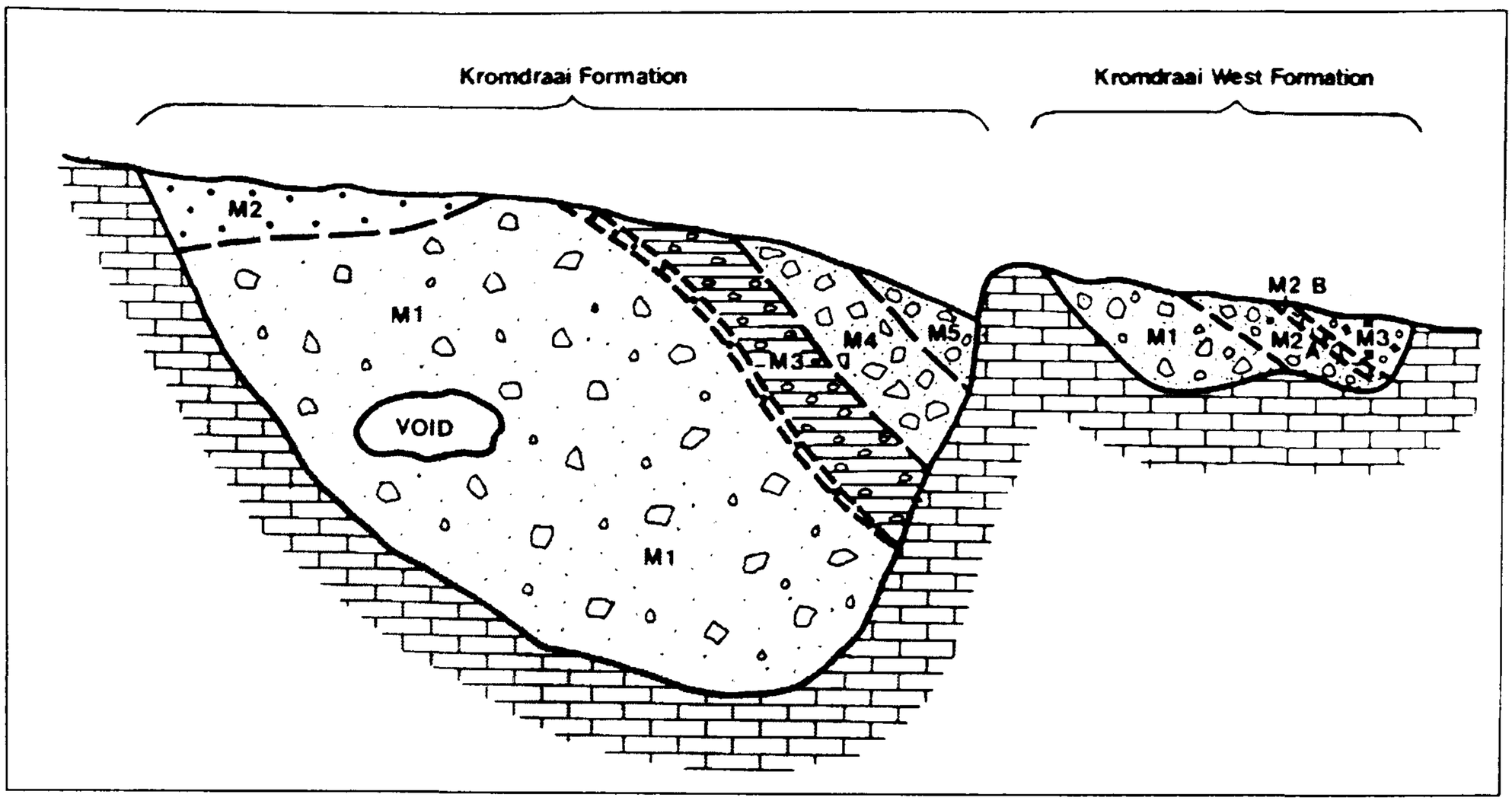

Figure 2.8: Cross-section through the Kromdraai B and Kromdraai B West formations. M1 = member 1, etc. Refer to Section (2.2.4) for full descriptions of each member deposit. From Partridge (1982).

Kromdraai formation and are taken from Partridge (1982) and Partridge (2000) unless specified otherwise.

Member 1

This deposit comprises up to 13m of red-brown breccia with abundant clasts but rare bone fragments. Most of the fauna derived from member 1 is microfauna, indicating that the opening to the surface was very small at this time and the cave was probably serving as an owl roost.

Member 2

Member 2 represents a period of slower sediment deposition. Consisting up to 2m of red-brown breccia with scattered clasts, it built up on the side of the debris cone formed by member 1. This member has yielded few bone fragments, not enough to be effectively analysed.

Figure 2.9: Photograph of Francis Thackeray behind a block of member 3 breccia (reddish deposits) from the Kromdraai B formation. The white deposit on top is a layer of flowstone and the grey blocks in the background are dolomite.

Member 3

Up to 4m of pale red-brown breccia makes up this member, which is preserved on the western side of the cone. It houses abundant weathered clasts and abundant bone fragments. At the base some speleothem growths can be observed interlayered with the breccia. Member 3 has yielded nearly all of the hominid fossils from Kromdraai B, including the type specimen[2] of *Australopithecus robustus*. The accumulation is interpreted as a "death-trap assemblage", much like that of member 2 at Sterkfontein, where animals fell in through the shaft entrance above. Figure (2.9) shows a block of member 3 breccia with a flowstone layer running through it.

Member 4

Member 4 comprises up to 3m of red-yellow breccia containing few bone remains. This deposit has been severely decalcified in certain areas.

[2]A type specimen is the specimen that was first assigned that particular species name.

Figure 2.10: View of Swartkrans hill from bottom of Bloubank river valley.

Member 5

Member 5 is found west of the member 4 outcrop and consists of up to 1m of red-brown breccia with abundant weathered clasts. This deposit contains few bones and occasional broken speleothems.

2.2.5 Swartkrans

Swartkrans is situated on the northern slope of the Bloubank valley on the opposite side to Sterkfontein, see Figure (1.1) and Figure (2.10). The two sites are less than a mile apart (Brain, 1958).

The dimensions of the cave are about $45m^2$ at the surface (Brain, 1995). Figure (2.11) gives an indication of the extent of the cave. The dolomite in which Swartkrans formed is extensively faulted and the cave has formed at an intersection of two fault lines (Brain and Watson, 1992). As with the other caves, Swartkrans is both a feature of solutional activity and subsidence, with the original solution cavern resulting in the subsidence cave seen today (Brain, 1958). An integral part of this was the removal of the roof over the outer part of the cave by erosion (Brain, 1958). The form of the cave and its deposits indicates that it has undergone repeated episodes of deposition and erosion (Brain and Watson, 1992). It

is thought that these correlate with interglacial-glacial cycles (Brain and Watson, 1992). Brain (1995) suggested that at the beginning of interglacials, when the vegetation cover was low but the precipitation levels were increasing, soil was washed into the cave in relatively large quantities. During drier glacial periods the amount of rainfall was too low to redeposit the soil in the cave, but it was high enough to result in periods of erosion (Partridge, 2000).

Brain (1958) and Brain and Watson (1992), divided the cave site into three parts; an inner cave in the north west corner, protected by a dolomite roof; an unroofed outer cave; and a lower cave that can be entered via an entrance from the inner cave, or via a shaft in the north east corner. The deposits are known as the Swartkrans formation and are divided into five members (Brain and Watson, 1992).

The following description of the Swartkrans formation is taken from Partridge (2000) unless indicated otherwise. Figure (2.12) shows how the cave deposits are thought to have formed.

Member 1

Member 1 is subdivided into units A-C.

Unit A is the basal flowstone which accumulated prior to an opening to the surface being established. The main flowstone layer at Swartkrans was deposited directly on to the dolomite floor, with the fossil rich breccia lying on top (Brain, 1958). The flowstone reached a maximum thickness of $\approx$ 8m (Brain, 1958).

The poorly calcified debris cone that is unit B entered the cave through a shaft opening post-formation of unit A. This deposit is known as the Lower Bank deposit and contains an abundant fauna including hominid remains, and an Oldowan stone tool assemblage.

Unit C is also known as the Hanging Remnant. This is a pale, red-brown breccia with many hominid remains, which are believed to be the result of carnivore activity. Together the deposits of the Hanging Remnant and the Lower Bank have produced the largest number of hominid remains so far (Brain and Watson, 1992).

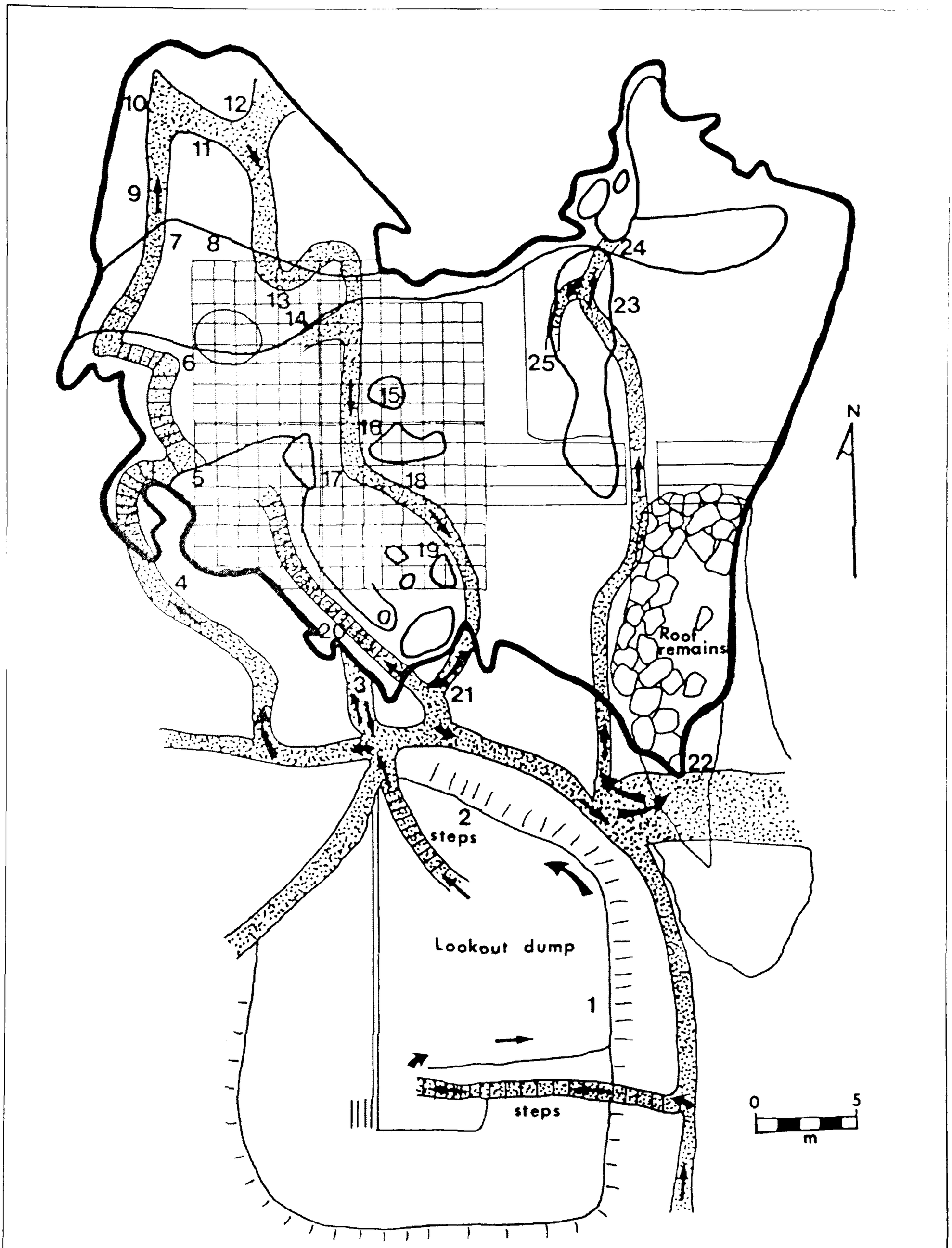

Figure 2.11: Plan of Swartkrans with the dark line showing the extent of the cave system. The grid represents the excavation grid in situ at Swartkrans. The numbers are tourist beacons painted on rocks. From Brain and Watson (1992).

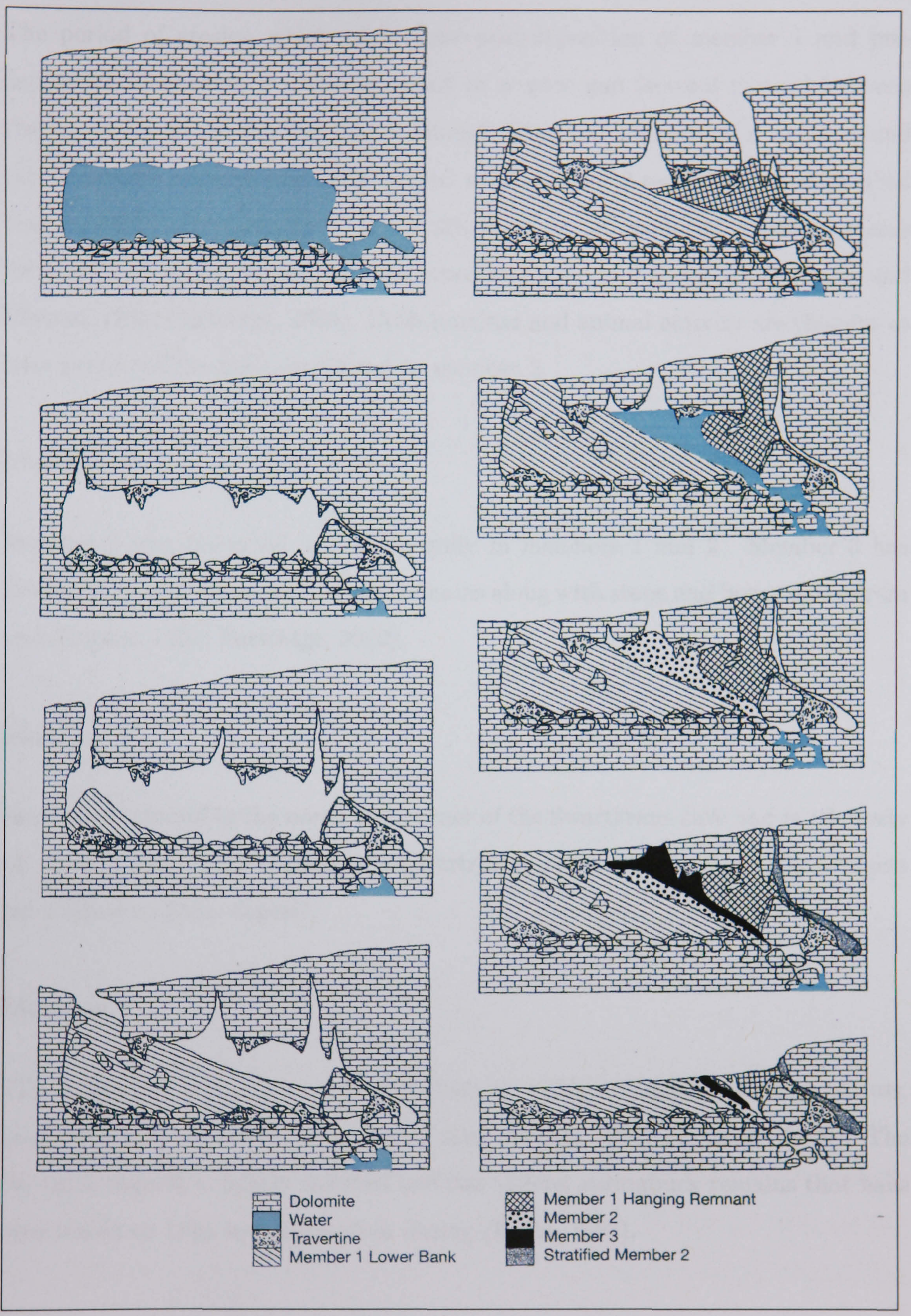

Figure 2.12: The stages in the evolution of the Swartkrans formation, showing the positions of members 1-3. Refer to Section (2.2.5) for full descriptions of each member deposit. From Partridge (2000), after Brain (1992) and Brain (1993).

Member 2

The period of erosion which took place post-deposition of member 1 and pre-deposition of member 2 is characterised by a wide gap (several metres) between the Lower Bank and the Hanging Remnant. This gap, along with a space behind the Hanging Remnant, was then infilled with member 2 red-brown. well calcified breccia. With a rich associated fauna this member has produced *Australopithecus robustus* and *Homo erectus* remains, stone and bone tool assemblages (Brain and Watson, 1992; Partridge, 2000). Both hominid and animal activity are thought to have produced the finds attributed to member 2.

Member 3

Member 3 was deposited in a steep gully in members 1 and 2. Member 3 has produced *Australopithecus robustus* remains along with stone and bone tools (Brain and Watson, 1992; Partridge, 2000).

Member 4

Member 4 is found in the north east corner of the Swartkrans cave and is relatively uncalcified (Brain and Watson, 1992; Partridge, 2000). Middle Stone Age artifacts are a feature of this deposit.

Member 5

This member is found in an erosional channel, which surrounds a stalagmite boss, near the north wall of the cave (Brain and Watson, 1992; Partridge, 2000). The 4m thick deposit is lightly calcified and has yielded springbuck remains that have been dated to 11 ka by radiocarbon dating (Brain, 1993).

Figure 2.13: View of the Makapansgat valley to the east of the Limeworks.

2.2.6 The Limeworks

Formation

The Limeworks at Makapansgat is found about 10 miles east of Makopane[3], whose grid reference is 24°10'S, 28°59'E, in the Limpopo Province[4], Figure (1.1).

Of the hominid caves this is the largest. The surface extent of the Limeworks is ≈ 200 × 115m with an average thickness of 20m (Partridge, 1979; Partridge, 2000), Figure (2.15). Columns of speleothem above the cone mouth indicate that the roof was considerably higher than the present surface (Latham *et al.*, 1999). The maximum height of the original roof is thought to have been ≈ 20m (Partridge, 1979; Latham *et al.*, 2003) to 50m (Partridge, 2000) above the present height.

The Limeworks developed in a slightly different environment to Sterkfontein, Swartkrans and Kromdraai, in that the karst at the Limeworks was mountainous rather than gently sloping (Latham *et al.*, 2003). Figures (2.13) and (2.14) show the Makapansgat valley looking out from the edge of the Limeworks cave. A solutional cave existed originally below the main cave and roof collapses into this space resulted in the formation of a large subsidence chamber above it (Brain, 1958). The devel-

[3]Formerly known as Potgietersrus

[4]Formally known as the Northern Province

Figure 2.14: View of the Makapansgat valley to the west of the Limeworks.

opment of very pure speleothems indicate that this did not lead to an immediate opening to the surface (Brain, 1958). The main period of speleothem deposition led to an arc of conjoined stalagmite bosses that divided the site into separate compartments. The Limeworks is now recognised to represent several repositories rather than one stratigraphically linked sequence (Latham *et al.*, 2003). When an opening to the surface did develop it remained small in comparison to the cave size allowing the slow accumulation of bone-rich breccias and contaminated speleothems (Brain, 1958). Early deposition was characterised by a shaft opening at the northern end of the site (Partridge, 2000). A sudden enlargement in the cave entrance resulted in the rapid accumulation of a large breccia deposit (Brain, 1958). Hiatuses in clastic deposition, sometimes followed by speleothem formation, indicate cycles of allogenic material entering the cave (Partridge, 1979). Figure (2.15) shows the plan of the cave as it is today.

The speleothem deposits in general, as at Swartkrans, lay below the main breccia directly on the dolomite floor (Brain, 1958). The cave contained a large amount of pure flowstone prior to the arrival of the limeminers. After this was removed a gap was left between the overlying breccia and the dolomite. In one area this has resulted in the collapse of less consolidated breccia known as the Collapse Cone (Brain, 1958).

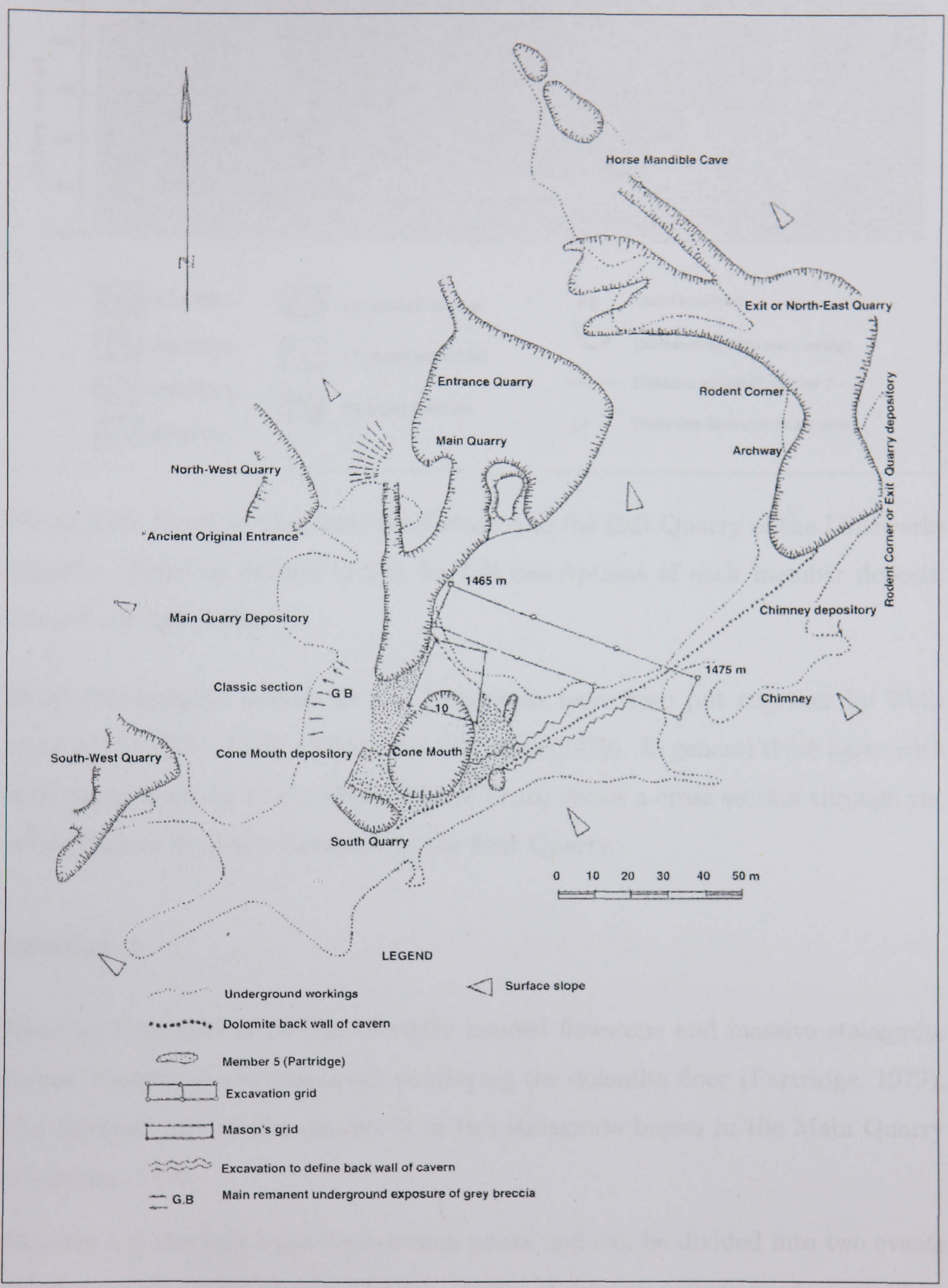

Figure 2.15: Plan of the Limeworks showing the extent of the cave system. From Latham *et al.* (2003), after Maguire *et al.* (1980)

.

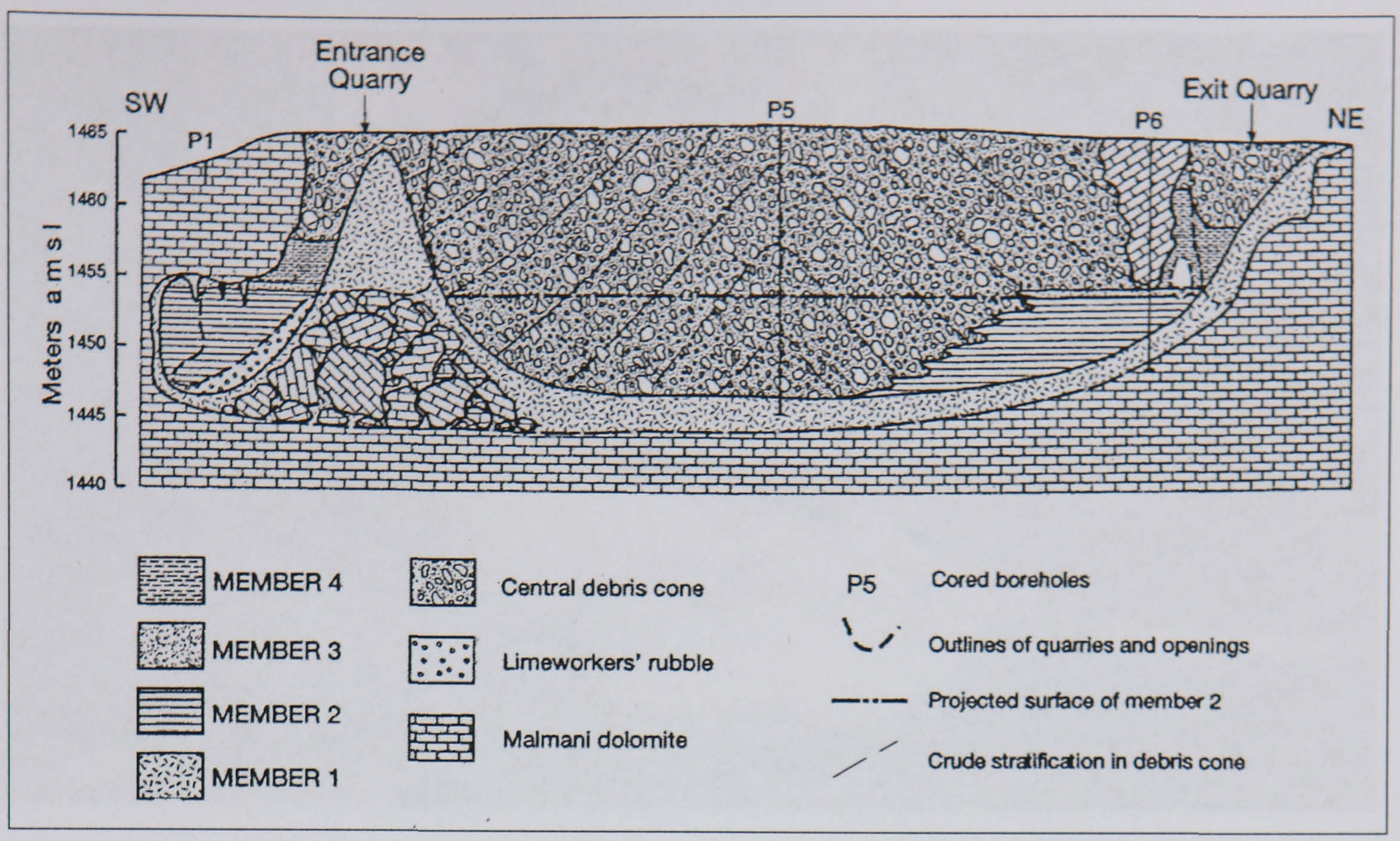

Figure 2.16: Cross-section from the Entrance to the Exit Quarry of the Limeworks deposits. Refer to Section (2.2.6) for full descriptions of each member deposit. From Partridge (2000).

Early stratigraphic models for the Limeworks have been put together by Wells and Cooke (1956), Brain (1958), and Partridge (1979). In general these agree with each other (Latham *et al.*, 1999). Figure (2.16) shows a cross section through the entire deposit from the Entrance to the Exit Quarry.

Member 1

Member 1 consists of to 15m of white banded flowstone and massive stalagmite bosses, sometimes contaminated, overlaying the dolomite floor (Partridge, 1979). The thickest part of this deposit is in two stalagmite bosses in the Main Quarry (Partridge, 1979).

Member 1 is the first large depositional phase and can be divided into two events (Latham *et al.*, 1999). Member 1A is a coating of subaqueously formed mammillary speleothem which extended across floors, walls and roofs (Latham *et al.*, 1999). Member 1B is the main subaerial flowstone deposit. This was a substantial deposit with two large speleothem bosses situated in the entrance and exit quarries, reaching in places up to 30m in height and width (Latham *et al.*, 2003). The Entrance

Figure 2.17: Photograph of Entrance Quarry looking into Main Quarry which was occupied by the arc of speleothem.

Quarry boss is thought to have been ≈ 15m high and 20m in diameter (Partridge, 2000). These existed as an arc in the shape of a horseshoe effectively dividing the cave into several closed compartments (Latham *et al.*, 1999; Partridge, 2000; Latham *et al.*, 2003). Figure (2.17) shows the Entrance Quarry (looking into the Main Quarry) at one end of the flowstone arc and Figure (2.18) the Exit Quarry at the other end of the arc.

Fine sediment contaminates this deposit in some localities, post-formation of member 1A (Latham *et al.*, 1999). Partridge (1979) suggests that at this time allogenic material was entering through a small opening in the northern end of the cave.

Member 2

Member 2 is a deposit of red-purple silts with a maximum thickness of 8m (Partridge, 2000; Latham *et al.*, 2003). Deposition seems to have occurred in an environment of fluctuating water levels (Partridge, 1979). Evidence of the recurrence of pooling and drying of water is left in the form of mud cracks and thin calcite deposits (Latham *et al.*, 1999).

Member 2 was deposited in two separate areas of the cave, which were divided by the stalagmite boss (Partridge, 1979). In the Entrance Quarry the fine deposits

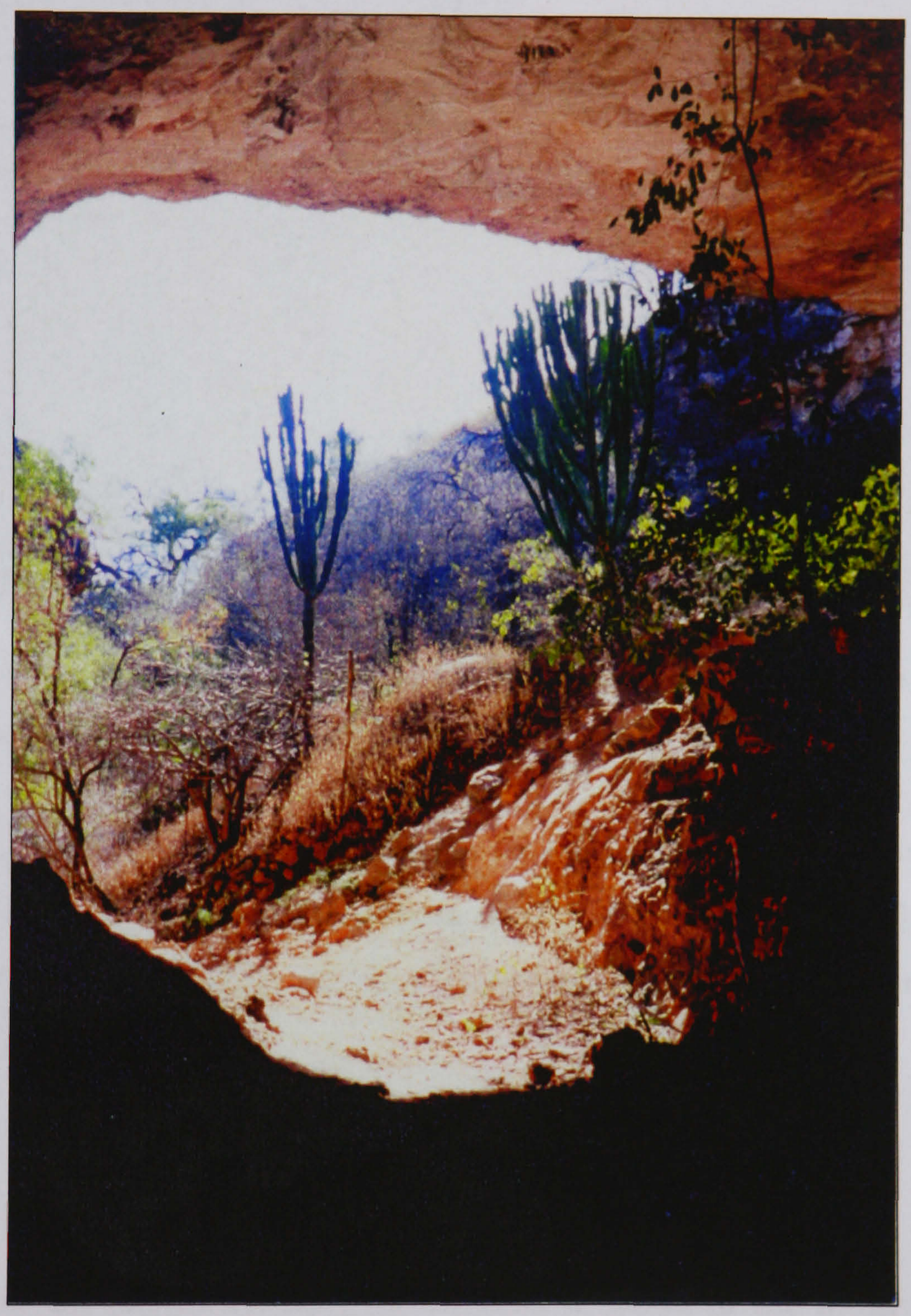

Figure 2.18: Photograph of opening into the Exit Quarry through which the arc of speleothem lay. The space represents, mostly, the quarried speleothem.

Figure 2.19: Photograph of member 3 in the Classic Section at the Limeworks. Member is found at same height as person's hand.

of member 2, containing fragments of bone and broken speleothem, are found against the member 1 flowstone (Latham *et al.*, 1999). In the Exit Quarry where the deposit formed separately, member 2 appears as 2m of red sediments (Latham *et al.*, 1999).

Member 3 or Grey bone-rich breccia

Member 3, better known as the Grey Breccia, is found in the Main Quarry and does not exist beyond the Cone deposit (Latham *et al.*, 1999). It consists of a contaminated flowstone containing abundant bone fragments, calcite growths and small clasts in a pale-brown matrix (Partridge, 1979). The thickness of this flowstone is $\approx$ 1m (Latham *et al.*, 1999; Maguire, 1980; Partridge, 2000) in the area of the cave known informally as the Classic Section, see Figure (2.19). It can been seen sandwiched between the overhang of the dolomite roof and the underlying member 2 sediments (Latham *et al.*, 1999; Latham *et al.*, 2003). The sediment that makes up the Classic Section entered the cave via an opening called

the Original Ancient Entrance (OAE) (Latham *et al.*, 2003).

The majority of the fauna found at the Limeworks derived from the grey bone-rich breccias of member 3, as found in the Classic Section. The faunal remains were mostly recovered from the limeworker's dumps but were correlated with the in situ deposits. The faunal remains are thought to be the result of hyena denning, where the bones rolled down a slope and were concentrated at the rear of the cave (Latham *et al.*, 1999; Partridge, 2000).

Member 4 and the Central Debris Pile

Member 4 is a coarse red-pink breccia that occupies the centre of the site. It contains dolomite and flowstone clasts of varying size (Latham *et al.*, 1999). This breccia represents a period when the cave opening had dramatically grown by roof collapse (Brain, 1958). It is the most extensive deposit covering 75% of the surface area of the site and reaching the present surface (Maguire, 1980). This member produced the only *Australopithecus africanus* not attributed to member 3 (Partridge, 2000).

Partridge (1979) split member 4 into Beds A and B. A is a pink-red breccia up to 2m thick found in the Entrance Quarry and in the Exit Quarry at Rodent Corner; although Latham *et al.* (2003) says that the deposits in the Exit Quarry can not be reliably related to the Entrance Quarry ones or assigned to the member system. A in the Entrance Quarry is similar to that at Rodent Corner but is more heavily calcified (Partridge, 2000). Rodent Corner is a dense accumulation of rodent bones in a fine matrix which mark the spot of an owl roost (Partridge, 1979). At Rodent Corner this deposit appears as red muds and sands (Latham *et al.*, 1999).

Bed B is also known as the Central Debris Pile (after Latham *et al.* (2003)) and is composed of up to 20m of red-brown breccia with abundant dolomite and sometimes chert clasts (Partridge, 1979; Maguire, 1980). The Central Debris Pile takes up the entire area in between the Entrance and Exit Quarries and inside the arc of speleothem (Latham *et al.*, 1999). Some in situ *Australopithecus africanus* fragments[5] have been retrieved from this deposit although this deposit is generally

[5]Specimens MLD 37/38

Figure 2.20: Photograph looking into the Original Ancient Entrance from the opening to the North-West Quarry.

lacking in fossil remains (Partridge, 2000).

Member 5

Member 5 is found around the edges of the collapsed cone at the southern end of the cave, where it reaches a thickness of ≈ 20m (Partridge, 2000; Partridge, 1979). This deposit is less well calcified and like member 4 extends to the present surface (Maguire, 1980). The Cone Mouth was created by a series of collapses after undermining of this member, resulting in a debris cone ≈ 15m high and 50m broad at its base (Maguire, 1980). The opening to daylight is ≈ 25m across, with surrounding deposits composed of speleothem, breccia and red sediment (Maguire, 1980; Latham *et al.*, 1999).

Original Ancient Entrance (OAE)

This is an artificially mined entrance but it was once part of a larger passage (Latham *et al.*, 2003), see Figure (2.20). A series of flowstones contaminated with red muds are found just inside the entrance. These lie between two subaqueous flowstone layers (Latham *et al.*, 2003). Further in, the horizontal red silt layers of member 2 have butted up against the huge flowstone boss which came in from the

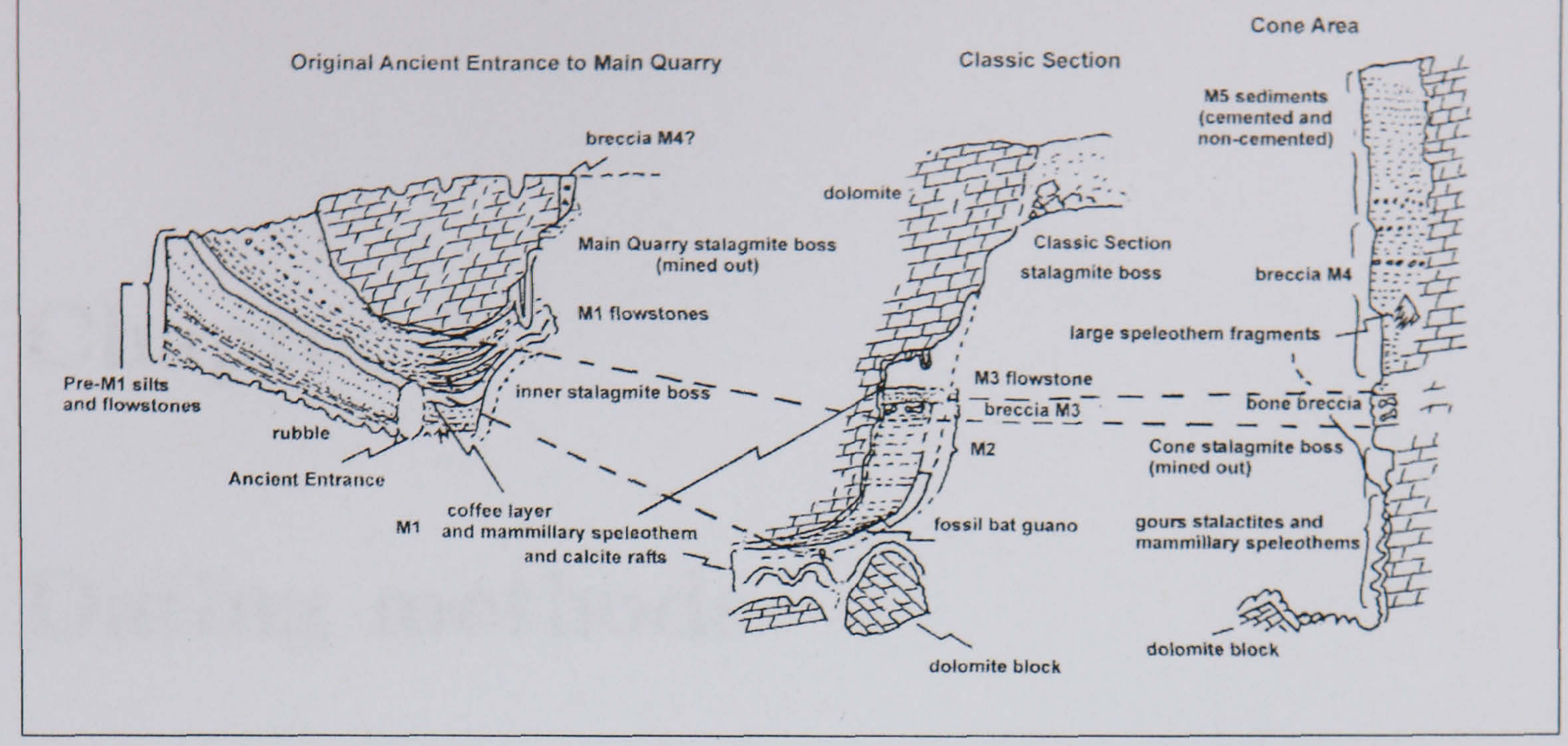

Figure 2.21: Schematic of the OAE, Classic Section and Cone area deposits showing how their stratigraphy is linked. From Latham *et al.* (2003).

Entrance Quarry above. This boss had formed according to Latham *et al.* (2003) prior to the subaqueous speleothem, although flowstones continued to form during the deposition of member 2 and can be seen interbedded with the red sediments (Latham *et al.*, 2003). The OAE still has an intact roof so this area was relatively well protected from the environment. Figure (2.21) shows how the deposits of the OAE are linked with those of the Cone and the Classic Section.

Chapter 3

Dating methods

The setting of the South African hominid sites has meant that they have not been as easy to date as their East African counterparts. East African sites are set in volcanic deposits and have been relatively easily dated using the K-Ar technique. Since this and other traditional radiogenic techniques are not applicable at the South African cave sites, other alternatives have had to be found. The techniques applied previously are discussed below.

3.1 Faunal dating

Faunal dating is a purely qualitative method that looks at the faunal assemblages within a deposit, and by comparing them to other confidently dated assemblages, attempts to estimate an age. This type of dating has been the most widely used at the hominid cave sites in South Africa.

Refer to Figure (3.1) for a diagrammatic representation of the following faunal evidence.

3.1.1 Faunal dating in the Bloubank and Makapansgat valleys

Two groups of fauna were initially distinguished in these regions (Tobias, 1973). The faunas of Sterkfontein and Makapansgat were assigned to an older group

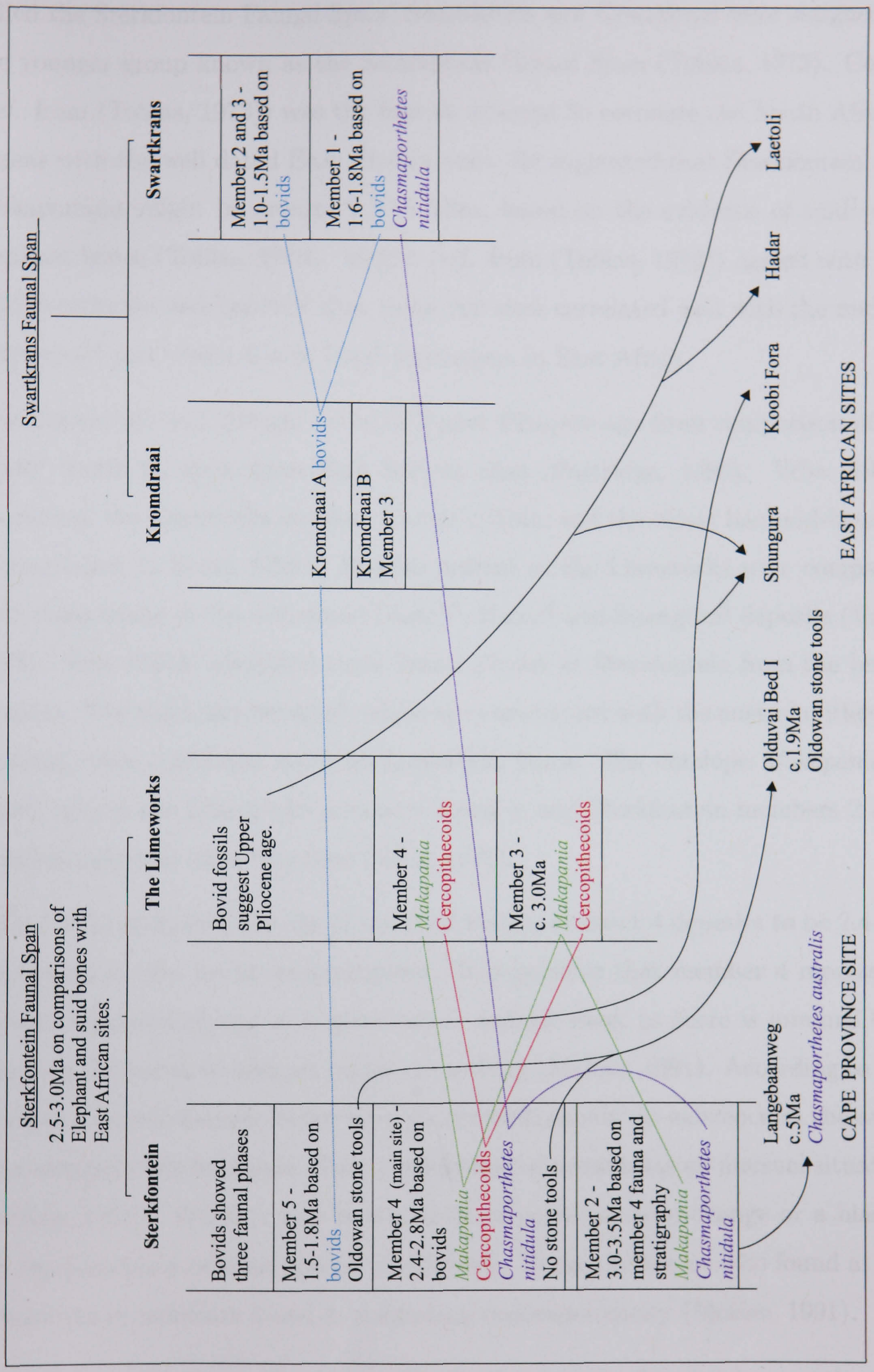

Figure 3.1: Diagram to show how the faunal evidence over the sequence of deposits at the South African cave sites is interpreted for the purpose of age determinations, and how it is linked across these sites and with other hominid sites in Africa. The arrows depict faunal correlations with other sites in Africa. The coloured lines link same species evidence at the four South African sites relevant to this study. Refer to Section (2.2) for geological descriptions of deposits at each site.

called the Sterkfontein Faunal Span. Swartkrans and Kromdraai were assigned to the younger group known as the Swartkrans Faunal Span (Tobias, 1973). Cooke (ref. from (Tobias, 1973)) was the first to attempt to correlate the South African faunas with the well dated East African ones. He suggested that Sterkfontein and Makapansgat might be around 2.5 to 3 Ma, based on the evidence of suid[1] and elephant bones (Tobias, 1973). Maglio (ref. from (Tobias, 1973)) agreed with the 2.5 Ma estimate and believed that these two sites correlated well with the middle Shungura[§2] and lowest Koobi Fora[§] formations in East Africa.

The Limeworks was thought to be of Upper Pliocene age from comparison of its bovid[3] fossils to those from East African sites (Partridge, 1986). Vrba (1985) considered the Limeworks member 3 to be *c.* 3 Ma, and the oldest hominid-bearing accumulation in South Africa. Species present at the Limeworks were compared with those found at the well dated Laetoli[§], Hadar[§] and Shungura[§] deposits (Vrba, 1985). Vrba (1974) identified three faunal phases at Sterkfontein from the bovid remains. The main site remains[4], which were associated with the australopithecine material, were correlated with the Limeworks fauna. The antelope *Makapania* is found only in the Limeworks members 3 and 4, and Sterkfontein members 2 and 4 and is unknown after this time (Vrba, 1985).

Vrba (1985) estimated the age of the Sterkfontein member 4 deposits to be 2.4-2.8 Ma, based on the bovid accumulations. It is possible that member 4 represents a death trap assemblage or a place where animals died, as there is minimal evidence on the bones to indicate carnivore activity (McKee, 1991). According to the member 4 faunal remains there were six cercopithecoids[5] in existence at the same time alongside the hominids. Such a saturation of primates is an unusual situation (McKee, 1991). Whether this is the result of environmental change or a bias in the representation of some species is unknown. These species are also found at the Limeworks in members 3 and 4, suggesting contemporaneity (McKee, 1991).

One of the main pieces of evidence for placing member 4 beyond a certain date

---

[1]Pigs.

[2]East African sites marked with an §.

[3]Family which includes cattle, sheep and antelopes.

[4]Known as STS = Sterkfontein type locality.

[5]Old world monkeys.

is the radiometric dating of Olduvai§ Bed I at *c.*1.9 Ma (Clarke, 2002b). Olduvai§ Bed I contains abundant Oldowan stone tools. These are not found at Sterkfontein until member 5 times. Therefore it seems reasonable to estimate that member 4 preceded Olduvai§ Bed I. Vrba (1982) estimated member 5 to be in the order of 1.5 to 1.8 Ma based on the bovid evidence. The bovids from the later faunal span[6] at Sterkfontein (equivalent to member 5) were linked to the Kromdraai A and Swartkrans fauna (Vrba, 1974).

Cooke considered Swartkrans to be as old as Olduvai§ Bed I (*c.* 1.9 Ma) at the very least (ref. from (Tobias, 1973)). From the bovid evidence at Swartkrans Vrba (1985) assigned a date of 1.6 to 1.8 Ma to Swartkrans member 1 and 1.0 to 1.5 Ma for members 2 and 3 (Vrba, 1982). Brain (1993) believes the Lower Bank deposit of member 1 at Swartkrans is at least 1.7 Ma. The Swartkrans member 1 fauna was originally considered to be older than that of Kromdraai (Tobias, 1973; Vrba, 1975). However following further research Vrba (1985) placed Kromdraai B member 3 in a time period just after Sterkfontein member 4 but before, and closer to, Swartkrans member 1. According to Partridge (1986) the dental morphology of the hominid fossils from Kromdraai B also suggests that they may be older than those from Swartkrans member 1.

3.1.2 Faunal dating of Sterkfontein member 2

The member 2 fauna is severely lacking in bovid fossils and so could not be dated in the same way as some of the other faunal assemblages. This provides a clue to how the Silberberg Grotto must have looked at the time and is indicative of how inaccessible the cave was during member 2 formation. The deposit appears biased towards animals which were relatively good climbers (primates and carnivores) even though these were not necessarily the most abundant creatures on the ground at that time (Pickering *et al.*, 2004). In addition to this the fauna is time-averaged and represents an evolving ecosystem over a considerable period of time (Pickering *et al.*, 2004). None of the fauna used to date the member 2 two deposits was actually near to the hominid skeleton StW 573. All of the fauna came from the eastern end of the member 2 deposit.

[6]Known as SE = West Pit of the Sterkfontein extension locality

The faunal dating of member 2 was based on two pieces of evidence; (i) the faunal dating of member 4 and the stratigraphic separation between these two units. (ii) the occurrence of a *Chasmaporthetes*[7] specimen.

The upper contact of member 4 is separated from member 2 by a 15m deep deposit. Partridge (in Clarke and Tobias 1995), estimates that member 3 alone would have taken between 0.3 Ma and 0.5 Ma to accumulate. Based on this Clarke and Tobias (1995) stated that member 2 could not be dated at less than 3.0 Ma and a preliminary age was given to member 2 of 3.0-3.5 Ma (Partridge, 2000). The *Chasmaporthetes nitidula* found in member 2 has also been used to infer an age for this deposit. Turner (1997) says that the teeth of this specimen are generally similar to the specimen found in member 4, but importantly he also draws a comparison between the dentition of the member 2 *C. nitidula* and that of a *C. australis* at the Cape Province site of Langebaanweg[8]. Langebaanweg was dated to *c.* 5 Ma but Turner (1997) stresses that it is not yet clear whether these two specimens are conspecific. There are only three such specimens within the Transvaal deposits that have been assigned to this genus that display the same dentition formation, the third of which was found in member 1 at Swartkrans. Due to its presence in both members 2 and 4 at Sterkfontein and at Swartkrans, Berger *et al.* (2002) do not think that this taxon is a sensitive chronological indicator.

Some researchers disagree with this dating method and these dates. McKee (1996) says that the dating of member 2 is "tenuous", as it assumes uniform sedimentation rates. McKee (1996) considers the member 2 fauna are suggestive of a more recent age and places member 2 just prior to member 4 and after the Limeworks. Berger *et al.* (2002) also do not agree with the current faunal dating of the deposits at Sterkfontein, citing the appearance of *Equus*[9] remains as evidence for the maximum age for the member 4 deposit[10] Berger *et al.* (2002) also claim that only 4 of the taxa assigned to member 4, all of which are endemic to South Africa, are not found in other late Pliocene or early Pleistocene sites such as Kromdraai or Swartkrans. The rest of the fauna, states Berger *et al.* (2002), almost completely overlaps with

[7]Hyena

[8]South African site.

[9]Horse

[10]Berger *et al.* (2002) say that *Equus* remains in Africa are unlikely to surpass an age of 2.36Ma.

supposedly younger sites. However it has been shown before that species can exist relatively unaltered for many thousands if not millions of years. Due to the wide temporal ranges of some of the member 4 species, whilst Berger *et al.* (2002) "tentatively support" the theory that Sterkfontein member 4 is older than the member 5, Swartkrans and Kromdraai deposits, they suggest a maximum age for member 4 of 2.5 Ma. In view of this Berger *et al.* (2002) then suggest that the minimum age for member 2 and StW 573 should then be set at 1.5 Ma and that the faunal evidence does not indicate an age in excess of 2.5 Ma.

Summary

Faunal dating has certainly been the most widely applied dating technique in the South African caves, but it is by no means ideal. Comparing fauna between South and East Africa is always going to have its difficulties. The climates are not exactly matched and the mode of fossil accumulation is completely different. The cave environments in South Africa have often been biased towards certain types of animals, just as they are today. Faunal assemblages may further be affected by factors such as preservational bias, predation or scavenging by carnivores, and the inclination of an animal to enter or climb into a cave (McKee, 1991). These factors mean that assemblages are difficult to compare to East African sites and may not even provide a true representation of the ecosystem that existed within the South African valleys.

3.2 Palaeomagnetic dating

The following theory of palaeomagnetic dating is taken from Verosub (2000).

Over time the earth's magnetic field fluctuates. During formation, magnetic grains in rocks and sediments, are magnetised parallel to the earth's magnetic field. These deposits then preserve a record of the direction of the magnetic field in which they formed. The largest variations in the magnetic field involve complete reversals in the polarity. These are known as polarity transitions. The field is termed normal when it is orientated in the same direction as the present day and reversed when it is orientated in the opposite direction. By measuring the shifts from normal

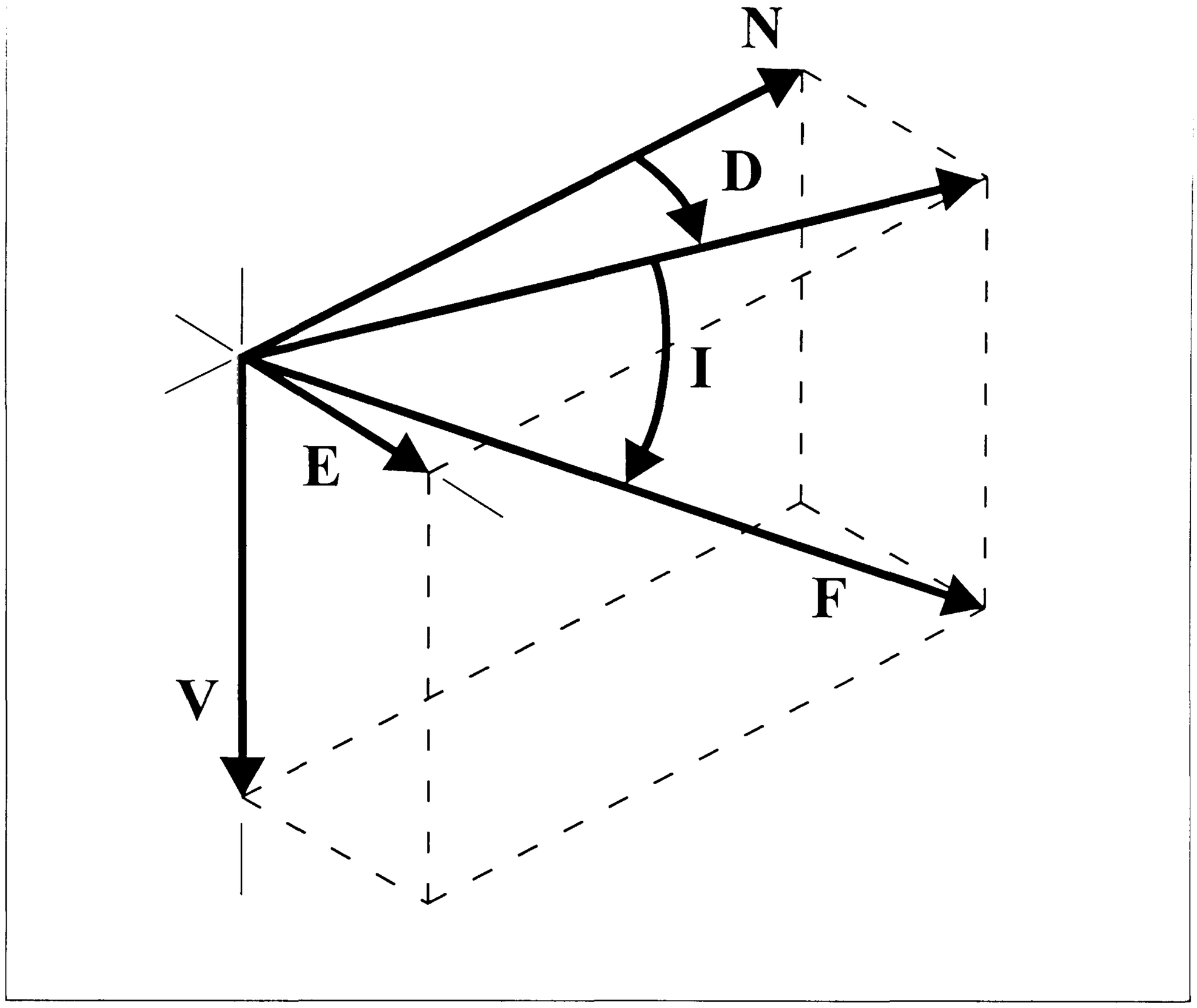

Figure 3.2: Schematic to show the relationship between the Intensity (F), the Inclination (I) and the Declination (D) - used to infer directions of polarity preserved during rock formation - with the cartesian components North (N), East (E) and Vertical (V). From Verosub (2000).

to reversed over a sedimentary deposit and correlating this with a known Global Polarity Timescale (GPTS), see Figure (3.3) a sequence of rocks can be dated.

The earth's magnetic field is a vector field and can be defined by Intensity (F), Inclination (I) and Declination (D), which are related to the cartesian components North (N), East (E) and Vertical (V), Figure (3.2). In a normal polarity field the inclinations are downward in the Northern hemisphere and upward in the Southern hemisphere. Declinations are usually northwards in both hemispheres. When the field is reversed the inclinations are upward in the Northern hemisphere and downward in the Southern hemisphere. The declinations are usually southwards in both hemispheres.

A normal or reversed polarity state can endure from 50,000 to millions of years and it takes a few thousand years to convert from normal to reversed or vice versa. The last full-scale polarity transition was 780,000 y ago. Figure (3.3) shows the GPTS for last 5.7 Ma.

Palaeomagnetic dating of sedimentary deposits is best applied to silts, siltstones, muds and mudstones; occasionally sands and sandstones. Limestones are usually weakly magnetised but are very reliable when magnetisation can be measured. In order to date the sequence it is necessary to have a prior estimate of the age, otherwise several possible correlations of polarity transitions to the GPTS could be made. A correlation between the pattern of the undated sequence and the GPTS can be made if you believe the sedimentation rate to be uniform. However this is often an inappropriate assumption. Correlation therefore usually requires tight biostratigraphic control or one well dated horizon. Better still would be the knowledge that the uppermost horizon is modern, of normal polarity and therefore represents the Bruhnes chron.

The issues for cave dating then are ones of poor magnetisation in limestones, growth hiatuses and physical movement of samples after magnetisation. A break in the sedimentary record could lead to misinterpretation of the palaeomagnetic sequence as could a sample which has been reorientated.

3.2.1 Palaeomagnetic dating at Sterkfontein

At Sterkfontein palaeomagnetic dating was applied across the sequence from member 1 to member 6 by Jones *et al.* (1986). The samples were often found to be unstably or intermediately magnetised, and this was put down to a high level of disturbance during deposition, i.e. collapse of cave roofs, walls or collapse of sediments into lower chambers (Jones *et al.*, 1986). Samples from the top of the sequence, members 5 and 6 were very "confused" and were not considered when dating the deposits. Overall the remainder of samples seemed to have been formed during a normal polarity event, excepting a couple of reversed periods at the top of members 2 and 3. The trouble with such normally magnetised samples is that it is sometimes not clear whether this is a relict of their formation, or remagnetisation by a modern magnetic field. Members 2, 3 and 4 were assigned to the Gauss

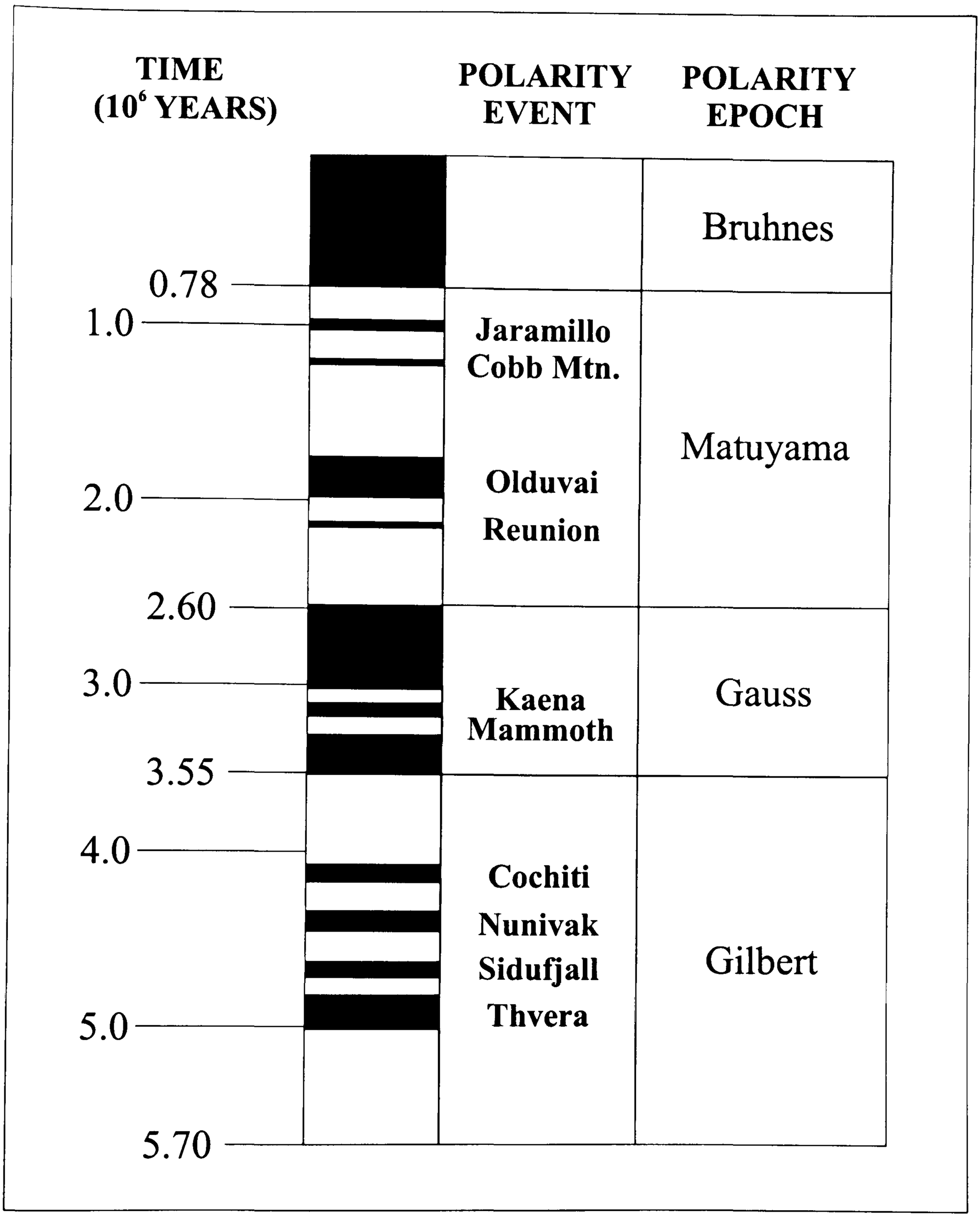

Figure 3.3: Global Polarity Timescale (GPTS) for the last 5.7 Ma. The black bands represent periods where the field was of normal polarity and the white bands when it was reversed. The Gauss epoch, for example, was generally a normal polarity epoch with two reversed events, the Kaena and the Mammoth. From Verosub (2000).

normal epoch which stretches from 2.58 to 3.58 Ma[11], with two alterative interpretations of the positioning of the reversals. These results seemed consistent with the faunal interpretation and revealed that Sterkfontein was probably younger than the Limeworks member 3. Nonetheless Jones *et al.* (1986) recommended further palaeomagnetic work at Sterkfontein in order to achieve a "less shadowy result."

A study by Partridge *et al.* (1999) built on the work done by Jones *et al.* (1986). Instead of using breccia, which does not appear to preserve a stable magnetic signal, Partridge *et al.* (1999) used member 2 flowstone horizons which are interbedded with the StW 573 bearing breccia within the Silberberg Grotto. According to the faunal evidence, see Section (3.1.2), the limits for the member 2 sequence were set at 2.7 Ma and 4.0 Ma. A total of five magnetic reversals were identified within the sequence. Following correlation of the observed polarity with the GPTS of Cande and Kent (1995) the hominid was placed between 3.22 and 3.58 Ma. By interpolating sedimentation rates and assuming uniform deposition in the different flowstone layers this age was refined to 3.30 to 3.33 Ma for StW 573. See interpretation A in Figure (3.4)

The negative aspects of the Partridge *et al.* (1999) study are that a complete stratigraphic sequence is not represented as the interlayered breccias have been ignored; the law of superposition is assumed to apply; and assumptions have been made about the rate of sedimentation. There is also the possibility of magnetic remanence caused by drilling of the samples (Partridge *et al.*, 2000).

Following doubts regarding the faunal dating of members 2 and 4, see Section (3.1.2), Berger *et al.* (2002) have produced an alternative interpretation of the palaeomagnetic data, Figure (3.4). If this hypothesis is indeed true this would give the hominid StW 573 an age of between 2.15 and 3.04 Ma (Berger *et al.*, 2002). Berger *et al.* (2002) present several other interpretations of the palaeomagnetic data and conclude that StW 573 is not older than 3.04 Ma and could be as young as 1.07 to 1.95 Ma.

[11] Dates of Gauss normal epoch at time of publication were 2.48 to 3.4 Ma.

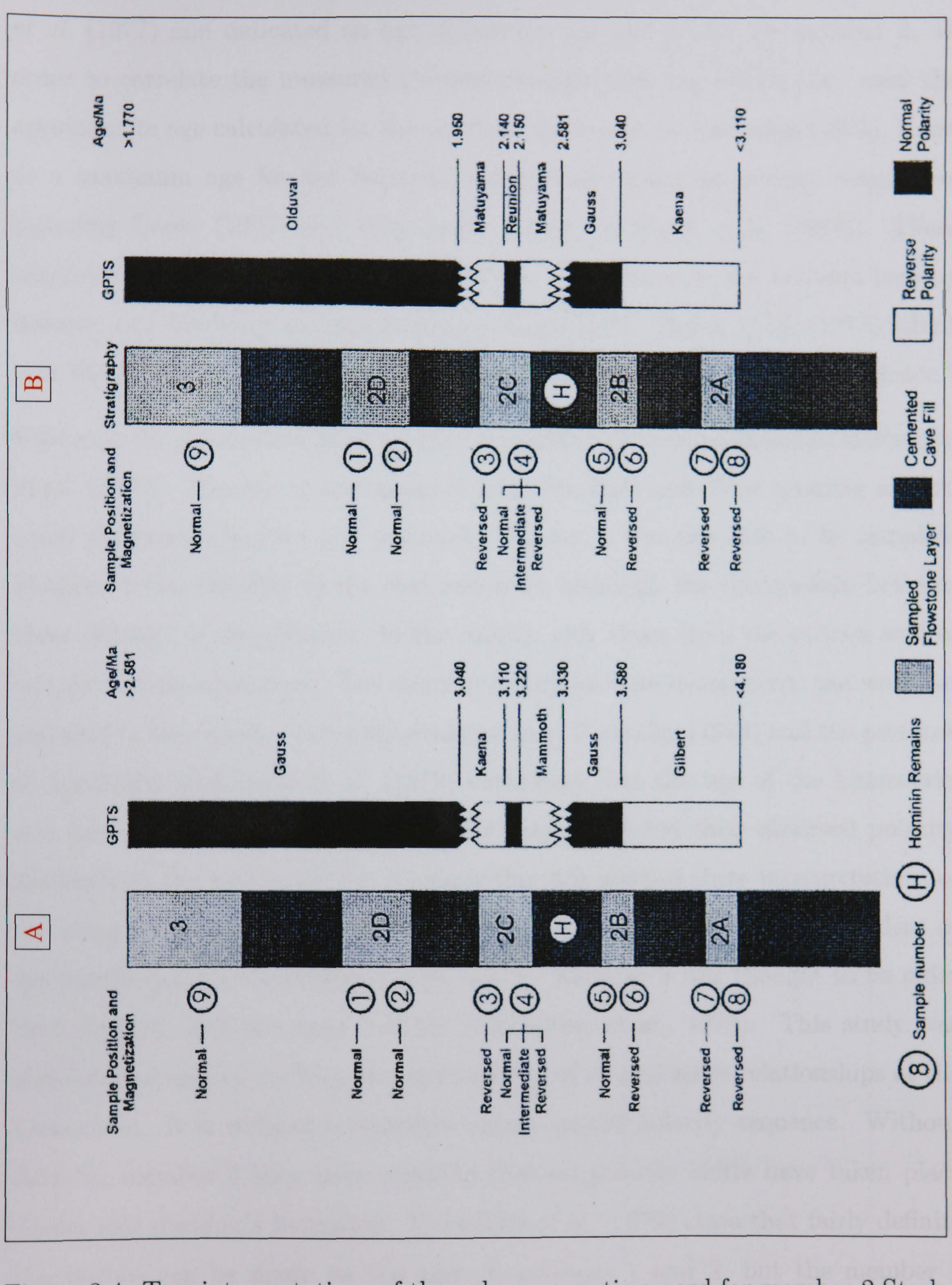

Figure 3.4: Two interpretations of the palaeomagnetic record for member 2 Sterkfontein using the GPTS. Interpretation A is from Partridge *et al.* (1999). Interpretation B is from Berger *et al.* (2002). Figure from Berger *et al.* (2002).

3.2.2 Palaeomagnetic dating at the Limeworks

Preliminary palaeomagnetic studies were undertaken at the Limeworks by Brock *et al.* (1977) and indicated an age of between 2.8 and 3.3 Ma for member 2. In order to correlate the measured polarity changes with the GPTS they used the approximate age calculated for the opening of the cave by Partridge (1973). (used as a maximum age for the deposits) and faunal dating by various researchers including Cooke (1970) and Vrba (pers. comm. in Brock *et al.* (1977)). These suggested an age of between 2.5 and 3.0 Ma for member 3, the hominid-bearing breccia, and therefore an approximate younger limit. Brock *et al.* (1977) admit that their date "depends heavily upon the limits provided by the other evidence."

Following the preliminary work a more extensive study was published in McFadden *et al.* (1979). Member 2 was sampled from the East and West quarries and an equal sedimentation rate was assumed. Member 3 was not able to be sampled. Member 4 was sampled in the east and west, although the relationship between these deposits is complicated. In the results, only those from the eastern wall of member 4 were considered. The member 5 samples were inconsistent and were not included in the results. Using the evidence from Partridge (1973) and the presence of hominids, McFadden *et al.* (1979) concluded that the age of the Limeworks was less than 5 Ma. From this evidence they correlated their observed polarity timescale to the known GPTS. However this still allowed three interpretations of the observed polarity changes. These interpretations were made independent of the faunal evidence (McFadden *et al.*, 1979). Member 3 was thought to be older than 2.90 Ma, but less than 3.32 Ma (McFadden *et al.*, 1979). This study was criticised because of the lack of understanding of stratigraphic relationships at the Limeworks. It is without a complete uninterrupted polarity sequence. Without data for member 3 they have assumed that no polarity shifts have taken place during this member's formation. McFadden *et al.* (1979) state that fairly definite conclusions can be made on the ages of members 1 and 2, but the member 1 samples had a weak magnetic signal and in order to make this assumption they have assumed that the geomorphological date is accurate. The GPTS has also been updated since this paper was published.

Subsequently Partridge *et al.* (2000) took cores of sediment for palaeomagnetic

analysis through the entire thickness of the Limeworks deposit. It was found that the drilling sometimes affected the magnetic signal. Additional difficulties included an absence of horizontal orientation, and in some cases multiple samples from the same stratigraphic horizon showed differing directions of magnetisation (Partridge *et al.*, 2000). The data from this study were thought to be of poor quality and half the data set had to be discarded (Partridge *et al.*, 2000).

The most recent palaeomagnetic work at the Limeworks was based on a complete stratigraphic sequence and found eight reversals over the depth of the deposit (Herries and Latham, 2002). Against the GPTS the most probable age span for the sequence is thought to be from 2.0 to 4.0 Ma. Further to this, the date for the sequence has been refined to between 2.1 and 4.29 Ma, with the *A. africanus* remains from member 3 being between 2.58 and 3.04 Ma (Herries, 2003).

3.2.3 Palaeomagnetic dating at Kromdraai B

The first palaeomagnetic study at Kromdraai B was that of Jones *et al.* (1986). The samples indicated a mostly reversed polarity. By comparing the result to the faunal estimates of Vrba (1981), they were able to place the Kromdraai B deposit within the Matuyama reversed epoch, between 0.73 Ma and 2.48 Ma. In spite of the trend of the magnetic field towards a reversed state, the results were not unequivocal. Jones *et al.* (1986) believe that "further study is likely to prove unprofitable" as Kromdraai B has few sedimentary remains, suffers from modification by the subsidence of cave walls and roofs, and is characteristic of a magnetic field in a wholly reversed state.

The recent palaeomagnetic work at Kromdraai B by Thackeray *et al.* (2002) seems to have been more successful. This used flowstones and calcified sediments as opposed to the breccias used by Jones *et al.* (1986). Through faunal correlations with East African sites, the Kromdraai B deposits are thought to be between 1.5 and 2.0 Ma. Samples KBM 7 and 8, which came from a flowstone layer that overlies the grey breccia associated with the hominids, were thought to relate to a reversed polarity event *c.* 2.0 Ma. Normally magnetised samples KBM 3, 4, 5 and 6 were placed in the following Olduvai interval of 1.95 to 1.77 Ma. From these, the hominid TM 1517 was inferred as being associated with a period of deposition

which correlates with the beginning of the Olduvai Event, *c.* 1.9 Ma.

3.2.4 Palaeomagnetic dating at Swartkrans

The preliminary palaeomagnetic studies by Brock *et al.* (1977) at Swartkrans, showed that the polarity of the samples was often unstable. Accordingly, it was felt that the results were not chronologically meaningful. No further palaeomagnetic studies have been carried out here.

3.3 Electron Spin Resonance (ESR) dating

ESR dating is a radiogenic method that can be applied to a wide range of insulating solids, varying in age from a few thousand to a few million years (Schwarcz and Lee, 2000). Unpaired electrons form in crystals that are exposed to ionising radiation (Grün *et al.*, 1987). These pairs can then be detected by an ESR spectrometer, which exposes the samples to a fixed microwave frequency while holding them in a varying magnetic field (Schwarcz and Lee, 2000). The amount of energy absorbed is a measure of the number of trapped charges. The intensity of the ESR signal increases as the sample is exposed to more irradiation over time (Schwarcz and Lee, 2000). Where the dose rate (grays per annum) is constant the age may be calculated by the formula;

$$\text{Age} = \text{accumulated dose} \,/\, \text{dose rate} \tag{3.1}$$

Where accumulated dose is the radiation received by the sample since it formed, and dose rate is the rate at which the sample was irradiated by radioactive elements (Grün *et al.*, 1987). Dose rate is made up of two constituents, the internal dose and the external dose. In some samples, such as quartz, the internal dose is negligible due to the lack of radioactive components in the material (Schwarcz and Lee, 2000). It becomes problematic when dealing with samples such as carbonates, which commonly contain initial amounts of U, or teeth, which have a tendency to uptake U after burial. Both of these affect the dose rate. The age can be corrected for U uptake by considering two possible uptake models; linear uptake (LU), where U was integrated at a constant rate; or early uptake (EU), where U was acquired

soon after burial. Disequilibrium within the U-series decay chain can cause further problems, and the dose rates of the ^{238}U decay must be corrected where this is found (Grün *et al.*, 1987). Events such as heating, stress or recrystallisation, also limit the applicability of ESR, as they can reset the signal to zero (Grün *et al.*, 1987).

3.3.1 ESR dating in South Africa

In South Africa, teeth from bovids and hominids were sampled for ESR dating. Within these it is the mineral hydroxyapatite[12] that is subject to alteration by radiation. Tooth enamel, as opposed to dentine or cement, is the favoured material because; (i) it has the largest crystals (leaving it less susceptible to recrystallisation and therefore resetting of the ESR signal), (ii) it is the least likely to uptake U as it ages, and (iii) the ESR signal appears to remain stable even when samples are exposed to light or erosion (Grün *et al.*, 1987).

3.3.2 ESR dating at Sterkfontein

An ESR study by Schwarcz *et al.* (1994) focused on bovid tooth enamel as a means of dating the member 4 deposits at Sterkfontein. The tooth enamel was exposed to radiation doses from internal and external U sources. These doses are in part controlled by the U uptake history of the tooth. Schwarcz *et al.* (1994) calculated both EU and LU ages. The samples were taken from random positions within member 4. Separations between the stratigraphic units within this member are difficult to differentiate, which made the samples difficult to compare (Schwarcz *et al.*, 1994). The spread in age across the results appeared greater than those expected for routine experimental errors, and Schwarcz *et al.* (1994) believe this to be the result of varying dose rate within the deposits, which they did not account for. It is also possible that diagenetic activity may have partially reset the ESR signal in the enamel of the teeth (Schwarcz *et al.*, 1994). Schwarcz *et al.* (1994) found the average ages of member 4 were;

EU = 1.36 ± 0.30 Ma; LU = 2.08 ± 0.46 Ma.

[12] $Ca_{10}(PO_4)_6(OH)_2$

3.3.3 ESR dating at Swartkrans

The hominid SKW11, assigned to *Australopithecus robustus* (Grine. 1993) was excavated from the Hanging Remnant, member 1. Curnoe *et al.* (2001) applied ESR dating to teeth from bovids and the hominid, SKW11, at Swartkrans. Four bovid teeth were sampled in total. Two of these were believed to be from the Hanging Remnant and two from member 2, although the exact provenance of the bovid teeth was unknown (Curnoe *et al.*, 2001). Because it is important to be able to estimate the external dose rate from in-situ sediments, this could lessen the credibility of the results. The location of the hominid sample SKW11, was much better known. A piece of enamel was selected from the SKW11 tooth for analysis by the non-destructive ESR technique suggested by Grün (1995). However this meant that the U content of the sample could not be measured. The fragments were composed of both enamel and dentine (Curnoe *et al.*, 2001). The bovid teeth were analysed using conventional ESR procedures (Curnoe *et al.*, 2001). Combining ESR with U-Series, the study produced "reasonable" results for these deposits. The best age estimate for the Hanging Remnant was 1630 ± 160 ka with a maximum age of 2110 ± 210 ka (Curnoe *et al.*, 2001).

3.3.4 ESR dating at Kromdraai B

A single bovid tooth from a block of breccia known to post-date the layer of flowstone dated by palaeomagnetic analyses, Section (3.2.3), was subjected to ESR dating by Curnoe *et al.* (2002). Weighted average dates were achieved of 568 ± 27 ka for an EU model and 814 ± 32 ka for a LU model.

3.4 Cosmogenic burial dating

The following description of cosmogenic burial dating is from Granger *et al.* (1997) and Granger *et al.* (2001) unless stated otherwise.

Cosmogenic burial dating is based on the decay of the cosmogenic nuclides ^{26}Al and ^{10}Be in quartz grains. In caves where deposits in the range of 0.3 to 5 Ma have been buried and shielded from cosmic rays this technique can be applied.

At the ground's surface the cosmogenic nuclides ^{26}Al and ^{10}Be are produced in quartz by reactions with secondary cosmic ray neutrons and muons. When the quartz grains are subsequently buried, the production of these cosmogenic nuclides dramatically decreases or ceases altogether. As the radionuclides decay at different rates the ratio of ^{26}Al/^{10}Be lowers over time, and this can be used to infer the time elapsed since the rock was buried.

In order to determine burial age the ratio of ^{26}Al/^{10}Be prior to burial must be calculated. This is estimated by assuming a uniform erosion rate for the exposed surface rock;

$$\left(\frac{N_{26}}{N_{10}}\right)_0 = \frac{P_{26}\left(\frac{1}{\tau_{10}} + \frac{E}{\Lambda}\right)}{P_{10}\left(\frac{1}{\tau_{26}} + \frac{E}{\Lambda}\right)} \tag{3.2}$$

Where N_{26}, N_{10}, P_{26}, and P_{10} are the concentrations and production rates of ^{26}Al and ^{10}Be; E is the erosion rate; Λ is the cosmic ray penetration depth[13]; τ_{26} and τ_{10} are the radioactive meanlifes of ^{26}Al and ^{10}Be[14]

Concentrations of ^{26}Al and ^{10}Be in buried deposits depend on two unknowns; burial time and preburial concentrations. Production rates are assumed to be constant since any variations in production rates affect the two isotopes the same and should have little effect on the ratio. Such variations may however have an effect on the erosion rate estimation.

After production has ceased, the radionuclides will decay according to the following equation;

$$N_i = (N_i)_0 e^{-t_{\text{burial}}/\tau_i} \tag{3.3}$$

Where N_i is the concentration of either ^{26}Al or ^{10}Be, $(N_i)_0$ is the concentration of either initially, τ_i is the radioactive meanlife of either ^{26}Al or ^{10}Be, and t is time since burial. ^{26}Al decays faster than ^{10}Be so over time the ratio decreases exponentially;

$$\frac{N_{26}}{N_{10}} = \left(\frac{N_{26}}{N_{10}}\right)_0 e^{-t_{\text{burial}}(1/\tau_{26} - 1/\tau_{10})} \tag{3.4}$$

---

[13] 60cm in a rock of density 2.6g cm^{-3}

[14] $\tau_{26} = 1.02 \pm 0.04$my; $\tau_{10} = 2.18 \pm 0.09$my

Granger *et al.* (1997) solved these equations iteratively. One iteration involves inputting a guess for the erosion rate into Equation (3.2), then solving Equation (3.4) for t_{burial} before solving Equations (3.3) for initial concentrations of ^{26}Al and ^{10}Be. The resulting initial concentrations can be divided to give a new value for the initial ratio, $\left(\frac{N_{26}}{N_{10}}\right)_0$. This can be input back into Equation (3.2) to obtain a new estimate of the erosion rate. This process is repeated until convergence is achieved, i.e. the difference between consecutive erosion rates is negligible. The first iteration is different to subsequent iterations as it assumes a value for E rather than $\left(\frac{N_{26}}{N_{10}}\right)_0$[15].

These equations can be used to calculate pre-burial erosion rates and estimate burial times where the following conditions are satisfied; (i) initial ^{26}Al and ^{10}Be in sample were not subject to previous burial. This technique makes the assumption that the sediment was not buried before it was deposited in its current position in the cave. If it had been buried for a significant period of time prior to this then the burial time would be overestimated. Errors associated with prior burial or departure from a steady erosion state are estimated by calculating the burial age of modern surface sediment - this should be indistinguishable from zero - and by replicate analyses of different but related samples from one or more sites. Although replicate samples may have varying ^{26}Al and ^{10}Be concentrations they should still have the same burial age; (ii) the sediment was buried quickly (with respect to radioactive decay and total burial time); (iii) sediment was buried deep enough so production of cosmogenic radionuclides ceased - for age errors of $\leq 10\%$, sediment buried for 4 my would need to have been buried at a depth of > 26m. Production of nuclides after burial will increase ages with increasing burial time and pre-burial erosion rate, and decrease ages with increasing burial depth.

Overall errors on ages are reported in two ways. Initial errors reflect analytical uncertainty only. When comparing burial dates between specimens this error is sufficient. The second error represents parenthetical uncertainty and encompasses

[15]This is the method of calculation assumed from the information given in Granger *et al.* (1997) although the method in the paper is slightly unclear. Granger *et al.* (2001) and Partridge *et al.* (2003) use the same equations but do not mention iteration.

Sample	Location	Depth (m)	Burial age (Ma)†	Burial age (Ma)‡	Burial age (Ma)§
Upper	0.8m above StW 573	24	4.72 ± 1.08	4.26 ± 1.08	4.09 ± 1.08
Middle	Adjacent to StW 573	25	4.17 ± 0.35	3.88 ± 0.35	3.57 ± 0.35
Lower	0.7m below StW 573	26	3.78 ± 0.44	3.56 ± 0.44	3.19 ± 0.44
Surface		0	0.01 ± 0.14	N/A	0.03 ± 0.14

Table 3.1: Table of results of cosmogenic burial dating, member 2 Sterkfontein. † = Calculated burial age following all corrections; ‡ = burial age if effect of muon activity were ignored; § = burial age if alternative ^{10}Be meanlife were applied. Uncertainties on burial ages are total uncertainties.

the systematic errors in radioactive decay rates, production rates, and uncertainty in the Be ratio in the spike. These total uncertainties are applicable when trying to calculate a calendar age.

3.4.1 Cosmogenic dating of StW 573

Prior to the application of this technique at Sterkfontein, cosmogenic burial dating had only been applied twice previously; refer to Granger *et al.* (1997) and Granger *et al.* (2001). The following information regarding the cosmogenic work done at Sterkfontein is taken from Partridge *et al.* (2003), and the online supporting material for this paper, unless otherwise indicated.

Three samples were collected from the member 2 calcified breccia near to the StW 573 skeleton. These were between 24 and 26m below the surface. The burial ages were found to agree within analytical uncertainty. Table (3.1) shows the results for the three different layers and their connected errors. Also included is a surface sample which was taken to test for a modern day burial age of zero. Partridge *et al.* (2003) state that these results indicate that the previous palaeomagnetic results sequence was placed two reversals too young.

Some criticism has been directed at the Partridge *et al.* (2003) paper. Gibbons (2003) writes that many researchers are wary of these results as Sterkfontein has a complicated stratigraphy, with collapsed ceilings and open shafts which may

have allowed mixing of sediment. In response to this Clarke *et al.* (2003) state that the Sterkfontein stratigraphy is not in fact particularly complex and that the overall cave stratigraphy is not important in the validation of these results. However there certainly seems to be a real possibility that the sediments used for cosmogenic studies may have originated in caves now extinct, where collapse or subsidence moved sediments into other chambers. In both Partridge (1978) and Partridge and Watt (1991) the modification of the sedimentary sequence at Sterkfontein by subsidence into underlying cavities is discussed. In such a case the sediments would have already been buried for hundreds of thousands, perhaps millions of years, before they became part of the breccia into which StW 573 was cemented.

The depth at which these samples were collected is not beyond the penetrating influence of muons according to Partridge *et al.* (2003). For an accurate age to be calculated the effect of muons must also be considered. Partridge *et al.* (2003) made the assumption that the quartz tested, originated in a landscape experiencing steady state erosion. This allowed for calculation of a correction for the effect of muon activity on the age. This correction however is only applicable if the samples were exposed to a constant amount of muon activity since they formed. Most of the hominid caves in South Africa had roofs that were considerably higher than the present day land surface, so it is possible that their present elevation is the closest to the surface these samples have been in a long time. Below such depths as these they would not experience enough muon activity to justify correction. If the effect of muons was ignored then the burial dates would decrease, as shown in Table (3.1).

Further to this there is some debate as to the meanlife which has been assumed for ^{10}Be. The meanlife of ^{10}Be used by Partridge *et al.* (2003) of $\tau_{10} = 1.93 \pm 0.10$ is 14% lower than that previously accepted by many researchers. Using the previously accepted meanlife of $\tau_{10} = 2.18 \pm 0.09$ would reduce the calculated burial ages by roughly this percentage too, see Table (3.1).

In view of these issues it is suggested in Gibbons (2003) that this method should be tested on a South African cave with a known chronology, and over a sequence of sediments to confirm that ages increase in the correct direction. This seems a

sensible idea, in that it would ascertain whether this technique is really suitable for these deposits, and it would give future results more grounding.

Chapter 4

Radiogenic Isotope Dating

4.1 The laws of radioactive decay

In 1902 Rutherford and Soddy performed a series of experiments that enabled them to explain the radioactive decay process. They concluded that radioactive decay is a spontaneous process whereby atoms of a certain element decay to atoms of another element, and the rate of this decay is directly related to the number of atoms present (Faure, 1986). The following equations describe the basics of radioactive decay and growth. Sections (4.1.1) to (4.1.4) are based on Faure (1986), except where specified.

4.1.1 Decay of parent to a stable daughter

If we consider firstly the decay of an unstable parent nuclide to a stable daughter. The parent nuclide will decay at a rate that is proportional to the number of atoms, N, present at time, t;

$$-\frac{dN}{dt} \propto N \tag{4.1}$$

Where $-dN/dt$ is the rate of change of parent atoms (this is negative because the rate decreases over time). Since each radionuclide decays at a different rate a proportionality constant, λ, is introduced, that is particular to the radionuclide in question. This represents the probability that an atom will decay within a certain

unit of time. Therefore;

$$-\frac{dN}{dt} = \lambda N \tag{4.2}$$

By integrating and assuming that $N = N_0$ at $t = 0$ the number of parent atoms remaining at any time t can be calculated;

$$N = N_0 e^{-\lambda t} \tag{4.3}$$

Where there are no daughter atoms present initially, $D_0 = 0$, the number of daughter atoms, D^*, at time t can be calculated;

$$D^* = N_0 - N \tag{4.4}$$

Therefore;

$$D^* = N_0(1 - e^{-\lambda t}) \tag{4.5}$$

Where D^* is the number is stable daughter atoms produced by the decay of a radiogenic parent whose abundance was N_0 at $t = 0$.

When $D_0 \neq 0$, and since it is more useful to relate the number of daughters at time t to the number of parents remaining at that time (because the parents abundance can be measured), it is necessary to further manipulate this equation. From Equation (4.3);

$$N_0 = Ne^{\lambda t} \tag{4.6}$$

Substituting this into Equation (4.4);

$$D^* = N(e^{\lambda t} - 1) \tag{4.7}$$

The total number of daughter atoms at time t can then be given as;

$$D = D_0 + N(e^{\lambda t} - 1) \tag{4.8}$$

This equation is the basis of geochronological dating.

4.1.2 Half life

The rate of decay of a radionuclide can also be expressed in terms of its half life, $t_{1/2}$. This is the time required for half of the number of atoms to decay. When $t = t_{1/2}$, then $N/N_0 = \frac{1}{2}$. Substituting these into Equation (4.3) it is found that;

$$t_{1/2} = \frac{\ln 2}{\lambda} = \frac{0.693}{\lambda} \tag{4.9}$$

4.1.3 Decay series

Among naturally occurring U and Th species it is common to find that the daughter product is itself radioactive and is subject to decay. Bateman (1910) wrote a solution to a system of differential equations that allowed the above calculations to be extended to calculate the number of atoms of any radionuclide within a decay series. For example, the rate of decay of the daughter nuclide, N_2, is found by calculating the difference between the rate at which the parent, N_1, decays to produce the daughter, and the rate at which it decays itself;

$$\frac{dN_2}{dt} = \lambda_1 N_1 - \lambda_2 N_2 \tag{4.10}$$

Where N_1 and N_2 are the numbers of atoms at any time, t, and λ_1 and λ_2 their respective decay constants. Combined, Equations (4.3) and (4.10) yield;

$$\frac{dN_2}{dt} + \lambda_2 N_2 - \lambda_1 N_1^0 e^{\lambda_1 t} = 0 \tag{4.11}$$

The solution to this equation is given by

$$N_2 = \frac{\lambda_1}{\lambda_2 - \lambda_1} N_1^0 (e^{-\lambda_1 t} - e^{-\lambda_2 t}) + N_2^0 e^{-\lambda_2 t} \tag{4.12}$$

The first set of terms describe the growth and decay of daughter atoms that originated from the parent. The second term describes the contribution of any daughter atoms present initially (Faure, 1986; Friedlander *et al.*, 1981). Using the Bateman equations it is possible to solve firstly for a series of successive decays where the assumption is made that at $t = 0$, $N_2^0 = N_3^0 = \cdots N_n^0 = 0$, resulting in (Faure, 1986; Friedlander *et al.*, 1981);

$$N_n = C_1 e^{-\lambda_1 t} + C_2 e^{-\lambda_2 t} + \cdots C_n e^{-\lambda_n t} \tag{4.13}$$

Where;

$$C_1 = \frac{\lambda_1 \lambda_2 \cdots \lambda_{n-1}}{(\lambda_2 - \lambda_1)(\lambda_3 - \lambda_1) \cdots (\lambda_n - \lambda_1)} N_1^0. \tag{4.14}$$

$$C_2 = \frac{\lambda_1 \lambda_2 \cdots \lambda_{n-1}}{(\lambda_1 - \lambda_2)(\lambda_3 - \lambda_2) \cdots (\lambda_n - \lambda_2)} N_1^0, \text{etc} \ldots \tag{4.15}$$

Where $N_2^0, N_3^0 \ldots N_n^0 \neq 0$, a Bateman solution for N_n in an $(N-1)$-membered series can be added where the first daughter acts as the parent and at $t = 0, N_2 = N_2^0$ and so on for further members of the decay series (Friedlander *et al.*, 1981).

4.1.4 Secular equilibrium

In a decay series where the parent isotope is much longer lived than its daughters, ie. $\lambda_1 \ll \lambda_2, \lambda_3 \cdots \lambda_n$, the decay of all daughters will be limited by the decay rate of the parent. In time, a state of equilibrium is reached where the decay rate (also known as the activity) of each daughter equals that of the parent nuclide. This is also true for the rate of growth of the stable daughter product (Dickin, 1997);

$$\text{Activity} = \lambda_0 N_0 = \lambda_1 N_1 = \lambda_2 N_2 = \lambda_n N_n \tag{4.16}$$

This is known as Secular Equilibrium. Where only the parent nuclide is present initially the number of radiogenic daughters that form from its decay can be treated as the number of stable daughter atoms;

$$D^* = N_1(e^{\lambda_1 t} - 1) \tag{4.17}$$

Isotope	Half-life($t_{1/2}$, y)	Decay Constant(λ, y^{-1})
^{238}U	4.47×10^9	1.55125×10^{-10}
^{235}U	0.704×10^9	9.8485×10^{-10}
^{232}Th	14.01×10^9	4.9475×10^{-11}

Table 4.1: Half-lives and Decay Constants of Parent U and Th isotopes. Steiger and Jäger (1977).

4.2 Uranium- Thorium-Lead methods of dating

These methods of radiogenic dating are based on the decay of ^{238}U,^{235}U and ^{232}Th to stable isotopes of Pb.

The actinides U and Th generally have a low abundance in the solar system but are enriched in rocks such as granites, shales, sandstones and carbonates. U and Th both exist in several oxidation states on the surface of the earth. U is generally found in the 6+ state and Th only in the 4+ state. There are three naturally occurring isotopes of U - ^{234}U, ^{235}U and ^{238}U - all of which are radioactive. Th is present primarily as ^{232}Th, with five other isotopes acting as intermediate daughters within the ^{238}U, ^{235}U and ^{232}Th decay chains. Of the four stable isotopes of Pb, three are the end daughter products of the ^{238}U, ^{235}U and ^{232}Th decay chains. The fourth one, ^{204}Pb, is the only non-radiogenic Pb isotope occurring naturally.

The half-lives of all three of these parent isotopes are large relative to their daughters meaning secular equilibrium can be readily achieved by each decay series. The half-lives of ^{238}U and ^{232}Th are comparable with the age of the earth, and the age of the universe, respectively. ^{235}U, however, has a much shorter half-life, meaning that most primordial ^{235}U has by now decayed to ^{207}Pb. See Table (4.1).

Ages can be calculated from these radioactive systems by two methods; (i) decrease in concentration of a radionuclide from an initial amount, or build-up of a stable daughter product (U-Pb or Th-Pb dating); (ii) measurement of return to secular equilibrium within a decay series following a disturbance (U-series disequilibrium dating).

Criteria which must be satisfied for these techniques to be employed are;

1. Concentrations of parent and daughter nuclides must be sufficiently high that they can be accurately measured.

2. The decay constants must be accurately known. These were agreed by the IUGS Subcommission on Geochronology in 1977 (Steiger and Jäger, 1977).

3. The sample being analysed must be representative of the rock being dated.

4. The system must have been closed to parent or daughter nuclides since formation, or perturbation in the case of disequilibrium dating.

5. Daughter products have not have been present initially or amounts present must be accounted for.

Where these are all taken into account the three decay series should give a concordant age.

4.2.1 Uranium-series disequilibrium dating

Geological processes such as weathering, transportation and deposition often result in elemental and isotopic fractionation of nuclides (Ku, 1976). As a result of this, U and Th decay chains in newly formed deposits are often in disequilibrium. This can be used to date a deposit by taking advantage of the relationship between U and Th and their relatively short-lived radiogenic daughters.

U-series disequilibrium dating falls into two categories; daughter excess methods; daughter deficiency methods. Reviews of these methods have been covered most recently by Bourdon *et al.* (2003). These methods have proved useful for dating Pleistocene carbonates, and more importantly for dating or improving understanding of dating speleothem and hominid remains.

Daughter excess methods

Daughter excess methods are applicable when a deposit is formed with an excess of a daughter product which can not be supported by the decay of its parent. Providing the initial excess is known, samples can be dated by measuring the degree of excess remaining, as the system returns to secular equilibrium.

An example of this is the ^{234}U-^{238}U method. ^{234}U is formed by the rapid decay of two intermediate daughters from ^{238}U. The nature of these decay processes mean that ^{234}U may be more easily removed from the crystal lattice, or may exist in the more soluble 6+ valency (Ku, 1976). Both result in the fractionation of U and ^{234}U/^{238}U activity ratios larger than unity in natural waters. The ^{234}U-^{238}U technique can date deposits back to *c.* 1.5 Ma depending on the initial ^{234}U excess (Gascoyne *et al.*, 1978). The general equation applied is;

$$[(^{234}\mathrm{U}/^{238}\mathrm{U}) - 1] = [(^{234}\mathrm{U}/^{238}\mathrm{U})_0 - 1]e^{-\lambda_{234}t} \quad (4.18)$$

Where ^{234}U/^{238}U and ^{234}U/^{238}U$_0$ are the current and initial activity ratios respectively.

Daughter deficiency methods

Daughter deficiency methods can be used where a parent nuclide is incorporated during the formation of a deposit but the daughter nuclide is not. The age is determined by measuring the growth of the daughter towards secular equilibrium. This could span up to seven of the daughter's half-lives.

The ^{230}Th-^{234}U method is possible because of the fractionation of U and Th in the hydrosphere. In oxidising environments U exists as the highly soluble UO_2^{2+} ion, whereas Th remains in the insoluble tetravalent state. Th is almost exclusively adsorbed onto sediment grains as soon as it is formed, leaving groundwater depleted. When deposits form from this groundwater, appreciable U is co-precipitated. The deposit will however be essentially free of initial Th. The ingrowth of ^{230}Th towards secular equilibrium can then be used as a dating tool. This method along with the corresponding nuclides from the ^{235}U decay chain (^{231}Pa-^{235}U dating) can be successfully applied to freshwater carbonates such as speleothems up to *c.* 0.4 Ma. Such an age limit was possible with the improvement of mass spectrometry for this technique. Taking into account the disequilibrium of ^{234}U/^{238}U in natural waters the ^{230}Th-^{234}U relationship can be defined as;

$$^{230}\mathrm{Th}/^{234}\mathrm{U} = \frac{1 - e^{-\lambda_{230}t}}{^{234}\mathrm{U}/^{238}\mathrm{U}} + \frac{\lambda_{230}}{\lambda_{230} - \lambda_{234}}\left[1 - \frac{1}{^{234}\mathrm{U}/^{238}\mathrm{U}}\right]\left(1 - e^{-(\lambda_{230} - \lambda_{234})t}\right) \quad (4.19)$$

Where $^{230}\mathrm{Th}/^{234}\mathrm{U}$ and $^{234}\mathrm{U}/^{238}\mathrm{U}$ are the current activity ratios.

Dating speleothem with uranium-series techniques

The concentration of U in speleothems is dependant on the U content of the overlying bedrock and the duration that the groundwater is in contact with this bedrock. U concentrations in speleothem are known to be diverse both spatially and temporally, and have been found to vary from < 0.01 ppm to > 90 ppm (Thompson *et al.*, 1975b; Gascoyne *et al.*, 1978).

The most successful U-series dating technique, as far as speleothems are concerned, is ^{230}Th-^{234}U. This technique requires that all ^{230}Th within the speleothem is the result of ^{238}U and ^{234}U decay. If the speleothem contains any detrital material such as sand or clay particles this may not necessarily be the case. Where large ^{232}Th signals appear on a spectrum it can be assumed that some detrital material was incorporated in the deposit. A correction must then be made to account for the non-authigenic ^{230}Th. This is not a simple correction as the $^{230}\mathrm{Th}/^{232}\mathrm{Th}$ ratio in sediments varies.

^{234}U-^{238}U disequilibrium has been used to date speleothems beyond the range of ^{230}Th dates. In this case it is critical to know the initial $^{234}\mathrm{U}/^{238}\mathrm{U}$ activity ratio. Estimating such initial ratios has proven to be extremely difficult. This problem can be overcome where there is an overlap between the ^{234}U-^{238}U range and the ^{230}Th-^{234}U range. If a stalagmite can be reliably dated by ^{230}Th-^{234}U and over that time range display relatively constant $^{234}\mathrm{U}/^{238}\mathrm{U}$ activities then these activities can be assumed to be true for older sections of the same stalagmite (Gascoyne *et al.*, 1978). Thompson *et al.* (1975b) found that although initial $^{234}\mathrm{U}/^{238}\mathrm{U}$ ratios differed between stalagmites they were fairly constant throughout the individual stalagmite.

Initial $^{234}\mathrm{U}/^{238}\mathrm{U}$ activities are also important considerations for U-Pb dating of

speleothems and will be discussed further in Section (4.2.3).

Dating hominid deposits

Caves and their deposits act as traps for sediment and archaeological materials. Deposits that can be related to archaeological remains are ideal for use as a dating tool. U-series can provide useful *ante* or *post quem* dates for remains which lie in between two speleothem layers (Schwarcz and Blackwell, 1992). In such circumstances it is vital to have an understanding of the stratigraphy of the surrounding deposits.

U-series techniques have been used successfully to date speleothem deposits which are related to hominids, for example, the dating of Nanjing Man (Zhao *et al.*, 2001). Unfortunately it is rare to find datable calcite alongside hominid remains (Pike and Pettitt, 2003). Hominids generally only resided in the outermost chambers of cave systems where the speleothems formed are more likely to contain detrital material. In such cases care must be taken to sample clean speleothem, in order to avoid erroneous ^{230}Th-^{234}U dates. A good review of this and other archaeological applications of U-series is provided by Schwarcz and Blackwell (1992).

Primary archaeological deposits such as bones and teeth have also been subjected to U-series techniques, but there are often problems with these materials. Bones and teeth are open-systems, meaning U can move in or out. They contain relatively high amounts of U, but most of this appears to accumulate after death. Living bone contains only a few ppb of U, whereas fossil bone can contain 1-100 ppm (Pike and Pettitt, 2003). There have been new developments in this field, such as modelling U uptake and distribution, or combining U-series with techniques such as ESR. A good review of these is provided by Pike and Pettitt (2003). Despite this the technique is still in its infancy. Zhao *et al.* (2001) confirmed the merits of speleothem and the limitations of teeth and bones when using this method. Ages from the teeth and bones came out significantly younger than those from the speleothem, suggesting that the U uptake by such artifacts was far more complex than present modelling could predict (Zhao *et al.*, 2001).

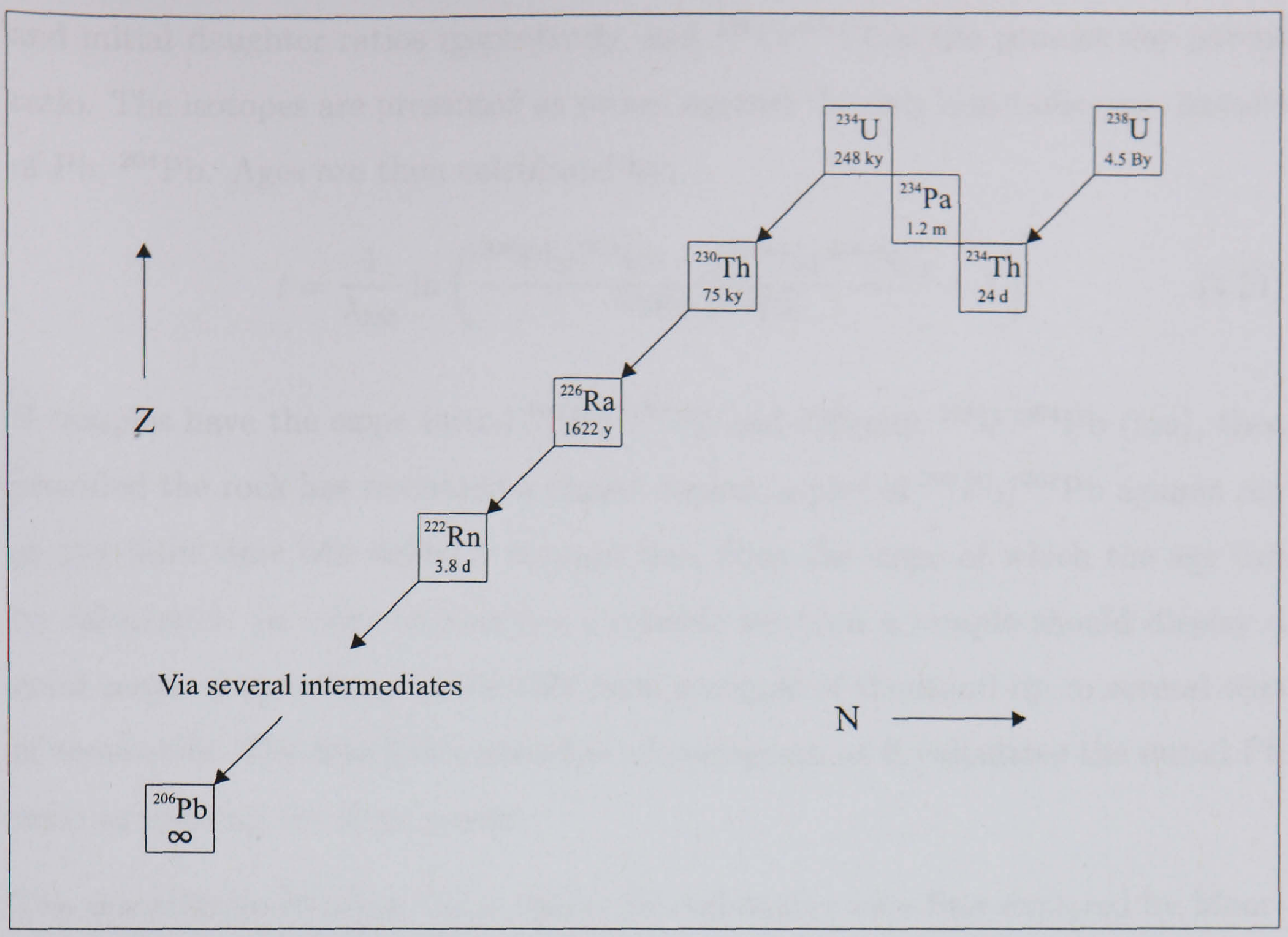

Figure 4.1: ^{238}U decay chain showing important nuclides and their half-lives. After Dickin, 1997. Where N = Neutron No. and Z = Proton No.

In terms of the South African cave deposits the age ranges of U-series techniques were the limiting factor. Despite the lack of absolute dates the current chronological evidence showed that the caves were all likely to be older than 1 Ma, and Sterkfontein and the Limeworks considerably older than this. However, one of the younger hominid bearing caves, Gladysvale, has been successfully dated by ^{230}Th-^{234}U methods (Pickering, 2004).

4.2.2 Uranium-Lead dating of young carbonates

Figure (4.1) shows the main isotopes of interest in the ^{238}U decay chain. Where a decay chain is considered to be in secular equilibrium initially, the intermediate daughters can be eliminated from age calculations and the parent can be considered as having decayed directly to its stable daughter;

$$\frac{^{206}\mathrm{Pb}}{^{204}\mathrm{Pb}} = \left(\frac{^{206}\mathrm{Pb}}{^{204}\mathrm{Pb}}\right)_i + \frac{^{238}\mathrm{Pb}}{^{204}\mathrm{Pb}}(e^{\lambda_{238}t} - 1) \tag{4.20}$$

As per Equation (4.8), where ^{206}Pb/^{204}Pb and $(^{206}\mathrm{Pb}/^{204}\mathrm{Pb})_i$ are the present day

and initial daughter ratios respectively, and $^{238}U/^{204}Pb$ is the present day parent ratio. The isotopes are presented as ratios, against the only non-radiogenic isotope of Pb, ^{204}Pb. Ages are then calculated by;

$$t = \frac{1}{\lambda_{238}} \ln \left(\frac{^{206}Pb/^{204}Pb - (^{206}Pb/^{204}Pb)_i}{^{238}Pb/^{204}Pb} + 1 \right) \tag{4.21}$$

If samples have the same initial $^{206}Pb/^{204}Pb$ and different $^{238}U/^{204}Pb$ (mu), then provided the rock has remained a closed system, a plot of $^{206}Pb/^{204}Pb$ against mu at any later time will define a straight line, from the slope of which the age can be calculated. In order to produce a reliable isochron a sample should display a good range of mu values, preferably from a couple of thousand up to several tens of thousands. The isochron method is advantageous as it calculates the initial Pb ratio in plotting the data points.

The possibilities of using U-Pb dating on carbonates were first explored by Moorbath *et al.* (1987). They used a Pb-Pb isochron to date the Mushandike stromatolitic limestones of Zimbabwe. Following on from this Smith and Farquhar (1989) used a ^{238}U-^{206}Pb isochron to date marine carbonates, Israelson *et al.* (1996) dated calcite concretions and Rasbury *et al.* (1997) paleosol calcite. It was thought that U-Pb dating could not be applied to rocks less than a few million years old due to the long half-lives of the parent isotopes and the tiny amounts of Pb that accumulate from this decay. Carbonates however, may have low Pb contents coupled with relatively high U contents. This results in a range of U-Pb ratios and measurable changes in the growth of radiogenic end daughter products (Richards *et al.*, 1998). A general review of Pb-Pb and U-Pb geochronology is provided by Jahn and Cuvellier (1994).

4.2.3 Uranium-Lead dating of South African flowstones

Previous work

This study follows on from the U-Pb dating of speleothem from Winnats Head Cave in the Peak District by Richards *et al.* (1998). They achieved ^{238}U-^{206}Pb dates within error of an α-spectrometric U-Th age, for deposits of *c.* 250 ka. Richards

et al. (1998) reported U concentrations of up to 37.1 μg g^{-1} and Pb concentrations as low as 2.3ng g^{-1}. Mu values for the same samples ranged from 700 to 1,141,000.

Initial work done at Sterkfontein on flowstone layer 2C of member 2. see Figure (5.1), revealed promising results. An age of 3.04 ± 0.08 Ma was achieved, Figure (4.2). Unfortunately the South African flowstones do not have the benefit of multiple tests of concordance like the Winnats Head material as they are too old to be dated by U-Th, and do not contain enough ^{235}U for a concordia plot.

There were several issues to consider when applying this technique to these deposits;

Closed system behaviour

The requirement of closed system behaviour sometimes limits the application of U-Pb dating where limestones are concerned. Closed systems in nature are rare because of the mobility of U and its daughter products (Smith and Farquhar, 1989). Consequently these techniques are often thought to date early diagenesis rather than primary deposition (Jahn and Cuvellier, 1994; Jones *et al.*, 1995).

When diagenetic alteration occurs, U/Pb ratios may be affected by U or Pb expulsion or incorporation (Jahn and Cuvellier, 1994). U loss is generally deemed to be the most likely because of the increased mobility of U in oxidising conditions and the insoluble nature of Pb (Jahn and Cuvellier, 1994). U has a low distribution coefficient into carbonate, and abundant data shows that it will tend to move out of U-rich primary carbonate during alteration events (Winter and Johnson, 1995; Jones *et al.*, 1995). U movement has been identified by discordance between the two U-Pb schemes but concordance in the corresponding Pb-Pb plots (Israelson *et al.*, 1996; Jones *et al.*, 1995). Jones *et al.* (1995) found that there was more scatter associated with a U-Pb isochron than the corresponding Pb-Pb one. This confirmed that the dominant cause of the scatter in this case was U loss or gain. A study by Israelson *et al.* (1996) found that U loss had occurred on more than one occasion since sediment deposition. This was thought to be the cause of scatter on the isochron as Pb gain would have substantially lowered the ^{206}Pb/^{204}Pb values.

Pb, in contrast to U, tends to behave like Th, adsorbing onto suspended detrital

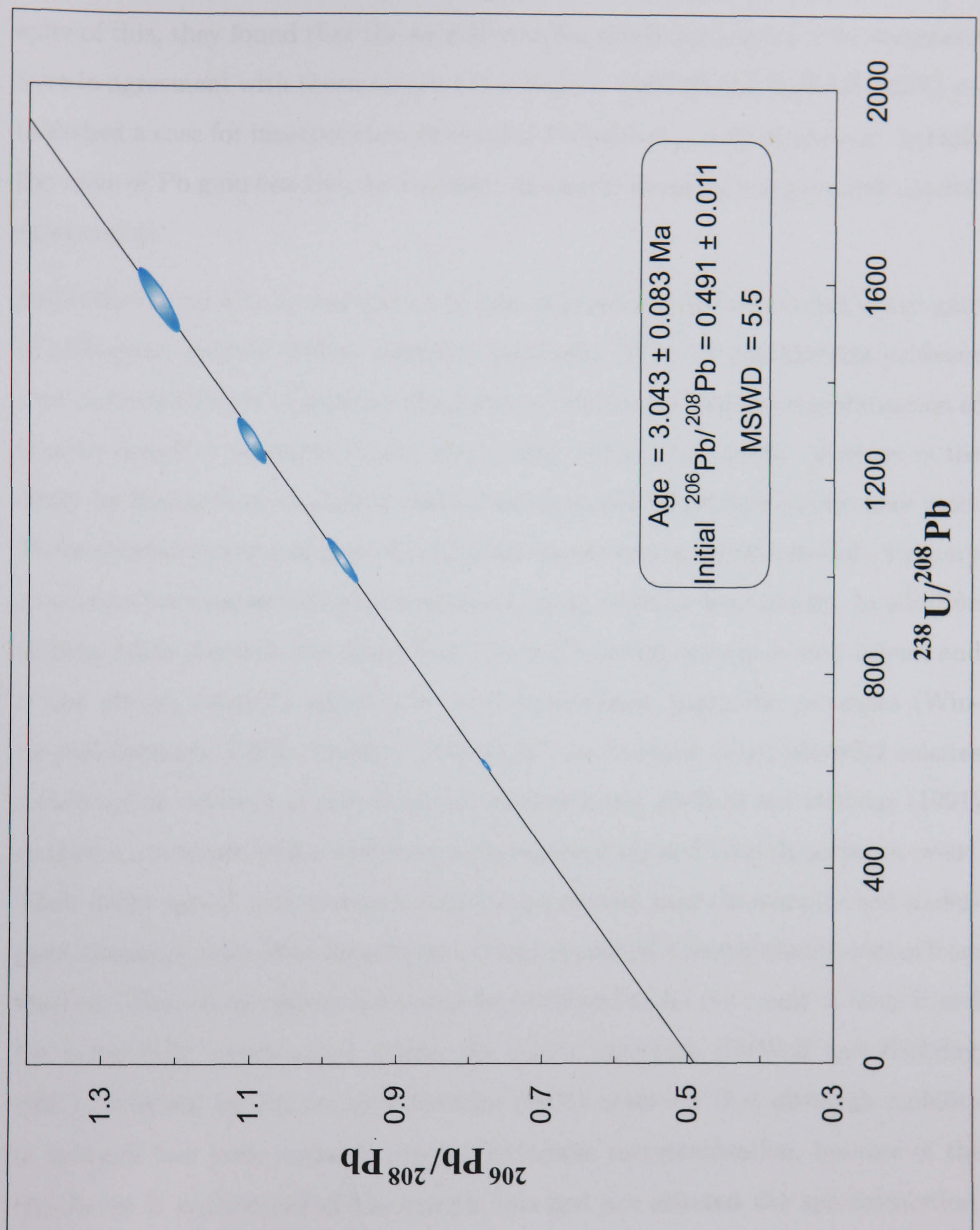

Figure 4.2: SK3 isochron from initial analyses at Sterkfontein by Cliff, R. A. Full data are not included in this thesis. Age calculated is a maximum age. Error ellipses are plotted at 2σ level. Sample is from flowstone layer 2C.

particles (Jahn and Cuvellier, 1994). It does not therefore possess the same mobility as U. However, Smith *et al.* (1994) found that the transformation of fossil nautiloids from aragonite to low magnesium calcite resulted in a net loss of Pb. In spite of this, they found that the ages of samples which had experienced diagenesis were in agreement with those samples that hadn't. DeWolf and Halliday (1991) established a case for incorporation of detrital Pb following early diagenesis. Luckily the issue of Pb gain can thus be rectified, by simply avoiding samples with detrital components.

Speleothems can also be susceptible to post-depositional alteration and loss or gain of radiogenic parents and/or daughter products. There is considerable evidence that recrystallisation of primary aragonite to calcite can result in remobilisation of U or its daughter products (Smith *et al.*, 1991; Jones *et al.*, 1995). However in the study by Richards *et al.* (1998), stalactites composed of pristine calcite were used. These showed no signs of post-depositional dissolution or reprecipitation. Primary structures were preserved and secondary mineral growths were absent. In addition to this, much research has found that the U-Pb dating system is very robust and is not always seriously affected by post-depositional diagenetic processes (Winter and Johnson, 1995). Rasbury *et al.* (1997) successfully dated palaeosol calcites and found no evidence of post-depositional diagenesis. DeWolf and Halliday (1991) studied a limestone with a well known depositional age and later disturbance event. Their dates agreed with previous studies and showed that the samples had undergone alteration soon after deposition but had remained a nearly closed system from then on. The closed system behaviour was believed to be the result of both U and Pb being fully incorporated within the calcite structure (DeWolf and Halliday, 1991). A study by Winter and Johnson (1995) observed that although mobility in isotopes had been initiated through extensive recrystallisation, because of the significant U enrichment of the sample this had not affected the age calculation. They regarded the age to be geologically meaningful because of the spread in the U/Pb values, and the concordance between this and a precursory dating method. These studies prove that alteration does not necessarily result in ages which are incorrect.

What is clear from the previous studies is that there is often no way to tell whether U or Pb movement has occurred. Partitioning of U and Pb during secondary

carbonate precipitation is not well understood (Smith *et al.*, 1994). Even if an isochron is produced, this can not provide definitive evidence as to geochemical changes during the rocks history. Some diagenetic events have proved to be so soon after deposition that they do not affect the calculated ages, whilst other later events that have the potential to affect the U-Pb system have not. Jones *et al.* (1995) could not trace U movement with any of the petrographic or geochemical studies they undertook to supplement their geochronological research. Neither could these studies confirm or disprove the ages calculated. In the absence of any other solution to this problem Jones *et al.* (1995) recommend picking "the solidest, freshest looking samples possible."

As the only gas in the ^{238}U decay chain, loss of ^{222}Rn is also something to consider. However, by measuring the activities of ^{230}Th and ^{210}Po (nuclides either side of ^{222}Rn in ^{238}U decay chain) Richards *et al.* (1998) showed that ^{222}Rn loss in dense columnar crystal speleothems is negligible. In the present study ^{222}Rn loss was not further investigated, but every effort was made to ensure that only dense speleothem was analysed.

Common lead and initial lead ratios

The U-Pb isochron represents the mixture of radiogenic and common Pb present in the sample. To achieve high mu values when dealing with young rocks, low initial levels of common Pb are essential. Contamination by common Pb will result in lower $^{206}Pb/^{204}Pb$ ratios and the radiogenic signal will be indistinguishable (Israelson *et al.*, 1996). Fortunately due to the ionic size of Pb its incorporation into calcite is much less favourable than that of U. However, detrital material, which is free of the calcite lattice, is also known to add common Pb to limestone and will contribute to its isotopic signature (DeWolf and Halliday, 1991).

Initial Pb compositions of secondary carbonates are generally determined by the fluid from which they precipitated (Smith *et al.*, 1991), which in turn reflects the lithology of the aquifer and soil through which the fluid passes (Jahn and Cuvellier, 1994). If Pb is incorporated from a variety of sources this may result in heterogeneity in the forming deposit. Initial Pb heterogeneity can cause complications when isochrons are used as the isochron method assumes initial isotopic homogeneity.

Winter and Johnson (1995), Smith *et al.* (1994) and DeWolf and Halliday (1991) all reported variation in initial Pb ratios, which can lead to scatter on the isochron. To counteract this, ages should be governed by samples with high mu values, as these are less sensitive to the initial isotopic composition and therefore give the lowest age uncertainties (Jones *et al.*, 1995).

Initial $^{234}U/^{238}U$ disequilibrium

The standard calculations of U-Pb ages, as in Equation (4.21), make the assumption that the ^{238}U decay series is in secular equilibrium at the time of deposition. However, when a sedimentary deposit forms it is normal for a state of disequilibrium to exist between ^{238}U and its daughters (Ku, 2000). In speleothem this is the result of radioactive disequilibrium within the meteoric waters forming the deposits.

In using U-Pb dating for such young material, initial U-series disequilibrium must be taken into account when calculating ages (Ludwig, 1977; Wendt and Carl, 1985). Initial disequilibrium will only affect those daughter nuclides that have a half-life within the age range of the sample ie. age is $\approx$ 6-7 times the half-life. In the ^{238}U decay series, where deposits of a few million years are being dated, this includes ^{234}U and ^{230}Th.

The main causes of ^{234}U enrichment in groundwater are believed to be recoil of ^{234}Th from the alpha-decay of ^{238}U, and preferential leaching of ^{234}U from areas of the lattice which have been damaged by radiation (Porcelli and Swarzenski, 2003). In freshwater the $^{234}U/^{238}U$ activity is usually greater than unity and can reach values >10. When excess ^{234}U is incorporated in cave deposits the resulting accumulation of ^{206}Pb is a product of this as well as the parent isotope ^{238}U. Standard age calculations assume that all the accumulated ^{206}Pb originated from the parent ^{238}U isotope, and do not account for any additional ^{206}Pb produced via initial disequilibrium. Where initial disequilibrium was present (activity of $^{234}U/^{238}U > 1$) the calculated age will be older than the true age and can only be treated as a maximum age for the given deposit.

The accumulation of radiogenic ^{206}Pb is also influenced by the discrimination

against the incorporation of Th in the forming deposit. This results in a deficiency of ^{206}Pb from the decay of the intermediate daughter ^{230}Th, although this effect is usually more than cancelled out by the ^{206}Pb produced from initial ^{234}U excess. Some excess ^{226}Ra will also be incorporated in speleothems when they form. Regardless, as it is unsupported by its parent ^{230}Th and only has a half-life of 1600 y, it won't significantly affect samples that are older than 200 ka (Richards *et al.*, 1998; Faure and Mensing, 2005).

Ignoring initial disequilibrium can have significant effects on the age estimate. In the Richards *et al.* (1998) study, the results would have yielded an age of 187$\pm$9 ka, as opposed to 248$\pm$10 ka, if disequilibrium had not been considered. The true age is higher because the standard age calculations do not take into account the deficit in ^{206}Pb in rocks as young as these. In the South African flowstones this effect would be negligible in comparison to the increase in the true age resulting from the initial excess ^{234}U. Figure (4.3) shows how different degrees of disequilibrium alter the outcome of the age calculation.

A study of the disequilibria present in the Transvaal dolomite aquifer was undertaken by Kronfeld *et al.* (1994). By sampling water from bore holes and conducting an isotopic study of speleothem they demonstrated how U isotope fractionation occurs and changes over time in this region. Unlike the accepted mechanism for alpha-recoil where the aquifer is U rich and the waters reducing, the Transvaal aquifer has low U concentrations, below 0.2 ppm, whilst the water is O_2 rich (Kronfeld *et al.*, 1994). In the Transvaal dolomite aquifer the disequilibrium is thought to be the result of ion exchange processes. Thin coatings of U may form on carbonate surfaces and act as a medium for alpha-recoil transfer of ^{234}U. This results in progressively higher activity ratios the longer the groundwater remains in contact with the aquifer. Evidence of extreme variation in ^{234}U/^{238}U, and in U concentrations, between different speleothems and within individual speleothems was found. Records from the Wolkberg cave show that this process has been in effect for at least the last 350 ka in this area. There is still a great deal of debate about how elevated activity ratios such as these come about. Porcelli and Swarzenski (2003) doubt this ion-exchange mechanism because the "reservoir would isotopically exchange U with the water" so that high activity ratios must stem from ^{238}U which is irreversibly bound in the aquifer. Bonotto and Andrews (2000) also suggest that

alpha-recoil can not elevate activity ratios in groundwaters of carbonate limestone regions and that chemical etching/leaching is a more important process.

Correcting for initial disequilibrium is an extremely contentious issue. It has been suggested that modern day groundwaters can be used to adjust for initial disequilibrium. Thompson *et al.* (1975b) used modern dripwaters to estimate initial $^{234}U/^{238}U$ activity. However there is much evidence to suggest that this method is flawed due to the wide temporal and spatial variation of initial $^{234}U/^{238}U$ in groundwater (Thompson *et al.*, 1975a). Gascoyne *et al.* (1978) state that assuming that modern dripwater values can be applied to initial $^{234}U/^{238}U$ is of "dubious validity." $^{234}U/^{238}U$ ratios vary in both time and space, and Thompson *et al.* (1975b) found that average values for dripwater can vary significantly from the values in the stalagmite being produced. Kronfeld *et al.* (1994) further support this apprehension following their results.

It is clear that groundwaters in the Transvaal dolomite were most likely in disequilibrium with respect to U, when the flowstones formed in the caves of interest. Furthermore, the initial extent of this disequilibrium can not easily be estimated for the purpose of age calculations.

4.2.4 Summary

There are several issues to take into account when attempting to calculate dates for the South African flowstones. Previous work indicates the importance of selecting material which is clean, dense, free of detrital contamination and wherever possible preserves primary depositional features. This should ensure that the samples do not suffer from unwanted incorporation of detrital Th or Pb and that they have the least likely chance of post-depositional alteration. With no way of accurately modelling movement of parent or daughter isotopes, it was hoped that this method of sample selection would guard against open-system behaviour. Furthermore the issue of initial Pb heterogeneity and initial ^{234}U excess would have to be taken into account. Without any information regarding initial ^{234}U excess or a method for correction, any ages calculated would serve as maximum ages for a deposit rather than best estimates.

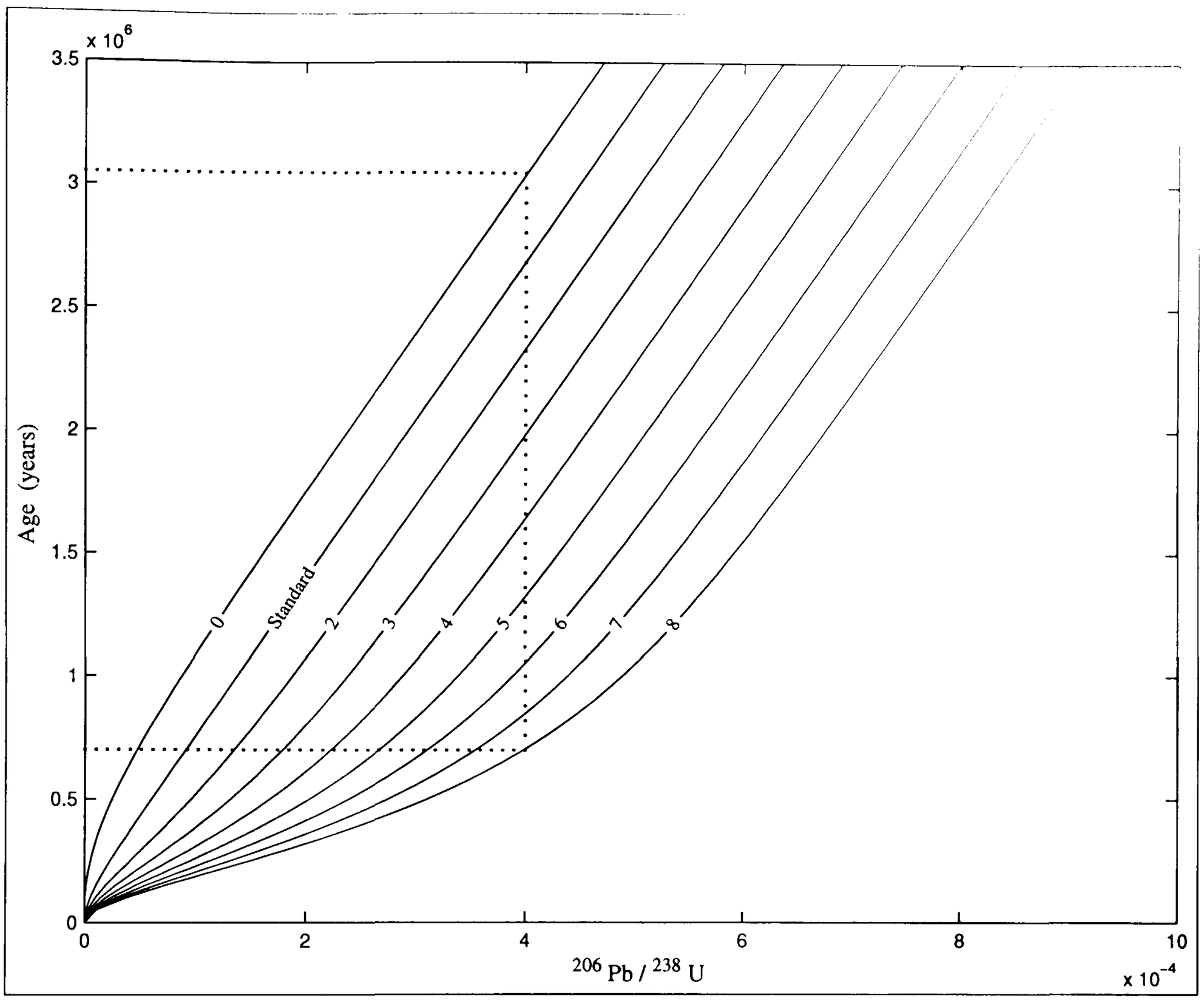

Figure 4.3: Effect of initial $^{234}U/^{238}U$ disequilibrium on $^{238}U/^{206}Pb$ age. Lines show ingrowth of $^{206}Pb/^{238}U$ for varying initial disequilibrium. Numbers represent initial activity ratios. Standard shows ingrowth assuming initial secular equilibrium, Total activity = 1; 0 = no daughters present initially ∴ Total activity = 0. Dotted lines show how age can vary depending on correction for initial disequilibrium; using Standard, where $^{206}Pb/^{238}U = 4$, Age $\simeq 2.7$ Ma (no disequilibrium correction); but where initial activity of $^{234}U/^{238}U = 8$ and $^{206}Pb/^{238}U = 4$. Age $\simeq 0.7$ Ma (with disequilibrium correction).

Chapter 5

Methodology

The following chapter deals with the various methods employed in the U-Pb dating of speleothem associated with the South African hominid fossils. Section (5.1) deals with sample selection in the field and in the laboratory; Section (5.2) covers the chemistry theory and lab methods; Section (5.3) looks briefly at the processing of the raw sample data and more specifically at the use of the data from the blanks and standards analysed; lastly Section (5.4) covers the methodology applied to the critical assessment of results.

5.1 Sampling techniques

5.1.1 Sample selection in the field

Samples were selected according to several criteria;

- Proximity to fauna (hominid or other) and clarity of stratigraphic position - could sample be reliably linked to position of fauna?
- Colour, texture, and apparent detrital content of flowstone.
- Ease of removal of sample.

The aim of the study was to clarify the dates of hominid finds, so the first sampling criteria was to sample flowstone which was within centimetres of the fossil(s). In

addition to this, the flowstone had to be suitable for the U-Pb technique. To minimise the issues associated with open-system behaviour and common Pb, samples that appear clean and non-porous should be carefully selected. Smith and Farquhar (1989) found that corals which displayed discordant behaviour had a more porous structure. They suggest that air pockets may facilitate the movement of fluids which can remove U and less frequently Pb. Porous speleothem is also known to be susceptible to loss of ^{222}Rn (Richards *et al.*, 1998). Flowstone samples that appeared free of detrital material and dense in structure were selected. However, no deliberate attempt was made to avoid samples which were on surfaces that were exposed to the cave environment. If these criteria were met, sampling was only subject to removal. Since most sampling was done only with a rock hammer and chisel it was not always possible to remove a first choice sample.

Sterkfontein sampling

Sampling at Sterkfontein was concentrated on the member 2 deposits in the Silberberg Grotto. This was a small, not easily accessible cave, and contained a fossil hominid, StW 573, in situ. This meant that sampling was more limited than at the other sites, as the cave could not be moved about in freely. The stratigraphy in the grotto was the most uniform of all the sites and the easiest to interpret. The hominid skeleton was in breccia sandwiched in between two layers of flowstone, and a further two layers of flowstone were found either side of these, one above and one below; see Figure (5.1), and Figure (6.1) for a cross-sectional view. In general the layers followed a layer cake stratigraphy model, with the oldest at the base of the sequence and the youngest at the top. If dates could be assigned to each of the layers this would give an age gap which would correspond to the age of StW 573. Removal of samples was relatively easy as most of the areas being sampled were sloping with layers protruding like steps. In certain places a layer of flowstone could be approached from above, on top of the growth layer, as well as from the side.

Sixteen samples were taken in total, as shown in Figure (5.1). Seven samples, STA01-STA07-C, were taken from the top (youngest) layer of flowstone, layer 2D, $\approx$ 1m above the skull of StW 573. Samples STA08-STA13 were taken from the

layer of flowstone which lies directly above the skeleton, layer 2C (Figure (5.2)). A further three samples, STA14-STA16, were sampled from the oldest flowstone layer $\approx$ 1m below the skull, layer 2B.

Additional pictures of layers 2B, 2C and 2D can be seen in Section (A.2.1) along with pictures of the samples taken, in situ.

Limeworks sampling

The Limeworks was the largest of the cave sites and had the largest amounts of flowstone to choose from. However, it was not possible to sample flowstone that was in close proximity to hominid fossils. Most of the hominid finds here were retrieved from the mineworkers dumps. A significant amount of the hominid finds were traced back to a bone-rich breccia which was part of the member 3 deposit (Wells and Cooke, 1956; Brain, 1958; Partridge, 1979). Unfortunately there were no suitable areas of flowstone in context with this deposit.

The area chosen for sampling was the Original Ancient Entrance (OAE). This was believed to be one of the oldest areas of the cave. This cavern had a fully intact roof and was almost completely enclosed, which meant it had been less exposed to weathering than other areas of the site. It also had several areas of dense, detritus free flowstone. Nine samples were taken, LAB03-LAB11, along a large section of the member 1B speleothem boss which came in from the Entrance Quarry, against the side of the cave wall, see Figures (5.3) and (5.4). As these samples were on a flat surface, some had to be removed with the help of an angle grinder.

Further views of the flowstone band from which the LAB- samples were taken and an in situ photograph of LAB03 can be consulted in Section (A.2.2).

Kromdraai B sampling

Kromdraai B was the smallest of the cave sites, and the most exposed to external weathering. It had no roof remaining at all. Sampling was limited due to the small amounts flowstone present at the site, so was concentrated on the deposits which could be related to the fauna there. Unlike the Limeworks or Sterkfontein there were no easily discernable sequences of strata with which to correlate samples with

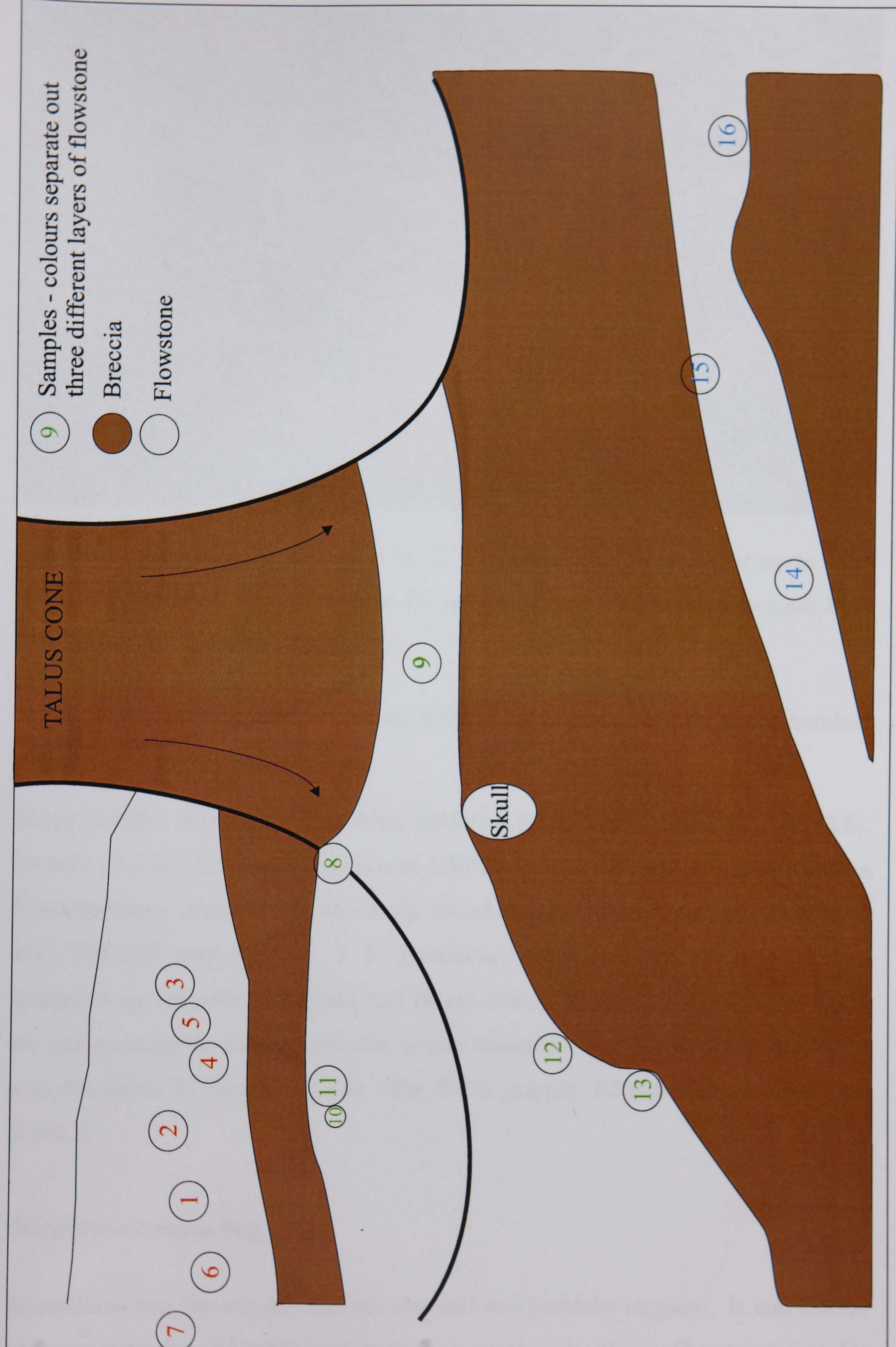

Figure 5.1: Schematic of STA- sample suite from the Silberberg Grotto, Sterkfontein. Not to scale. Compare with Figure (5.2) for context and Figure (6.1) for the view in cross-section.

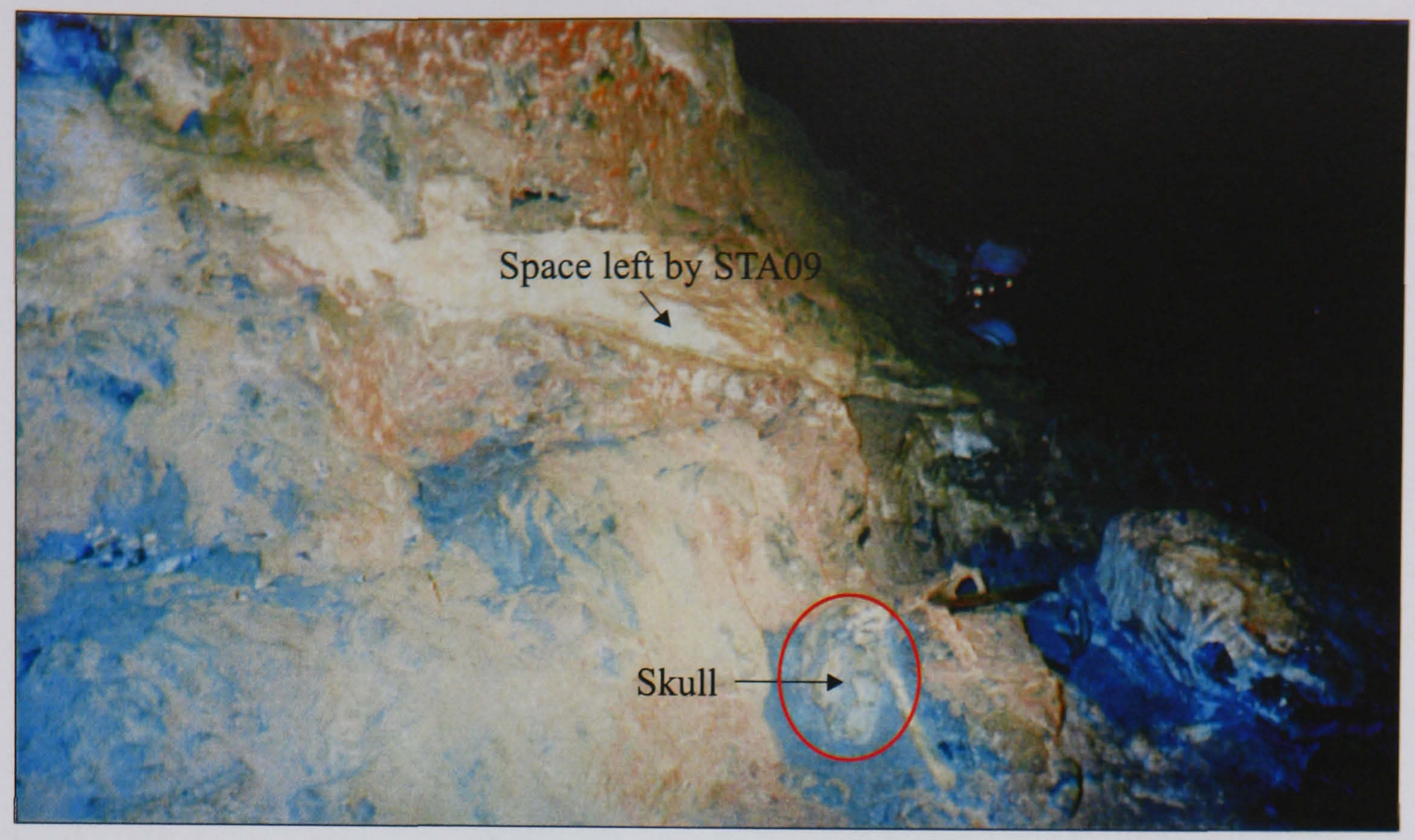

Figure 5.2: Photograph of section of STA- sample suite from Sterkfontein. Positions of Flowstone 2C and sample STA09 are shown with respect to fossil StW 573. Compare also with Figure (2.6).

fauna. There was however suitable material in very close proximity to the hominid remains with a clear association.

Three samples were taken from here, KBP02-KBP04, see Figures (5.5) and (5.6). Section (A.2.3) also shows a photo of KBP03 in situ. These were taken from a flowstone layer immediately above the member 3 breccia, of the kind associated with TM 1517 (pers. comm., J. F. Thackeray, 2002), the type specimen of *Australopithecus robustus* (Johanson and Edgar, 2001). Samples KBM 7 and 8 taken for palaeomagnetic dating were also in this flowstone, see Thackeray *et al.* (2002) and discussion in Section (3.2.3). The U-Pb sample, KPB03 was $\approx$ 12cm from KBM 8.

Swartkrans sampling

Swartkrans was the second smallest site and was partially exposed. It had a complex stratigraphy and contained several areas of clean, dense, flowstone, suitable for sampling. A flowstone seam at the rear of the inner cave (north wall), adjacent to public viewpoint 10, was selected. Three samples, SKF01-SKF03 were taken from a flowstone that lies between members 1 and 2, see Figure (5.7) and Fig-

Figure 5.3: Schematic of LAB- sample suite from large speleothem boss in the Original Ancient Entrance, the Limeworks. Not to scale.

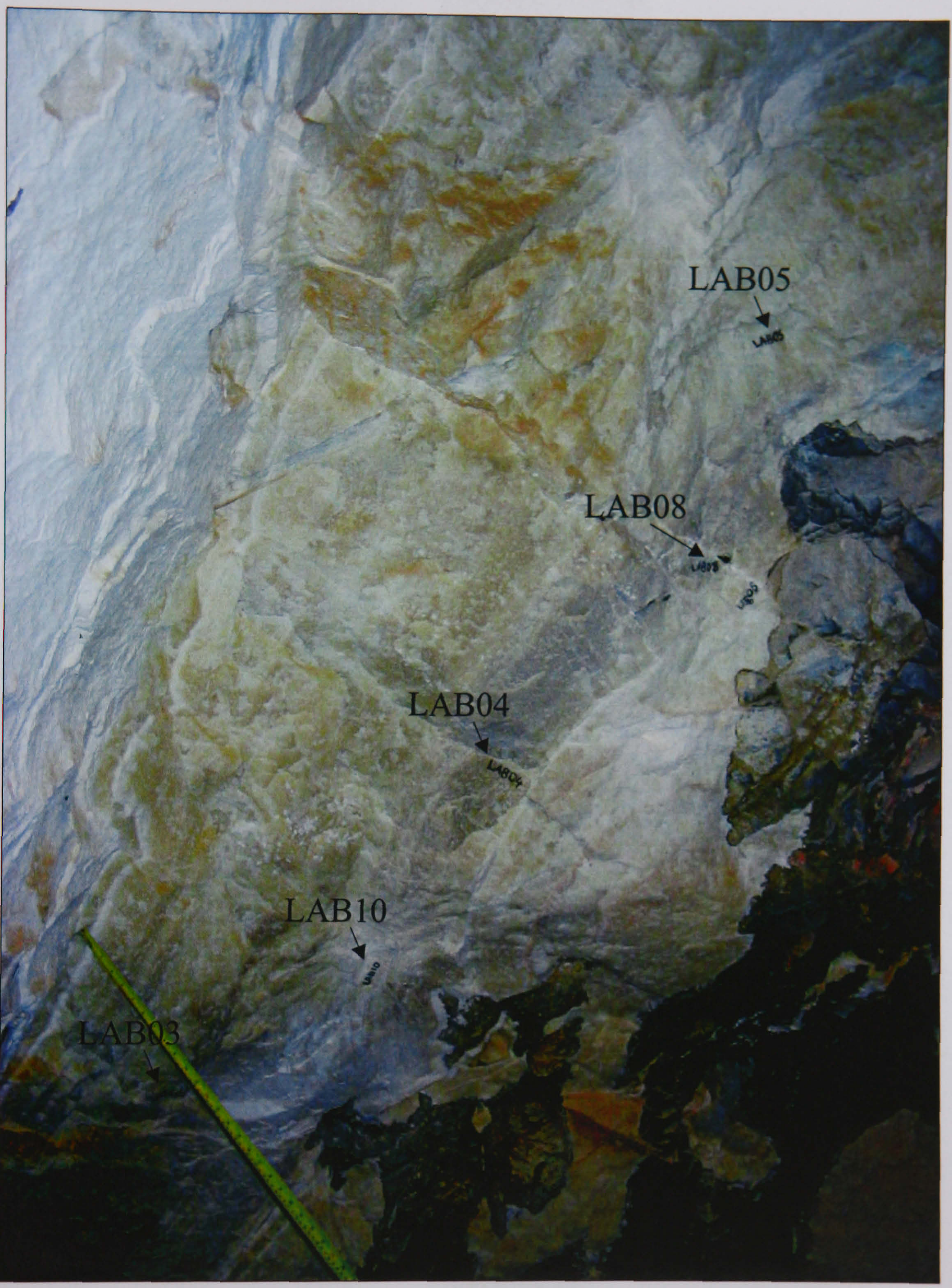

Figure 5.4: Photograph of section of LAB- sample suite from the Limeworks showing type of material sampled for LAB- suite and position of five of samples after removal. Apart from the grey/brown material, which is dolomite, all material is flowstone.

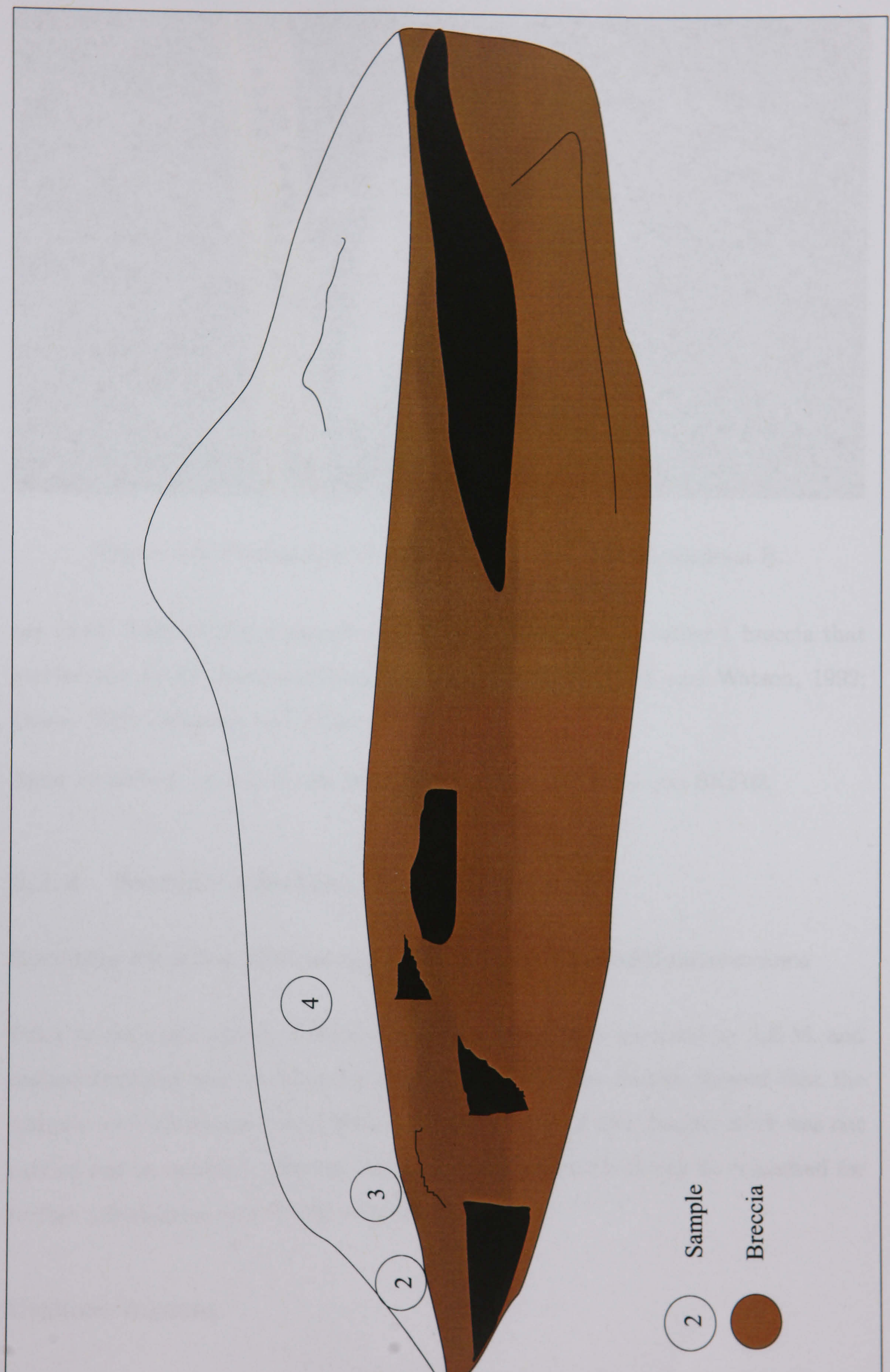

Figure 5.5: Schematic of KBP- sample suite from Kromdraai B. Not to scale. Compare with Figure (2.9) and Figure (5.6) for context with respect to surrounding deposits.

Figure 5.6: Photograph of KBP- sample suite from Kromdraai B.

ure (5.8). This overlies a pocket of the Hanging Remnant member 1 breccia that yielded the SK23 *Australopithecus robustus* mandible (Brain and Watson, 1992; Brain, 1993; Johanson and Edgar, 2001).

Refer to Section (A.2.4) for an in situ photograph of SKF01 and SKF02.

5.1.2 Sample selection in the laboratory

Scanning Electron Microscopy (S.E.M.) and Cathodoluminescence

Prior to the main period of fieldwork, two samples[1] were screened by S.E.M. and cathodoluminescence to check for detrital content. The results showed that the samples were relatively free of detritus. On the basis of this, further work was not carried out on samples collected subsequently. Section (A.1) can be consulted for further information and S.E.M images.

Uranium imaging

Samples from each site were selected for initial U content assessment. An indication of the U content was derived by phosphor imaging. This is a form of digital

[1]SK3 from Sterkfontein and LAB03 from the Limeworks

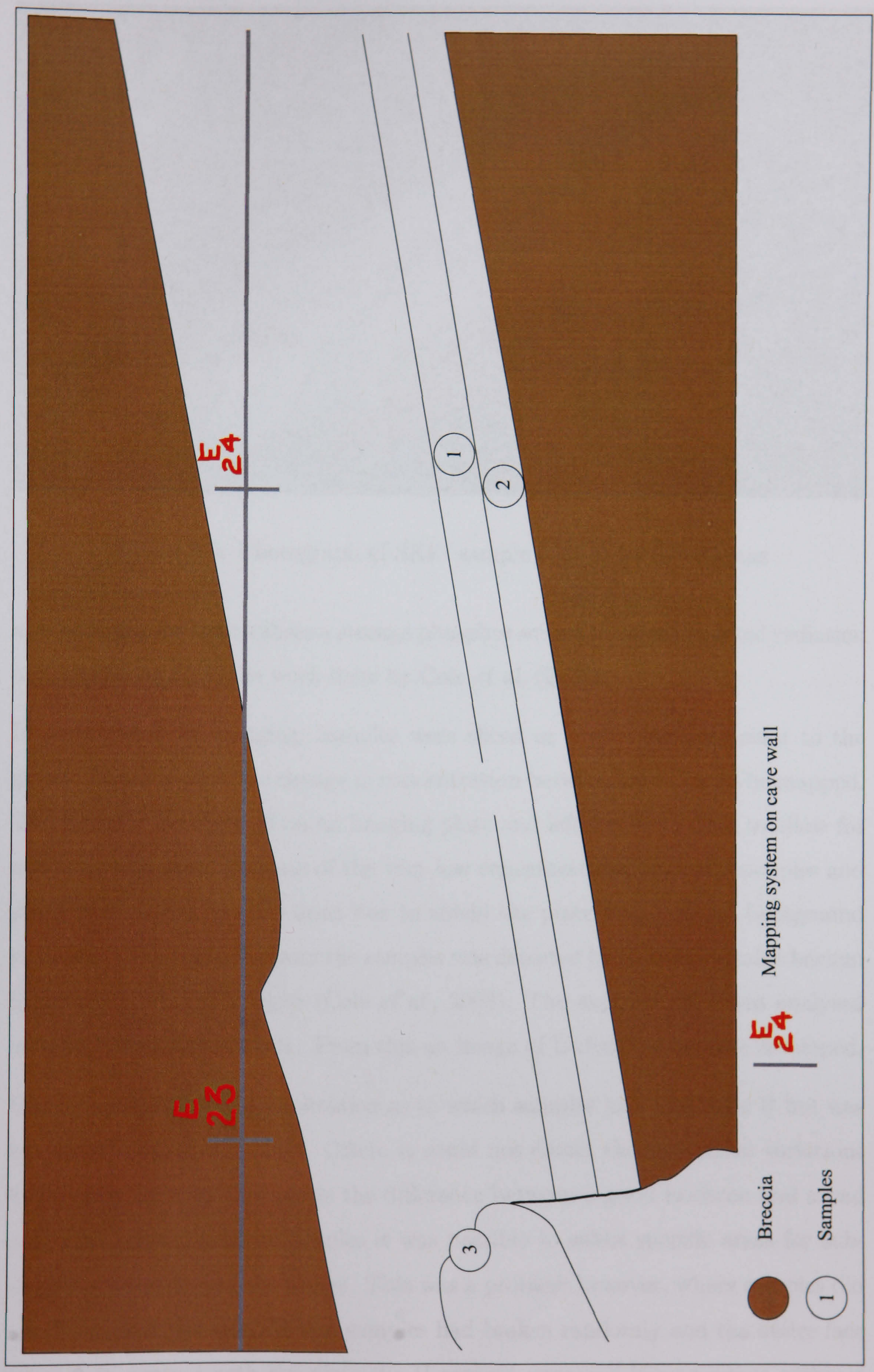

Figure 5.7: Schematic of SKF- sample suite from Swartkrans. Not to scale. Compare with Figure (5.8) for context in terms of surrounding deposits.

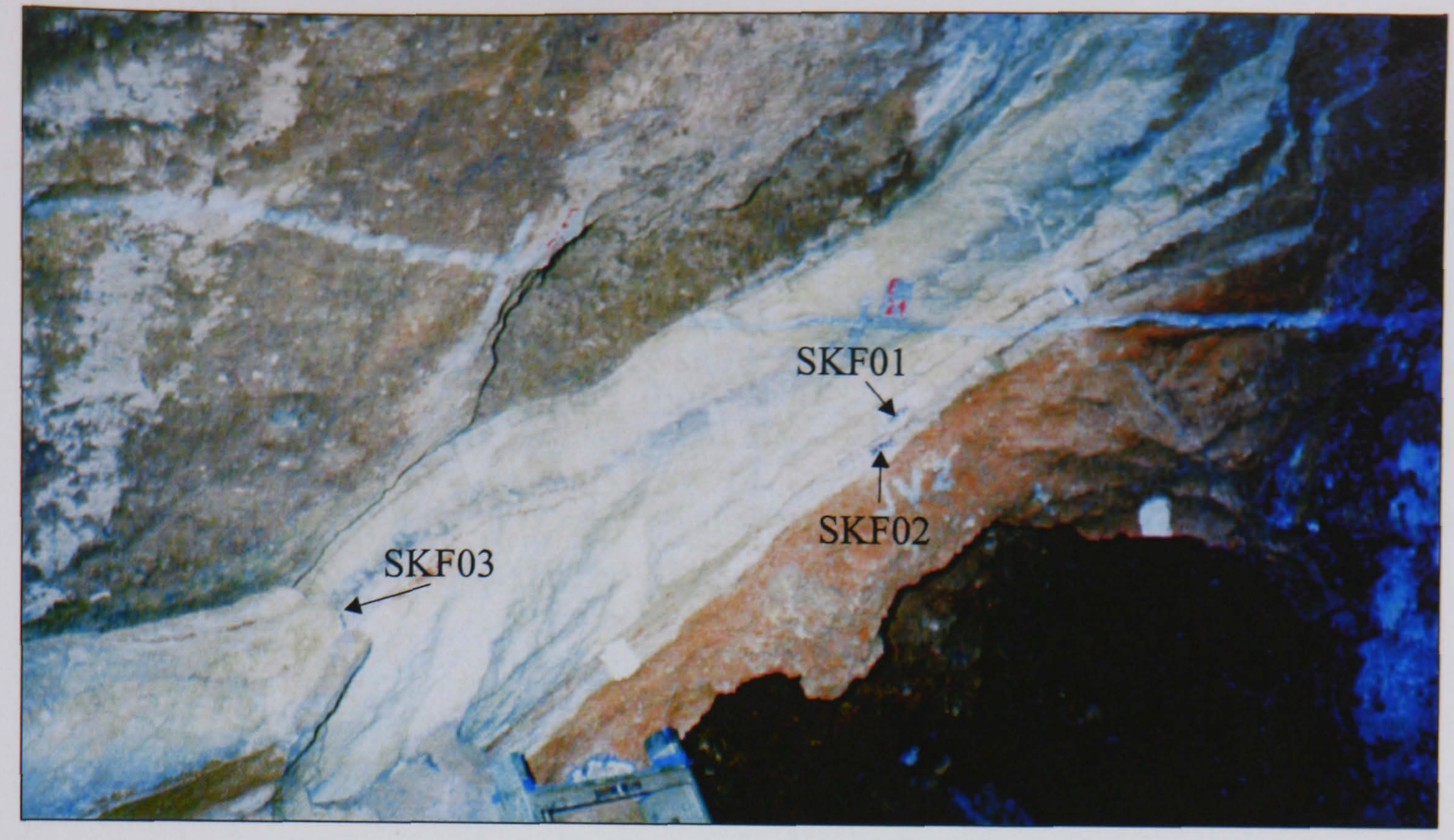

Figure 5.8: Photograph of SKF- sample suite from Swartkrans

autoradiography that utilises a storage phosphor screen to record emitted radiation and follows on from the work done by Cole *et al.* (2003).

In preparation for imaging, samples were sliced or broken perpendicular to the growth layers so that the change in concentration between layers could be mapped. The samples were placed on an imaging plate and left for 10-14 days to allow for adequate exposure. Because of the very low concentrations of U, the samples and plate were placed in a Pb-lined box to shield the plate from natural background radiation. The radiation from the samples was detected by photostimulable barium fluorobromide[2] on the plate (Cole *et al.*, 2003). The exposed plate was analysed on a Fuji BAS1000 scanner. From this an image of U distribution was developed.

U imaging did give some indication as to which samples had very little U but was not always sensitive enough. Often, it could not detect the very small variations in U concentrations that made the difference between a good isochron and a bad one. On individual hand samples it was possible to select specific areas for sub-sampling according to the image. This was a problem however, where samples did not have a cut flat face. Where samples had broken randomly and the entire face was not in contact with the plate the U content appeared homogeneous within a hand sample, even across growth layers.

[2]BaFBr

Sub-sampling

Samples with apparently the highest U content were then sub-sampled using a tungsten carbide chisel. Sub-sampling was at times random as it depended on how the material broke when force was applied, although some of the samples had been cut initially using a rock saw. In general, samples were selected from areas with a clean appearance. Sampling from the face which had been exposed in the cave was avoided when possible. Each sample was photographed and drawn, and the positions of the sub-samples were recorded on the drawings.

5.2 Experimental techniques

5.2.1 Chemistry theory

Samples were analysed by thermal ionisation mass spectrometry (TIMS). This requires chemical separation of the elements under observation from the bulk of the sample. This was done by;

- Dissolution of samples
- Separation of Pb
- Purification of Pb
- Separation of U

In order to understand the lab technique employed the theories behind it must first be addressed.

Anion exchange chromatography

U and Pb were separated from bulk samples using anion exchange chromatography. In the past Pb and U have been separated from samples, such as zircons, simultaneously using anion exchange columns and HCl. Where Fe is present this is not possible (Dickin, 1997). An alternative to this is to separate Pb initially

from all the elements, on a miniature anion exchange column with dilute HBr. as per Chen and Wasserburg (1981), Manhes *et al.* (1978) and Manhes (1982).

When Pb in solution is loaded onto a column containing anion exchange resin it will display different affinities for the solvent and the resin. The ratio of the concentration of Pb in the two phases is known as a distribution coefficient, and is affected by the solvent used and its concentration.

Pb was separated from the bulk samples using HBr. Complexes formed by the sample Pb and Br^- ions were strongly retained by the resin while other major elements, including U, passed through. The distribution coefficient of the Pb complexes onto the resin was at a maximum just below 1M. The Pb could then be stripped from the column in 6M HCl or water (Korkisch and Hazan, 1965).

Separation of U can be carried out using the same resin but in a nitrate environment. Using 6-8M HNO_3, U is sufficiently retained by the resin while most other elements are not. U can then be eluted using weak acid or water (Carswell, 1957; Faris and Buchanan, 1964; Tilton, 1973; Chen and Wasserburg, 1981).

Isotope dilution

Sample concentrations of Pb and U were determined by isotope dilution. The sample is mixed with a spike that contains known quantities of an element but is artificially enriched in one or more isotope. When known quantities of both sample and spike are combined, the resulting isotopic composition can be used to calculate the amount of the element in the sample (Faure, 1986; Dickin, 1997). The spike used was ^{202}Pb-^{233}U-^{236}U. Using a mixed spike enabled calculation of the amounts of both elements simultaneously. The U-Pb ratio can be measured precisely and is independent of any weighing errors.

Blanks

When attempting to measure amounts of Pb in the ppb region it is necessary to minimise sources of contamination wherever possible. Industrial activities mean that Pb has a much higher abundance in nature than U. Therefore, U contamination is not as important as Pb contamination. Major sources of Pb contamination

are;

- Analyst - care and attention to detail was the best way to reduce this source.
- Reagents - contamination from reagents was minimised by using UpA (Romil) reagents wherever possible or doubly distilled reagents. The UpA reagents guarantee certain levels of purity. In addition to these, 18.2MΩ water was used throughout. Contamination levels in the reagents used can be consulted in Table (B.1).
- Equipment - equipment that was reused ie. beakers and columns, was boiled in 50% HCl and filled with a mix of acids or stored in 6M HCl. Equipment that was used once and then thrown away eg. frits or pipette tips, was stored in 6M HCl. All equipment was thoroughly rinsed in 18.2MΩ water before using.
- Atmosphere - All separations were performed in a Class 10 workstation[3].

To accurately quantify contamination a blank was processed for every set of five samples. Excluding dissolution the blanks were subjected to the same procedure as the samples.

5.2.2 Lab technique

A comprehensive description of the following techniques can be found in Appendix (B). Texts which can be consulted for reference to these techniques are Carswell (1957); Faris and Buchanan (1964); Korkisch and Hazan (1965); Tilton (1973); Manhes *et al.* (1978); Chen and Wasserburg (1981); Manhes (1982); Bourdon (1992); Rehkämper (1995); additionally Smith *et al.* (1991) and Smith *et al.* (1994) more specifically for the fluoride precipitation step.

Preparation of reagents

The HBr used in the Pb separation was prepared from UpA HBr. Immediately prior to a separation it was purified further on an anion exchange column of AG1x8

[3]This is a laminar flow workstation defined by Federal Standard 209E

200-400 resin to further reduce possible Pb contamination. The concentration of CPHBr (column-passed) was 0.5M.

Sample preparation

Sub-samples of up to 3g were removed from the hand samples. Superficial contamination was removed by cleaning in an ultrasonic bath before etching in 3M HCl to remove the surface layers. Typically $\approx$ 0.3g was removed by etching. Where samples were unusually small (< 0.5g) or unusually large (> 5g), this amount could be as little as 0.04g, or as much as 3g.

For the columns to flow efficiently it was necessary to remove the calcium from the samples. This was done by adding HF and discarding the CaF_2 precipitate that formed. HF was added in amounts that were slightly above what was stoichiometrically required (Smith *et al.*, 1991; Smith *et al.*, 1994).

Following some poor U results, yield tests were performed to test the effectiveness of the fluoride precipitation and the column chemistry. This was done by spiking a sample with two different spikes. Spike one (236B) was added following the fluoride precipitation and spike two (MS1) was added following the column separation. The results showed that the precipitation step removed 82% of the U, whereas the column separation was nearly 100% efficient. It was decided that the precipitate fraction should be processed twice for the Pb separation and again for the U separation. Prior to this the precipitate was only rinsed once, for the Pb separation, after which it was discarded. In the new method, following precipitation and removal of the first supernate, the CaF_2 precipitate was mixed with CPHBr and centrifuged again. The resulting supernate was added to the first one, after which the Pb separation was performed as normal. The precipitate was retained and was rinsed and centrifuged twice in 8M HNO_3 for the U separation. The two supernates produced were added to the U sample eluted from the Pb separation and the U separation was then performed as standard.

Lead separation

After the precipitates were rinsed in CPHBr and the resulting supernate was added to the sample solution, Pb samples were loaded onto the column in CPHBr and rinsed in with the same. The U passed through the column at this stage so the collective waste eluates were saved for later U separation. The Pb was then collected using 6M HCl. The Pb sample was purified by repeating the separation procedure.

Uranium separation

The fluoride precipitates were rinsed twice in 8M HNO_3 and the supernates were added to the eluates from the Pb separation. Chen and Wasserburg (1981), Bourdon (1992) and Rehkämper (1995) all mention the possible retention of U and Th in dissolved rock residues, although Chen and Wasserburg (1981) found that this accounted for no greater than 6.5% of the whole sample.

The U samples (eluate + supernates) were separated using AG1x8 in a nitrate environment. The U salt was highly soluble in HNO_3 and was loaded in 8M HNO_3. Most elements were eluted from the column by rinsing the sample in with further 8M HNO_3. U was then collected with 0.25M HNO_3.

Preparing the sample for loading

Final drying of samples was done with a couple of drops of Aldrich 0.002M H_3PO_4 to prevent the samples drying down entirely and to make them more visible in the vials, which eased loading (Manhes *et al.*, 1978; Bourdon, 1992).

A couple of drops of concentrated HNO_3 was then added to the samples and they were dried down again. This was intended to reduce the organic content of the sample which was a problem when loading.

Loading samples

Samples were loaded onto rhenium (Re) filaments. Pb samples, in 1μl of 18.2MΩ water, were loaded onto single filaments that had already been loaded with 1μl of silica gel. U samples were loaded onto double filaments in 1μl of 18.2MΩ water.

5.2.3 Mass spectrometry

All samples were run[4] on a TIMS - Finnigan Triton.

Running techniques for lead samples and blanks

Pb samples and blanks were measured using a static method. Pb filaments were raised to a temperature that enabled volatilisation and ionisation of the sample at the same time. ^{204}Pb in samples was measured in the centre cup on the faraday, or the SEM (Secondary Electron Multiplier) where the signal was $\leq$ 2mV (0.02pA). All other isotopes were measured on the faraday. For blanks the ^{204}Pb was always measured on the SEM.

Running techniques for uranium samples and blanks

The U evaporation filament (bearing the sample) was heated to a temperature where stable volatilisation of the sample occurred. The ionisation filament was raised to a much higher temperature where it acted as a source to ionise the sample atoms. U samples were measured using a multidynamic method with the ^{236}U, ^{235}U and ^{233}U in the centre cup, measured on the SEM. The ^{238}U was measured continuously by switching between three faraday cups. The resulting three ratios between the isotopes measured on the SEM and the three ^{238}U measurements meant that any variation in signal intensity could be taken into account. Running U samples on a multidynamic method also meant both ^{233}U and ^{236}U could be measured on the SEM. These isotopes were found only in the spike and so the ratio was used to correct for fractionation.

U blanks were measured using a dynamic method where all four of the isotopes - ^{238}U, ^{236}U, ^{235}U and ^{233}U - were measured in the centre cup on the SEM detector.

---

[4]Run is used throughout the thesis as the name for a set of measurements taken on the TIMS for a U or Pb sample.

Calibrations

Samples were measured using a multi-collection method so a gain calibration was done at the beginning of each new set of samples. This tested how each individual cup measured the same signal slightly differently, and then corrected for this in the raw data. Only samples measured using a dynamic method were unaffected by gain as all isotopes were measured in the same cup. This applied to U blanks.

A yield calibration was done for each sample that was measured on both the faraday and SEM detectors. This calibrated the gain of the SEM relative to a nominal value of 60,000cps (counts per second) per mV (millivolt). For Pb, the ^{208}Pb or ^{206}Pb beam was focused into the centre cup and a yield calibration was performed by switching between measuring on the SEM and the faraday and comparing the difference in signal intensity. The same was done for U, but using a ^{187}Re beam, produced by heating up the ionisation filament only. The result was given as a reading of % yield. The TIMS applied this correction to all subsequent measurements. Yield calibrations for U ranged between 90.5% and 96.8% but were generally over 95%. Pb yield calibrations were between 89.7% and 92.1% and were systematically lower than for U under identical conditions. U yield variation was further corrected for in the calculations. ^{238}U was the only isotope measured on the faraday so the ^{238}U/^{235}U ratio was used as a correction for bias by comparing the accepted value in nature with that measured.

Following a set of Pb runs which had particularly low signals, additional experiments were performed to test fractionation, and bias on the SEM (yield and non-linearity). Firstly the sample, STA14-B4, was run at varying intensities and the fractionation compared. The higher temperatures improved the signal, but the ratios were within error, so fractionation was not greatly affected. SRM981 was also run at varying intensities. These results showed that there was no basis for correcting for non-linearity variations in the yield.

5.3 Processing results, standards and blanks

The raw data from the TIMS were exported to a spreadsheet where outliers highlighted by the TIMS were removed. Outliers were further removed by hand with

the help of a macro with a window of acceptance based on the mean and the absolute standard deviation (see Section (B.0.14)) and the data were prepared for importing to an Error Propagation (EP) package. The EP package collated the raw Pb and U data (inclusive of errors and correlations) along with the data for the blank correction, the spike composition, the fractionation correction for Pb, and the values of sample and spike weights. The resulting ratios were suitable for plotting isochrons using the Excel add-in Isoplot (Ludwig, 2003).

5.3.1 Standards

Standards are firstly a test of instrumental bias. Secondly they test the mass fractionation effects on a filament over the duration of a run. Samples have a tendency to fractionate, whereby lighter isotopes are preferentially released from a hot filament due to their lower bond energies. This results in a discrepancy between the measured ratio of two isotopes and the true ratio (Dickin, 1997). Pb samples were corrected for isotope fractionation by running the standard, SRM981. Two standards were run for each set of Pb samples loaded and mass fractionation was averaged over sets of 8-10 results.

Standards, $\approx 1\mu$l in volume and containing in the region of 4ng of Pb, were loaded onto filaments that had already been loaded with 1μl of silica gel. They were run using the same technique as that used for Pb samples, with ^{204}Pb in the centre cup, but all isotopes were measured on the faraday detector.

The raw data for SRM981 runs was exported to a spreadsheet in Excel. Mean ^{207}Pb/^{206}Pb, ^{208}Pb/^{206}Pb and ^{206}Pb/^{204}Pb ratios were collated in another worksheet. The permil fractionation of each of the ratios was calculated by ;

$$\text{fractionation } ‰ = \left[\left(\frac{\text{measured value}}{\text{true value}}\right) - 1\right] \times 1000 \tag{5.1}$$

The ^{208}Pb/^{206}Pb and ^{206}Pb/^{204}Pb ratios were corrected for mass difference by dividing this value by 2. The overall fractionation factor was calculated thus;

$$\text{Fractionation factor} = \frac{\text{Average fractionation } ‰^{8/6,7/6,6/4}}{1000} \tag{5.2}$$

Date applied from	Fractionation factor	Error (1σ abs.)
04/12/2002	-0.00068	0.00049
14/10/2003	-0.00084	0.00027
29/01/2004	-0.00095	0.00036
11/03/2004	-0.00065	0.00044
25/03/2004	-0.00062	0.00016
12/05/2004	-0.00090	0.00011
02/07/2004	-0.00060	0.00030
23/08/2004	-0.00085	0.00020

Table 5.1: Fractionation Factors applied to samples and dates applicable from.

Around 8-10 fractionation factors were calculated like this and then averaged to give a value to the fractionation factor over a certain period of time. Samples run during that time period were corrected for this fractionation factor. The error for the fractionation factor was the standard deviation of the 8-10 fractionation values. Table (5.1) shows the fractionation factors that were applied over the course of the study. The full set of standards data can be consulted in Section (C.0.18).

5.3.2 Blanks

A blank was run for each set of samples analysed. However there is no way of knowing how representative this was of each individual sample. Blank levels were observed to vary in both sample replicates analysed on separate occasions and those analysed on the same day. It was felt that it was better to take an average of all the blank runs in order to provide a more representative blank. This averaged out the scatter between batches and was more indicative of scatter within a batch. Since each sample was corrected by the same absolute amount this gave better scope for comparing samples which were not analysed contemporaneously. Table (5.2) displays the blank results that were used to calculate an average blank size and composition; a small number of blanks that were spuriously large were excluded, these can be found in Table (C.3). Figure (5.9) shows how the blank size and associated error varied over time.

Blank	Date	Pb(ng)	Error(1σ)	206pM	Error(1σ)	$^{206}Pb/^{204}Pb$	Error(1σ)	$^{207}Pb/^{204}Pb$	Error(1σ)	$^{208}Pb/^{204}Pb$	Error(1σ)
360	25/03/2003	0.062	0.002	0.076	0.003	17.004	1.411	14.232	1.171	34.386	2.862
429	25/11/2003	0.102	0.004	0.126	0.005	17.028	0.298	14.671	0.247	34.103	0.596
428b	09/12/2003	0.078	0.003	0.094	0.004	18.288	0.022	15.710	0.024	38.074	0.060
355	27/01/2004	0.094	0.004	0.113	0.004	15.625	0.857	13.517	0.730	32.446	1.759
419	16/03/2004	0.092	0.004	0.111	0.004	19.104	0.032	16.493	0.034	39.801	0.052
428	29/03/2004	0.082	0.003	0.097	0.004	17.535	0.181	16.022	0.215	37.570	0.202
412	27/04/2004	0.134	0.005	0.162	0.006	18.389	0.021	15.813	0.026	38.245	0.037
424	24/05/2004	0.116	0.005	0.140	0.005	18.078	0.026	15.554	0.028	37.551	0.043
429	09/08/2004	0.068	0.003	0.082	0.003	18.703	0.059	15.964	0.055	38.479	0.127
404	23/08/2004	0.128	0.005	0.153	0.006	19.260	0.133	17.204	0.203	39.991	0.197
418	04/10/2004	0.066	0.003	0.079	0.003	17.804	0.061	15.537	0.080	37.281	0.097
	Mean	0.093	Mean	0.112	Wtd Mean	18.323	Wtd Mean	15.751	Wtd Mean	38.213	
	Std dev.	0.017	Std dev.	0.03	Error(2σ)	0.214	Error(2σ)	0.211	Error(2σ)	0.540	

Table 5.2: Blank results and weighted averages of these applied to samples as blank correction.

5.4 Evaluation of results

U-Pb ratios are generally normalised by ^{204}Pb as this is the only non-radiogenic isotope. In speleothems normalising is not limited to ^{204}Pb alone. ^{208}Pb can essentially be considered non-radiogenic because of the insoluble nature of its parent ^{232}Th. This is not incorporated in the speleothem as it forms so the initial ^{208}Pb does not change significantly over time. Thorogenic ingrowth within these deposits is estimated to be $\ll 0.1\%$ (Cliff, R. A. (2005) pers. comm.).

Ages were calculated by plotting $^{206}Pb/^{208}Pb$ against $^{238}U/^{208}Pb$ to produce an isochron, a line of equal age. How well the points fit the isochron was inferred from a measurement called MSWD (mean square of weighted deviates). This is a measure of scatter. MSWD values much greater than 1 indicated that either the analytical error was underestimated or that some non-analytical source of error was causing the scatter (Ludwig, 2003). There were several possible causes of scatter about the isochrons to consider in this study. Firstly, underestimation of analytical errors. It is possible, due to certain oversights, that the error estimates were too optimistic;

- Fractionation factor. This is likely to be greater than that estimated from the standard, as the samples are unlikely to behave as ideally as a standard.

- TIMS interference. Background interference can affect samples which have low Pb concentrations, in particular those isotopes with low signals.

- Blank composition. If the composition is significantly different from the initial Pb composition of the sample this can dislocate the sample on the isochron. This may be more exaggerated where the blank correction is large. Where the assigned errors are justified this should not affect the scatter.

- Change in analytical technique. Samples that were processed before 18/06/03 were not subjected to the revised fluoride precipitation step, as per Section (5.2.2). This could have affected the quality of the results.

- Contamination due to lapse of time between dissolution and analysis - samples not analysed for several months after the original dissolution may have

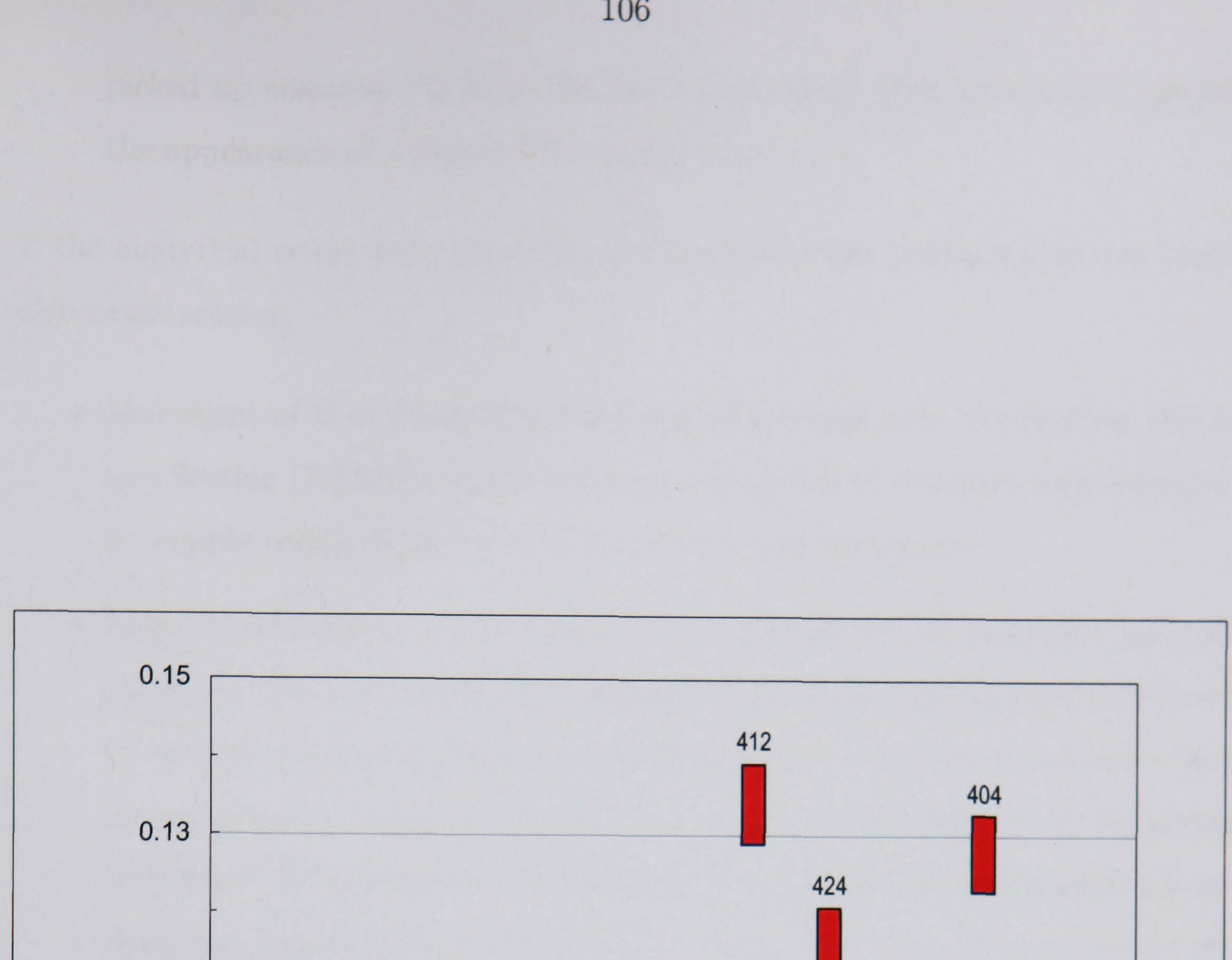

Figure 5.9: Graph showing how blank size varied over time. Blue line shows average blank size. Boxes are at 2σ level.

picked up common Pb from the labware in which they were stored, giving the appearance of a higher Pb concentration.

If the analytical errors were correctly accounted for, then geological factors could also cause scatter;

- Movement of U or Pb in situ, following recrystallisation. See Section (4.2.3) and Section (7.3.2) for explanation and discussion of this issue with reference to sample results from both previous work and this study.

- Initial heterogeneity of Pb isotopes in the deposit. If the true initial isotopic signature differs in individual samples then the initial composition calculated by the isochron method will be an average of these resulting in samples which do not lie on the isochron but have evolved on lines parallel to it. If variations in $^{208}Pb/^{204}Pb$ are greater that analytical uncertainty then this suggests more than one common Pb source (Romer, 2001). The main Pb sources for the samples will have been the aquifer and the surrounding soil.

- Variation in initial $^{234}U/^{238}U$ between layers. This ratio may vary temporally as the growth rate of the speleothem varies. Taking this into account it is quite possible that samples only cm apart may have had differing initial ratios. On an isochron these samples would evolve along different age lines which, when not accounted for, would cause scatter on the isochron.

In addition to scatter, errors could move a sample up or down the isochron. This should not affect the resulting age unless there is excess scatter already present, but these errors are something to be aware of;

- Variation between blank correction and true blank amount. There is no way of knowing how close the average blank correction was to the true blank value of each sample. Consequently individual samples may suffer from over- or under-correction. Such correction can cause problems with scatter when combined with one or more of the issues described above.

Aside from scatter the U or Pb concentrations could be affected by the following issues, therefore it was important to take these into account when comparing sample replicates;

- The sample amounts were calculated from the volume of the dispensed aliquot. The error in the pipette was estimated by measuring out and weighing ten aliquots of 1.3ml to be on average 6.5‰. The EP package only accounts for 0.25mg error whereas this actually equates to 2.81mg. However when input at the EP stage this did not have a great effect on the final concentrations.

- Spike weights. The error on the spike weight was estimated over 20 spike weights to be on average 1%. The error propagation accounts for a 0.25mg error so on most samples, which had a spike weight of over 30mg, this is slightly lower than the estimated error, although this does not greatly affect the final concentrations.

Chapter 6

Results

Of the hand samples that were analysed, three produced good isochrons[1] from which a maximum age and a best estimate age for the associated deposits could be deduced. These samples were from Sterkfontein and were associated with the fossil hominid, StW 573. The results are quoted initially as maximum ages, without taking into account initial disequilibrium. ^{234}U disequilibrium is dealt with in Section (6.3), where the original results are corrected and presented as best estimates. The results present the age information for this fossil that has long been sought.

Although the remaining 16 hand samples analysed were not chronologically important they played a part in producing an interesting picture of the variation in chemistry and formation of the speleothem deposits at the sites. The information they have presented is extremely useful for any future work that may be carried out.

6.1 Results selection

Results were screened for suitability on samples STA07-C; STA09; STA12; STA15; LAB03. Rejected results were affected by one or more of the following factors:

- Large blank correction - when the amount of Pb (ng) analysed was around

[1]The term isochron is used throughout the following chapter to denote plotted lines with an MSWD ≤ 10.

the same magnitude as the blank or less than it, it was usually felt that confidence could not be placed in the result. Sometimes blank corrections on particularly small samples resulted in a large increase in errors relative to the original run error. However, providing that the original run error and error correlation was good, this only affected the error ellipse by drawing it out along the isochron/plotted line.

- Errors relating to mass spectrometry - a) Samples that were subject to large errors on one or more than one of their associated measurements, eg. Pb or U run errors. b) Samples with runs that had few measurements. c) Low ^{208}Pb signal - signals below $\approx$ 2mV (0.02pA) were generally considered to be unreliable.

- Variation from expected ratios - sample results $^{207}Pb/^{204}Pb$ and $^{208}Pb/^{204}Pb$ ratios were checked against common Pb values and across sample suites. Ratios should be relatively uniform within a hand sample otherwise a mu_{208} plot could not be applied. Where ratios were spurious, bearing in mind possible initial Pb heterogeneity, the result was discounted.

- Variation in U concentration - where there were large variations in U concentrations between repeats of a sub-sample the result with the best errors throughout was taken as being more reliable.

- Apparent contamination - this was usually obvious from the Pb concentration, and particularly where repeat analyses of the same sample were compared.

The rejected results from the above samples can be found in Section (C.0.16). Individual descriptions as to why samples were rejected are provided there.

6.2 Sterkfontein

Three flowstone layers were analysed from the member 2 deposits at Sterkfontein, refer to Sections (5.1.1) and (A.2.1) for provenance. These and the samples analysed from them are discussed below. Table (6.1) displays the accepted results of the Sterkfontein samples, including those from which ages were calculated. Rejected sample results are shown in Table (C.1).

6.2.1 Flowstone layers

Refer to Figure (5.1) and Figure (6.1) for context.

Layer 2D - upper most layer

Samples STA03, STA04 and STA07-C came from the uppermost deposit of flowstone, layer 2D. The thickness of the flowstone around STA03 and STA04 is $\approx$ 70cm. STA07-C was $\approx$ 300cm to the left horizontally of STA03 at around the same height. STA03 and STA04 were $\approx$ 35cm apart horizontally and STA03 was slightly higher than STA04. These samples were close to the roof of the cave and near where the cave opening is believed to have been. Speleothems at the mouths of caves often contain higher levels of sediment than those further in (Latham and Schwarcz, 1992).

Layer 2C - middle layer

Samples STA09 and STA12 originated in the middle flowstone deposit, layer 2C. This flowstone is in close proximity to the skeleton. The thickness of the flowstone around STA09 is $\approx$ 30cm. STA09 was $\approx$ 70cm above the skull and slightly to the right. STA12 was $\approx$ 90cm below STA09 and was $\approx$ 95cm away from the skull (this was measured obliquely down the slope). It is difficult to tell how they were positioned in terms of of how high or low they within this flowstone layer, and relative to one another. STA12 was almost certainly at the base of this layer but it was not as easy to tell if this was true of STA09.

Layer 2B - bottom layer

Samples STA14, STA15 and STA16 came from the lowest flowstone deposit sampled, layer 2B. STA15 was sampled from the very base of the flowstone layer, STA16 was taken from the very top and STA14 taken from the middle. At STA16 the flowstone is $\approx$ 30cm thick. STA15 was found $\approx$ 110cm to the right of STA16 and slightly below. STA14 was $\approx$ 100cm to the left of STA16 and $\approx$ 70cm below. The distance obliquely downslope from the skull to STA16 was $\approx$ 265cm.

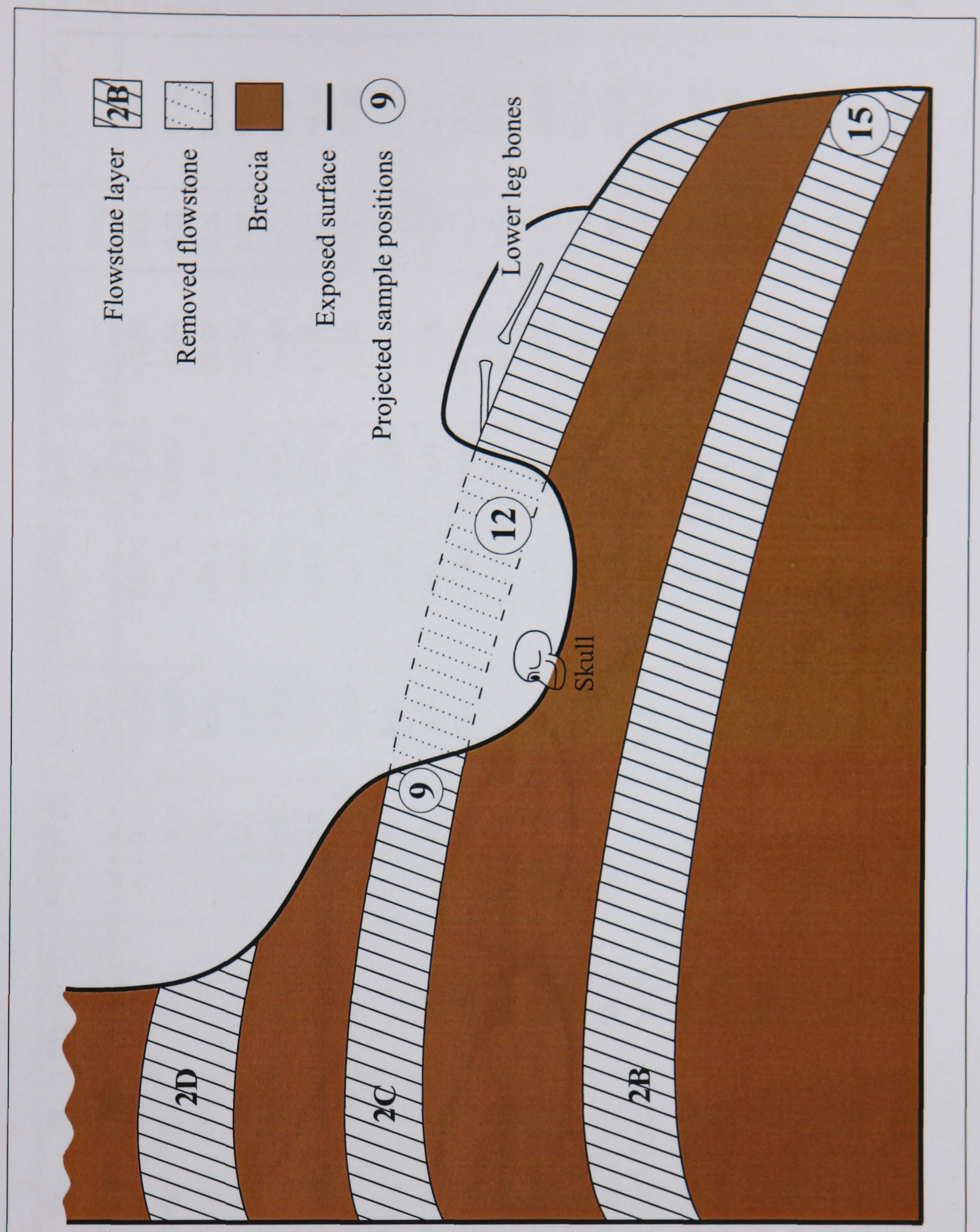

Figure 6.1: Schematic of the stratigraphy of the Silberberg Grotto showing flowstone layers 2B, 2C and 2D and the three U-Pb samples, STA09, STA12, and STA15, that yielded ages. Not to scale. Area of removed flowstone was excavated prior to sampling for the current study. Skeleton is dissected by flowstone layer 2C due to partial collapse of sediments before formation of this layer. See Section (2.2.3) for further information. After Clarke (2002a).

Sample	Date	U (ppm)	Pb (ppm)	Pb (ng)	$^{206}Pb/^{204}Pb$ before blank	$^{238}U/^{208}Pb$	Error (1σ)	$^{206}Pb/^{208}Pb$	Error (1σ)	$^{207}Pb/^{204}Pb$	Error (1σ)	$^{208}Pb/^{204}Pb$	Error (1σ)
STA03-B1-3n	16/03/04	0.022	0.0389	16.09	20.43	0.967	0.005	0.5127	0.0002	15.84	0.01	39.93	0.03
STA03-B1-3s	16/03/04	0.024	0.0425	17.59	20.69	0.949	0.005	0.5129	0.0002	16.04	0.03	40.43	0.08
STA03-B1-4▲	16/03/04	0.020	0.0254	8.978	20.55	1.301	0.011	0.5161	0.0002	15.82	0.01	39.92	0.03
STA03-B1-5△	16/03/04	0.025	0.0262	7.104	19.71	1.571	0.010	0.5030	0.0002	15.74	0.01	39.27	0.03
STA03-B1-7◇	17/02/04	0.024	0.0253	9.574	20.07	1.585	0.099	0.5074	0.0005	15.84	0.03	39.64	0.09
STA03-B2-3	16/03/04	0.030	0.0612	24.23	20.05	0.806	0.006	0.5068	0.0002	15.79	0.01	39.63	0.03
STA03-B2-4	16/03/04	0.028	0.0542	20.93	20.36	0.870	0.006	0.5107	0.0002	15.82	0.02	39.93	0.05
STA04-A4-2	17/02/04	0.015	0.0037	1.554	18.92	6.85	0.25	0.4962	0.0005	15.58	0.06	38.25	0.14
STA04-A4-3✱	17/02/04	0.021	0.0015	0.515	20.69	23.88	1.26	0.4919	0.0011	17.56	0.90	43.14	2.22
STA04-A7n	17/02/04	0.012	0.0027	1.14	19.00	7.652	0.20	0.4965	0.0006	15.65	0.03	38.44	0.09
STA04-A7s	17/02/04	0.136	0.0027	1.14	19.04	85.12	3.22	0.4975	0.0006	15.63	0.03	38.45	0.09
STA07-C5-A	09/08/04	0.510	0.0005	0.23	55.10	3068	643	2.226	0.366	17.28	0.36	38.14	0.45
STA07-C5-B	09/08/04	0.725	0.0006	0.25	71.41	5105	1269	3.263	0.691	18.01	0.58	37.02	0.59
STA07-C6-A	09/08/04	0.530	0.0005	0.228	54.66	3203	673	2.208	0.363	17.19	0.35	38.13	0.45
STA07-C6-B	09/08/04	0.658	0.0017	0.75	32.27	779.7	32.4	0.921	0.018	15.90	0.04	37.45	0.11
STA09-A2-2	24/05/04	0.807	0.0011	0.493	41.11	1652	119	1.235	0.054	17.05	0.11	38.49	0.16
STA09-B2-1	24/05/04	0.852	0.0026	1.125	28.49	626.6	16.3	0.768	0.007	16.04	0.04	38.50	0.07
STA09-B2-1	04/10/04	0.866	0.0036	1.562	25.45	441	8	0.683	0.004	15.84	0.02	38.02	0.05
STA09-C1-1	24/05/04	0.577	0.0015	0.629	29.61	776.9	36.7	0.822	0.016	16.12	0.05	38.63	0.11
STA09-C2-1A	27/01/04	0.764	0.0031	0.479	25.46	454.2	9.6	0.680	0.004	15.94	0.04	38.37	0.09
STA09-C2-1A	29/03/04	0.904	0.0034	1.329	⋆	490.5	28.7	0.694	0.012	⋆	⋆	⋆	⋆
STA09-C2-1B	15/10/03	0.957	0.0032	1.354	26.46	570.4	12.1	0.726	0.005	15.71	0.09	37.39	0.2

Sample	Date	U (ppm)	Pb (ppm)	Pb (ng)	$^{206}Pb/^{204}Pb$ before blank	$^{238}U/^{208}Pb$	Error (1σ)	$^{206}Pb/^{208}Pb$	Error (1σ)	$^{207}Pb/^{204}Pb$	Error (1σ)	$^{208}Pb/^{204}Pb$	Error (1σ)
STA09-C2-1B	29/03/04	1.345	0.0048	0.396	⋆	525.1	37.2	0.710	0.016	⋆	⋆	⋆	⋆
STA09-C2-1C	29/03/04	1.341	0.0014	0.593	⋆	2472	164	1.541	0.07	⋆	⋆	⋆	⋆
STA09-C2-1D	27/01/04	1.158	0.0043	1.853	25.58	496.6	7.7	0.692	0.003	15.86	0.04	37.66	0.11
STA09-C2-1D	29/03/04	1.287	0.0020	0.871	⋆	1389	53	1.075	0.023	⋆	⋆	⋆	⋆
STA09-C2-2	15/10/03	0.860	0.0021	0.885	30.07	823.3	27.8	0.834	0.012	16.04	0.13	37.93	0.31
STA09-C2-2	27/01/04	0.961	0.0025	1.061	28.94	758.7	21.2	0.807	0.009	15.70	0.1	37.30	0.23
STA09-C2-2	29/03/04	0.933	0.0024	0.907	⋆	747.9	24.3	0.803	0.010	⋆	⋆	⋆	⋆
STA12-A1♦	27/04/04	0.429	0.0014	0.453	26.06	595.1	37.4	0.733	0.016	16.01	0.06	38.17	0.14
STA12-A2	27/04/04	0.494	0.0004	0.186	45.03	3276	757	1.814	0.308	17.57	0.46	37.92	0.49
STA12-B2-A1	27/04/04	0.374	0.0008	0.366	29.41	882.3	72.6	0.853	0.031	16.50	0.09	38.69	0.18
STA12-B3-A	04/10/04	0.312	0.0011	0.46	25.46	548.9	33.7	0.719	0.015	15.66	0.06	37.82	0.14
STA12-C1-A2s	27/04/04	0.469	0.0009	0.383	31.56	1095	89	0.940	0.037	16.34	0.09	38.07	0.18
STA12-C1-A2	04/10/04	0.493	0.0012	0.529	28.23	789.6	44.2	0.817	0.019	15.71	0.05	37.15	0.13
STA14-A1	09/12/03	0.059	0.0042	1.82	19.51	23.33	0.34	0.4965	0.0005	16.11	0.03	39.49	0.07
STA14-A2	28/07/04	0.260	0.0015	0.649	23.45	311.7	13.1	0.638	0.007	15.81	0.04	38.12	0.11
STA14-A3	28/07/04	0.369	0.0029	1.263	23.90	226.4	4.9	0.631	0.003	15.90	0.03	38.67	0.08
STA14-A4	28/07/04	0.170	0.0033	1.41	21.68	90.15	1.71	0.564	0.002	15.93	0.04	38.92	0.08
STA14-B3	09/12/03	0.050	0.0023	0.968	18.94	37.39	0.99	0.504	0.0008	15.59	0.04	37.77	0.1
STA14-B4	09/12/03	0.048	0.0115	4.93	18.71	6.97	0.04	0.4912	0.0003	15.65	0.02	38.17	0.05
STA14-B5-A	28/07/04	0.045	0.0033	1.422	18.85	23.12	0.42	0.5004	0.0005	15.60	0.02	37.80	0.06
STA14-B5-B	28/07/04	0.052	0.0016	0.702	18.88	53.20	1.93	0.505	0.001	15.56	0.04	37.62	0.09
STA14-C1	09/12/03	0.039	0.022	9.453	18.94	2.92	0.01	0.4924	0.0003	15.70	0.02	38.54	0.05
STA14-C2	09/12/03	0.043	0.0061	2.627	17.96	11.69	0.12	0.4823	0.0003	15.44	0.02	37.29	0.05

Sample	Date	U (ppm)	Pb (ppm)	Pb (ng)	$^{206}Pb/^{204}Pb$ before blank	$^{238}U/^{208}Pb$	Error (1σ)	$^{206}Pb/^{208}Pb$	Error (1σ)	$^{207}Pb/^{204}Pb$	Error (1σ)	$^{208}Pb/^{204}Pb$	Error (1σ)
STA15-01	25/03/03	1.009	0.0043	2.125	25.42	430.2	6	0.691	0.003	15.80	0.13	37.38	0.31
STA15-02	25/03/03	1.246	0.0068	2.852	24.09	332.3	3.6	0.645	0.002	16.00	0.14	37.75	0.33
STA15-03	25/03/03	0.528	0.0052	2.202	22.14	175.9	2.3	0.5822	0.0014	15.89	0.07	38.39	0.18
STA15-04	25/11/03	1.269	0.0102	4.098	21.87	217.5	1.6	0.5858	0.0008	15.72	0.03	37.55	0.08
STA15-05◊	25/11/03	1.248	0.0031	0.86	31.24	825.8	29.4	0.885	0.014	15.94	0.22	37.34	0.51
STA15-A2-B	23/08/04	0.838	0.0024	1.055	30.62	670.2	18.8	0.811	0.009	16.65	0.05	39.55	0.09
STA15-A2-C	23/08/04	1.103	0.0018	0.76	40.71	1406	63	1.131	0.029	17.25	0.09	39.54	0.13
STA15-A2-D	23/08/04	0.930	0.0023	0.99	31.91	809.7	24.7	0.853	0.011	16.80	0.04	39.41	0.09
STA15-A2-F	23/08/04	0.737	0.0024	1.04	29.19	587.6	16.4	0.766	0.008	16.93	0.05	39.75	0.09
STA15-B2-A1	14/06/04	1.176	0.0043	1.863	26.72	512.3	7.9	0.724	0.004	15.84	0.02	37.68	0.04
STA15-B2-A2	14/06/04	1.109	0.0039	1.668	27.23	543.8	9.5	0.739	0.004	15.86	0.02	37.69	0.04
STA15-B2-A3	14/06/04	1.021	0.0033	1.441	28.27	585.6	11.9	0.761	0.006	16.12	0.03	38.22	0.06
STA15-B3-A	14/06/04	1.362	0.0047	2.016	27.87	558.6	8.2	0.758	0.004	15.93	0.01	37.51	0.04
STA15-B3-B	14/06/04	1.291	0.0049	2.115	26.68	495.5	6.8	0.721	0.003	15.91	0.01	37.67	0.04
STA16-A1	25/11/03	0.025	0.0048	2.054	19.59	8.866	0.117	0.4968	0.0004	16.20	0.15	39.63	0.36
STA16-A2⊠	25/11/03	0.024	0.0069	1.665	18.73	5.733	0.096	0.4916	0.0003	15.65	0.04	38.21	0.1
STA16-A3	25/11/03	0.025	0.0115	4.927	18.91	3.667	0.031	0.4941	0.0003	15.68	0.02	38.37	0.06
STA16-A5⊡	09/12/03	0.045	0.0093	0.926	18.86	8.063	0.782	0.4933	0.0005	15.72	0.03	38.42	0.08

Table 6.1: Table of Sterkfontein sub-sample suite results. Sub-sample weights are 430 ± 50mg apart from the following samples; ▲ - 353mg; △ - 271mg; ◎ - 378mg; ⊛ - 345mg; ♦ - 334mg; ◊ - 282mg; ⊠ - 242mg; ⊡ - 100mg. The blank applied was 92.9 ± 0.25pg. Blank corrections ranged between 0.383% and 49.94%. ⋆ - STA09-C2 samples from 29/03/04 were run with the ^{204}Pb on the SEM without an appropriate yield correction, resulting in a bias in all of the ^{204}Pb ratios - therefore these have been removed.

6.2.2 STA03

Petrography

STA03 is a clean-looking sample with a dark band $\approx$ 1.5cm thick running through the middle, see Figures (6.2), (6.3) and (6.4). This could be of organic or detrital origin. The material below this band is slightly darker than that above it. The crystals are small and some mm sized cavities can be seen in between. The top surface of the sample is very white and powdery. A thin layer of sediment is attached to the lower surface of the sample.

U and Pb concentrations and distribution

Refer to Figures (6.3) and (6.4) for positioning of STA03 sub-samples.

There appears to be a higher concentration of U in the centre of the sample on the U image, Figure (6.2), although it is not very clear. This could coincide with the darker band. U concentrations are uniformly low for this sample, ranging from 19.8 ppb to 29.5 ppb, Table (6.1). Unfortunately this is coupled with high Pb concentrations of 25.3 ppb to 61.2 ppb. When combined, these result in very low mu_{208} values and a narrow range in mu_{208}, from which a meaningful plot can not be constructed. It is evident that this sample had incorporated a significant amount of common Pb. It could be that the darker layer present in this sample is a layer of detritus, and that the cave at this time was more open and sediments were being incorporated with the speleothem as it formed.

6.2.3 STA04

Petrography

STA04 is a very dense sample. Cutting vertically through the sample reveals elongated crystals, $\approx$ 0.5cm in length. The exposed face appears dusty and chalky, refer to Figure (6.5) and Figure (6.7). The face of the sample that was not exposed to the cave environment has large tightly packed crystals, see Figure (6.6). Although the material seems pure, some colouration is apparent; in cross-section

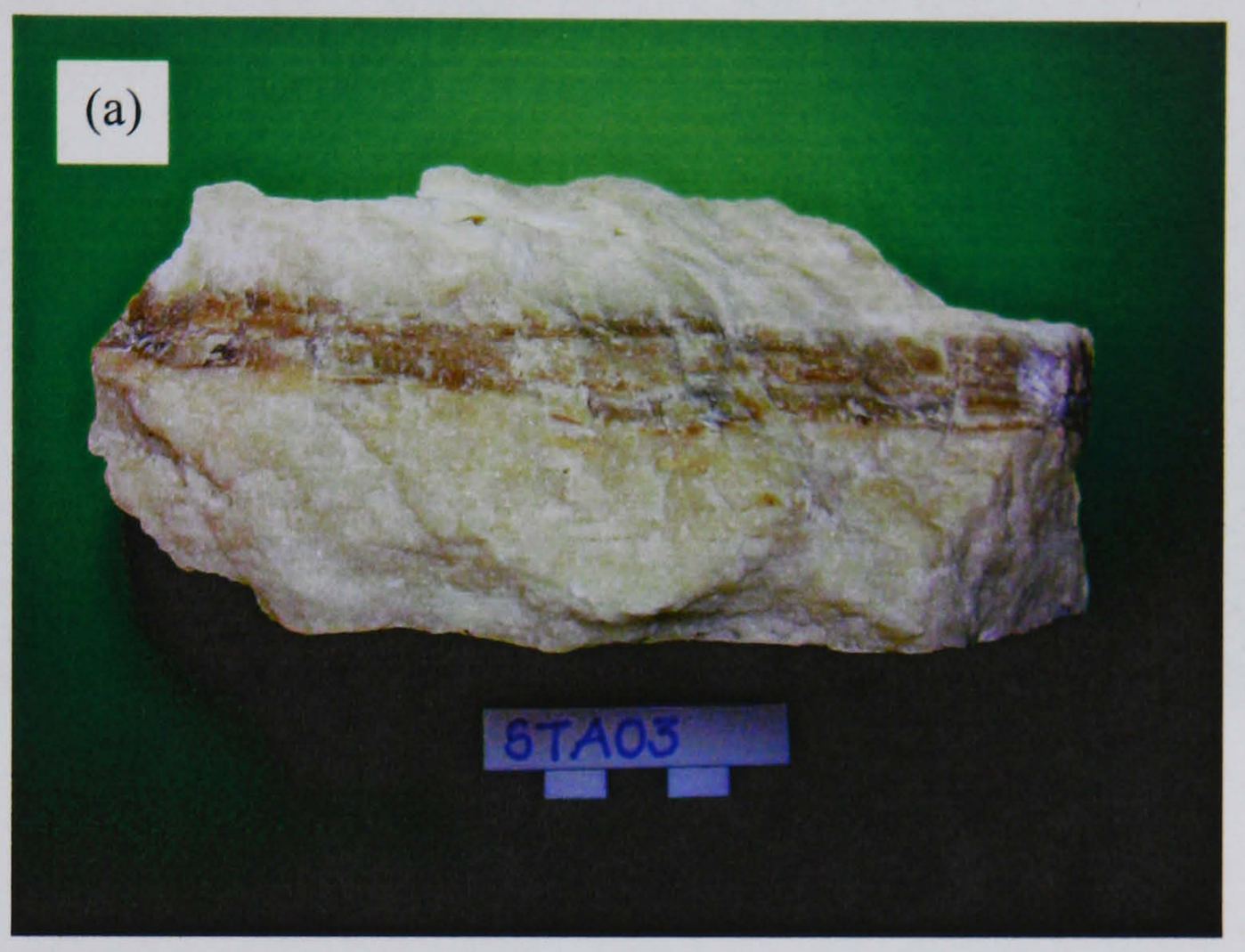

Figure 6.2: Photograph of sample STA03 before sub-sampling (a) showing darker band of flowstone near the top - scale shown in cm; uranium image of the same (b).

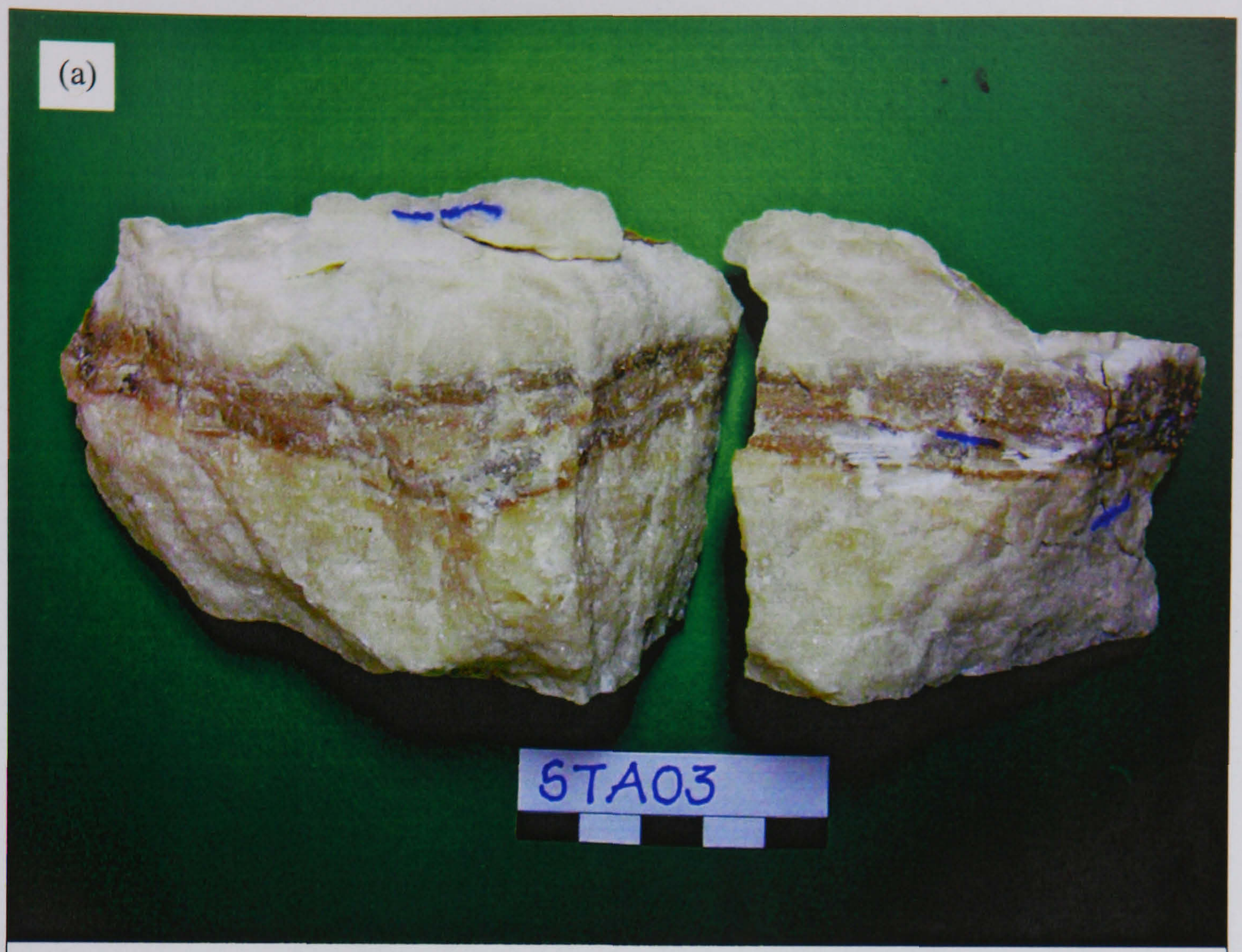

Figure 6.3: Photograph of STA03-A and STA03-B (a) - scale shown in cm; corresponding schematic of sub-samples taken from these (b). The arrow shows the vertical orientation of the sample in situ.

(b)

STA03-B2

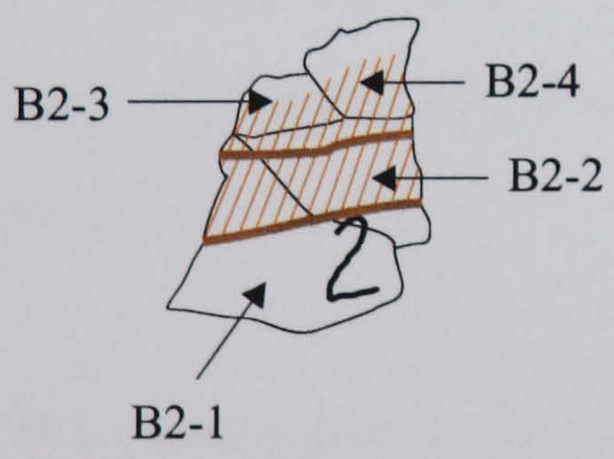

STA03-B1

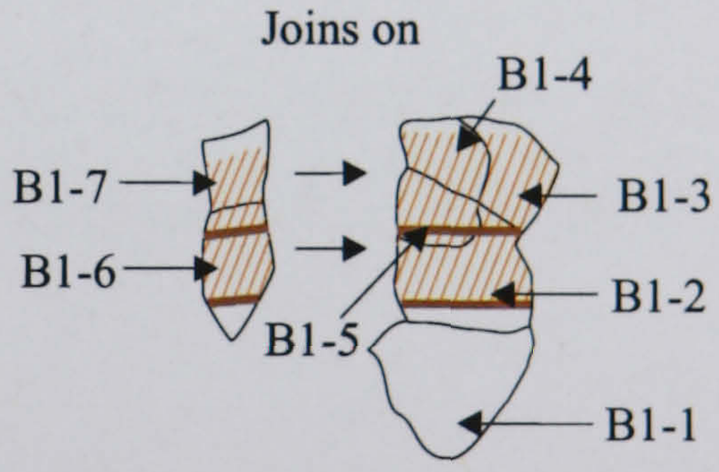

4 & 5 overlay 3 & 2)

Figure 6.4: Photograph of sample STA03-B with sub-samples B1 and B2 detached, but in place (a) - scale shown in cm; schematic of sub-samples B1 and B2 following further separation (b). Brown shading relates to darker layers of flowstone. The arrow shows the vertical orientation of the sample in situ.

bands of light brown material can be seen running through the calcite. These bands vary in thickness from ≈ 1mm to >1cm. The top surface of the sample has a rind of very white, fine-grained material, 3 or 4mm in thickness.

U and Pb concentrations and distribution

Refer to Figures (6.6) and (6.7) for positioning of STA04 sub-samples.

The U image, Figure (6.5) shows a very even distribution of U in slightly lower concentration than in STA03. Like STA03, STA04 suffers from very low U concentrations, with a minimum of 12.2 ppb and a maximum of 136 ppb, Table (6.1). Pb concentrations are considerably lower than STA03 though. They range from 1.5 ppb to 3.7 ppb. Despite a wider range in mu_{208} values than STA03, the data do not define a line.

6.2.4 STA07-C

Petrography

STA07-C appears to be a very pure sample. It is composed of large colourless columnar crystals, which are densely packed. There is an outer rind of dirt, and the material on the exposed faces of the fragments has a slightly different texture, see Figure (6.8).

U and Pb concentrations and distribution

Refer to Figure (6.8) for positioning of STA07-C sub-samples.

Despite being in the same flowstone layer as STA03 and STA04 this sample has much higher U concentrations. These vary between 0.51 ppm and 1.25 ppm, Table (6.1). The visual appearance of purity in this sample is confirmed by the Pb concentrations, which are as low as 0.53 ppb and peak at 1.7 ppb. C2 has double the U concentration of the other sub-samples, although apart from the brown layer there is not much visible difference in the material sampled to indicate why this is the case.

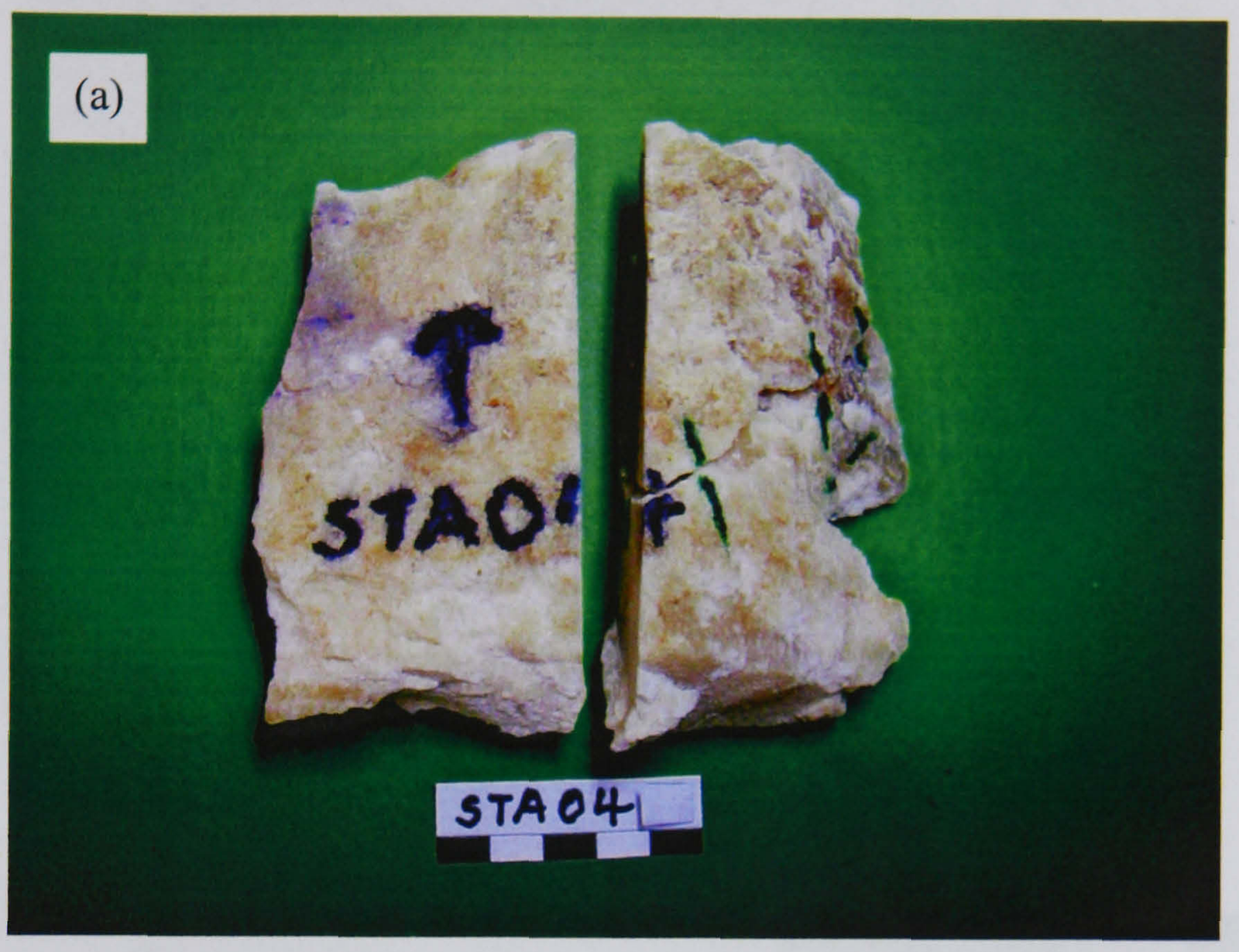

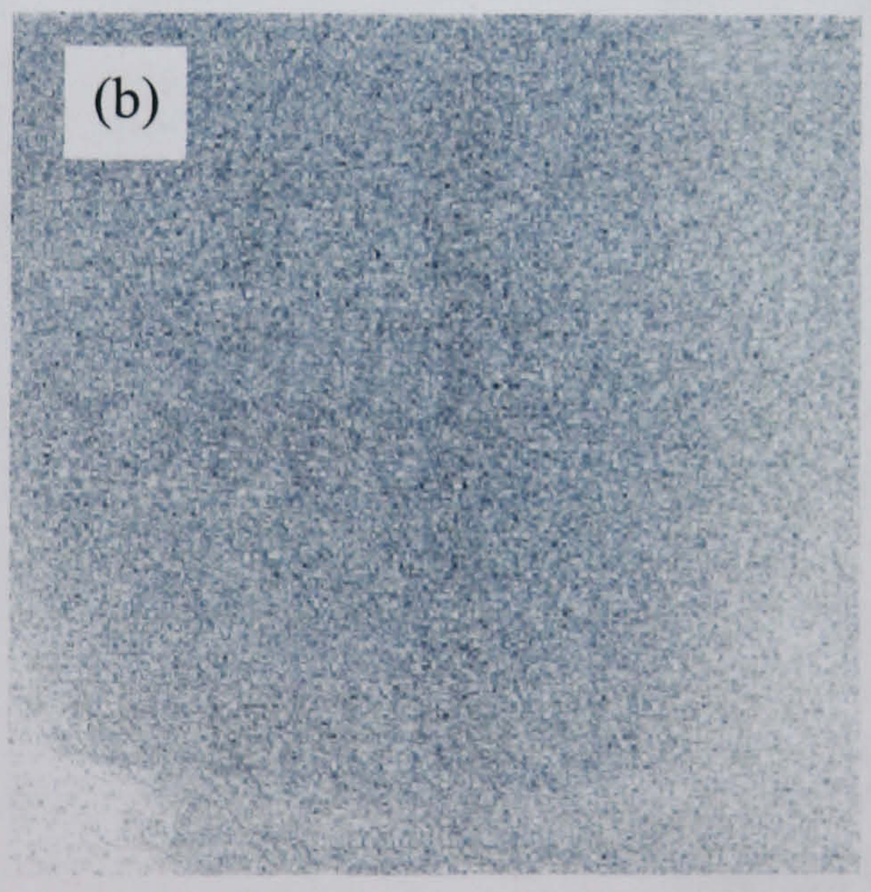

Figure 6.5: Photograph of front of sample STA04 after initial dissection but prior to sub-sampling (a) - scale shown in cm; uranium image of STA04 before any dissection (b).

(c)

STA04 sign facing down

Orientation

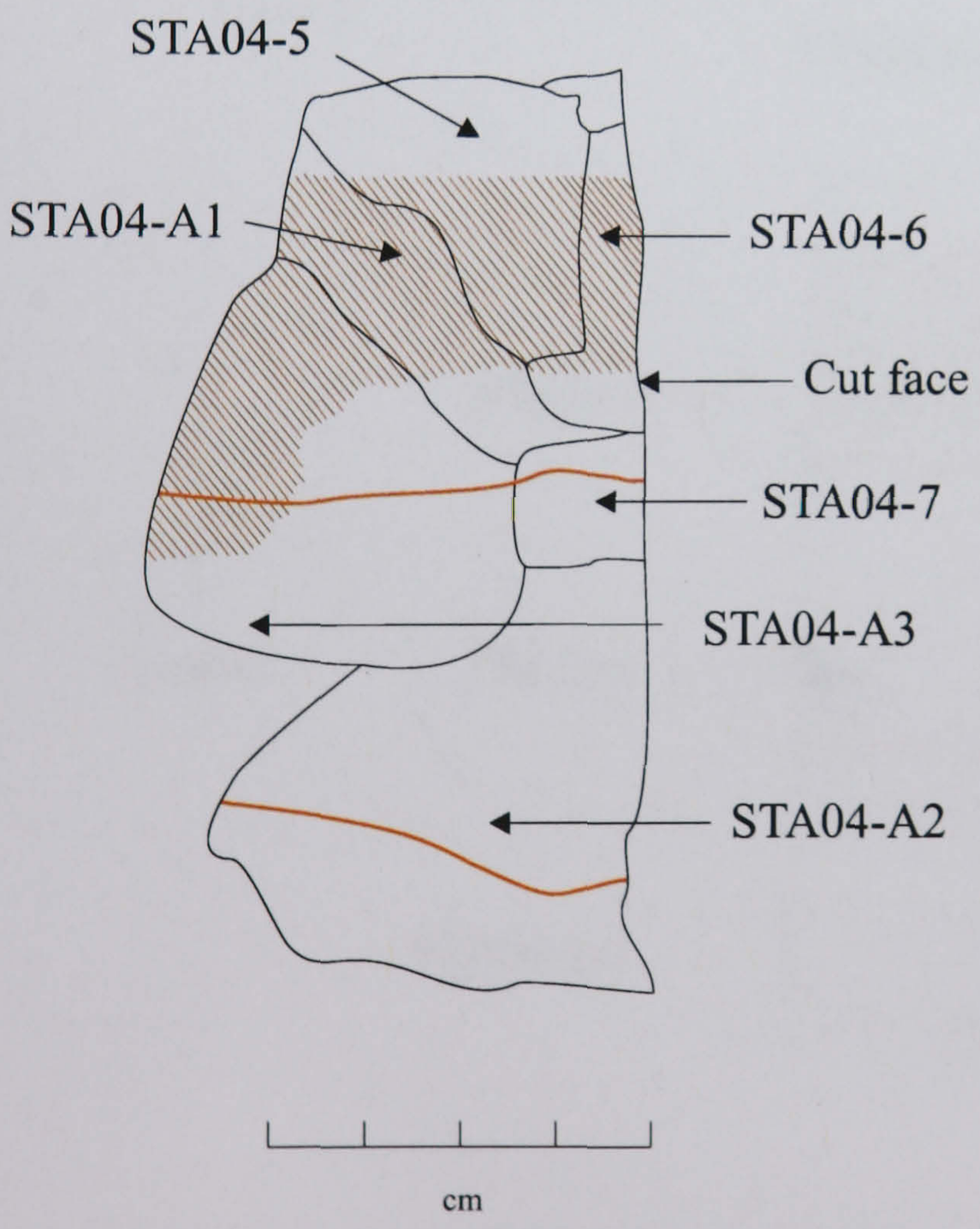

Figure 6.6: Photograph of reverse side of STA04 after sub-sampling (a). Photograph of reverse of STA04-A showing divisions into sub-samples (b); schematic of the same (c). Scale on (a) and (b) shown in cm. The arrow shows the vertical orientation of the sample in situ. Brown shading relates to darker layers of flowstone.

(a)

STA04-A

(b)

STA04 sign facing up

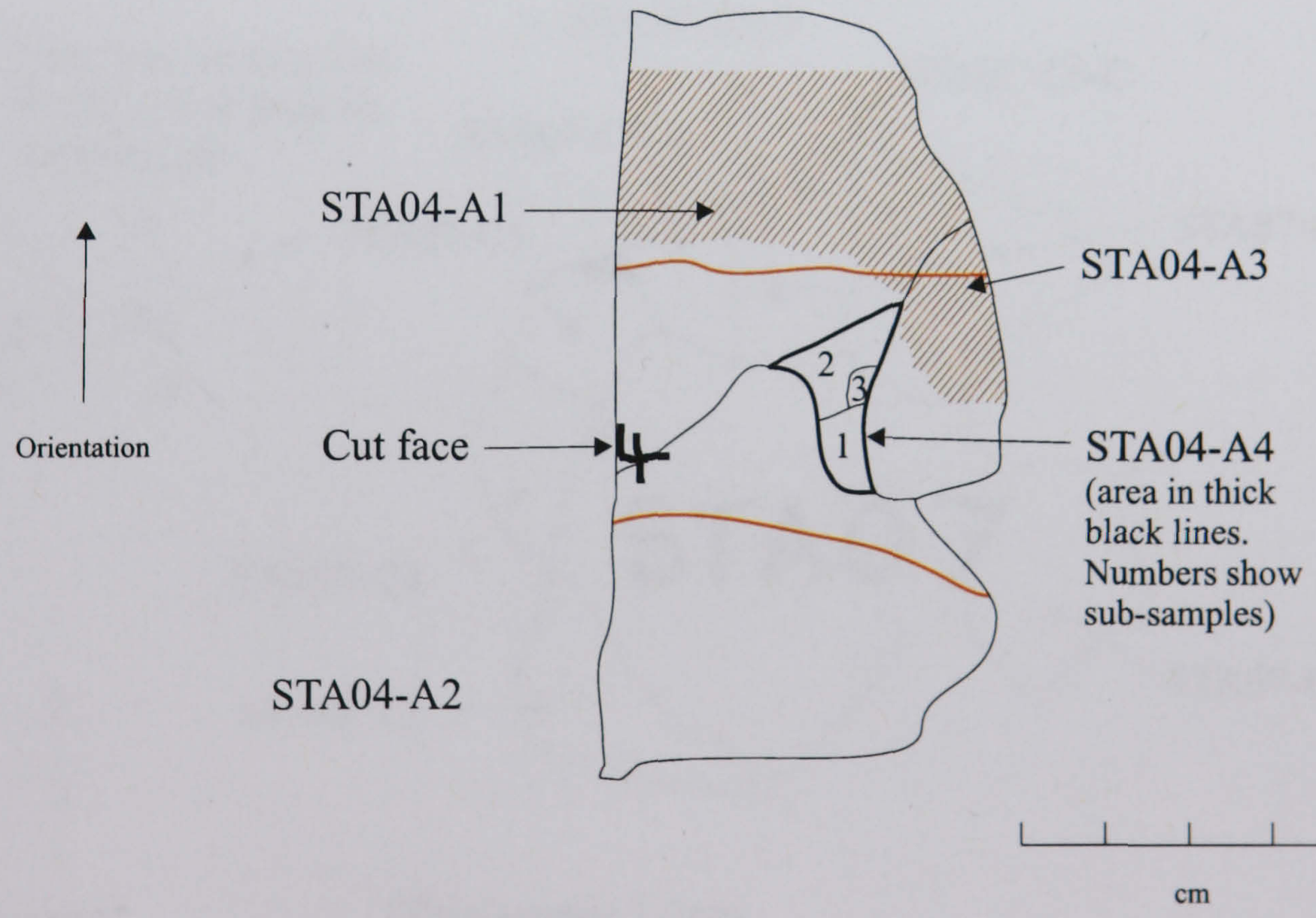

Figure 6.7: Photograph of front of STA04-A showing sub-sample divisions (a) - scale shown in cm; schematic of the same but also showing further sub-sampling of STA04-A4 (b). The arrow shows the vertical orientation of the sample in situ. Brown shading relates to darker layers of flowstone.

(a)

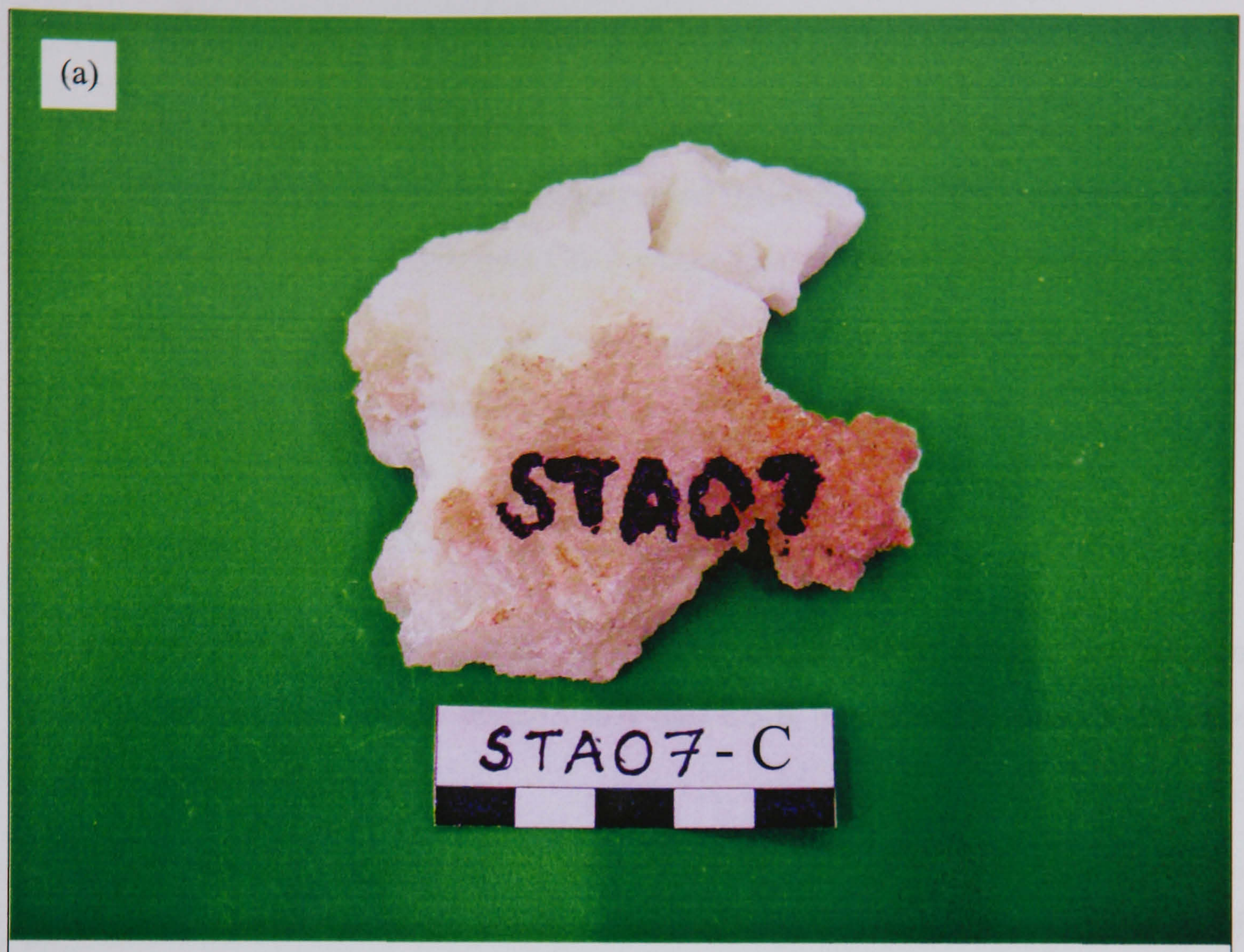

(b)

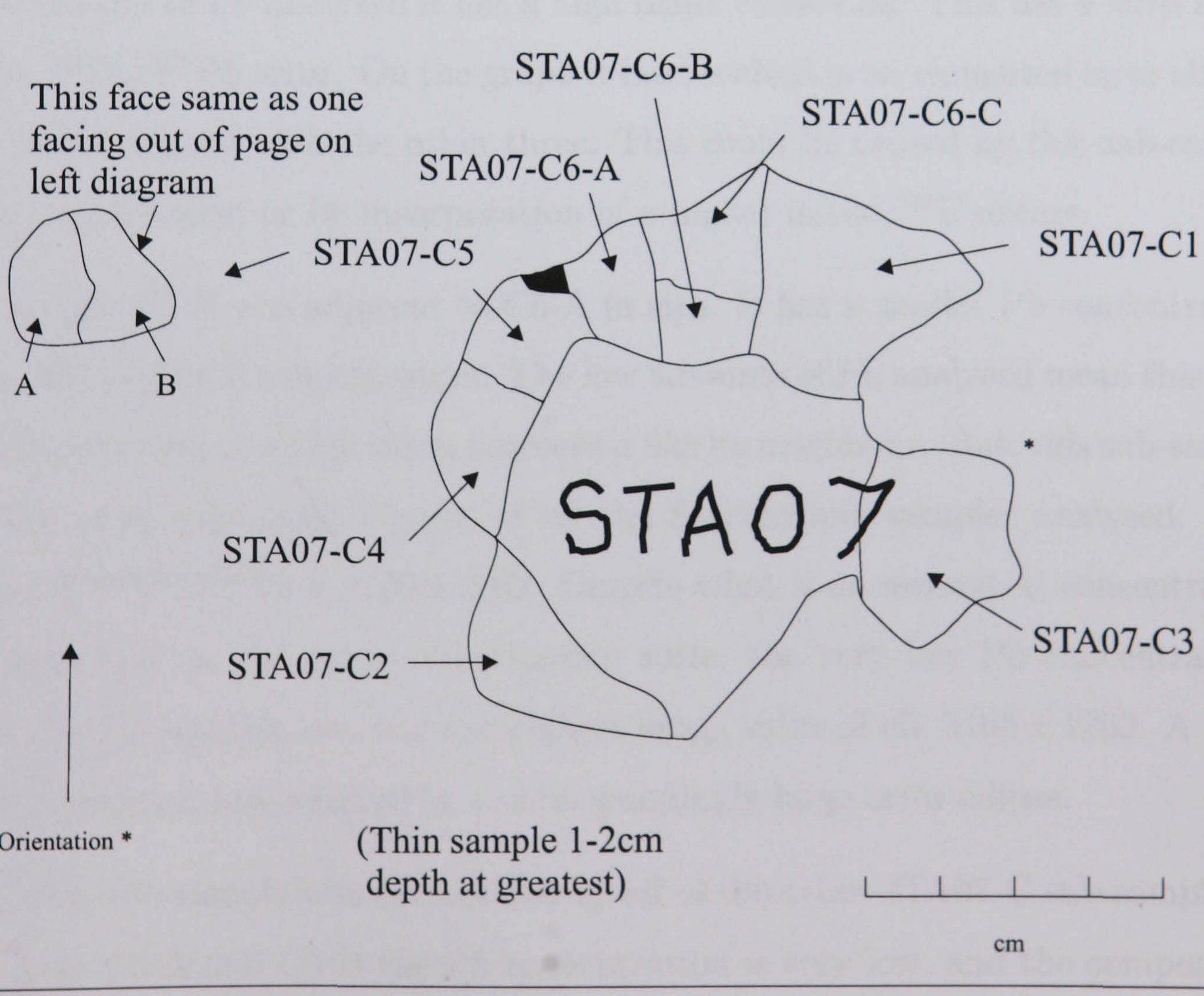

Figure 6.8: Photograph of STA07-C prior to sub-sampling (a) - scale shown in cm; schematic showing positions of sub-samples after sample division (b). The arrow shows the vertical orientation of the sample in situ.

Isochrons

The STA07-C data are displayed on one plot, Figure (6.9). Due to the positioning of the data points no line could be constructed using Isoplot. This is probably due to positioning of results C5-A and C6-A either side of where the line would lie.

Refer to Table (6.1) for numerical results plotted. Rejected numerical results can be found in Table (C.1) in the Appendix.

Sub-samples C5-A, C5-B, C6-A and C6-B

On the STA07-C plot these samples show a general alignment along a line but are fairly scattered. The scatter of the C5-A and C6-A points either side of this line makes it unresolvable.

C5-A has the lowest U concentration and the second lowest Pb concentration, resulting in a relatively high mu_{208}. This sub-sample has a high proportion of radiogenic Pb; the corrected $^{206}Pb/^{208}Pb$ is 2.23 ± 0.37. However, because of the small amount of Pb analysed it has a high blank correction. This has a large effect on the $^{206}Pb/^{208}Pb$ error. On the graph it has resulted in an elongated error ellipse. This is not aligned with the other three. This could be caused by this sub-sample being slightly older or by incorporation of a higher initial ^{234}U excess.

Sub-sample C5-B was adjacent to C5-A in situ. It has a similar Pb concentration but a 30% higher U concentration. The low amounts of Pb analysed mean this sub-sample is subject to a high blank correction like its neighbour. But, this sub-sample has the most radiogenic Pb out of all the Sterkfontein samples analysed. The corrected $^{206}Pb/^{208}Pb$ is 3.26 ± 0.69. Despite what is an average U concentration in comparison to the entire Sterkfontein suite, the very low Pb concentrations mean this sub-sample also has the highest mu_{208} value of all, 5105 ± 1269. A large blank correction has resulted in a correspondingly large error ellipse.

The C6-A sub-sample was surrounded by all of the other STA07-C sub-samples in situ. Like C5-A and C5-B the Pb concentration is very low, and the composition of this sample is most comparable to C5-A. However on the graph these two points are diverging from each other.

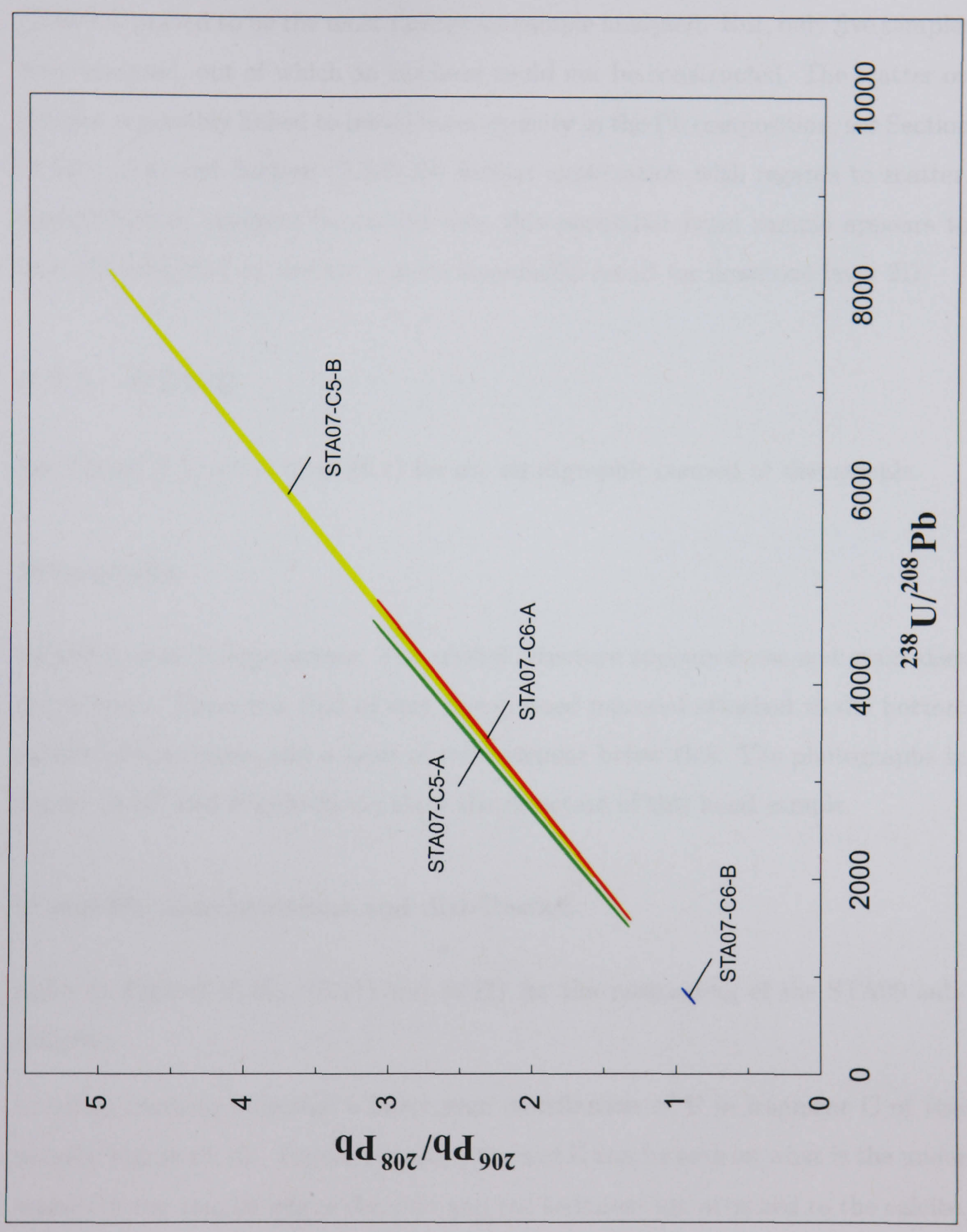

Figure 6.9: STA07-C data plot. Error ellipses are plotted at 2σ level. Each colour represents an individual sub-sample. Sample is from flowstone layer 2D.

Although the C6-B sub-sample has a comparable U concentration to its neighbour, C6-A, its Pb concentration of 1.73ppb is more than three times higher. This means this sub-sample is the lowest point on the graph.

STA07-C proved to be the most radiogenic sample analysed. But, only five samples were analysed, out of which an isochron could not be constructed. The scatter on the plot is possibly linked to initial heterogeneity in the Pb composition; see Section (4.2.3), (5.4) and Section (7.3.2) for further explanation with regards to scatter. Should further analyses be carried out, this particular hand sample appears to have the potential to provide a more meaningful result for flowstone layer 2D.

6.2.5 STA09

See Figure (5.1) and Figure (6.1) for the stratigraphic context of this sample.

Petrography

STA09 is clean in appearance. The crystal structure appears dense and grain sizes are $\approx$ 1mm. There is a rind of very fine-grained material attached to the bottom surface of the calcite and a layer of red sediment below this. The photographs in Figure (6.10) and Figure (6.11) show the structure of this hand sample.

U and Pb concentrations and distribution

Refer to Figures (6.10), (6.11) and (6.12) for the positioning of the STA09 sub-samples.

Uranium imaging indicates a fairly even distribution of U in fragment C of this sample, Figure (6.10). Higher concentrations of U can be seen on what is the under surface of the sample where the rind and red sediment are attached to the calcite. This would seem to suggest that the higher concentrations of U are actually found in the areas which contain detrital material. There also appears to be a fine layer of higher U concentration running through the middle of fragment C.

The U concentrations in the sub-samples range from 0.58ppm to 1.35ppm, see Table (6.1). The highest concentrations are found in the sub-samples analysed

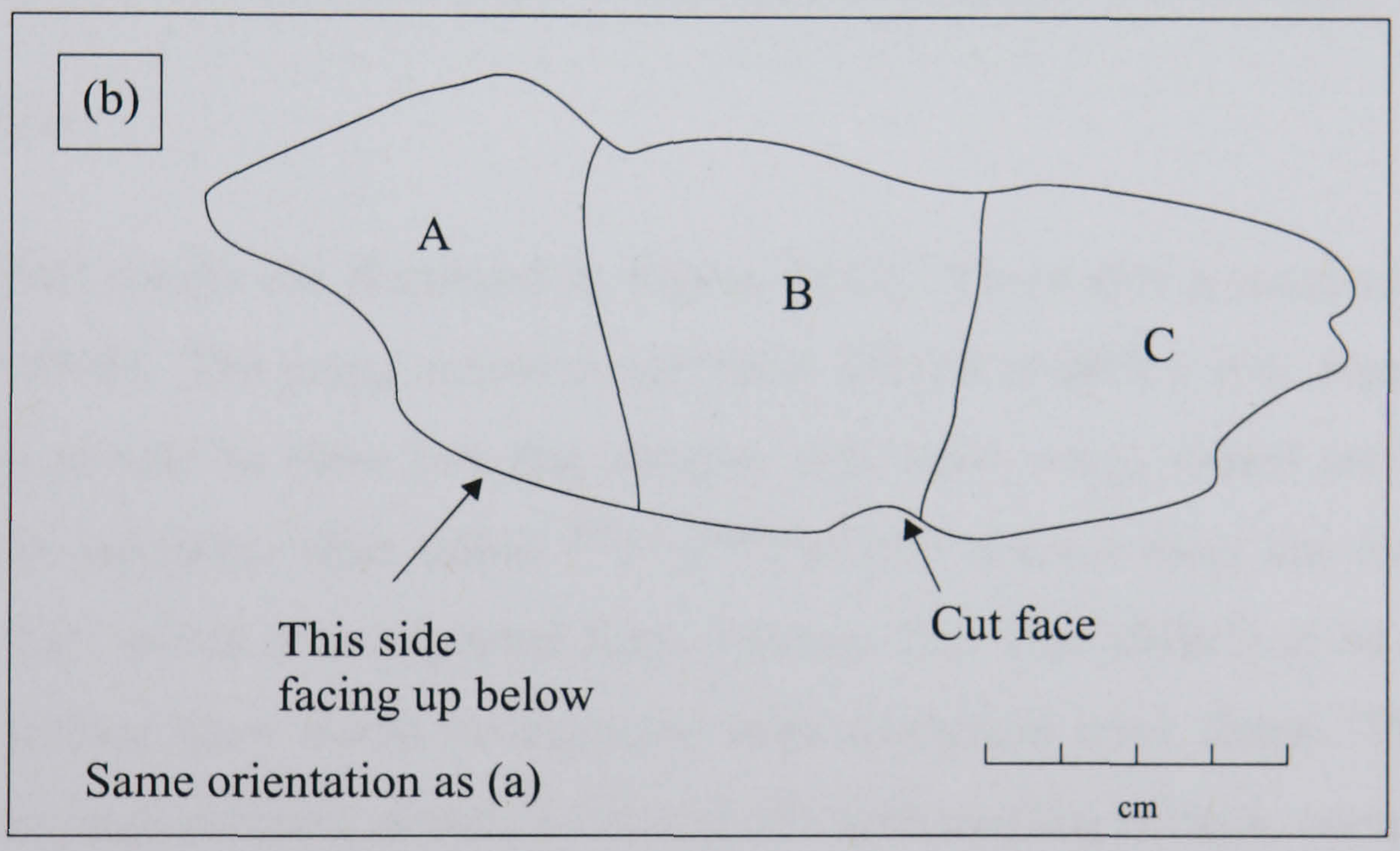

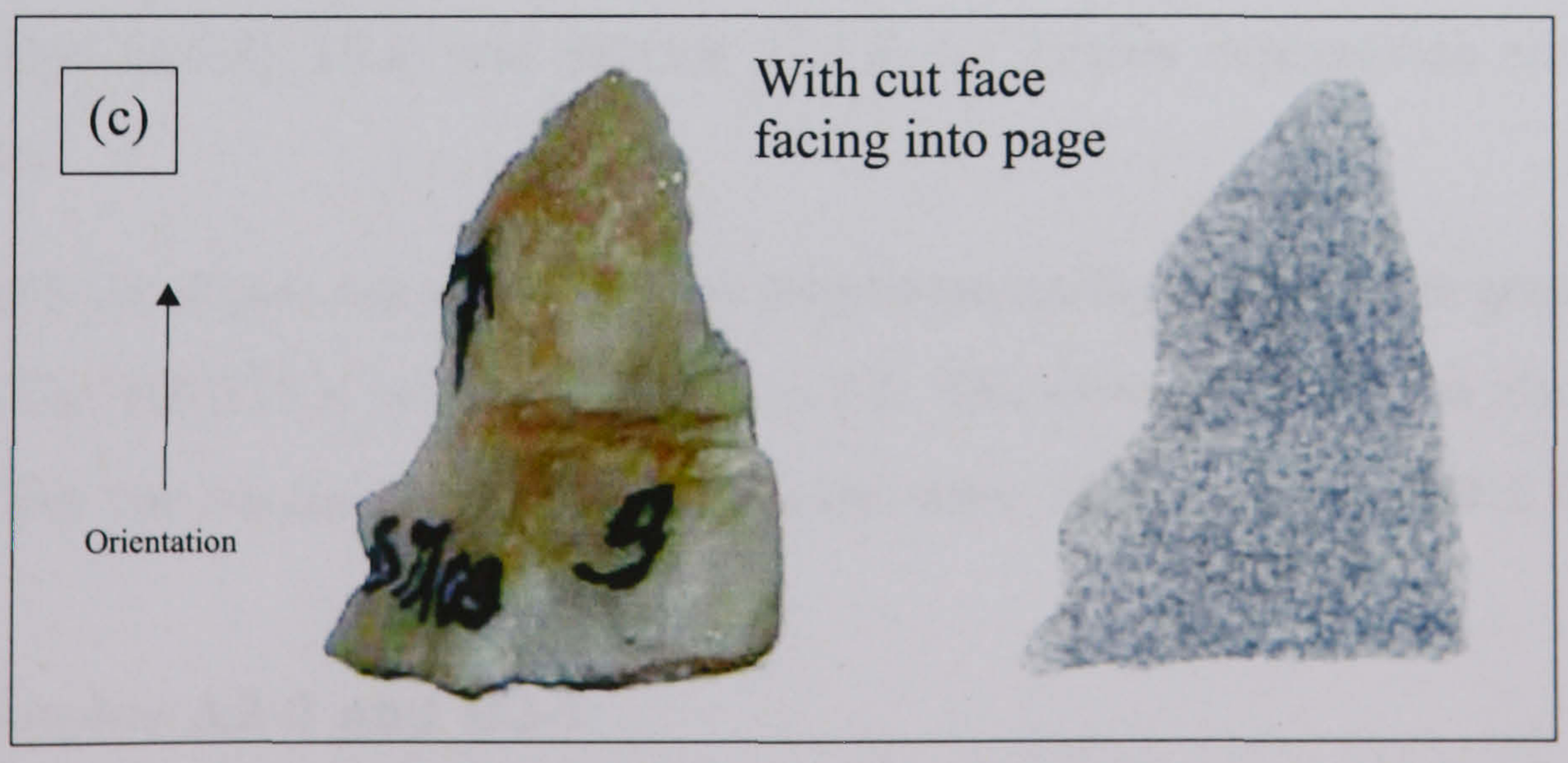

Figure 6.10: Photograph of STA09 from above after division into three pieces (a) - scale shown in cm; schematic (plan view) of the same (b). Photograph of front face of STA09-C and corresponding uranium image (c). The arrow shows the vertical orientation of the sample in situ.

from fragment C2. Concentrations in C2 are $\geq$ 0.76ppm. Fragments A2, B2 and C1, meanwhile, all have concentrations which are $\leq$ 0.87ppm. Sub-sample C1-1 comes from the lower half of STA09 (fragments A1, B1 and C1) and is the only point plotted on the isochron from these fragments. Inspection of the hand sample shows that the top half, represented by fragments A2, B2 and C2, is made of the larger crystals which are tightly packed, whereas the lower half of the hand sample is more fine-grained. The results seem to indicate that the U content of the upper half is slightly higher. The highest U concentrations in the main fragment analysed, C2, are to be found in the sub-samples, 1B and 1C. Although adjacent to each other they had no features to distinguish them from the other sub-samples of C2.

Pb concentrations in the sub-samples are as low as 1.1 ppb, ranging up to 4.8 ppb.

Isochrons

The STA09 results are displayed in Figure (6.13). These give a maximum age of 2.72 ± 0.10 Ma. The mu_{208} values ranged from 441 ± 8 to 2472 ± 164. Figure (6.14) has been plotted to show how the samples with lower mu_{208} values are arranged about the isochron. The initial $^{206}Pb/^{208}Pb$ ratio derived from the isochron is 0.489 ± 0.01 which is as expected from common Pb. The MSWD of 39 indicates greater scatter than would be expected from analytical error alone. This could be due to incorporation of initial detrital Pb with varying isotopic compositions. See Section (4.2.3), (5.4) and Section (7.3.2) for further explanation with regard to scatter.

If an isochron of just C2 is plotted the improvement in the scatter is great, Figure (6.15). The MSWD is reduced from 39 to 7.9. The error on the age is also reduced by half but the maximum age itself does not alter significantly, 2.749 ± 0.051.

Sub-samples A2-2 and B2-1

Figure (6.13) and Figure (6.14).

Sub-sample A2-2 is one of the three high points on the isochron. The Pb concentration is very low - 1.1 ppb - and the U concentration is also low - 0.81 ppm. The

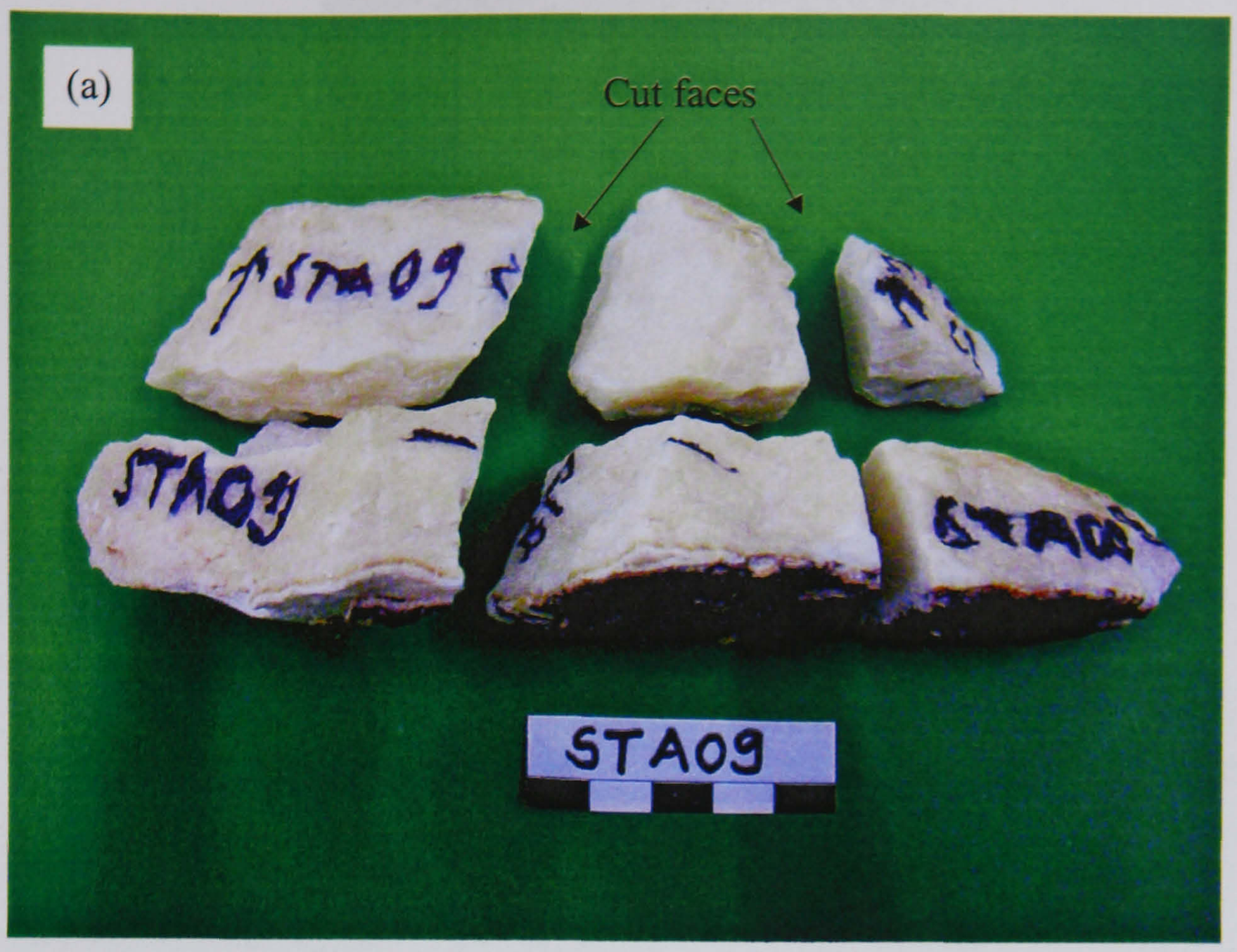

(b)

Orientation

STA09-A **STA09-B** **STA09-C**

STA09-A2
STA09-A1
STA09-B2
STA09-B1
STA09-C2
STA09-C2-2
STA09-C2-1
STA09-C1

Cut faces facing into page on STA09-A and STA09-B

STA09-C orientated as above

cm

Figure 6.11: Photograph of front face of STA09 after division into six pieces (a) - scale shown in cm; schematic of these pieces following further division (b). The arrow shows the vertical orientation of the sample in situ.

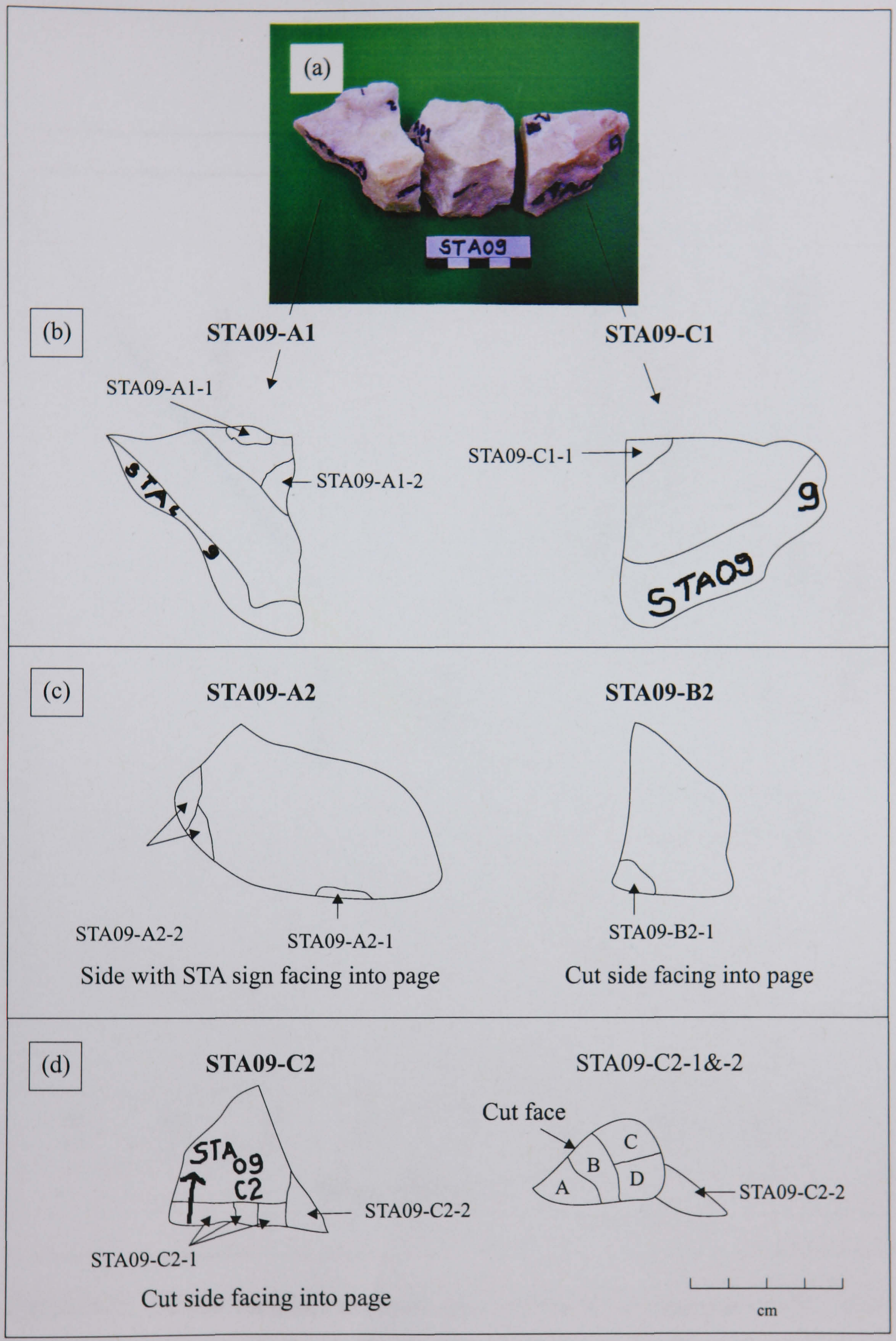

Figure 6.12: Photograph of STA09-A1, STA09-B1 and STA09-C1 from above (a) - scale shown in cm; corresponding schematic for A1 and C1 showing sub-samples (b). Schematic of STA09-A2 and STA09-B2 (c) and STA09-C2 (d), with sub-sample positions. Compare with Figure (6.11) for context of other sub-samples.

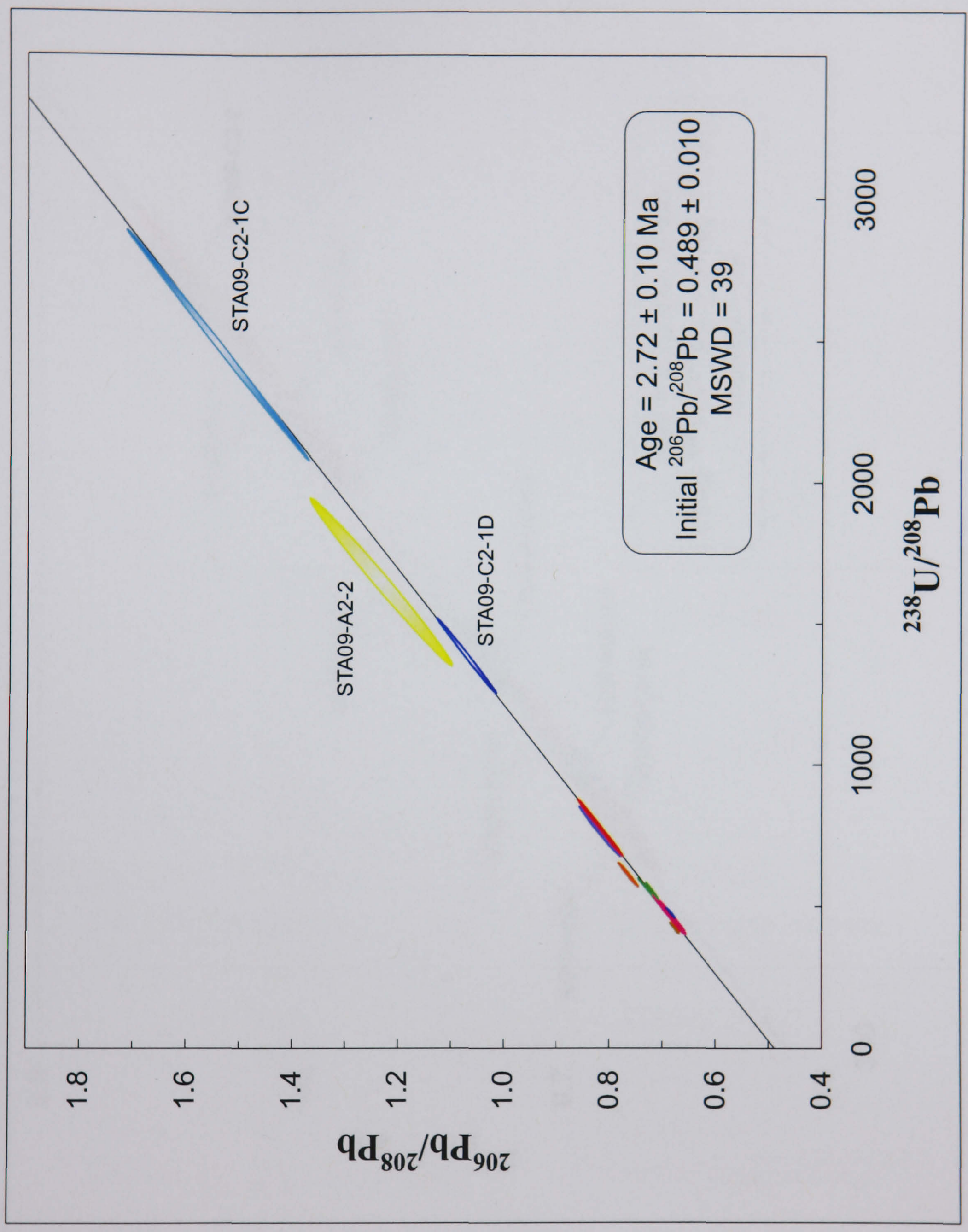

Figure 6.13: STA09 complete isochron. Age calculated is a maximum age. Error ellipses are plotted at 2σ level. Each colour represents an individual sub-sample. Sample is from flowstone layer 2C.

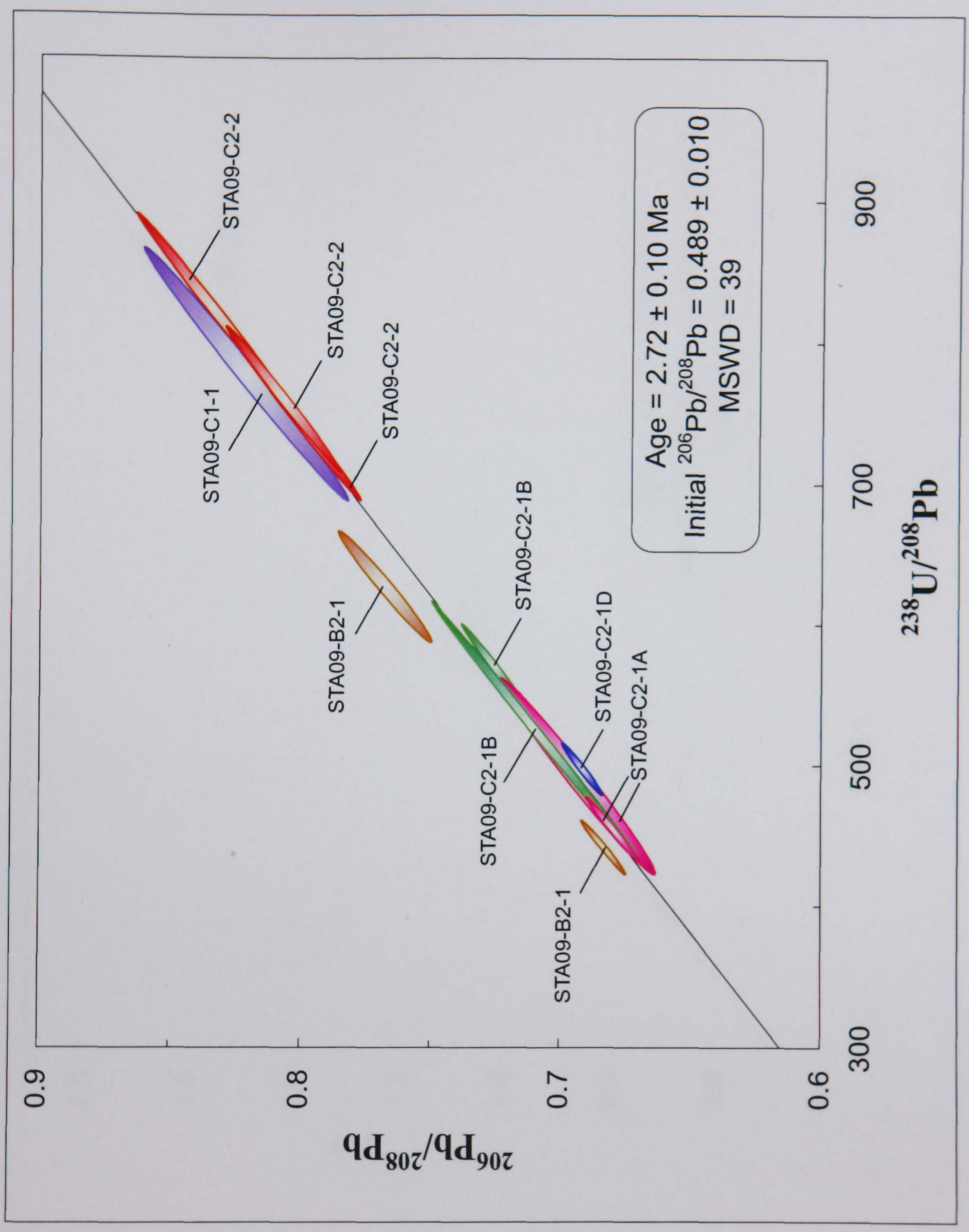

Figure 6.14: STA09 isochron showing points with $mu_{208} \leq 900$. Age calculated is a maximum age. Error ellipses are plotted at 2σ level. Each colour represents an individual sub-sample. Sample is from flowstone layer 2C.

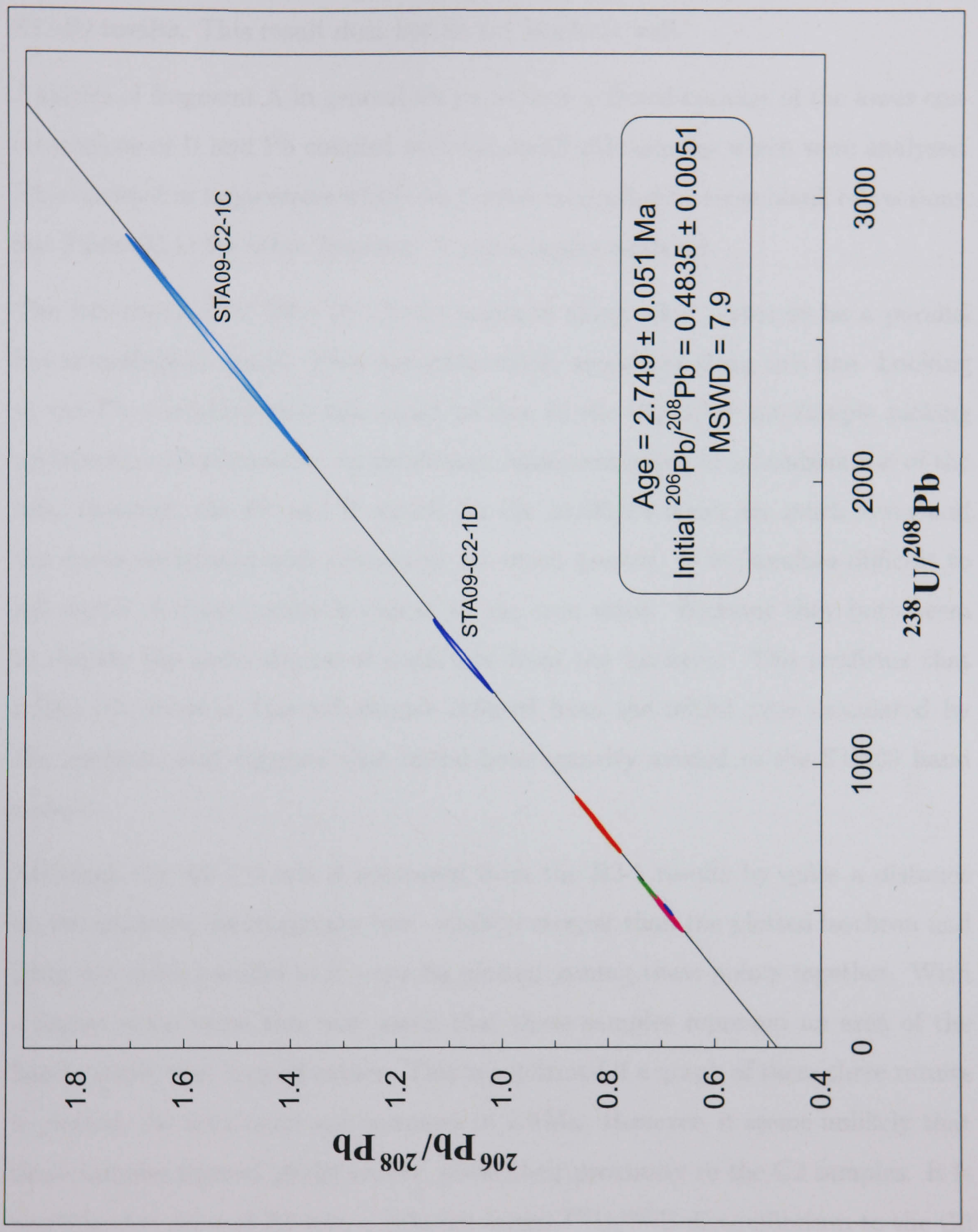

Figure 6.15: STA09 isochron of C2 sub-samples only. Age calculated is a maximum age. Error ellipses are plotted at 2σ level. Each colour represents an individual sub-sample. Sample is from flowstone layer 2C.

confidence in this result is lessened somewhat by the fact that it has no repeat to back it up, and because only 42% of the expected U measurements were recorded[2]. Despite this the errors pre-blank correction are comparable with the rest of the STA09 results. This result does not fit the isochron well.

Analysis of fragment A in general seems to have suffered because of the lower concentrations of U and Pb coupled with the small sub-samples which were analysed. This resulted in large errors which are further magnified by large blank corrections. See Table (C.1) for other fragment A sub-samples analysed.

The two repeats[3] of B2-1 lie off the isochron along what seems to be a parallel line of radiogenic decay. They are quite widely separated along this line. Looking at the Pb concentrations this could be due to the 04/10/04 sub-sample picking up labware contamination, an insufficient blank correction or a combination of the two. However, the Pb and U signals for the 24/05/04 result are much lower and the errors associated with this result are much greater. It is therefore difficult to tell which of these results is closest to the true value. However they both seem to display the same degree of departure from the isochron. This confirms that initial Pb ratios in this sub-sample differed from the initial ratio calculated by the isochron, and suggests that initial heterogeneity existed in the STA09 hand sample.

Although the A2-2 result is separated from the B2-1 results by quite a distance on the isochron, an imaginary line - slightly steeper than the plotted isochron and lying not quite parallel to it - can be plotted joining these points together. With a higher slope value this may mean that these samples represent an area of the hand sample that formed earlier. This is confirmed if a graph of these three results is plotted, the maximum age increases to 2.9 Ma. However, it seems unlikely that these samples formed 200 ky earlier, given their proximity to the C2 samples. It is possible that A2 and B2 had a different initial $^{234}U/^{238}U$ disequilibrium to the C2

---

[2]The TIMS was set up to measure the U signal 50 times for each run. Where there was a problem with a run, such as low signal intensity, this number of measurements was not always achieved. In this case only 21 measurements were taken; this is 42% of those expected.

[3]Where a sub-sample has been analysed more than once the repeats are differentiated from one another by being referred to by the date on which they were analysed, e.g. the B2-1 repeats of 04/10/04 and 24/05/04.

samples, making them appear older.

Sub-samples C2-1A, C2-1B, and C2-1D

Figure (6.13), Figure (6.14) and Figure (6.15).

Excepting the 29/03/04 repeat of C2-1D these results are found in a cluster on the lower half of the plot. Two repeats of each of the samples are plotted.

The results for the C2-1A repeats compare favourably with each other and agree within error. The 27/01/04 repeat has the lowest U concentration in the STA09-C2 suite of sub-samples. In spite of the lower U concentration, the 27/01/04 repeat has much better errors than the 29/03/04 repeat, on both the Pb and the U runs. The larger analytical errors on the 29/03/04 result are displayed by the much bigger error ellipse.

The C2-1B repeats agree within error, but show varying U and Pb concentrations. This could be due to volumetric or weighing errors on one of the samples. The blank correction on the 29/03/04 repeat is large but this is inevitable with such a small sample amount - 83.2 mg. But, the errors on the Pb run for 29/03/04 are better than the 15/10/03 repeat. The 15/10/03 lies just below the isochron on the plot, but its error ellipse overlaps that of the 29/03/04 result, which is found on the line.

The Pb and U concentration for the two repeats of C2-1D plotted on the isochron do not agree well. However, there is no evidence to reject either of these two. The 29/03/04 repeat has a 10% higher concentration of U but 50% less Pb than the 27/01/04 repeat. Pb variation can probably be accounted for by the difference in the actual blank level and the average blank applied. The difference in U is not as easy to understand, although the 29/03/04 repeat has much higher errors of 1‰ on the measured $^{238}U/^{236}U$ ratio. In Figure (6.14) and Figure (6.15) the 27/01/04 result is found within the cluster of STA09-C2 results. The 29/03/04 repeat is found in Figure (6.13) and Figure (6.15) although it is considerably higher up than the 27/01/04 repeat because of its much greater mu_{208} value.

Sub-sample C2-1C

Figure (6.13) and Figure (6.15).

Sub-sample C2-1C has the largest mu_{208} value and displays the largest errors on the STA09 isochron. This sub-sample has the second highest U concentration of the STA09 results associated with the second lowest Pb concentration. As a consequence of the low Pb concentration, the blank correction has had a significant effect on the error associated with this sub-sample.

Sub-samples C1-1 and C2-2

Figure (6.14) and Figure (6.15).

These two samples are grouped above the cluster of STA09-C2 results. The position of C1-1 slightly above the C2-2 results indicates that this part of the hand sample had a slightly different chemistry to that of C2-2.

C1-1 has one of the lowest U concentrations for STA09, 0.58 ppm, and a correspondingly low Pb concentration, 1.5 ppb. Pb measurements are good, despite a low signal intensity. However, the low signal intensity of the U results has resulted in errors of 4‰ on the final $^{238}U/^{236}U$ ratio. Since this sub-sample does not have a replicate it is impossible to assess how representative this result is of this sub-sample. Like the other samples from the lower half of STA09 (A1-1 and A1-2 - See Table (C.1)) this sub-sample has considerably lower U concentrations in comparison to the upper half results of STA09.

In contrast to the single C1-1 result, the three repeats of C2-2 confirm this result very well. The concentrations, $^{206}Pb/^{208}Pb$ ratios and mu_{208} values of these repeats are sometimes, but not always, within analytical error of each other. However, their excellent fit on the isochron and close proximity to each other supports the results. The associated errors are low and are not severely affected by the blank correction. The repeat from 15/10/03 is slightly higher up the isochron than the other two. This could be due to over correction for the blank, yet the U concentration is lower for this sub-sample too.

STA09-C2 results

The STA09-C2 results compliment each other well and define the isochron. In spite of variations in U and Pb concentrations within sub-sample repeats, these sub-samples formed with the same initial Pb ratios and can be seen to have evolved along an isochron. This is confirmed when these results are plotted on their own in Figure (6.15).

6.2.6 STA12

See Figure (5.1) and Figure (6.1) for the stratigraphic context of this sample.

Petrography

This sample has a white layer of calcite on top of of a dark layer, see Figure (6.16). The dark layer appears to be brown flowstone rather than flowstone that is contaminated with sediment. When compared with the red sediment attached to some of the hand samples this material is crystalline rather than grainy and it is translucent, where the red detrital sediment is not. The white material is composed of hexagonal shaped crystals of $\approx$ 0.5mm. There is no visible layering within the white material. This could mean that this is one layer in itself that was deposited rapidly, or it could mean that this material is recrystallised as this results in the loss of primary structures such as layering (Murphy, P. (2005) pers. comm.). The darker material appears to be denser than the white and has slightly larger grains which can be seen extending down through a growth layer. Some of the darker crystals appear quite needle-like in shape. This could be evidence of primary aragonite. On fragment A there is a rind of material with a denser texture in between the light and dark deposits, suggesting a break in deposition between these two. STA12 seems to be slightly less dense than STA09 and small cavities can be seen under the hand lens. The bottom of the sample has a thin coating of red mud very like that attached to the bottom of STA09.

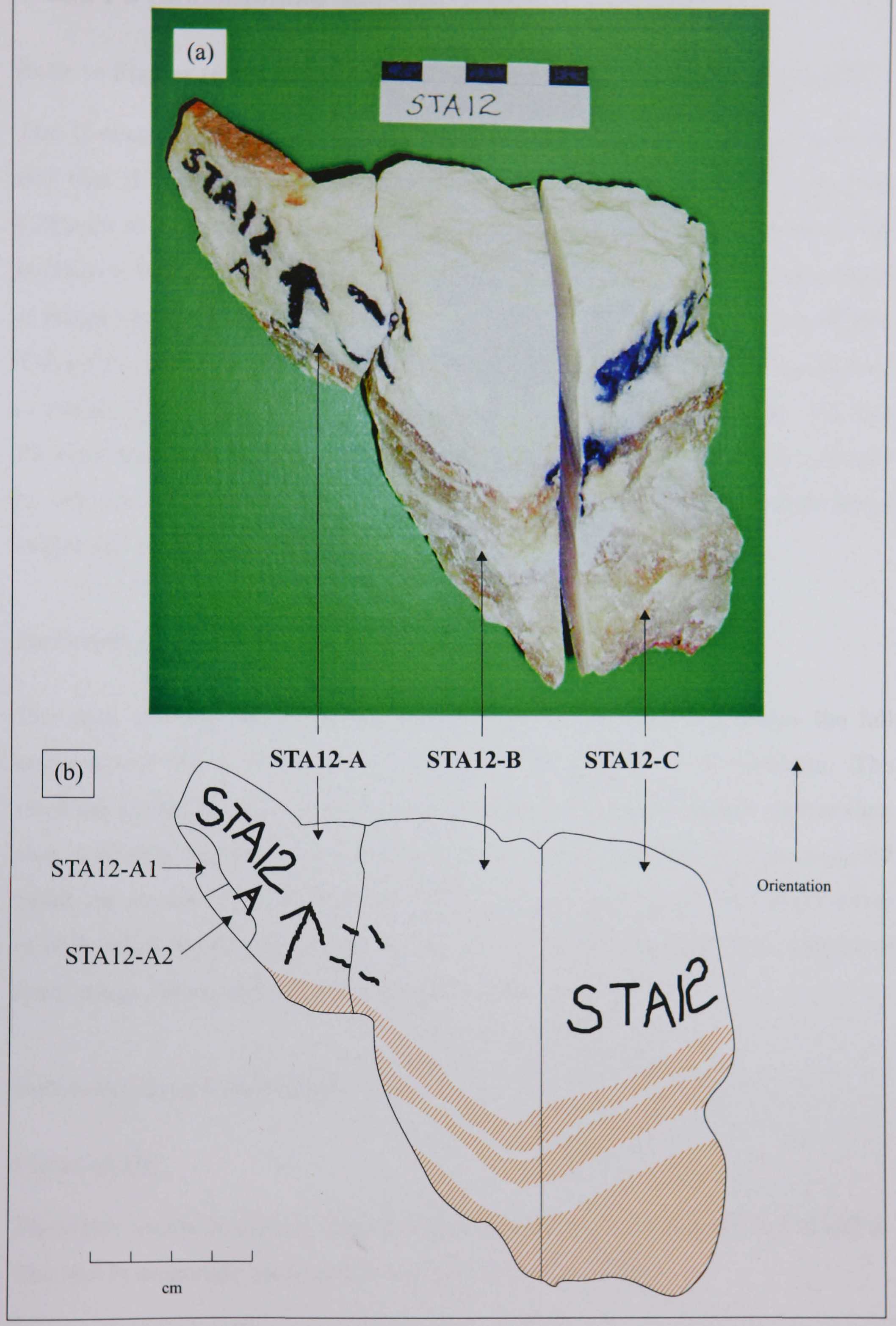

Figure 6.16: Photograph of STA12 after division into three pieces (a) - scale shown in cm; schematic of the same showing STA12-A sub-samples (b). Brown shading relates to darker layers of flowstone. The arrow shows the vertical orientation of the sample in situ.

U and Pb concentrations and distribution

Refer to Figures (6.16), (6.17) and (6.18) for positioning of STA12 sub-samples.

The U concentrations are considerably lower than those for STA09 despite the fact that they are in the same flowstone layer. They have a narrow range from 0.31 ppm to 0.54 ppm. The highest U concentration of the samples plotted on the isochron is 0.49 ppm. Fragment B seems to have low U concentrations whilst those of fragments A and C are higher. Pb concentrations are also lower than STA09. The lowest value being only 0.43ppb, and the highest 1.4ppb. B3-A was composed of mainly white material but did have some of the darker material too. The low Pb concentrations in this sample confirm that his darker layer has been coloured by organic acids rather than detrital sediment. STA12 has relatively high mu_{208} values and an adequate range from 595.1 ± 37.4 to 3276 ± 757.

Isochrons

The data are plotted in two figures for STA12. Figure (6.19), shows the full isochron and Figure (6.20) focuses just on the low points on the isochron. The resulting maximum age is 2.598 ± 0.052 Ma. Scatter on this isochron is better than that of STA09, MSWD is 2.8. If an isochron is plotted without the high mu_{208} A2 result the maximum age is 2.64 ± 0.12 Ma. The two ages are are well within error of each other showing that good isochrons can be still achieved with samples of lower mu_{208} values that have a relatively narrow range.

Sub-samples A1 and B3-A

Figure (6.20).

These two results lie slightly overlapping at the very bottom of the STA12 isochron. The line is seemingly anchored in between these two ellipses.

A1 has the highest Pb concentration of the samples on the isochron. It was adjacent to A2 in situ, and U concentrations between the two are comparable. Pb concentrations, however, are three times higher in A1. Good U and Pb measurements have resulted in low errors. Being low down the isochron means a relatively

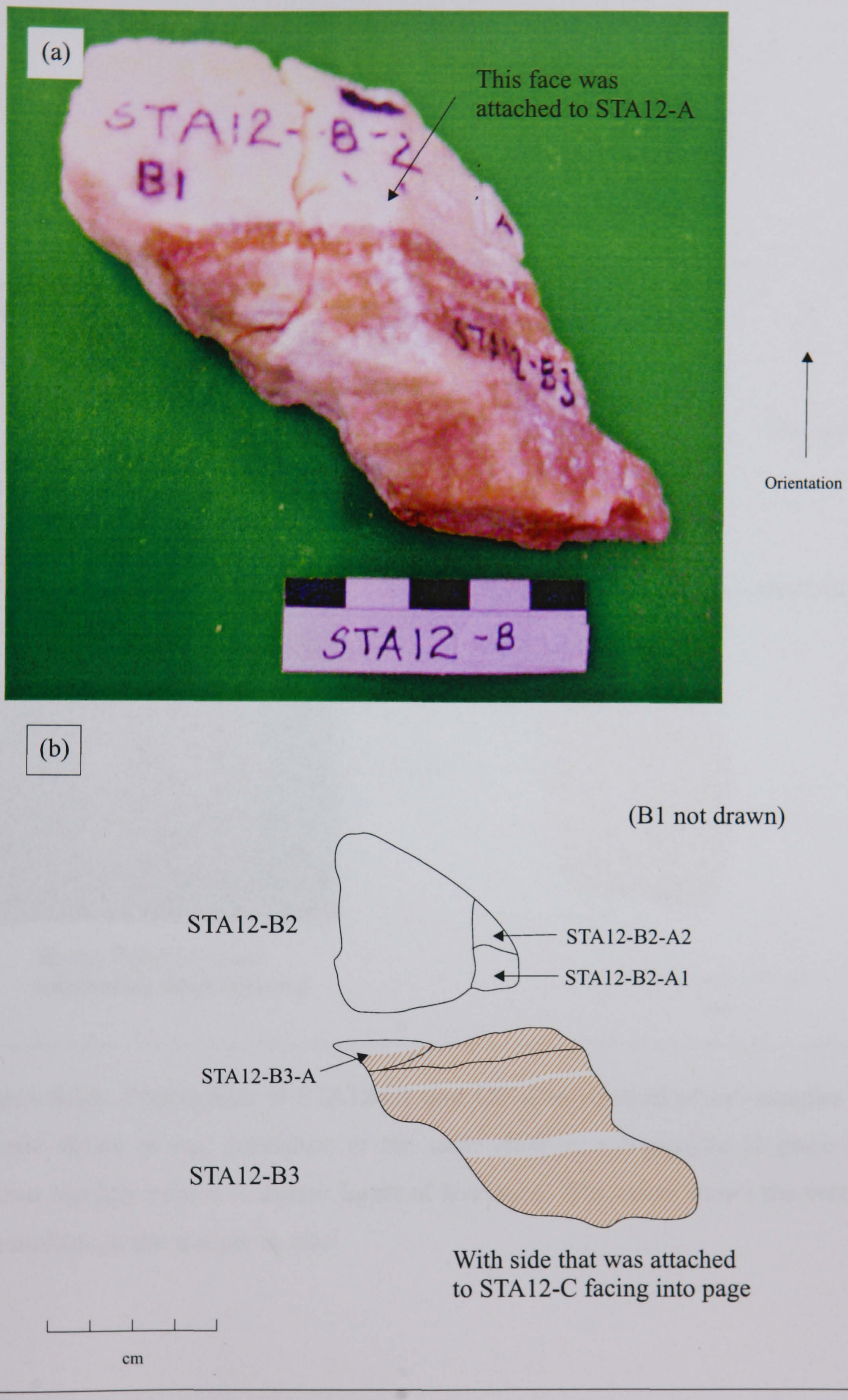

Figure 6.17: Photograph of STA12-B showing sub-samples (a) - scale shown in cm; schematic of the same, minus fragment B1 (b). Brown shading relates to darker layers of flowstone. The arrow shows the vertical orientation of the sample in situ.

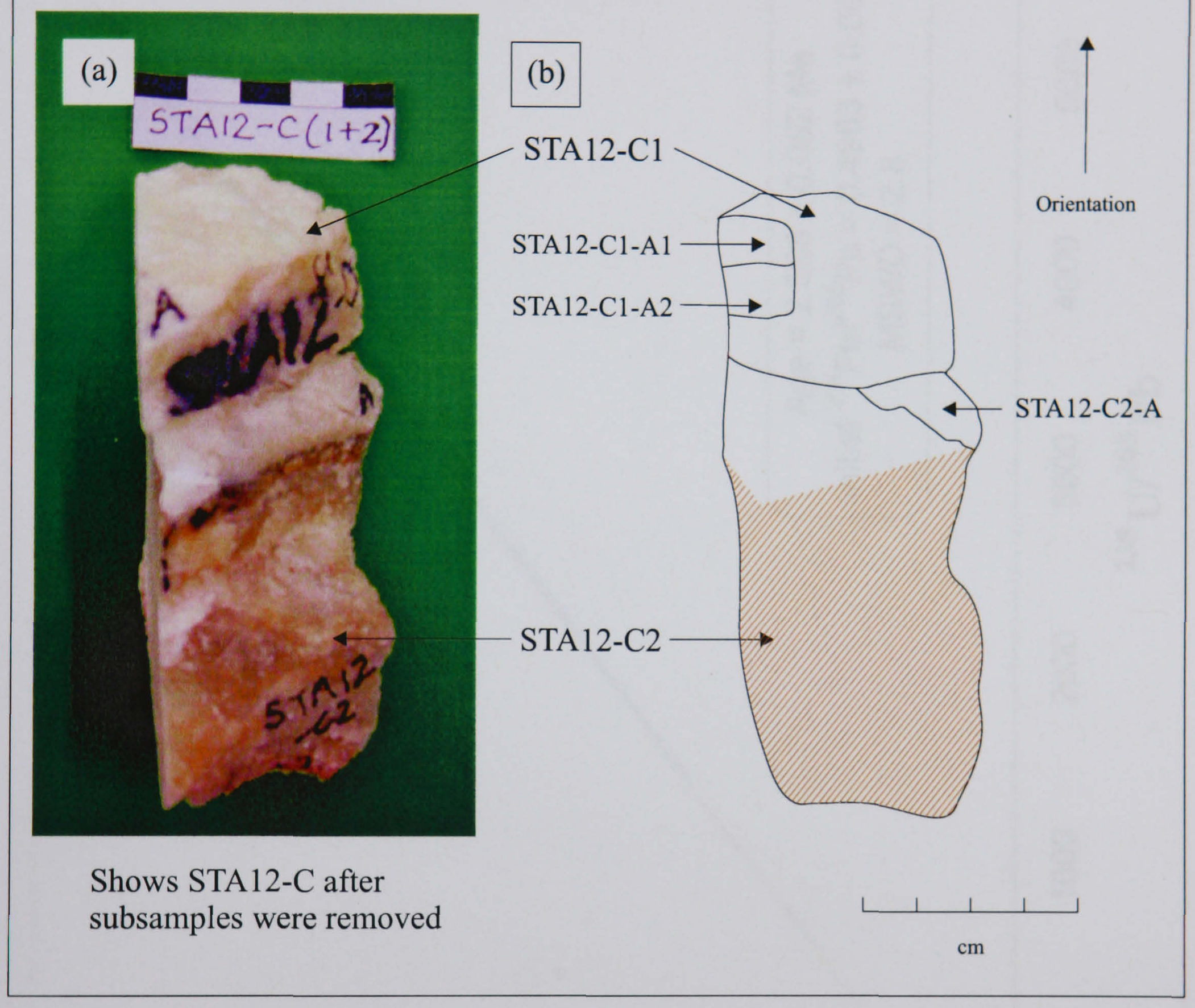

Figure 6.18: Photograph of STA12-C1 and C2 after removal of sub-samples (a) - scale shown in cm; schematic of the same showing sub-samples in place (b). Brown shading relates to darker layers of flowstone. The arrow shows the vertical orientation of the sample in situ.

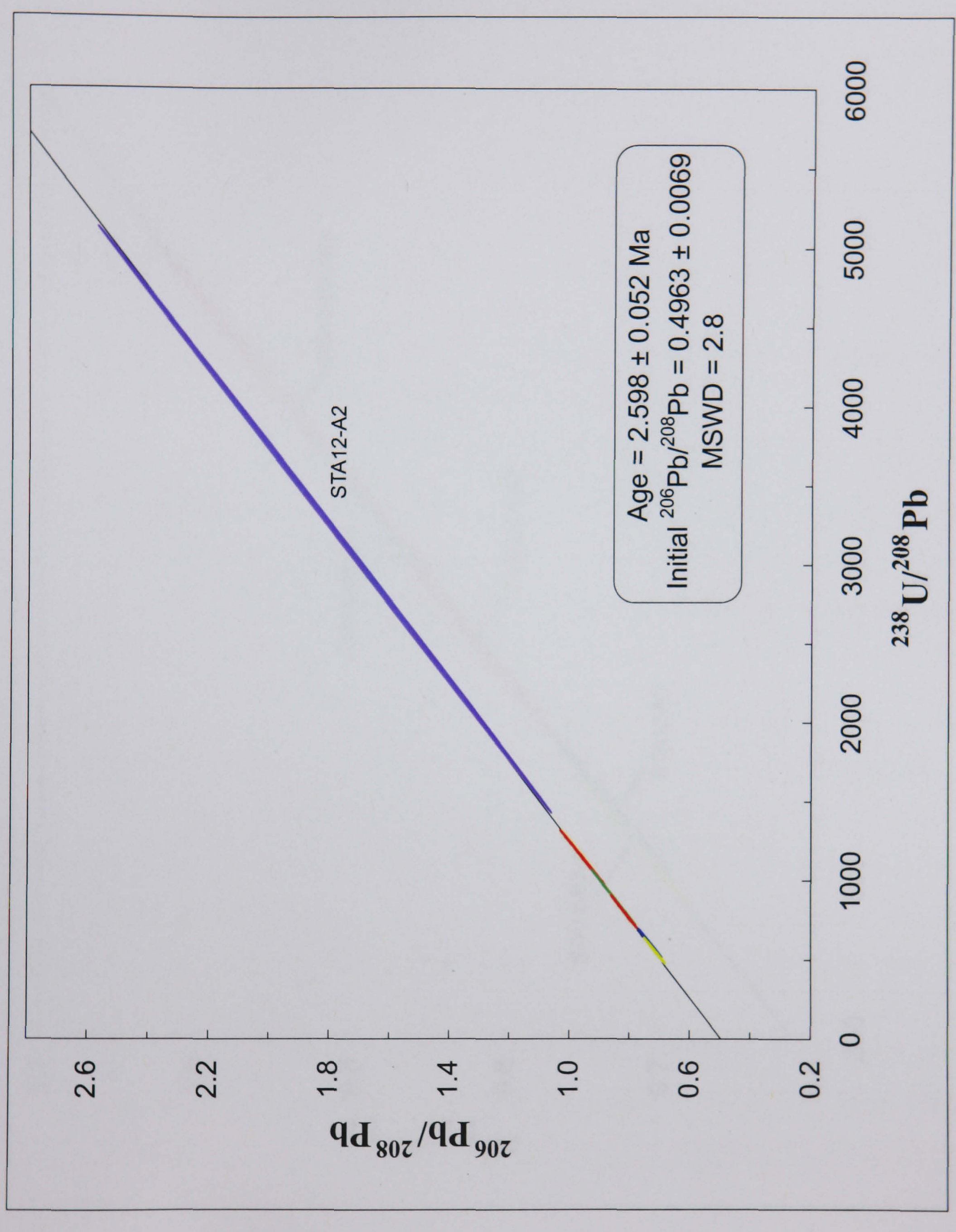

Figure 6.19: STA12 complete isochron. Age calculated is a maximum age. Error ellipses are plotted at 2σ level. Each colour represents an individual sub-sample. Sample is from flowstone layer 2C.

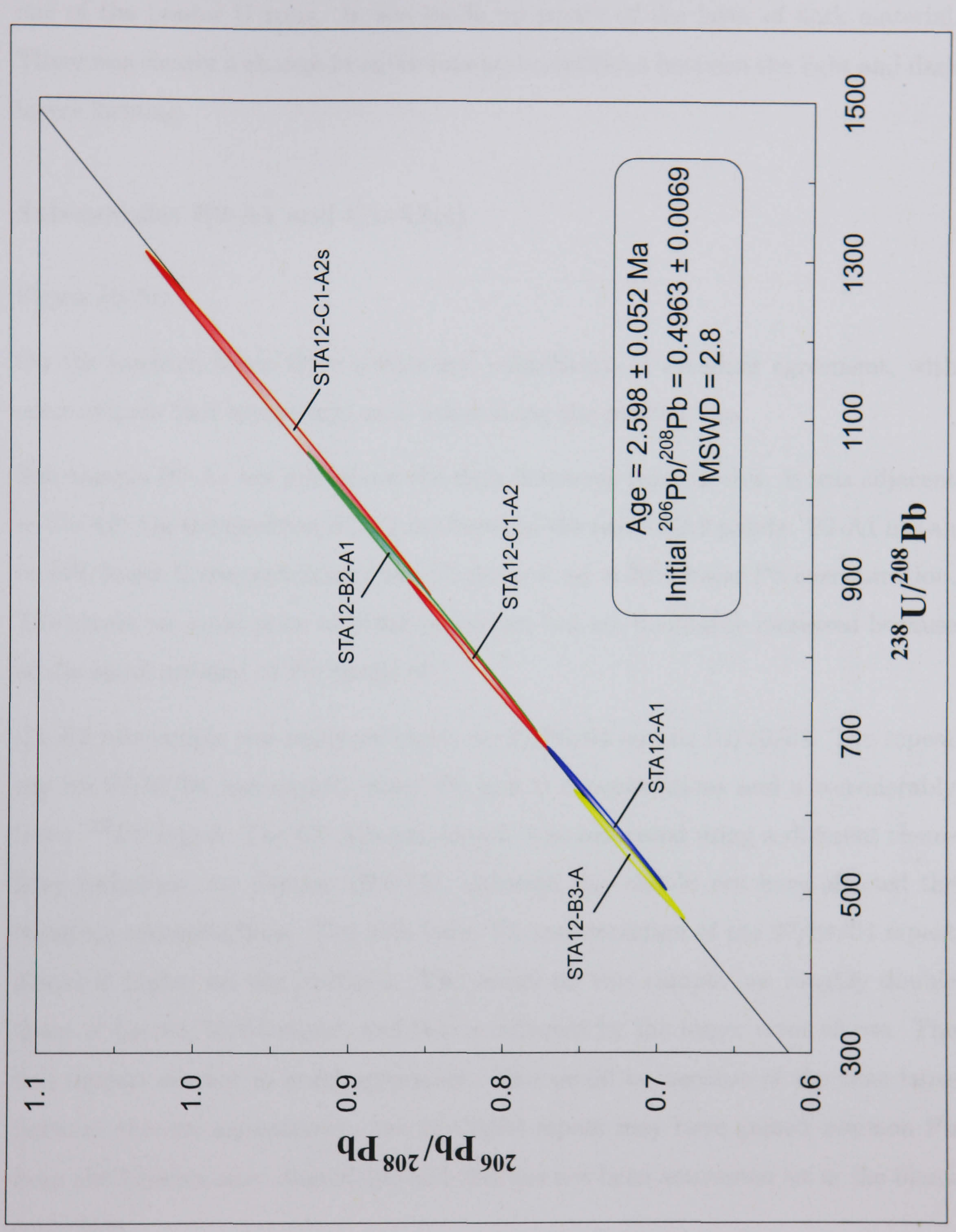

Figure 6.20: STA12 isochron showing points with $mu_{208} \leq 1300$. Age calculated is a maximum age. Error ellipses are plotted at 2σ level. Each colour represents an individual sub-sample. Sample is from flowstone layer 2C.

high blank correction has had little effect on the ratios.

B3-A lies on the isochron, and is the lowest point. B3-A has a good Pb run but one of the poorer U runs. It was made up partly of the layer of dark material. There was clearly a change in environmental conditions between the light and dark layers forming.

Sub-samples B2-A1 and C1-A2(s)

Figure (6.20).

On the isochron these three points are, collectively, in excellent agreement, with error ellipses that merge into each other along the plotted line.

Sub-sample B2-A1 lay just above the dark flowstone layer in situ. It was adjacent to C1-A2. On the isochron B2-A1 lies between the two C1-A2 points. B2-A1 has an $\approx 20\%$ lower U concentration than C1-A2 and an $\approx 30\%$ lower Pb concentration. The errors are good prior to blank correction but are inevitably increased because of the small amount of Pb analysed.

C1-A2 sub-sample was analysed twice, on 27/04/04 and on 04/10/04. The repeat run on 27/04/04 has slightly lower Pb and U concentrations and a considerably lower ^{208}Pb signal. The C1-A2s sub-sample was separated using a different chemistry technique, see Section (B.0.15), although this should not have affected the resulting concentrations. The 30% lower Pb concentration of the 27/04/04 repeat places it higher on the isochron. The errors on this sample are roughly double those of the 04/10/04 repeat and this is reflected by the larger error ellipse. The two repeats are not in good agreement. This could be because of the time lapse between the two separations - the 04/10/04 repeat may have gained common Pb from the labware after dissolution and this has not been accounted for in the blank correction.

6.2.7 STA14

Petrography

STA14 is composed of very pure very dense calcite, see Figure (6.21). No porosity can be seen with the naked eye. The crystals are quite large and elongated - several mm long. What appear to be several horizontal growth layers can be seen on the cut face. On the bottom of STA14 is a thin, 1-2mm, layer of red sediment shown on Figure (6.23).

U and Pb concentrations and distribution

Refer to Figures (6.21), (6.22) and (6.23) for positioning of STA14 sub-samples.

The U image, Figure (6.22) of this sample reveals generally even distribution of U with slightly higher concentrations on the bottom right edge of the sample. It is hard to tell whether this U is incorporated in the speleothem, or in the layer of sediment. U concentrations according to the U image do not differ that much from STA09. From the analytical data it is known that they are in fact much lower. This demonstrates the lack of sensitivity of U imaging to U concentrations at this level. Excluding A2, A3 and A4 the STA14 samples have, relatively speaking, very low U concentrations and quite high Pb concentrations. U ranged from 38.6 ppb to 59.2 ppb in samples excluding A2, A3 and A4 and from 170 ppb to 369.4 ppb in A2, A3 and A4. Pb ranged from 1.5 ppb to 22 ppb. With such low U levels, high levels of common Pb and a resulting insufficient range in mu_{208}, an age can not be determined.

Sub-samples A2, A3 and A4

During a visit to Sterkfontein in July 2004 it was noted that the base of STA14 seemed to overlap with the same material that STA15 is composed of. STA15 had already proved itself to be a promising sample, refer to results in Table (6.1), and on the basis of this three samples (STA14-A2, STA14-A3 and STA14-A4) were taken from the lowest clean material in STA14. These three samples seemed to confirm the theory that the base of STA14 is contemporaneous with STA15.

Figure 6.21: Photograph of front and internal structure of STA14 after initial sample division (a) - scale shown in cm; schematic of the same from the front view (b). The arrow shows the vertical orientation of the sample in situ.

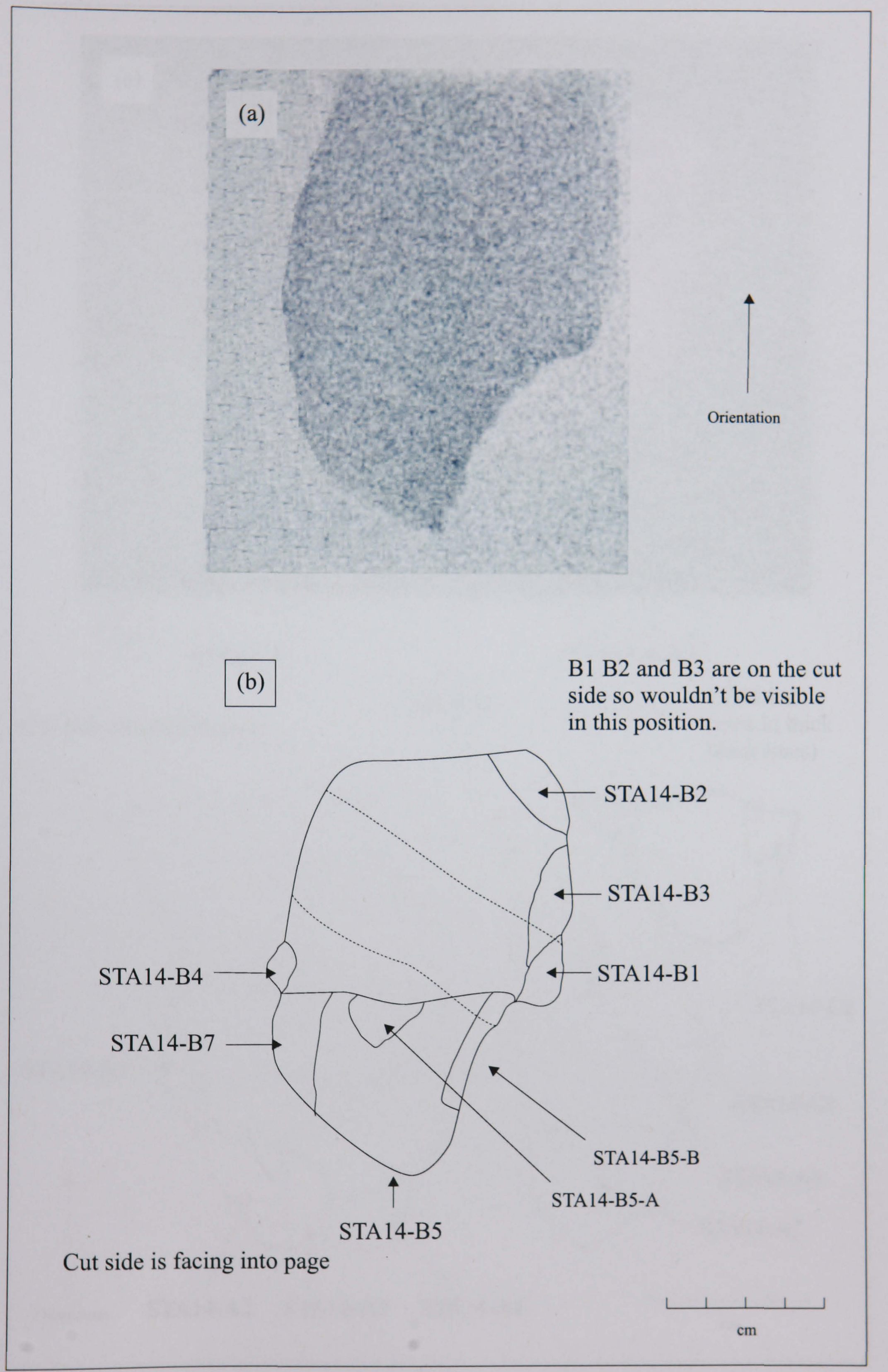

Figure 6.22: Uranium image of STA14-B (a); schematic showing sub-sample positions (b). Dashed lines show visible growth layers. The arrow shows the vertical orientation of the sample in situ.

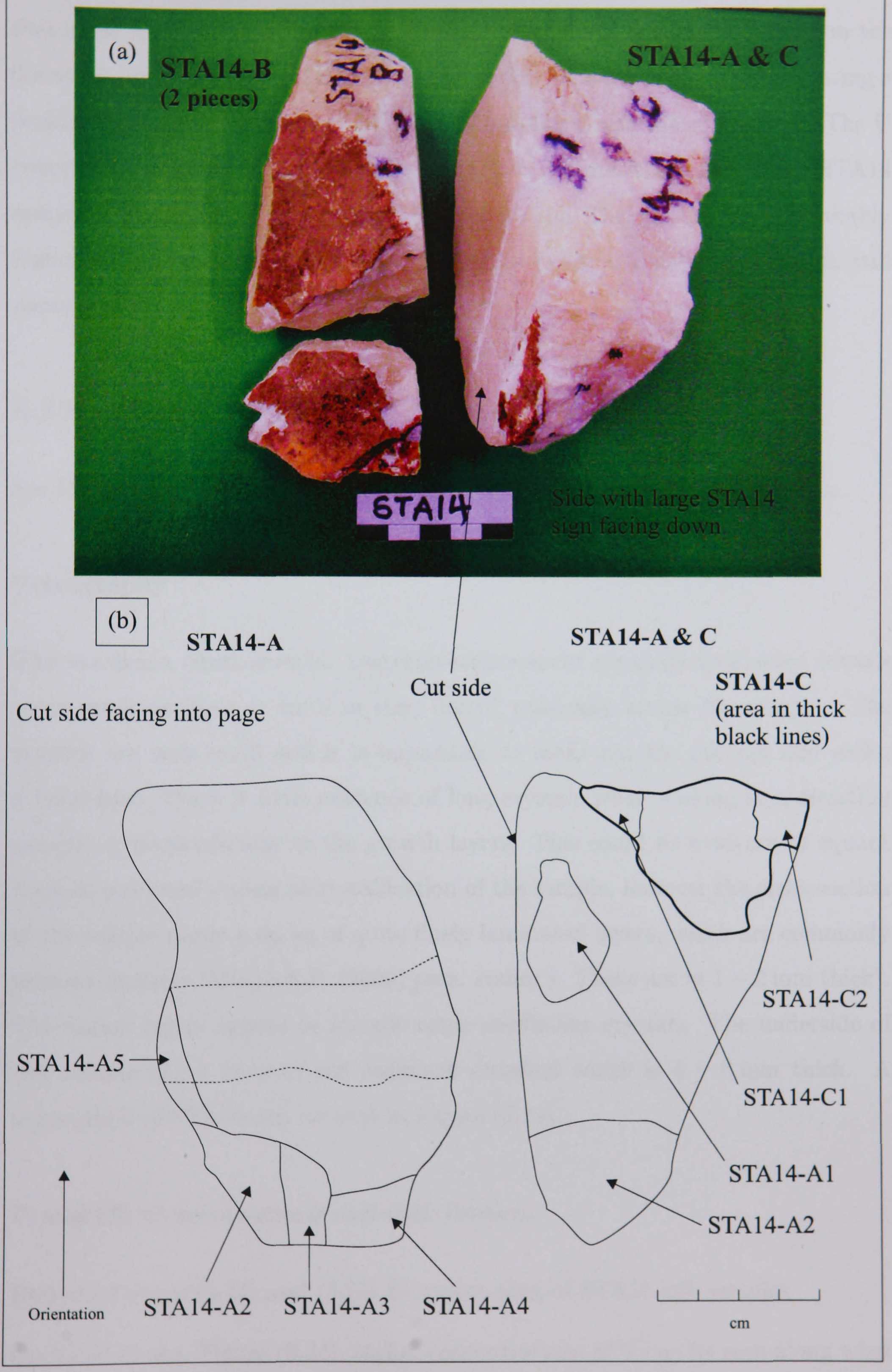

Figure 6.23: Photograph of reverse side of STA14 (a) - scale shown in cm; schematic of STA14-A and STA14-C and sub-samples (b). Dashed lines show visible growth layers. The arrow shows the vertical orientation of the sample in situ.

They have much higher U concentrations than the rest of the STA14 sub-samples that came from higher up in the STA14 hand sample, and therefore higher in the flowstone layer. The base of STA14 and all of STA15 seem to have formed during a period where greater amounts of U were incorporated into the speleothem. The U concentrations of these three samples are up to 6.5 times that of the other STA14 samples. In general they have lower Pb content too. Despite having considerably higher mu_{208} values than the other STA14 samples, a reliable isochron is still unresolvable.

6.2.8 STA15

See Figure (5.1) and Figure (6.1) for the stratigraphic context of this sample.

Petrography

This is a dense, clean, sample. The cross-sectional cut across growth layers, reveals some small cavities, $\approx$ 1mm in size, dotted randomly across the sample. The crystals are very small and it is impossible to make out the average size under a hand-lens. There is little evidence of long crystals when looking in a direction parallel or perpendicular to the growth layers. This could be evidence of equant crystals produced during recrystallisation of the sample, however the cross-section of the sample shows a series of quite finely laminated layers, which are commonly primary features (Murphy, P. (2005) pers. comm.). These are $\approx 1-2\,\text{mm}$ thick[4]. The darker layers appear to include some needle-like crystals. The underside of this sample has a layer of red sediment attached which is $1-3$ mm thick. A photograph of STA15 can be seen in Figure (6.24).

U and Pb concentrations and distribution

Refer to Figures (6.24) and (6.25) for positioning of STA15 sub-samples.

On the U image, Figure (6.24), higher concentrations of U can be seen along what is the top of the sample. Initial sampling of STA15-01 to STA15-05 followed this

[4]Layers are only visible on the cut faces of the sample and do not appear on the schematics.

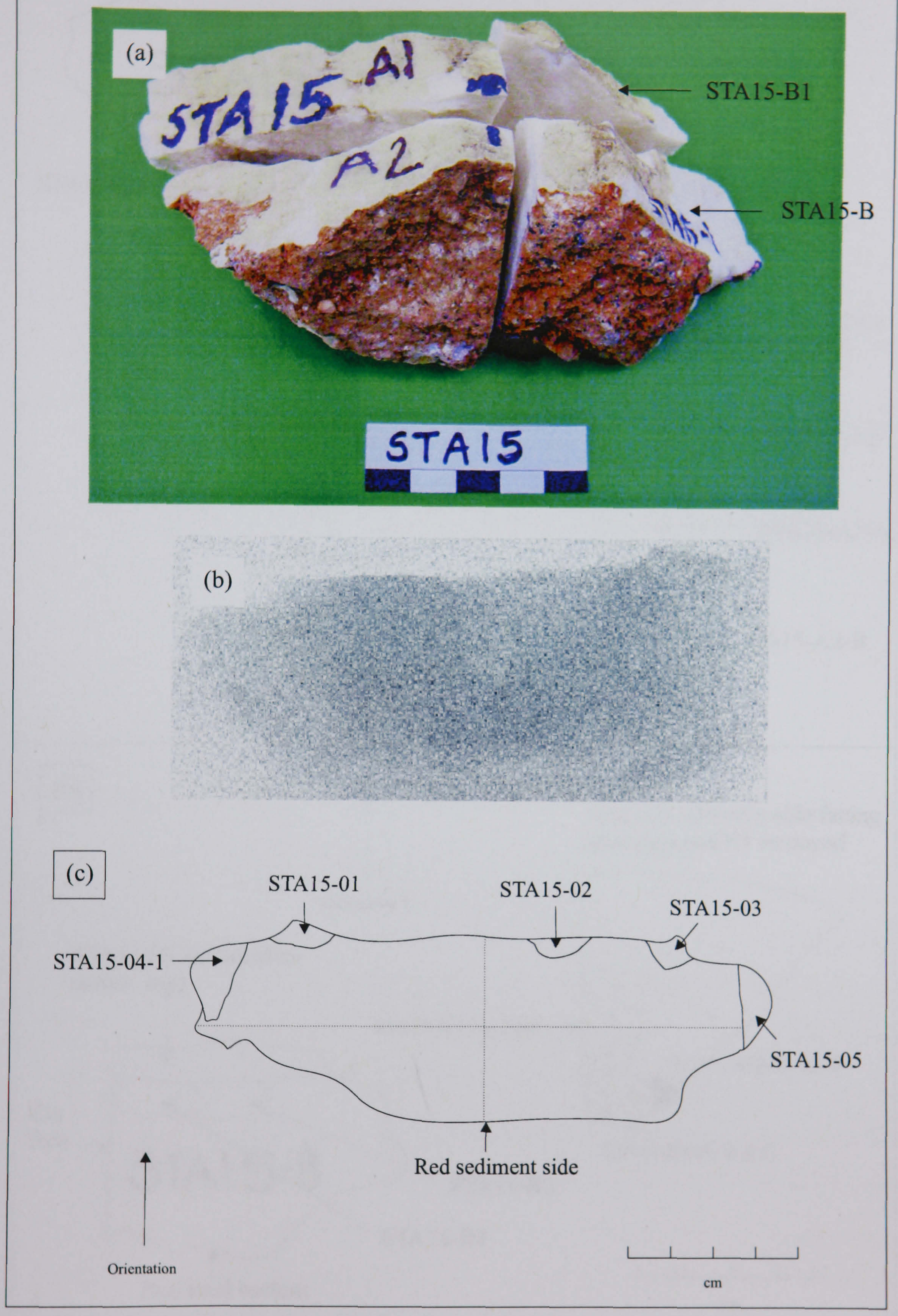

Figure 6.24: Photograph of initial division of STA15 (a) - scale shown in cm. Uranium image of STA15 prior to division (b); schematic of the same showing initial sub-sampling (c). Dotted lines on (c) show division after these sub-samples were taken. The arrow shows the vertical orientation of the sample in situ.

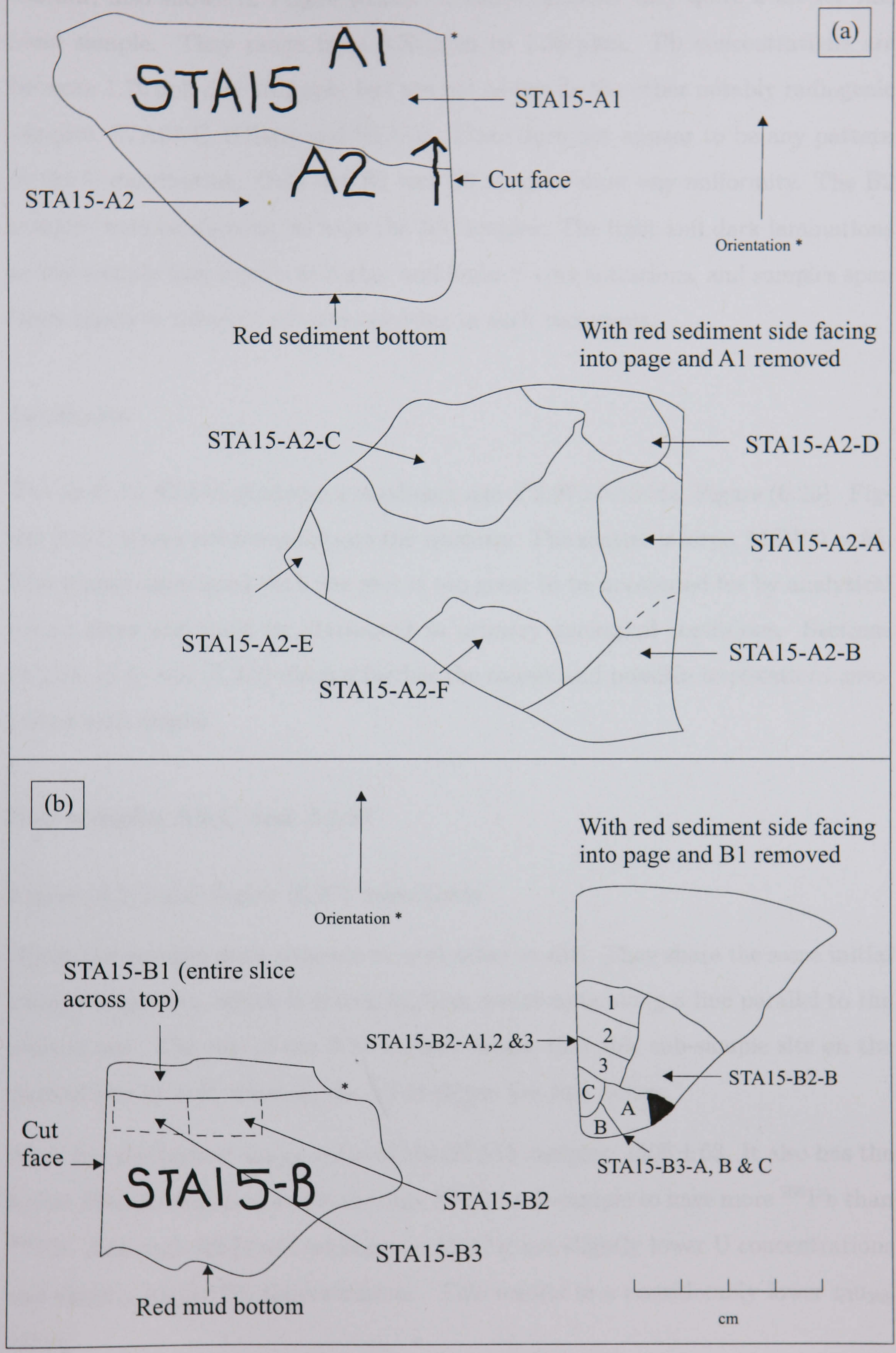

Figure 6.25: Schematic of STA15-A and associated sub-samples (a); schematic of STA15-B and associated sub-samples (b). The arrow shows the vertical orientation of the sample in situ.

contour, also shown in Figure (6.24). U concentrations vary quite a bit for this hand sample. They range from 0.53 ppm to 1.36 ppm. Pb concentrations are between 1.76 ppb and 10.2 ppb, but are not as low as the other notably radiogenic samples, STA07-C, STA09 and STA12. There does not appear to be any pattern to the U distribution. Only the B2 and B3 samples show any uniformity. The B2 samples were contiguous, as were the B3 samples. The light and dark laminations in this sample may represent higher and lower U concentrations, and samples span these layers to different extents resulting in such variations.

Isochrons

The plot[5] for STA15 produces a maximum age of 2.97 ± 0.13 Ma, Figure (6.26). Figure (6.27) shows the low points on the isochron. The scatter is large, MSWD = 85. The scatter associated with the plot is too great to be accounted for by analytical errors alone and must be attributed to primary geological conditions. Sections (4.2.3), (5.4) and (7.3.2) discuss further the causes and possible implications associated with scatter.

Sub-samples A2-C and A2-D

Figure (6.26) and Figure (6.27) respectively.

These two samples were adjacent to each other in situ. They share the same initial isotopic signature, which is shown by their positioning along a line parallel to the plotted one. The size of the A2-C ellipse means that this sub-sample sits on the plotted line as well, whereas the A2-D ellipse lies just below.

A2-C has the highest mu_{208} value of the STA15 samples, 1406 ± 63. It also has the lowest Pb concentration and is the only STA15 sub-sample to have more ^{206}Pb than ^{208}Pb. Although A2-D was adjacent to A2-C it has slightly lower U concentrations and slightly higher Pb concentrations. This results in a considerably lower mu_{208} value.

---

[5]The graphed data for STA15 is referred to as a plot rather than an isochron as the scatter is too great for it to be labelled as the latter.

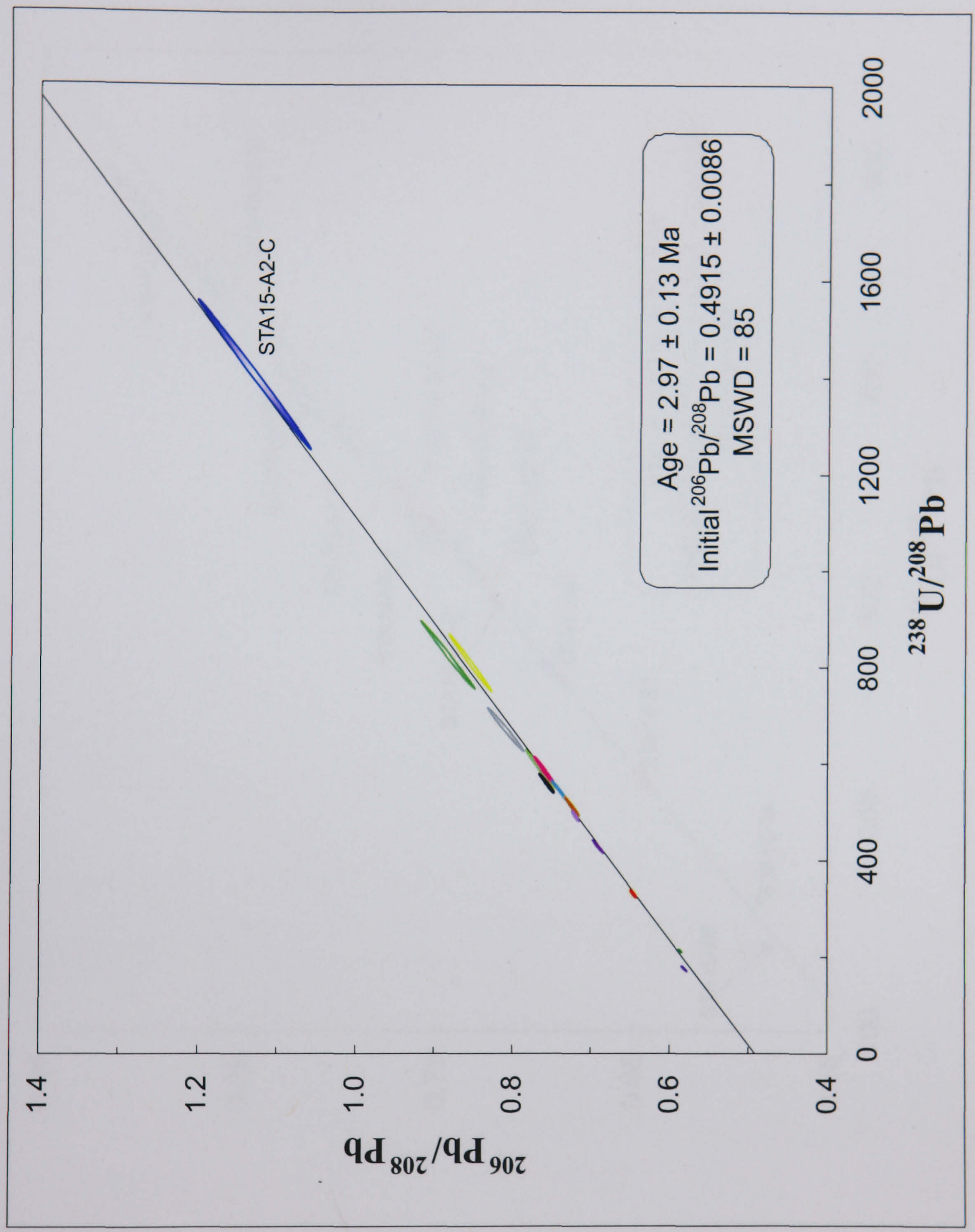

Figure 6.26: STA15 complete plot. Age calculated is a maximum age. Error ellipses are plotted at 2σ level. Each colour represents an individual sub-sample. Sample is from flowstone layer 2B.

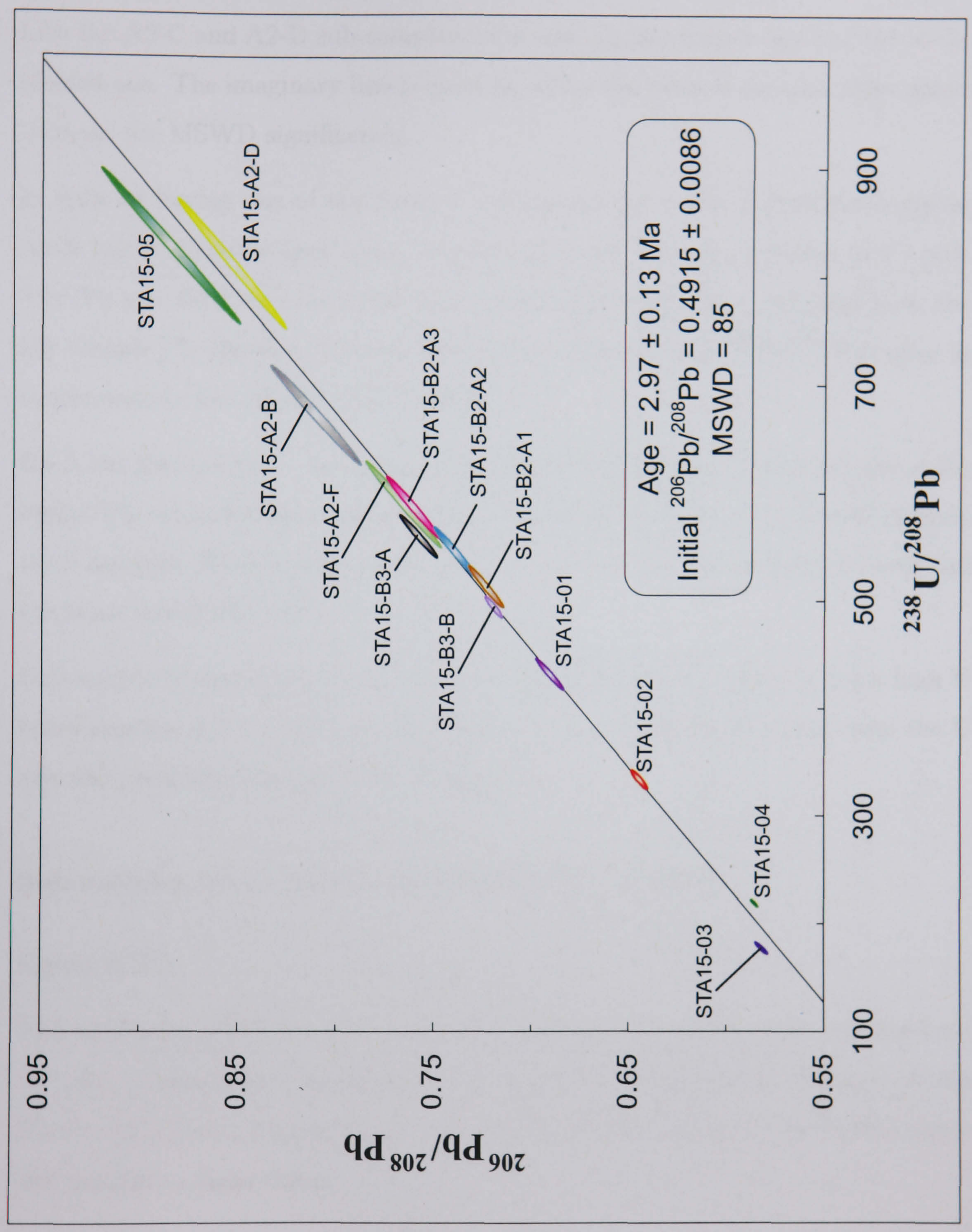

Figure 6.27: STA15 plot showing samples with a $mu_{208} \leq 900$. Age calculated is a maximum age. Error ellipses are plotted at 2σ level. Each colour represents an individual sub-sample. Sample is from flowstone layer 2B.

Sub-samples A2-B, B3-A and 05

Figure (6.27).

Like the A2-C and A2-D sub-samples these sub-samples form a line parallel to the plotted one. The imaginary line is quite far above the plotted one and these points increase the MSWD significantly.

In spite of having one of the lower U concentrations of the STA15 sub-samples, A2-B has a relatively high mu_{208} because of its low Pb concentration of 2.4 ppb. The Pb run for this sub-sample has a low signal and this, combined with the low sample Pb amounts, has resulted in large errors in the $^{206}Pb/^{208}Pb$ ratios in comparison to the other STA15 samples.

B3-A has the highest U concentration of the STA15 samples. It also has one of the higher Pb concentrations, which means that on the plot, it is the lowest of these three samples. B3-A was alongside B3-B in situ but they do not seem to have had the same initial Pb ratios.

Sub-sample 05 was taken from the outer edge of the hand sample. It has a high U concentration and a low Pb concentration. In spite of the small sample size the U run was good and Pb signal was adequate.

Sub-samples A2-F, B2-A1, B2-A2, B2-A3 and B3-B

Figure (6.27).

The results for these five sub-samples form a cluster of points quite low down on the plot. These points really define the lower part of the plot. Of these points B2-A1, B2-A2 and B2-A3 form a line. B3-B and A2-F form a line slightly above but parallel to these three.

A2-F was next to A2-B in situ. The U and Pb concentrations are similar. On the plot they are relatively close and both lie a little above the line. A2-F is slightly lower on the plot than A2-B.

B2-A1, B2-A2 and B2-A3 were originally one piece and were split into three for analysis. They agree well in terms of their position on the plot, suggesting a shared

chemical and geological history.

Sub-sample B2-A1 has an average U and Pb concentration, in relation to the other STA15 sub-samples, and a mu_{208} of 512.3 ± 7.9. It is positioned slightly below the plotted line and has a very similar Pb makeup to B3-B.

B2-A2 is alongside B2-A1, but it has a 10% lower Pb concentration which has shifted it higher up the plot.

B2-A3 has the lowest U and Pb concentrations of the three B2 samples. The Pb signal is low and the errors are higher than the other two samples because of this. Its higher position on the plot is the result of a lower Pb concentration.

Sub-sample B3-B is very similar in composition to its in situ neighbour B3-A. It has a marginally lower U concentration and a lower Pb concentration. B3-B lies on the line whereas B3-A doesn't. Whether this is a geological consequence or an analytical one is unknown.

Sub-samples 01, 02, 03 and 04

Figure (6.27).

These four samples are found on the bottom of the plot and are linked by their relatively high Pb concentrations and more specifically lack of radiogenic Pb. Sub-samples 01, 02 and 03 are also linked by the fact that they were subject to a slightly different separation technique than the remainder of the STA15 sub-samples. Taking into consideration the inexperience of the analyst at the time and the change in the fluoride precipitation step, Section (5.2.2), it seems reasonable to be suspicious of all the STA15 samples from the 25/03/03 analysis. This includes samples STA15-01, STA15-02 and STA15-03. When the U runs for these samples are compared with the next set analysed - STA09-C2 from 15/10/03 - the improvement is great. When the two repeats of STA15-05 are compared, again the improvement in the U result is noticeable, see Table (6.1) and Table (C.1). This indicates that the discrepancies in the 25/03/03 sub-samples are due to inadequacies in the analysis rather than their geological history.

These low points constitute an important area on the plot giving the mu_{208} a wider

range, although they also increase the level of scatter.

Sub-sample 01 has a relatively high U concentration but not a particularly low Pb concentration. The result of this is a mu_{208} value of 430 ± 6 with a small blank correction.

02 has one of the largest U concentrations of the STA15 suite, but also has the second highest Pb concentration. The U run was short, only 22.5% of the usual number of ratios were recorded. Sub-sample 02 is positioned low on the plot.

Out of all the STA15 samples, 03 has the lowest U concentration - only 0.55 ppm - and the third highest Pb concentration - 5.5 ppb. It is found low on the plot and has a poor fit with regards to the calculated line.

Sub-sample 04 has a large U concentration and the largest Pb concentration. This has produced a result where the ^{206}Pb enrichment is small. 04 appears to come from the same layer in the hand sample as 03. However 04 has double the concentration of U and of Pb.

Summary

The STA15 results seem to indicate there was a fair amount of variation in initial Pb composition within this hand sample. On the plot there appear to be several groups of points that shared the same initial Pb composition. Each group had a slightly different initial composition and the groups evolved radiogenically along lines parallel to each other. In such cases this results in a plot with a large scatter, which is not necessarily indicative of the applicability of the results. Although the groups may not be positioned along the same line, a synchronous decay history means that the slopes of the lines they define should be in agreement. Possible causes of scatter are discussed further in Section (4.2.3), (5.4) and Section (7.3.2).

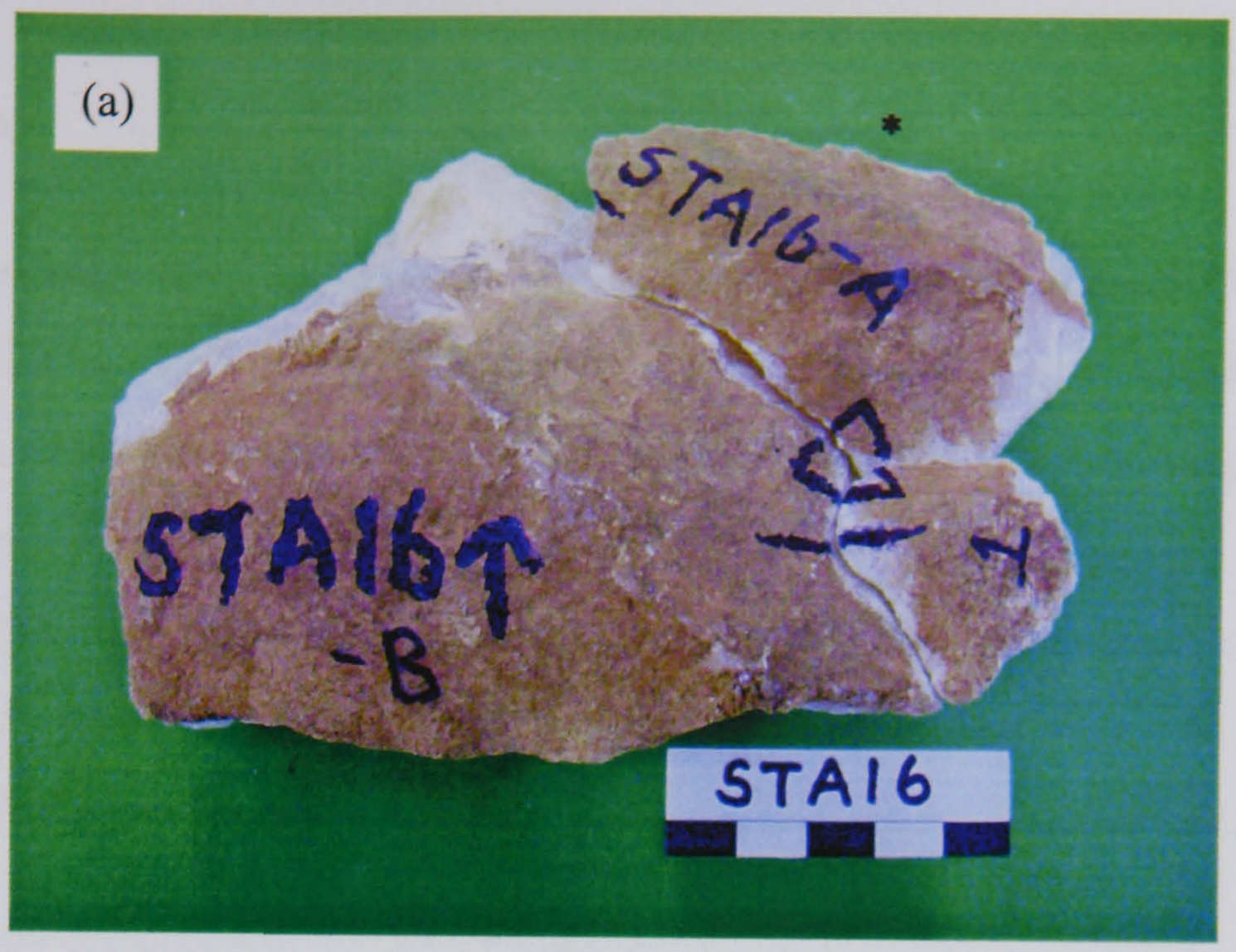

Figure 6.28: Photograph of STA16 after initial division into three pieces (a) - scale shown in cm; schematic of the same (b). Schematic of STA16-A sub-samples (c). Brown shading shows layers of darker flowstone. The arrow shows the vertical orientation of the sample in situ.

6.2.9 STA16

Petrography

STA16 came from the top of flowstone layer 2B. In appearance STA16 is very similar to STA14. It has the same pure, dense calcite, with no visible porosity. The crystals are quite large and variable in size. In cross-section, large crystals, which are several mm long, can be seen extending through the sample. STA16 is darker than STA14, in particular near the top of the sample where all the sub-samples but A5 were located. The surface of the sample exposed in the cave has a layer of red/brown sediment which comes off when rubbed. Refer to Figure (6.28)

U and Pb concentrations and distribution

Refer to Figure (6.28) for positioning of STA16 sub-samples.

STA16 has very low U concentrations ranging from 0.024 ppm to 0.045 ppm. These are lower than the other two hand samples from this flowstone, and are more similar to the concentrations of STA03 and STA04 from layer 2D. The low U concentrations seem to coincide with the top of flowstone layer 2B, as lower U concentrations are seen at the top of STA14. Pb concentrations are between 4.8ppb and 11.5 ppb. These are similar to STA14 and much higher than STA15. The STA16 sub-samples suffered from too much common Pb and too little U. No plot has been constructed from this data set.

6.2.10 Summary of layer 2D results

This is the only layer for which an age can not be produced. Out of the three hand samples analysed, STA03 and STA04 prove unsuitable for the technique. STA03 has very high Pb concentrations and very low U concentrations. The mu_{208} values are consequently low and have an extremely narrow range. STA04 has much lower Pb concentrations but is hampered by similarly low U concentrations. Although the mu_{208} values are much higher and have a wider range they are still very low in relation to the other Sterkfontein hand samples. In complete contrast to these, STA07-C is the most radiogenic sample analysed with a top mu_{208} of 5105 ± 1269.

Unfortunately an isochron can not be plotted from these results.

6.2.11 Summary of layer 2C results

Flowstone layer 2C is the most successful layer in that it has yielded two hand samples which produce dates[6]; STA09 produces a maximum age of 2.72 ± 0.10 Ma, and STA12 a maximum age of 2.598 ± 0.052 Ma. Importantly these maximum ages agree within error. STA12 produces a significantly better isochron. In terms of U and Pb concentrations STA12 has lower U concentrations but it also has lower Pb concentrations. The mu_{208} values for these samples therefore span a similar range. The higher Pb concentrations of STA09 do make resolution of radiogenic enrichment more difficult though. Greater U concentrations in STA12, and greater variation in U concentrations, could be primary features or a sign of subsequent alteration as indicated by the lack of primary features such as growth layers, and by visible porosity. Although STA12 was in the same layer as STA09 it certainly experienced different conditions because it includes a layer of dark flowstone that is lacking in STA09. Despite this, STA12 appears to be more suited to the U-Pb technique, and it produces an appreciably better isochron than STA09. This may be purely down to variable initial Pb compositions in STA09. If STA12 has recrystallised this probably occurred early after deposition, after which it remained a closed system. Together these samples provide evidence not only for the maximum age of this flowstone deposit but for the robustness of the U-Pb system in this kind of material.

6.2.12 Summary of layer 2B results

Like layer 2D this flowstone produces mixed results. Sample STA14 is like STA04 in that its Pb concentrations are relatively low but it is U deficient. STA16 has a comparable Pb content but is even more deficient of U. Whilst STA14 has some mu_{208} values as high as 311.7 ± 13.1, an isochron can not be determined for this hand sample. Regardless of this layer 2B yielded the third hand sample from which

[6]There are in fact three results when the preliminary SK3 result is included - See Section (4.2.3)

a maximum age is inferred; STA15 produced a maximum age of 2.97 ± 0.13 Ma. STA15 has a wide range in mu_{208} values, but does not have as high upper values as STA09 or STA12. The STA15 plot, and therefore the hand sample itself, is not as robust as those for layer 2C. The scatter and therefore the confidence in the age are not as great for those of the layer 2C results either. However it is felt that in view of the layer 2C results this scatter can most likely be attributed to initial Pb heterogeneity and that confidence can be placed in this maximum age.

6.3 U disequilibrium corrections

The following lab work and calculations are credited to Cliff, R. A., (2005).

Following the laboratory work carried out by the writer, giving the above results, the present day $^{234}U/^{238}U$ ratios of seven Sterkfontein samples were measured by Bob Cliff and Jan Kramers at the University of Bern. They were analysed on a Nu-Instruments MC-ICPMS using a sample/standard bracketing routine with an equilibrium uraninite solution as standard. Excess ^{234}U was detected in all the samples analysed, meaning the initial disequilibrium must have been relatively high. Flowstone layers 2C and 2B produced similar present day excesses, giving an overall average of $3.9 \pm 1.4‰$ for these two layers. Flowstone layer 2D produced significantly higher excesses, and a greater variation in excesses within a hand sample. Therefore, it was felt that an average excess for this layer was not appropriate. See Table (6.2) for all measured excesses.

Ages corrected for initial ^{234}U excess are calculated for each of the Sterkfontein samples by assuming a common level of excess ^{234}U. The isochron slope from the uncorrected maximum age is used as a first approximation. By inputting this into the calculation derived by Ludwig (1977)[7] and iterating until the results converge, a new initial disequilibrium value is established, from which a new age can be calculated. The calculations show that initial ^{234}U excess was as high as 2.5, see Table (6.2). The error in the disequilibrium corrected age is the quadratic combination of the propagated uncertainty in the disequilibrium correction and the error on the isochron slope.

[7]Equations are adapted from Bateman (1910), see Section (4.1.3)

Sample	Isochron Slope	Error (2σ)	Corrected Age	Estimated Error (2σ)	MSWD	Initial ^{234}U Excess	Error (2σ)
STA09	0.000427	0.000008	2.17	+7/-6	7.9	1.97	+0.16/-0.23
STA12	0.000403	0.000008	2.11	+7/-5	2.8	1.69	+0.18/-0.22
SK3	0.000466	0.000009	2.25	+8/-7	5.5	2.46	+0.22/-0.25
STA15	0.000461	0.000020	2.24	+9/-7	85	2.41	+0.31/-0.35

Table 6.2: Table of dated Sterkfontein samples with new ages corrected for initial ^{234}U disequilibrium.

The corrected ages are significantly different from the maximum age results, see Table (6.2). The new corrected age is the best estimate of the true age of the sample taking into account initial U disequilibrium conditions. The best estimate ages for flowstone layer 2C are plotted in Figure (6.29) and give a weighted average age for this horizon of 2.17 ± 0.17Ma. This combined with the best estimate STA15 result of $2.24 + 0.09/-0.07$Ma for layer 2B, suggests an age for StW 573 of around 2.2Ma (Cliff, R. A., (2005) pers. comm.).

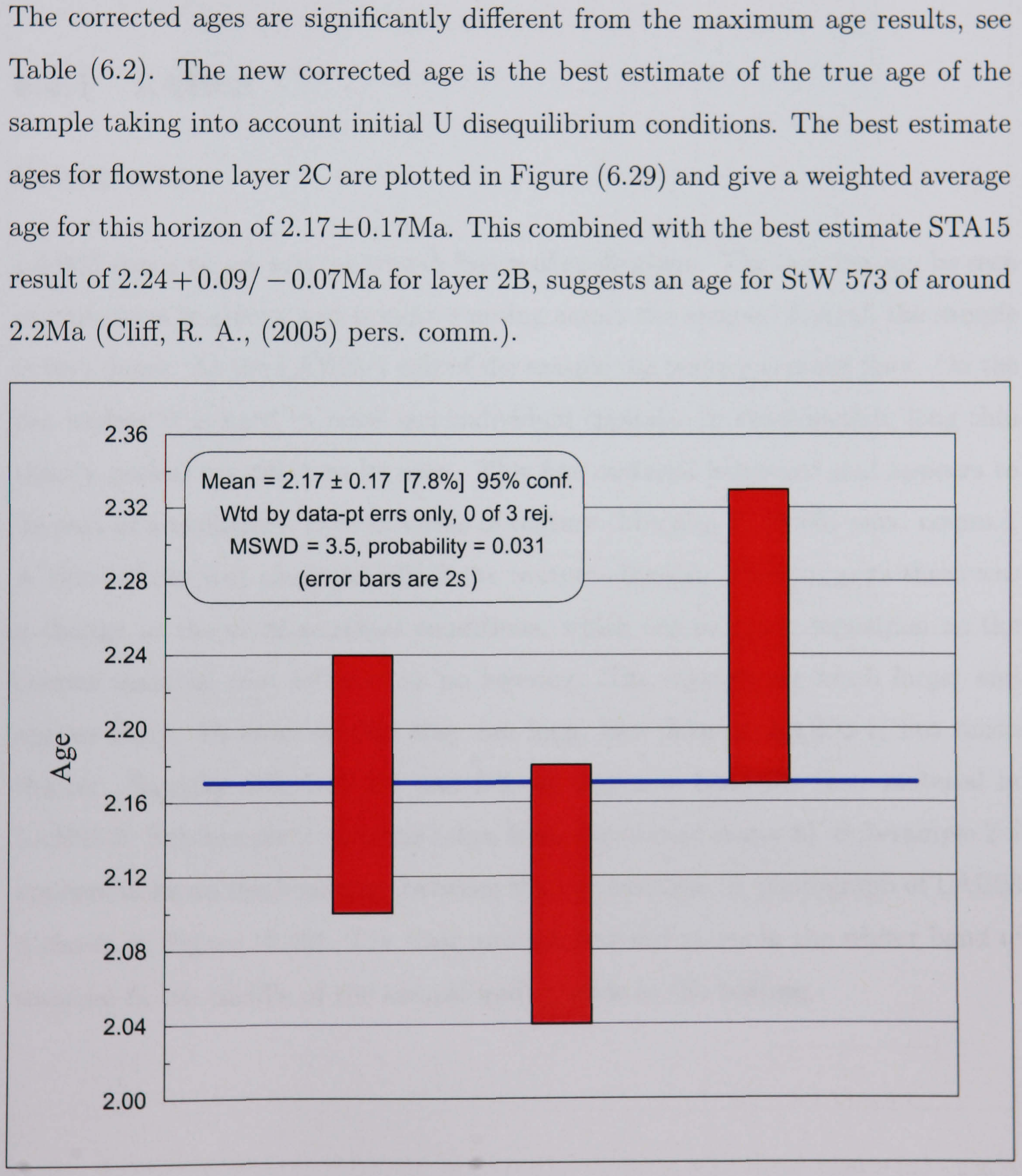

Figure 6.29: Weighted age calculation for flowstone 2C using best estimate ages for samples STA09, STA12 and SK3. Cliff, R. A., (2005) pers. comm.

6.4 The Limeworks

The Limeworks hand sample that was analysed, LAB03, was sampled from a member 1B extensive stalagmite boss that was very clean and dense in appearance. The speleothem deposit was several metres thick at this point and LAB03 was taken $\approx$ 30cm from the lower edge of the deposit. Refer to Sections (5.1.1) and (A.2.2) for provenance. The accepted results for this hand sample are displayed in Table (6.3), while the rejected results are shown in Table (C.2).

6.4.1 LAB03

Petrography

LAB03 spans across several growth layers of speleothem. The layering can be seen as variations in colour and texture running across the sample. Overall the sample is very dense. At the LAB03-1 end of the sample the texture is much finer. On the flat surface it is hard to make out individual crystals. In cross-section, long thin tightly packed crystals can be seen. This fine material is layered and appears to be part of a stalagmite boss in terms of texture (Murphy, P. (2005) pers. comm.). A third of the way along LAB03-2 the texture changes. This suggests there was a change in the environmental conditions, which led to rapid deposition as the coarser material that follows has no layering. The crystals are much larger and appear flaky. In cross section they are long, like those in LAB03-1, but much thicker. Samples 2-3, 2-4, 2-7 and 2-8, all originate from the finer material in LAB03-2. Sub-sample 2-11A was taken from the coarser material. Sub-sample 2-2 appears to lie on the boundary between the two textures. A photograph of LAB03 is shown in Figure (6.30). The finer grained material starts in the whiter band of material in the middle of the sample and extends to the bottom.

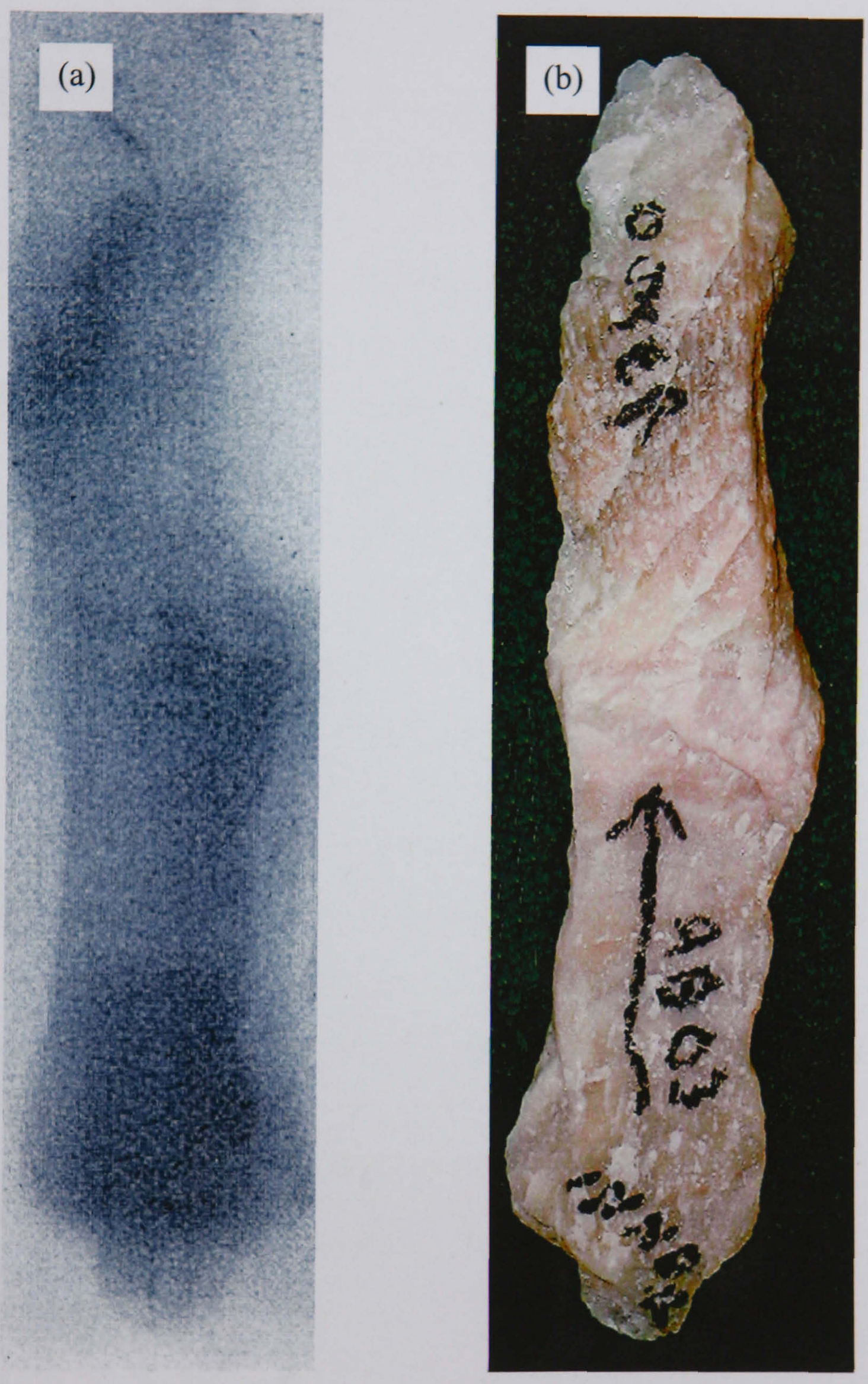

Figure 6.30: Uranium image of LAB03 (a) and corresponding photograph (b).

Sample	Date	U (ppm)	Pb (ppm)	Pb (ng)	$^{206}Pb/^{204}Pb$ before blank	$^{238}U/^{208}Pb$	Error (1σ)	$^{206}Pb/^{208}Pb$	Error (1σ)	$^{207}Pb/^{204}Pb$	Error (1σ)	$^{208}Pb/^{204}Pb$	Error (1σ)
LAB03-2-2▲	18/06/03	1.853	0.0078	3.937	40.74	529.7	5.1	1.122	0.006	16.21	0.03	36.99	0.08
LAB03-2-3	02/12/02	1.988	0.0095	3.904	37.85	453.9	4.3	1.046	0.005	15.93	0.05	36.79	0.13
LAB03-2-4△	18/06/03	1.666	0.0063	3.081	46.59	636.2	7.9	1.299	0.01	16.21	0.08	36.86	0.19
LAB03-2-7	06/11/02	1.684	0.0144	6.258	27.85	224.1	1.4	0.7564	0.0015	15.85	0.03	37.09	0.08
LAB03-2-8	18/06/03	1.797	0.0075	3.225	41.84	541.8	6.2	1.15	0.007	16.27	0.04	37.24	0.10
LAB03-2-11A	18/06/03	0.056	0.0027	1.191	19.62	34.8	0.78	0.526	0.001	15.68	0.04	37.58	0.10

Table 6.3: Table of the Limeworks LAB03 sub-sample results. Sub-sample weights are 430 ± 50mg apart from the following samples; ▲ - 504mg; △ - 493mg. The blank applied was 92.9 ± 0.25pg. Blank corrections ranged between 1.48% and 7.8%.

U and Pb concentrations and distribution

Refer to Figure (6.31) for positioning of LAB03 sub-samples.

The U image, Figure (6.30) shows some variation in U concentration for this sample. Higher U concentrations appear to be in LAB03-1 and in two areas of LAB03-2. These areas correspond to samples 2-8 and 2-7. These do have two of the higher U concentrations by analysis. U concentrations are, for the most part, high. They vary between 0.06 ppm and 1.99 ppm but most are well over 1.5 ppm. The highest concentrations are in samples 2-2, 2-3, and 2-8. Pb concentrations are very variable. Sub-sample 2-11A has a Pb concentration of 2.7 ppb whereas 2-7 has a concentration of 14.4 ppb. The higher Pb concentrations are in samples 2-3 and 2-7. There is no obvious physical explanation for this.

Isochrons

The plot[8] for LAB03 gives an age of 7.98 ± 0.29 Ma, but it has a MSWD of 50. The scatter of these samples could be the result of real age variation, differences in initial U disequilibrium, or initial Pb heterogeneity between the layers. Possible causes of scatter are discussed further in Section (4.2.3), (5.4) and Section (7.3.2). Sub-samples 2-3 and 2-7, which are plotted on the graph, were analysed prior to the alteration in the precipitation step, see Section (5.2.2).

The following sub-samples are all plotted in Figure (6.32).

Sub-samples 2-2, 2-3, 2-4 and 2-8

These four sub-samples form a cluster near the top of the LAB03 plot. In terms of their composition there are similarities between these sub-samples.

Of the repeats analysed of sub-sample 2-2 the 18/06/03 repeat is considered the most reliable as it has much better errors and was analysed with the improved fluoride precipitation step. This sub-sample has a high U concentration and a relatively radiogenic Pb isotopic signature. Like all the LAB03 results the relatively

[8]The graphed data for LAB03 is referred to as a plot rather than an isochron as the scatter is too great for it to be labelled as the latter.

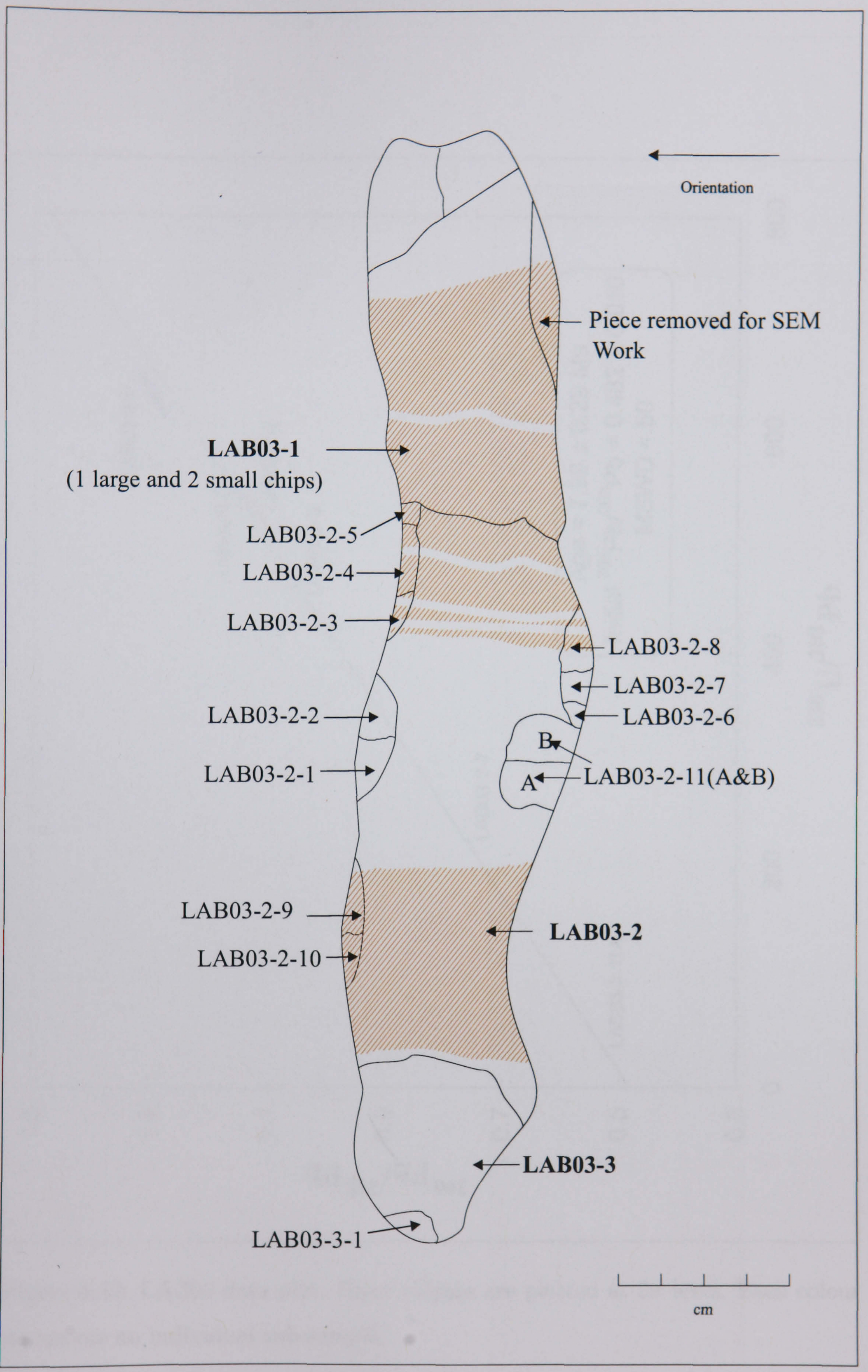

Figure 6.31: Schematic of LAB03 from front, showing sub-sample positions. Brown shading shows darker layers of flowstone. The arrow shows the vertical orientation of the sample in situ.

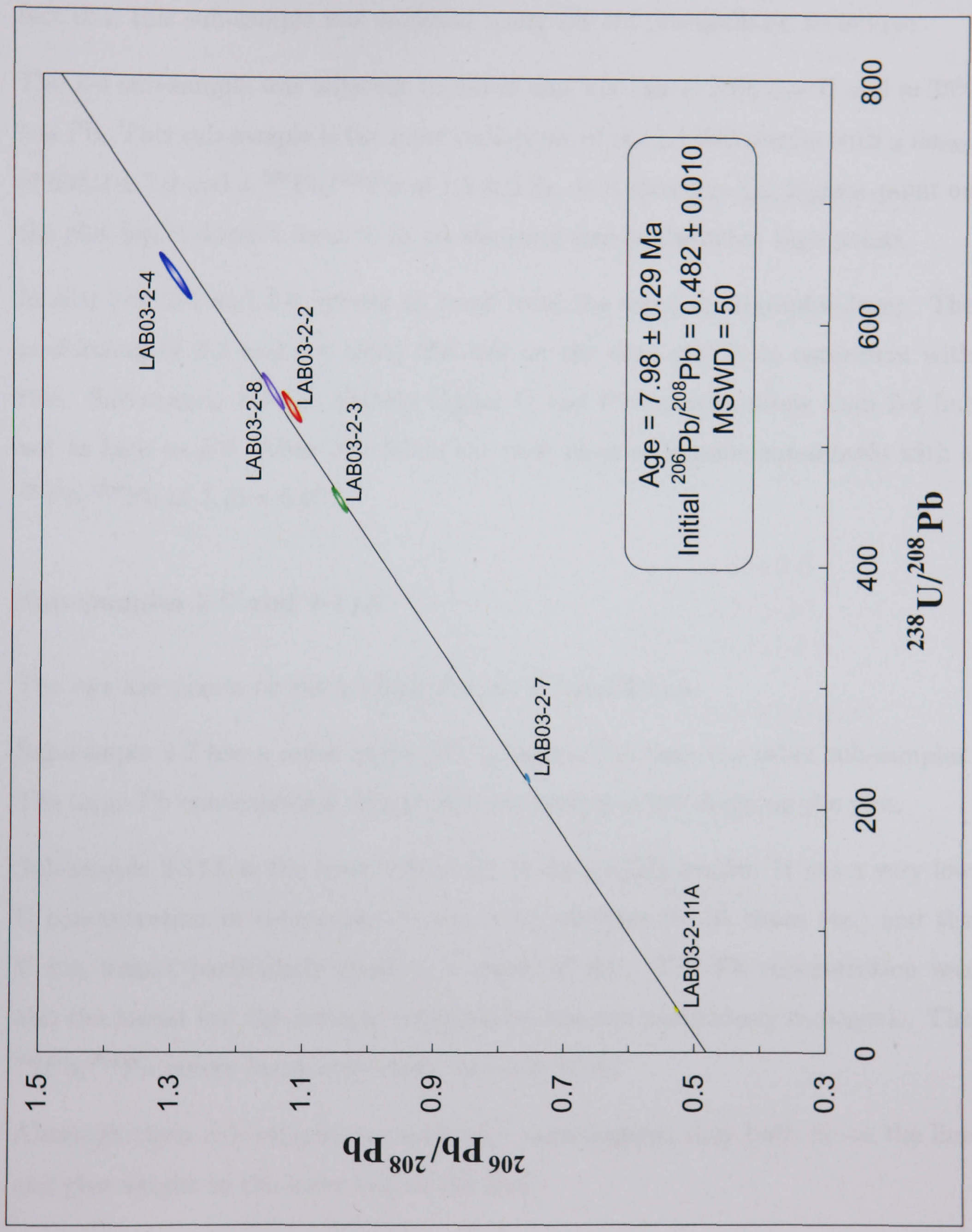

Figure 6.32: LAB03 data plot. Error ellipses are plotted at 2σ level. Each colour represents an individual sub-sample.

high Pb concentrations mean that the error ellipses are small.

Sub-sample 2-3 has the highest U concentration of all the LAB03 sub-samples. but it álso has a relatively high Pb concentration. It has a good U run in spite of the fact that this sub-sample was analysed using the old precipitation technique.

The 2-4 sub-sample was adjacent to 2-3 in situ but has $\approx 20\%$ less U and $\approx 35\%$ less Pb. This sub-sample is the most radiogenic of the LAB03 results with a mu_{208} of 636.2 ± 7.9 and a $^{206}Pb/^{208}Pb$ of 1.3 ± 0.01. It is therefore the highest point on the plot but it doesn't seem to fit on the same line as the other high points.

In situ 2-3, 2-4 and 2-8 appear to come from the same stratigraphic layer. The positioning of 2-3 and 2-8 along the line on the data plot is in agreement with this. Sub-sample 2-8 has slightly higher U and Pb concentrations than 2-4 but not as high as 2-3. After 2-4, 2-8 is the next most radiogenic sub-sample with a $^{206}Pb/^{208}Pb$ of 1.15 ± 0.007.

Sub-samples 2-7 and 2-11A

The two low points on the LAB03 plot are 2-7 and 2-11A.

Sub-sample 2-7 has a much higher Pb concentration than the other sub-samples. The large Pb concentration means this sub-sample is low down on the plot.

Sub-sample 2-11A is the least radiogenic of the LAB03 results. It has a very low U concentration in comparison to the other samples ($\approx$ 30 times less) and the U run wasn't particularly good as a result of this. The Pb concentration was also the lowest but the isotopic composition was not particularly radiogenic. The $^{206}Pb/^{204}Pb$ before blank correction was only 19.62.

Although these sub-samples are relatively unradiogenic, they both lie on the line and give weight to the lower end of the plot.

Summary

The LAB03 plot suffers from insufficient data, which is partially due to the timing of analysis. More than half the results were analysed prior to the alteration to the precipitation step, Section (5.2.2), and as a consequence of the poor analytical

quality of these results they have not been plotted. The 18/06/03 samples were the first to be run on the altered technique with the new precipitation steps. However following these separations it was evident that there was still a high level of scatter connected with the results and it was felt that pursuing with the analysis of this sample may very well prove futile. With such large scatter on the LAB03 plot, and without any supporting data plots for this result, it was felt that the maximum age produced could not be taken as meaningful.

6.5 Kromdraai B

The Kromdraai B sample analysed, KBP03, was removed from a thin band of flowstone on a block of member 3 breccia associated with the TM 1517 partial cranium and mandible, refer to Sections (5.1.1) and (A.2.3) for provenance. The results for this hand sample are shown in Table (6.4).

Sample	Date	U (ppm)	Pb (ppm)	Pb (ng)	$^{206}Pb/^{204}Pb$ before blank	$^{238}U/^{208}Pb$	Error (1σ)	$^{206}Pb/^{208}Pb$	Error (1σ)	$^{207}Pb/^{204}Pb$	Error (1σ)	$^{208}Pb/^{204}Pb$	Error (1σ)
KBP03-A1▲	13/05/2003	0.601	0.0174	3.48	18.66	58.26	0.62	0.5026	0.0005	15.63	0.03	37.19	0.08
KBP03-B2△	13/05/2003	0.408	0.0097	1.265	18.58	70.76	1.47	0.5037	0.0007	15.57	0.03	36.99	0.1
KBP03-B3◎	13/05/2003	0.367	0.0058	0.872	19.61	107.4	4.8	0.5287	0.0015	15.61	0.06	37.42	0.17

Table 6.4: Table of Kromdraai KBP03 sub-sample results. Sub-sample weights; ▲ - 200mg; △ - 130mg; ◎ - 150mg. The blank applied was 92.9 ± 0.25pg. Blank corrections ranged between 2.67% and 10.65%.

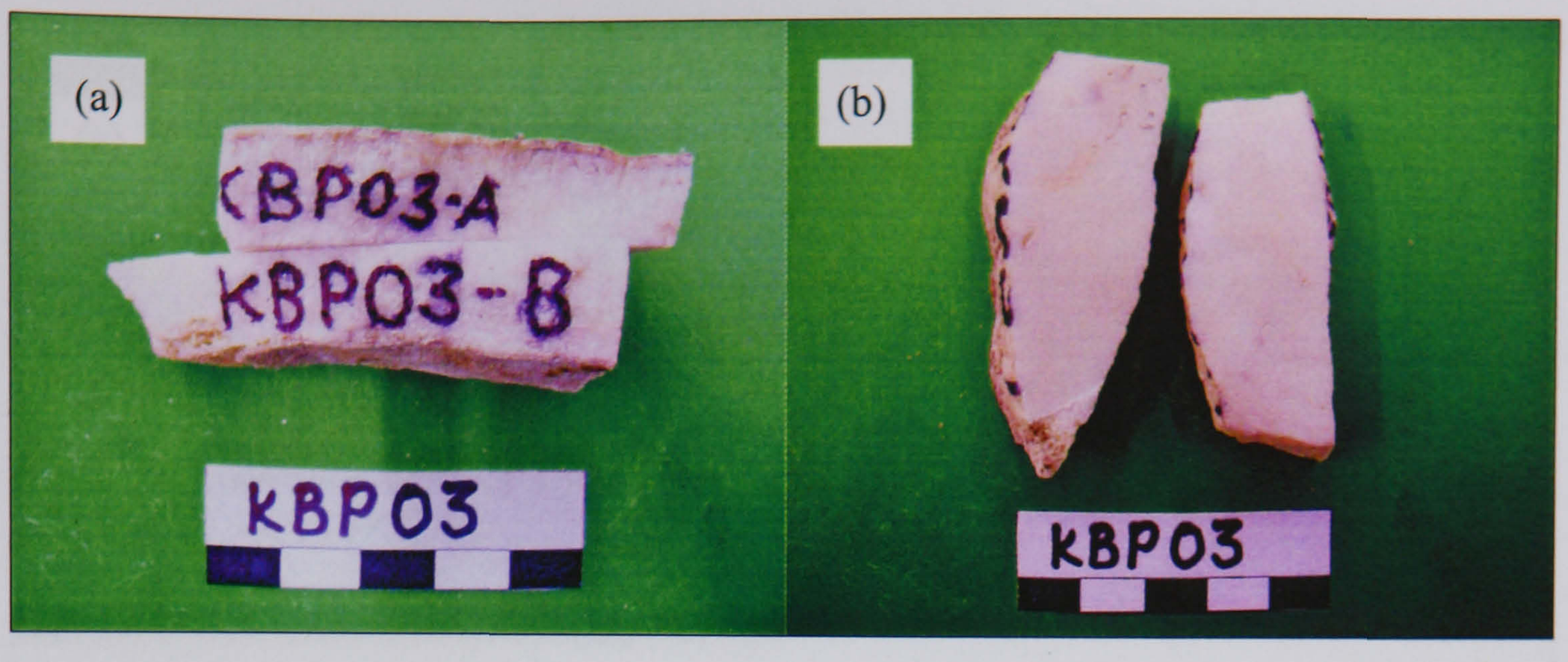

Figure 6.33: Photograph of reverse of KBP03 after sub-sampling (a); photograph of same showing internal texture (b) - scales shown in cm.

6.5.1 KBP03

Petrography

The majority of this sample appears clean and relatively dense. Some porous spaces can be seen under the hand-lens and the crystals are extremely fine. The outer surfaces of the samples appear more porous than the inner. This could be a primary or a secondary feature. The top surface of this sample has a rind $\approx 1\,\mathrm{mm}$ thick. This is grey in appearance and seems to be texturally different flowstone, rather than a layer of sediment. There is a similar but thinner layer on the bottom of the sample. Figures (6.33) and (6.34) show photographs of the different faces of KBP03.

U and Pb concentrations and distribution

Refer to Figure (6.35) for positioning of KBP03 sub-samples.

The U image, Figure (6.34), shows that U distribution is uniform. Only five Kromdraai samples were analysed, all from KBP03. Unfortunately, two of these were loaded with contaminated silica gel; the remaining three were analysed prior to the alteration in the fluoride precipitation step, see Section (5.2.2). The U concentrations in these three are not particularly high, between 0.37 ppm and 0.6ppm. The Pb concentrations are relatively high, in sub-sample A1 in particular. With only three points, having understandably low mu_{208} values, the data could

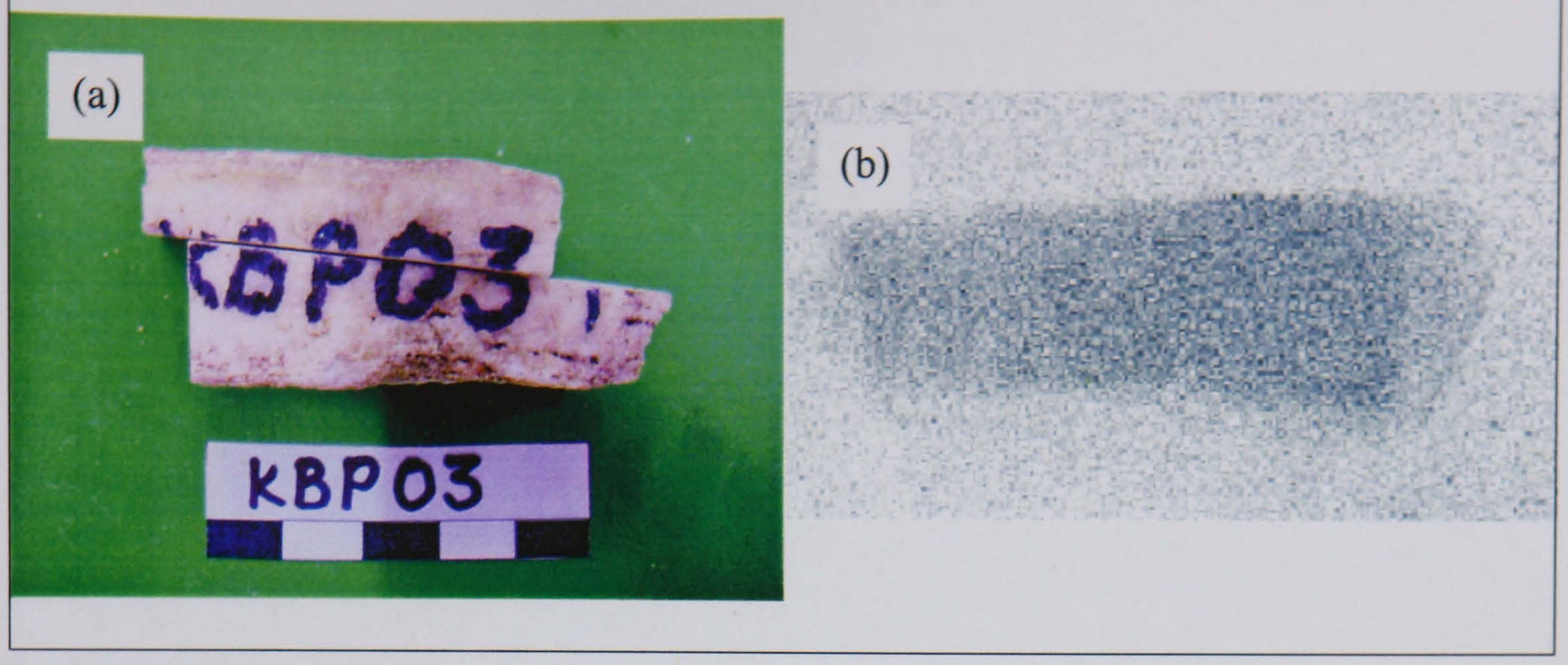

Figure 6.34: Photograph of front of KBP03 after sub-sampling (a) - scale shown in cm; corresponding uranium image (b). U image was taken prior to sub-sampling.

not be meaningfully plotted. This site is very exposed to erosion and has few flowstone deposits so it is unlikely to be ideal for U-Pb dating.

6.6 Swartkrans

The Swartkrans sample analysed, SKF01, was sampled from a band of flowstone in the rear north west corner of the inner cave above a pocket of member 1 breccia which produced the SK23 mandible. Refer to Sections (5.1.1) and (A.2.4) for provenance. The results for this hand sample are shown in Table (6.5).

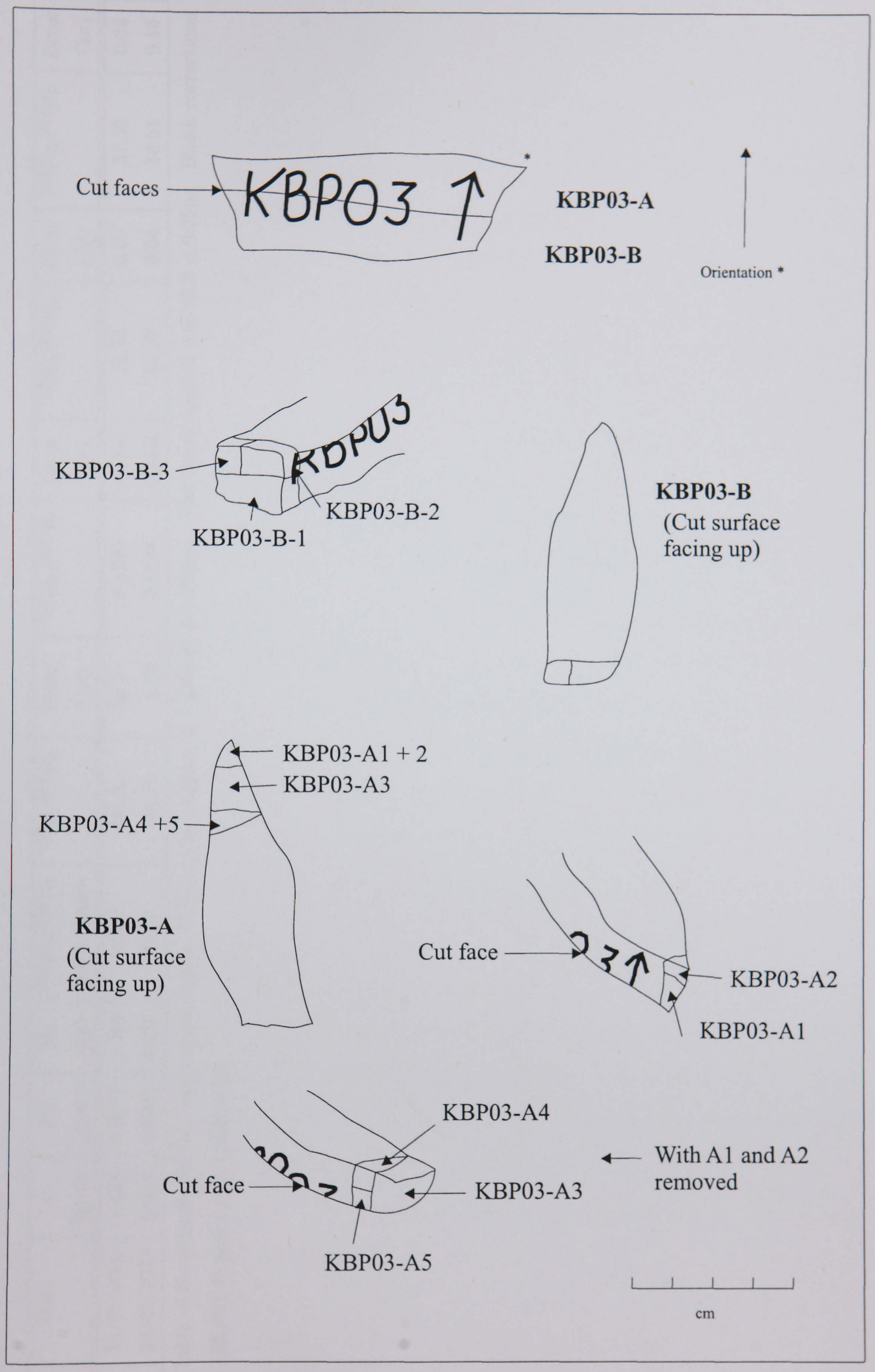

Figure 6.35: Schematic of KBP03 showing its progressive breaking up into sub-samples. The arrow shows the vertical orientation of the sample in situ.

Sample	Date	U (ppm)	Pb (ppm)	Pb (ng)	$^{206}Pb/^{204}Pb$ before blank	$^{238}U/^{208}Pb$	Error (1σ)	$^{206}Pb/^{208}Pb$	Error (1σ)	$^{207}Pb/^{204}Pb$	Error (1σ)	$^{208}Pb/^{204}Pb$	Error (1σ)
SKF01-1▲	13/05/2003	1.158	0.0071	3.065	20.88	281.5	25.1	0.5586	0.0009	15.75	0.03	37.59	0.08
SKF01-3Δ	13/05/2003	0.714	0.0249	4.972	19.49	48.28	0.36	0.5074	0.0005	15.79	0.06	38.51	0.16

Table 6.5: Table of Swartkrans SKF01 sub-sample results. Sub-sample weights; ▲ - 430mg; Δ - 200mg. The blank applied was 92.9 ± 0.25pg. Blank corrections were 3.03% (SKF01-1) and 1.87% (SKF01-3).

6.6.1 SKF01

Petrography

This sample is relatively clean, see Figure (6.36). The texture is dense, with grains that are easily visible to the naked eye and up to 2 or 3 mm long. The exposed top and front surfaces of the sample are discoloured by a light coating of sediment. There is a thin layer of dark red sediment on the underside and a lamina of the same material ≈ 1 cm from the base of the sample. Sub-sample 3 was abreast the red lamina.

U and Pb concentrations and distribution

Refer to Figure (6.36) for positioning of SKF01 sub-samples.

Two samples from SKF01 were analysed to assess their potential for dating. Both were analysed before the alteration to the fluoride precipitation step, see Section (5.2.2). Sub-sample 1 has a high U concentration of 1.2 ppm and a Pb concentration of 7.1 ppb, giving it a mu_{208} value of 281.5 ± 25.1. Sub-sample 3 has a lower U concentration and a high Pb concentration of 24.9 ppb. On the U image, Figure (6.36), the U concentration appears slightly higher at the base of the sample. Analysis of the samples does not show higher U in this area so it is reasonable to think that could be linked to the layer of red sediment there, which was not part of the analysed sub-samples.

Swartkrans results showed that the deposits do not appear to have sufficient quantities of U for this technique. The flowstone deposits and the fact that these are generally well protected from the elements means this site could produce U-Pb ages if samples with higher U concentrations could be sought out. However being a younger site than both the Limeworks or Sterkfontein could also mean that it falls just beyond the limits of this technique.

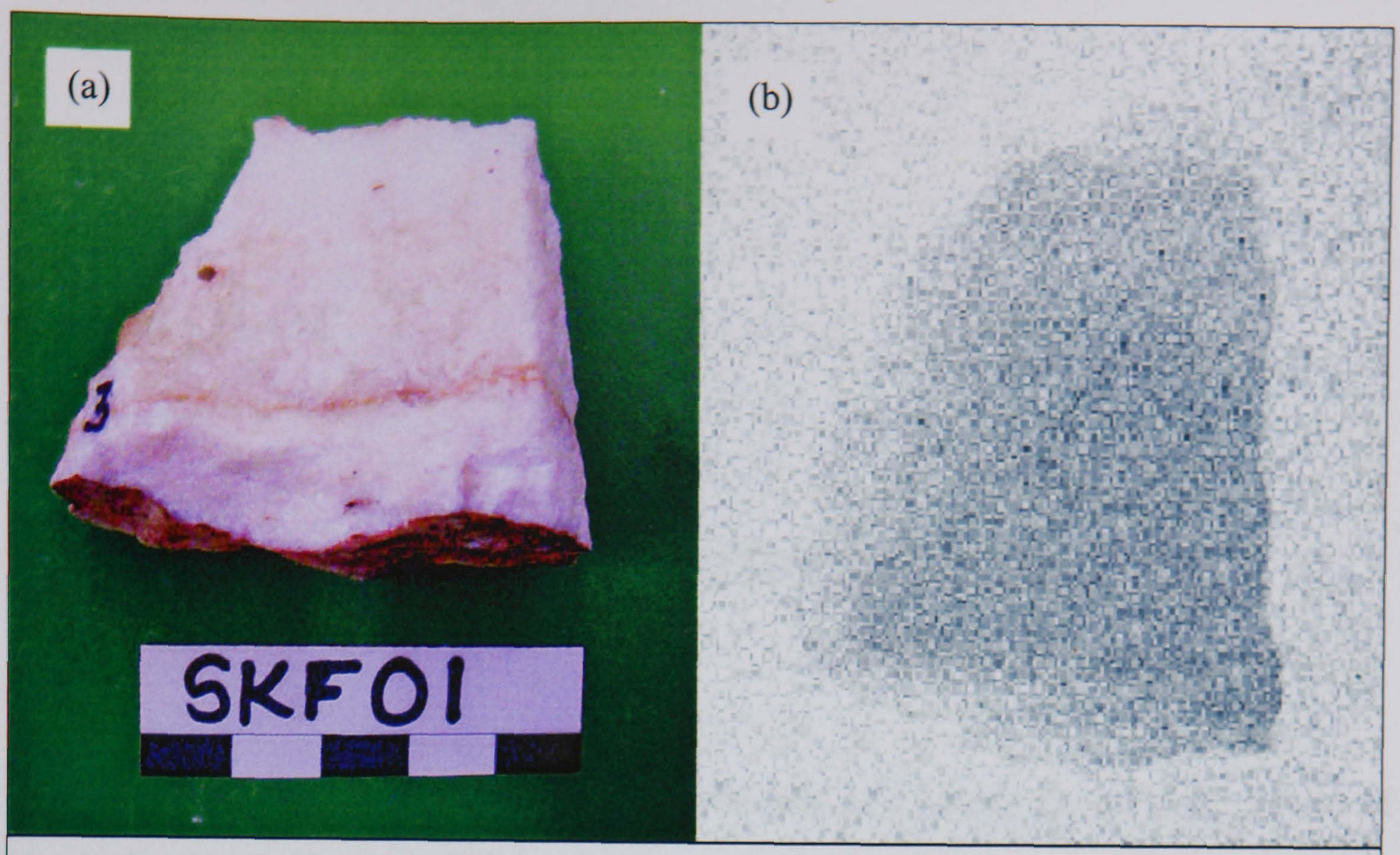

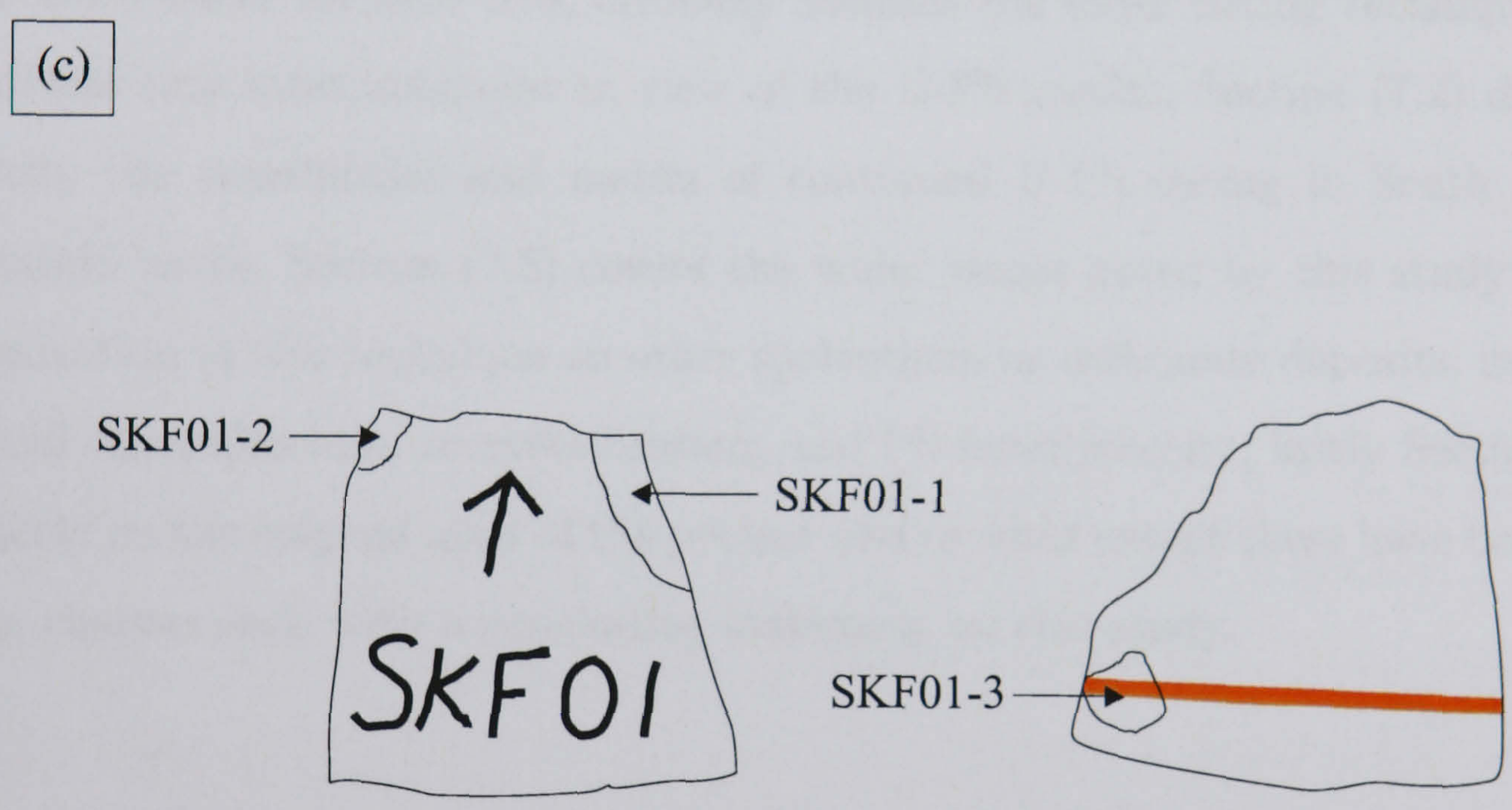

Figure 6.36: Photograph of reverse of SKF01 (a) - scale shown in cm; corresponding uranium image (b). Schematic of SKF01, from front and reverse angles, and sub-samples (c). Brown layer in schematic shows darker layer of flowstone and corresponds to one shown in photo.

Chapter 7

Discussion and conclusion

The discussion is split into four sections. Section (7.1) looks at the implications of the U-Pb dates for StW 573, critically assesses the other dating techniques, and provides new interpretations in view of the U-Pb results; Section (7.2) discusses briefly the possibilities and merits of continued U-Pb dating in South African hominid caves; Section (7.3) covers the wider issues noted by this study for the application of this technique on other speleothem or carbonate deposits, including initial disequilibrium, recrystallisation, and Pb heterogeneity; lastly Section (7.4) reflects on the original aims of the project and to what extent these have been met. The chapter ends with a concluding statement on this study.

7.1 Interpretation of the dates for Sterkfontein

The results of the dating techniques previously applied at Sterkfontein have, so far, not been able to reach an agreement for the age of the deposit, most notably for members 2 and 4, and the important hominid fossil, StW 573. Using the new U-Pb dates it is possible for some new interpretations to be made of the previous results and to better resolve the age issue for this fossil.

7.1.1 Uranium-Lead dating

The U-Pb results for Sterkfontein member 2 have important implications: not only for the age of StW 573, but also for the age and development of the cave itself.

The original maximum ages calculated by U-Pb dating for Sterkfontein are extremely useful in themselves. Even without disequilibrium correction these results improve the resolution of the age of this fossil. By using the results of the previous dating techniques as indicators of the possible range in age for StW 573, it was apparent from the maximum ages that these deposits had not incorporated exceptionally high ^{234}U disequilibrium, unlike some other speleothems in the Transvaal measured by Kronfeld *et al.* (1994). See Table (6.2) for calculated initial ^{234}U excess. Following correction for disequilibrium the best estimate ages were lower than the maximum ages by $\leq 0.94\,Ma$.

Implications of the new dates for Sterkfontein

The corrected U-Pb ages show that StW 573 is not as old as calculated by Partridge *et al.* (1999) and Partridge *et al.* (2003). This has implications for how this fossil fits in with other South and East African hominids, and thus for the origin of the human lineage. Firstly, these results confirm that the South African branch of the *Australopithecus* genus, which StW 573 most likely belongs to, is probably not as ancient as the East African branch. There is currently no fossil evidence to indicate that these early hominids had reached South African by 3 Ma. Secondly, the first evidence for the genus *Homo* appears in East Africa $\approx 2.5\,Ma$ (Johanson and Edgar, 2001), and therefore, at only 2.2 Ma, it is highly unlikely that StW 573 is a direct ancestor of modern humans. Whether this rules out all South African hominids as ancestral to *Homo sapiens* is questionable. There is still some debate as to whether East Africa is the first home of the later genus *Homo*. According to Pickford (2004), *Homo* appeared suddenly in East Africa suggesting that it evolved elsewhere. Pickford (2004) speculates that because Southern Africa suffered aridification much earlier than the rest of Africa, vertebrate species such as the Nile crocodile evolved over time in the dry southern environments, and having adapted to such conditions, could spread into other areas such as East Africa when these became drier. This may also have happened in the case of primitive hominids (Pickford, 2004). Until a fuller picture of human evolution is gained it is still entirely possible that *Homo sapiens* evolved via a *Homo* species which originated in South Africa before spreading across the African continent.

However at 2.2 Ma it is improbable that these individuals descended from the species represented by StW 573, although the two may have shared a common ancestor. A further question that arises from these results is, if the species that StW 573 represents did not evolve into modern humans, what happened to it? Did it simply die out, or did it evolve into other species such as *Australopithecus robustus*, as has previously been suggested? (Johanson and Edgar, 2001) In spite of the continued debate on human origins, what is certain is that StW 573 is the most complete hominid skeleton ever discovered, and it is vital that an age can be assigned in order to further clarify the path of human evolution.

A U-Pb age for StW 573 also provides interesting information on the history of the formation of this cave site. High levels of water flow are typically linked to flowstone deposition, and the age results for the two flowstone layers are testimony to the rate at which these deposits were forming. The U-Pb ages place flowstone layers 2C and 2B at the most 230 ka apart, although growth hiatuses in member 2 may actually account for the greatest proportion of the depositional time of this member. If the faunal dates for member 4 are credible, then combining them with the U-Pb results reveals that members 2 and 4 are contemporaneous, despite being vertically separated by several metres of sediment. This might be explained by periods of rapid sedimentation but it probably means that the stratigraphy is not as simple as has been assumed by previous dating techniques. The Sterkfontein deposits clearly do not conform to a straightforward depositional model, where member deposits were laid down sequentially on top of each other. This is an area which needs to be researched more thoroughly before using this as evidence for any other dating means. What is particularly interesting about the similar timing of deposition for members 2 and 4 is that Little Foot (StW 573) and Mrs Ples (Sts 5) may in fact turn out to be contemporaries, rather than being separated by several hominid generations.

7.1.2 Faunal dating

Refer to Figure (3.1) for previous interpretations of the faunal evidence.

The U-Pb ages agree with the original interpretation of the fauna by Cooke and Maglio (ref. from Tobias (1973)) prior to the discovery of StW 573. In spite of

this there are still questions over some of the assumptions made by this dating technique.

Comparing South African with East African sites is not necessarily reliable. As discussed earlier, the climatic conditions in these two regions were not guaranteed to be identical at that time (Pickford, 2004). In addition to this, the environments of accumulation are very different. The cave sites in South Africa therefore, evolved in entirely different landscapes and potentially different climates.

Faunal evidence is sometimes completely circumstantial. Is a sample representative of a species' actual proportion? Can one sample be taken as good evidence of its presence at that time? Turner (1997) notes how the number of specimens and number attributable to each species is generally low making faunal dating a difficult technique. Currently the faunal evidence for the dating of member 2 is one *Chasmaporthetes* fossil which is similar to one found at the 5 Ma site of Langebaanweg. However this same fossil is also likened to one from member 4 at Sterkfontein, and is not well represented in the Transvaal deposits. A *Dinofelis barlowi*[1] from member 4 has also been compared to some specimens from Langebaanweg and to a single specimen from the Limeworks member 3 (Turner, 1997). It is apparent then that some species and their features may span considerable periods of time. All the member 2 species do in fact exist in the member 4 deposits, and/or at younger sites. The two that don't appear in member 4, *Acinonyx jubatus*[2] and *Felis caracal*[3] are both found in the supposedly younger Swartkrans member 1 deposits (Brain and Watson, 1992).

Another factor that may bring faunal dating into question is the possibility of sedimentary, and therefore faunal, mixing between different members. If the deposits have been subjected to mixing it raises doubts over the faunal evidence. Although Clarke (2002b) asserts that though some of member 4 collapsed, fossils from member 4 or member 5 could not have found their way into the member 2 deposits.

---

[1]Sabre tooth cat.

[2]Cheetah. This specimen came from the limeminers dumps so it is uncertain as to whether this fossil can be assigned to member 2.

[3]Cat family. Caracal resembles a lynx.

Despite these problems with the faunal dating technique, this is still the most widely used out of all the dating techniques. It is possible that the sparse fauna in member 2 has been misinterpreted, for whatever reason. Taking the original estimate for member 4 by Vrba (1985), and using the faunal similarities between members 2 and 4 as evidence, the faunal date for StW 573 can easily be reconciled with the U-Pb result.

7.1.3 Palaeomagnetic dating

Palaeomagnetic dating in this context is immediately weakened by the fact that it relies on faunal dating for a guide and sedimentation rates as further chronological evidence.

The faunal guide for the palaeomagnetic dating of member 2 was between 2.7 and 4.0 Ma (Partridge *et al.*, 1999). This in turn was based on the evidence of one fossil and a stratigraphic separation of 15m between members 4 and 2. Partridge *et al.* (1999) identified five reversals within the member 2 deposits and in order to assign an age to StW 573 from these results, the sedimentation rate of the deposits was interpolated. Whether this is a safe assumption is debateable. The U-Pb dates and faunal dating of member 4 imply that the stratigraphy can not be interpreted in such a simplistic way, Section (7.1.1). Without precise knowledge of both sedimentation rates and how each deposit is related to every other, stratigraphic separation does not represent reliable evidence. Neither, for that matter, is a single fossil an adequate chronological indicator.

In spite of these issues, the measured palaeomagnetic sequence can be reinterpreted taking the U-Pb dates into account. In Figure (7.1) the palaeomagnetic sequence measured by Partridge *et al.* (1999) is reconsidered taking the U-Pb ages into account. The best estimate ages from layer 2C give a weighted average age of 2.17 ± 0.17Ma, see Figure (6.29), which can easily be matched to the Reunion 1 normal polarity event. The single STA15 best estimate age of $2.24+0.09/-0.07$Ma for layer 2B is not so easily resolved with the GPTS. Taking into account the polarity sequence measured by Partridge *et al.* (1999) the next reversal to which the lower portion of this flowstone can be assigned is the Reunion 2 normal polarity event (Cande and Kent, 1995). This event is dated at 2.42-2.44Ma, whereas the

STA15 best estimate can only accommodate a maximum of 2.33Ma. Whether this disparity is due to a poor U-Pb result or a mistake in the palaeomagnetic analyses cannot be determined.

7.1.4 Cosmogenic burial dating

Like U-Pb dating, cosmogenic burial dating is a relatively new dating technique in this context. However, like the palaeomagnetic and the faunal dating, this technique requires some very basic assumptions to be made about the history of mixing within the cave deposits. Aside from what the U-Pb dates imply with regards to the complex stratigraphy, it has been stated on many occasions previously that caves within the Malmani dolomite have all been subject to various periods of deposition, erosion, and subsidence of cave walls and roofs (Brain. 1958; Partridge, 1978; Jones *et al.*, 1986; Partridge and Watt, 1991; Brain and Watson, 1992; Clarke, 1994; Partridge, 2000; Clarke, 2002a). It is therefore highly likely that sediment was buried not only once but several times over before it reached its current location. In Partridge *et al.* (2003) it is stated that the mixing of the sample with older sediment is unlikely because of the "careful stratigraphic control." However other literature disputes this statement, see Partridge (1978), Partridge and Watt (1991), Schwarcz *et al.* (1994) and Gibbons (2003) for example.

The cosmogenic technique also applies a steady state erosion model in order to calculate the burial age. It is arguable as to whether an erosion rate can be presupposed. This site may indeed have been subject to slow uniform erosion but it was also subject to abrupt roof collapses where sediment was buried instantaneously.

It is stated in Granger *et al.* (2001) that burial dates "should be strictly considered as maximum ages, with the caveat that sediments could have conceivably undergone an earlier burial episode." In light of the U-Pb evidence this rule should also be applied to the cosmogenic burial dates for StW 573.

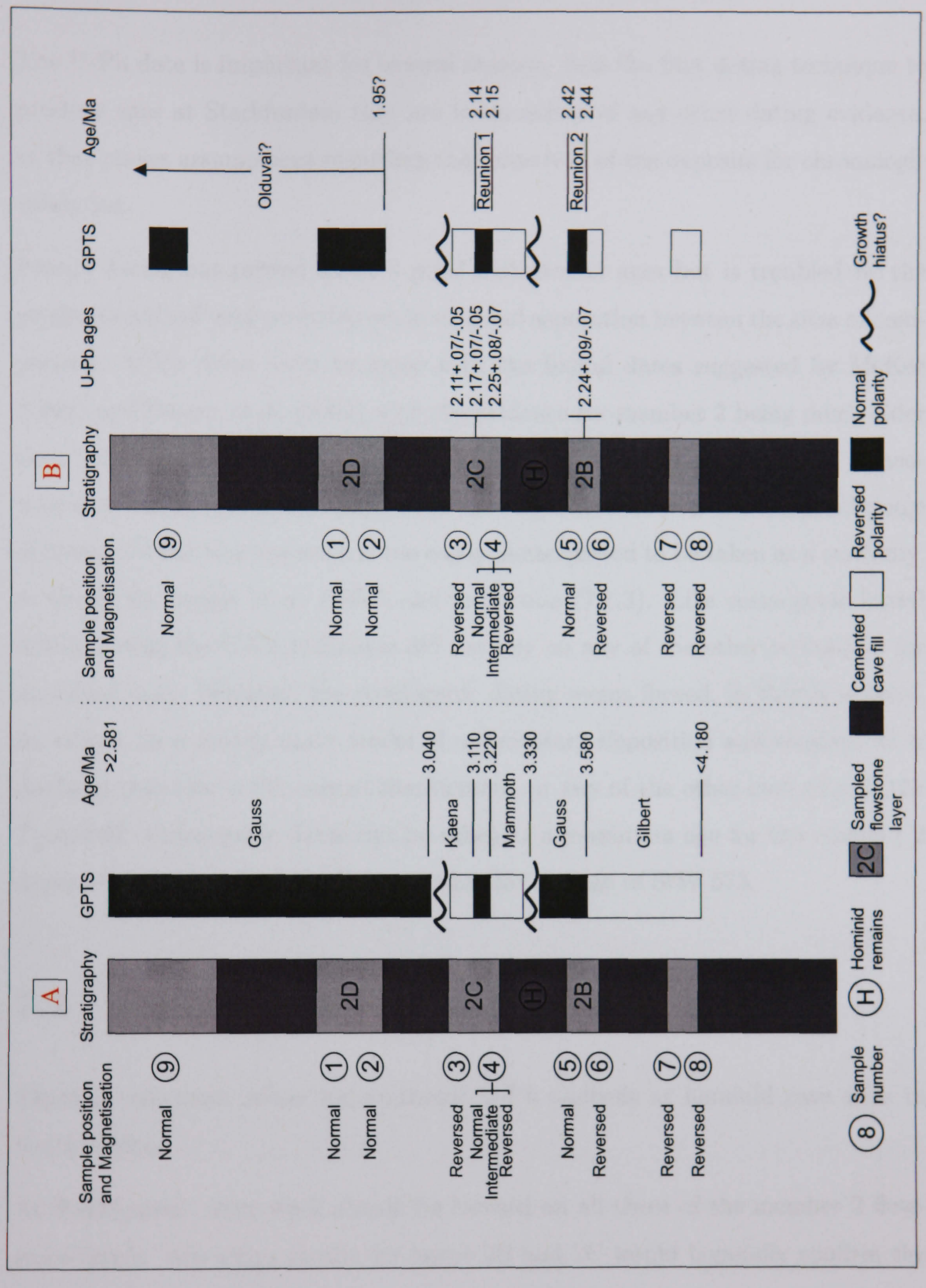

Figure 7.1: New interpretation of the palaeomagnetic record for member 2 Sterkfontein using the U-Pb ages. The original interpretation from Partridge *et al.* (1999) is shown in A, the new U-Pb based interpretation of this data is presented in B (Latham, A. G., (2005) pers. comm.). Figure is after Partridge *et al.* (1999) and Berger *et al.* (2002).

7.1.5 Summary and Conclusion

The U-Pb date is important for several reasons. It is the first dating technique to produce ages at Sterkfontein that are independent of any other dating evidence, or that makes assumptions regarding the formation of the deposits for chronologic validation.

Faunal dating has proved to be a good indicator of ages but is troubled by the geographical and very probable environmental separation between the sites of comparison. U-Pb dates seem to agree with the faunal dates suggested by McKee (1996) and Berger *et al.* (2002) with the evidence for member 2 being much older than member 4 being neither substantial nor convincing at present. The palaeomagnetic dating provides a snapshot of the magnetic field over the temporal range of member 2 but this sequence is too easily reinterpreted to be taken as a certainty, as shown by Berger *et al.* (2002) and in Section (7.1.3). Like cosmogenic burial dating dating the U-Pb technique did not rely on any of the other techniques for an initial date. However, the cosmogenic dating seems flawed, in that it is heavily reliant on a steady state model of sedimentary deposition and erosion. It is doubtful that this is the case at Sterkfontein, or any of the other cave sites in the Transvaal. Cosmogenic dates can be taken as a maximum age for the member 2 deposits, but not safely as a best estimate for the age of StW 573.

7.2 Future work in South Africa

There is still much scope for continued U-Pb analysis at hominid cave sites in South Africa.

At Sterkfontein, more work should be focused on all three of the member 2 flowstone layers. Any extra results for layers 2B and 2C would hopefully confirm the present results, and improve the scatter on the STA15 isochron for layer 2B. Layer 2D meanwhile is still undated. The STA07-C results indicate that this layer is datable, but a better understanding of ^{234}U disequilibrium would be required in order to turn any maximum ages into best estimates.

The Limeworks, despite being undated by this study has a great deal of potential

for further U-Pb dating. It is still believed to be the oldest of the caves and has the most extensive speleothem deposits. These deposits also display a wider variety of textures and colours. From these it may be possible to get a greater understanding of what types of material are better for U-Pb dating, and how or if visible features are related to U and Pb chemistry.

At the supposedly younger sites of Kromdraai B and Swartkrans there is less chance of success. This is firstly because they are believed to be considerably younger, but also because they do not have the same volumes or variety of speleothem available. Since this study only analysed very small amounts from these sites further work would be advisable to confirm their suitability for U-Pb, or not.

In addition to the sites studied here there are many other caves in the Transvaal that may benefit from this technique. There are several other caves that contain hominid remains such as Drimolen and Gladysvale. In addition to these there are many caves that are interesting in terms of climate change. Speleothems can preserve an excellent record of the environment in which they formed through stable O and C isotopes. These are all the more useful if dates can be assigned. Such studies have been applied at the Limeworks and at several other caves in the Makapansgat valley (Hopley, 2004).

7.3 Examination of the wider issues for Uranium-Lead dating

Having proven on two separate occasions the applicability of this technique, at Sterkfontein and by Richards *et al.* (1998), it is important to clarify any issues for further use of this technique either in South Africa or on other speleothem deposits.

7.3.1 Initial disequilibrium

At the outset of the project it was not anticipated how important isotopic heterogeneity would be. However this became a major part of the dating procedure,

firstly and most importantly for initial U disequilibrium, and secondly for initial Pb heterogeneity.

U compositions differed from those typical in nature, displaying an initial ^{234}U disequilibrium of around 2. This is relatively high but not as high as some of the values measured by Kronfeld *et al.* (1994). The high water flows that were required to produce the massive speleothem deposits in the Transvaal caves may have prevented such high excesses forming. Despite seemingly high water flows, U disequilibrium was still in effect in the aquifer, at that time, and it was important in terms of age calculations. Why U disequilibrium was so large in this context is still a mystery. But this is an issue which should be further investigated should more U-Pb dating be carried out in this area. In a wider context it is something that anyone intending to use this technique should be aware of. Initial disequilibrium may actually be useful in terms of palaeoclimate reconstruction. It is thought that high ^{234}U disequilibrium is linked to periods of low rainfall and retention of water in the aquifer (Kronfeld *et al.*, 1994). Temporal variations in ^{234}U disequilibrium may thus be demonstrative of changes in climatic conditions.

It was clear that U was not the only initially heterogeneous isotope when the isochrons were plotted. The U-Pb results are proof that Pb isotopic compositions varied spatially. The isochrons reflect a varied initial Pb composition for the forming flowstones. Even over short distances within a hand sample, initial Pb compositions were not always in agreement. The complete STA09 isochron, Figure (6.13) shows this variation. However some uniformity in the initial Pb signature can be seen when the STA09-C2 results are plotted on their own in Figure (6.15). These were samples that were contiguous and preserved initial Pb ratios that originated from the same Pb source. Initial Pb heterogeneity is even more apparent on the STA15 isochron. This is possibly because some of the STA15 sub-samples were more scattered across the hand sample than the STA09 sub-samples. It is evident from the STA15 isochron that even sub-samples which were close in situ sometimes had varying initial Pb isotopic compositions. Such initial heterogeneity is likely to have been caused by incorporation of Pb from a variety of sources. As with the U disequilibrium, further studies could be improved by gaining a better understanding of the provenance of initial Pb in speleothems. Certainly it is something to take into account when interpreting isochrons.

What has been shown by this study, is that initial ^{234}U excess can be accounted for. It was thought that a correction could not be made for the initial disequilibrium, but this was in fact possible. Issues such as this would previously have limited the capabilities of this technique. However, with continued improvements in technology, the measurement of remnant disequilibrium should no longer stand in the way of dating.

7.3.2 Recrystallisation

One of the initial considerations about the samples was whether they had been recrystallised, and if so, would this affect the results? The chronological problems associated with speleothem recrystallisation have already been introduced in Section (4.2.3). It is believed that speleothem at Sterkfontein recrystallised within a few thousand years of deposition (Partridge, T. C., (2004) pers. comm.). Early recrystallisation such as this would have a negligible effect on the final age. Analysis and interpretation of the Sterkfontein samples indicates that any diagenetic alteration such as recrystallisation that these samples may have been subjected to has not seriously affected the ages. The reasons for this conclusion are;

- Samples in general appeared clean and dense in terms of structure and had preserved primary depositional features. Sub-samples were carefully selected from the areas of material deemed most suitable for this technique.

- The STA09-C2 sub-samples define an isochron, Figure (6.15), with significantly less scatter than the complete STA09 isochron, Figure (6.13), suggesting that they were not subject to loss and/or gain of U or Pb but that they shared the same Pb isotopic signature, an isotopic signature that differed slightly from other sub-samples within the STA09 sub-sample suite. Data sets from the STA15 isochron, Figure (6.26), also show a similar trend.

- Agreement between results for SK3, STA09 and STA12. The maximum ages calculated for STA09 and STA12, which were at least 1 m apart in situ, are within error of one another. This is in spite of evidence of possible alteration in STA12, but preservation of primary features in STA09. Following disequilibrium correction, Section (6.3), the best estimate ages for all three samples

from flowstone 2C are within error of each other. The consistency of these results indicates that these samples were not subjected to a major alteration event, such as recrystallisation, long after deposition if at all.

These confirm that if the Sterkfontein samples were recrystallised then recrystallisation took place soon after the flowstone layers formed, and consequently the scatter associated with the plotted results is most likely related to initial Pb heterogeneity.

7.3.3 Sampling methods

Like all the other dating techniques U-Pb dating has its limitations. A certain type and quality of material was required but this was not always available. At Kromdraai B, for example, the amount of flowstone was limited. At Sterkfontein too, in member 4, where Sts 5 was removed from, flowstone was practically non-existent. It was extremely lucky that StW 573 was in an enclosed cave interlayered with flowstone that was often clean, dense, and entirely suitable for this technique.

What is noted from the work at the South African caves is that the cleanest densest samples weren't always the most successful in dating terms. STA12 for example, produced a considerably better isochron than STA09, yet STA09 appeared denser and had more perceptible primary structures. STA14 also was very clean and very dense but was of little use for dating because it had such low U concentrations. STA07-C was the most radiogenic sample and it was clean and dense in appearance. In spite of this a sensible isochron could not be plotted from the data.

Following selection of a hand sample it was important to then consider the sub-sampling and the position of sub-samples relative to each other. Sub-sampling may be improved by preliminary screening for higher U concentrations using phosphor imaging. This did not provide much information for this study but this is possibly because not all the analysed hand samples had a flat surface. For future reference it appears that this is necessary to ensure the strongest signal is received by the plate and to prevent interference from background radiation. At first sub-sampling was random, but it is clear from the isochrons that the sub-samples which were conjoined or in close proximity within a hand sample produced the better isochrons.

This can be seen by comparing the full STA09 isochron, Figure (6.13) and the isochron with the STA09-C2 sub-samples only, Figure (6.15). The isochron in the latter figure displays much better errors and scatter. What is also particular to these samples is that they all came from the same stratigraphic layer, as did the STA15-A2 suite and STA15-B2 and -B3 suite. Although the STA15-A2 sub-samples do not display the same uniformity as the STA09-C2 or the STA15-B2 and -B3 suites this is an important criteria for selecting sub-samples. Where there is no prior knowledge of sedimentation rate, sub-samples should be as closely related in terms of stratigraphy as possible in order that a reliable isochron can be plotted.

What the speleothems from South African demonstrate is that deposits can often be a hit or a miss for dating. Be that as it may, there is a much greater chance of producing ages where (i) the speleothem deposits are extensive and display a variety of textures and colours and (ii) sub-sampling is not a random procedure but is carefully thought out according to stratigraphy and relative sub-sample positions.

7.3.4 Analytical and data manipulation methods

When dealing with such small amounts of U and Pb it is inevitable that a relatively high percentage of the results may need to be rejected. In this study around 50% of analyses were rejected. This was due to a number of reasons such as Pb contamination and poor measurement of very small Pb signals. In such circumstances standard lab recipes may need to be adapted to best exploit the particular samples available. During this study further steps were added to the lab technique to ensure the highest possible U yield. Prior to the alterations the amount of U making it onto the column was inadequate for accurate measurement on the TIMS.

Because of the very low Pb amounts, factors such as the lapse in time between dissolution and analysis became important, see Section (5.4). This was only considered after lab work had finished, but some of the sample results where Pb concentrations can be seen to increase over time, suggest that this may be a problem. This is simple for a researcher to resolve; only dissolve what can be analysed immediately or within a short period of time thereafter. Although multiple sub-sampling and dissolution save time and effort, it is inadvisable to analyse samples

after months of storage. During this time they may have accumulated an unknown level of Pb contamination.

Running the TIMS is another area where very small amounts of sample mean extra care and attention is required. Despite a new automated Finnigan Triton machine a lot of the samples had to be run manually. After several analyses a method was decided for the running of Pb samples on the TIMS where the ^{204}Pb was always run on the SEM. An issue which is important to consider here is whether the difference in yield between the SEM and the faraday is sufficiently known. Providing it is known, a correction can easily be applied. Whether the TIMS is in fact the best machine for the job is also under consideration; the disequilibrium measurements were made on an ICP-MS. Calibration of the SEM on the TIMS was still in progress when this thesis was completed, so that accurate excess ^{234}U measurements at the permil level were not possible at Leeds. Choice of machine then may be something to investigate for future work.

The use of ^{208}Pb to normalise was an important part of this study. Using ^{208}Pb resulted in improved errors and therefore improved isochrons and ages. This may not be applicable to all speleothem deposits, particularly those that have incorporated a detrital component. Nonetheless this is a useful method since it does not rely on accurate measurement of ^{204}Pb which is much lower in abundance. It is also fairly simple to check whether ^{232}Th activity can be assumed to be negligible by comparing ^{208}Pb/^{204}Pb ratios between samples. An exception to this is when initial ^{232}Th activity can be assumed to be zero, and initial Pb is thought to have been heterogeneous. Variations were observed in the ^{208}Pb/^{204}Pb ratios from the Sterkfontein samples, but such variability was also present in the ^{207}Pb/^{204}Pb ratios. Since it was known that these deposits contained insignificant amounts of ^{235}U to account for the ^{207}Pb variations it was felt that the ^{208}Pb variations were the result of initial Pb conditions rather than thorogenic ingrowth.

Once samples have been analysed it is then necessary to consider whether the data are suitable for plotting an isochron. The South African samples had in general, very low U and Pb concentrations. In comparison to the U concentrations measured by Richards *et al.* (1998), those from South Africa were up to 27 times smaller. Ideally the U concentrations would have been higher. In spite of this,

isochrons were produced and this is promising for further research on material which is not exceptionally U rich. In addition to concentration requirements, a spread in U-Pb ratios is preferable for producing an accurate isochron. The spread on the Sterkfontein isochrons was good. However the STA12 results actually showed that the spread in mu_{208} can be as little as 500 and an isochron can still be produced. The difference in the error on the age between the small range isochron, 2.64 ± 0.12 Ma, and the full range isochron, Figure (6.19), is significant. However, the MSWD is nearly identical, and on its own the low range STA12 isochron is still adequate evidence for the age of this flowstone. The STA15 results however showed that even a large spread in mu_{208} can not compensate for scatter caused by geological effects.

A final issue to consider when dealing with very small amounts of Pb is the application of a blank correction. There is no way of testing how representative a blank is of the Pb accumulated by individual samples during analysis. Blank corrections in particular can cause a problem where any common Pb picked up by a sample during analysis differs in composition from Pb incorporated in the sample when it formed. This can displace the sample, as it is corrected according to the blank composition and not according to its initial Pb composition. Where the blank correction is perfect this is not a problem, but too great or too small a correction will dislocate the sample on the age plot. Comparisons between replicate samples analysed simultaneously, and between replicates analysed on separate dates showed that the amount of blank Pb incorporated by a sample varied in both scenarios. Accordingly, it was felt that the best method for blank correcting the South African samples was to take an average of the blank size and composition over time. Because all results were treated to the same correction they were much easier to compare. A small number of blanks that were spuriously large were not included in this calculation.

7.4 Re-examination of original aims

Refer to original aims laid out in Section (1.2).

The primary aim of this study was to assign ages with improved resolution to

the hominid fossils at selected sites in South Africa, through the U-Pb dating of associated speleothem deposits. Preliminary work done at Sterkfontein. see Section (4.2.3), had proved very promising. However it was known that this method may not be suitable for all the sites or even for any other material sampled from Sterkfontein. The main aim has been met to some degree then. Results have been produced for what is currently the most important hominid fossil in South Africa, StW 573. This in itself is a huge achievement for this research. It is only unfortunate that deposits at the other three sites, the Limeworks, Kromdraai B and Swartkrans did not yield dates.

The secondary aim of the study was to investigate further the applicability of this technique in this and similar contexts and to address any issues which arise from this. In particular the results have given added insight into the issues of initial ^{234}U disequilibrium and initial Pb heterogeneity. This study has also introduced new variations in sampling and analytical procedures, as summarised in Section (7.3.3) and Section (7.3.4), that future researchers may want to refer to.

7.5 Conclusions

The U-Pb ages calculated by this study show that the hominid fossil StW 573 is, at *c.* 2.2 Ma, considerably younger than previous researchers have estimated. This may have implications for the position of South African hominids in the evolutionary picture, and for the structure of the human family tree. It has also been shown that, like most caves, Sterkfontein has a complex stratigraphy that can not easily be determined. Previous dating techniques have relied too heavily on stratigraphic assumptions, but can be re-interpreted with the new U-Pb dates in mind. It is necessary when dealing with deposits such as these to have several dating techniques giving concordant results. With the introduction of the U-Pb data this is now possible.

Since the pioneering work of Moorbath *et al.* (1987) U-Pb dating has shown again how applicable it is for the dating of carbonates, and more specifically for dating young carbonates in what is a notoriously difficult geological period in geochronological terms.

References

Bateman, H. (1910). Solution of a system of differential equations occurring in the theory of radio-active transformations. *Proceedings of the Cambridge Philosophical Society* **15**, 423–427.

Berger, L. R., Lacruz, R. and de Ruiter, D. J. (2002). Brief Communication: Revised Age Estimates of *Australopithecus*-Bearing Deposits at Sterkfontein, South Africa. *American Journal of Physical Anthropology* **119**, 192–197.

Bonotto, D. M. and Andrews, J. N. (2000). The transfer of uranium isotopes ^{234}U and ^{238}U to the waters interacting with carbonates from Mendip Hills area (England). *Applied Radiation and Isotopes* **52**, 965–983.

Bourdon, B. (1992). U-Th chemistry and mass spectrometry at Lamont.

Bourdon, B., Henderson, G. M., Lundstrom, C. C. and Turner, S. P. (Eds.) (2003). *Reviews in Mineralogy & Geochemistry*, Volume 52; Uranium-series Geochemistry. Mineralogical Society of America.

Brain, C. K. (1958). The Transvaal ape-man-bearing cave deposits. *Transvaal Museum Memoir* 11, Transvaal Museum: Pretoria.

Brain, C. K. (1993). Structure and Stratigraphy of the Swartkrans Cave in the Light of the New Excavations. In C. K. Brain (Ed.), *Swartkrans: A Cave's Chronicle of Early Man.* Pretoria: Transvaal Museum Monograph No.8.

Brain, C. K. (1995). The Influence of Climatic Changes on the Completeness of the Early Hominid Record in the Southern African Caves, with Particular Reference to Swartkrans. In E. S. Vrba, G. H. Denton, T. C. Partridge and L. H. Burckle (Eds.), *Paleoclimate and Evolution with Emphasis on Human Origins*, Chapter 30, pp. 451–458. Yale University Press.

Brain, C. K. and Watson, V. (1992). A Guide to the Swartkrans Early Hominid Cave Site. *Annals of the Transvaal Museum* **35**:(25), 343-365, Transvaal Museum: Pretoria.

Brock, A., McFadden, P. L. and Partridge, T. C. (1977). Preliminary palaeomagnetic results from Makapansgat and Swartkrans. *Nature* **266**, 249–250.

Cande, S. C. and Kent, D. V. (1995). Revised calibration of the geomagnetic polarity timescale for the Late Cretaceous and Cenozoic. *Journal of Geophysical Research* **100**.

Carswell, D. J. (1957). Separation of Thorium and Uranium Nitrates by Anion Exchange. *Journal of Inorganic Nuclear Chemistry* **3**, 384–387.

Catuneanu, O. and Eriksson, P. G. (1999). The Sequence stratigraphic concept and the Precambrian rock record: an example from the 2.7-2.1Ga Transvaal Supergroup, Kaapvaal craton. *Precambrian Research* **97**, 215–251.

Chen, J. H. and Wasserburg, G. J. (1981). Isotopic Determination of Uranium in Picomole and Subpicomole Quantities. *Analytical Chemistry* **53**, 2060–2067.

Clarke, R. J. (1994). On some new interpretations of Sterkfontein stratigraphy. *South African Journal of Science* **90**, 211–214.

Clarke, R. J. (1998). First ever discovery of a well-preserved skull and associated skeleton of *Australopithecus*. *South African Journal of Science* **94**, 460–463.

Clarke, R. J. (2002a). Newly revealed information on the Sterkfontein Member 2 *Australopithecus* skeleton. *South African Journal of Science* **98**, 523–526.

Clarke, R. J. (2002b). On the unrealistic 'Revised age estimates' for Sterkfontein. *South African Journal of Science* **98**, 415–419.

Clarke, R. J., Partridge, T. C., Granger, D. E. and Caffee, M. W. (2003). Dating the Sterkfontein Fossils. *Science* **301**, 596–597.

Clarke, R. J. and Tobias, P. V. (1995). Sterkfontein Member 2 Foot Bones of the Oldest South African Hominid. *Science* **269**, 521–524.

Cole, J. M., J., Nienstedt, Spataro, G., Rasbury, E. T., Lanzirotti, A., Celestian, A. J., Nilsson, M. and Hanson, G. N. (2003). Phosphor imaging as a tool for in situ mapping of ppm levels of uranium and thorium in rocks and minerals. *Chemical Geology* **193**, 127–136.

Cooke, H. B. S. (1970). Notes from members. *Bulletin of the Society of Vertebrate Palaeontology* **90**, 2.

Curnoe, D., Grün, R., Taylor, L. and Thackeray, F. (2001). Direct ESR dating of a Pliocene hominin from Swartkrans. *Journal of Human Evolution* **40**, 379–391.

Curnoe, D., Grün, R. and Thackeray, J. F. (2002). Electron spin resonance dating of tooth enamel from Kromdraai B, South Africa. *South African Journal of Science* **98**, 540.

DeWolf, C. P. and Halliday, A. N. (1991). U-Pb dating of a remagnetized paleozoic limestone. *Geophysical Research Letters* **18**, 1445–1448.

Dickin, A. P. (1997). *Radiogenic Isotope Geology* (1st Paperback ed.). Cambridge University Press.

Faris, J. P. and Buchanan, R. F. (1964). Anion Exchange Characteristics of Elements in Nitric Acid Medium. *Analytical Chemistry* **36**, 1157–1158.

Faure, G. (1986). *Principles of Isotope Geology* (2nd ed.). John Wiley & Sons.

Faure, G. and Mensing, T. M. (2005). *Isotopes: Principles and Applications* (3rd ed.). John Wiley & Sons.

Ford, D. and Williams, P (1989). *Karst Geomorphology and Hydrology.* Unwin Hyman.

Friedlander, G., Kennedy, J. W., Macias, E. S. and Miller, J. M. (1981). *Nuclear and Radiochemistry* (3rd ed.). John Wiley & Sons.

Frisia, S. (1996). Petrographic Evidences of Diagenesis in Speleothems: Some examples. *Spéléochronos* **7**, 21–30.

Frisia, S., Borsato, A., Fairchild, I. J and McDermott, F. (2000). Calcite Fabrics, Growth Mechanisms, and Environments of Formation in Speleothems from the Italian Alps and Southwestern Ireland. *Sedimentary Research* **70**, 1183–1196.

Gascoyne, M., Schwarcz, H. P. and Ford, D. C. (1978). Uranium series dating and stable isotope studies of speleothems: Part 1. Theory and Techniques. *British Cave Research Association Transactions* **5**, 91–111.

Gibbons, A. (2003). Great Age suggested for South African Hominids. *Science* **300**, 562.

Granger, D. E., Fabel, D. and Palmer, A. N. (2001). Pliocene-Pleistocene incision of the Green River, Kentucky, determined from radioactive decay of cosmogenic ^{26}Al and ^{10}Be in Mammoth Cave sediments. *Geological Society of America Bulletin* **113**, 825–836.

Granger, D. E., Kirchner, J. W. and Finkel, R. C. (1997). Quaternary downcutting rate of the New River, Virginia, measured from differential decay of cosmogenic ^{26}Al and ^{10}Be in cave-deposited alluvium. *Geology* **25**, 107–110.

Grine, F. E. (1993). Description and Preliminary Analysis of New Hominid Craniodental Fossils from the Swartkrans Formation. In C. K. Brain (Ed.), *Swartkrans: A Cave's Chronicle of Early Man*, Chapter 3, pp. 75–116. Pretoria: Transvaal Museum Monograph No.8.

Grün, R. (1995). Semi-non-destructive, single aliquot ESR dating. *Ancient TL* **13**, 3–7.

Grün, R., Schwarcz, H. P. and Zymela, S. (1987). Electron Spin Resonance dating of tooth enamel. *Canadian Journal of Science* **24**.

Herries, A. and Latham, A. (2002). Dating of the depositional sequence and Australopithecine "Grey Breccia" of Makapansgat Limeworks using magnetostratigraphy. In *American Journal of Physical Anthropology: 71st Annual Meeting issue*, Volume 117, S34, pp. 84–85.

Herries, A. I. R. (2003). Magnetostratigraphy of the South African hominid palaeocaves. In *American Journal of Physical Anthropology: 72nd Annual Meeting issue*, Volume 120, S36, pp. 113.

Hopley, P. J. (2004). *Palaeoenvironmental reconstruction of South African hominin-bearing cave deposits using stable isotope geochemistry.* Ph. D. thesis, University of Liverpool.

Israelson, C., Halliday, A. N. and Buchardt, B. (1996). U-Pb dating of calcite concretions from Cambrian black shales and the Phanerozoic time scale. *Earth and Planetary Science Letters* **141**, 153–159.

Jahn, B. M. and Cuvellier, H. (1994). Pb-Pb and U-Pb geochronology of carbonate rocks: an assessment. *Chemical Geology* **115**, 125–151.

Johanson, D. and Edgar, B. (2001). *From Lucy to Language* (1st Paperback ed.). Casson.

Jones, C. E., Halliday, A. N. and Lohmann, K. C. (1995). The impact of diagenesis on high-precision U-Pb dating of ancient carbonates: An example from the Late Permian of New Mexico. *Earth and Planetary Science Letters* **134**, 409–423.

Jones, D. L., Brock, A. and McFadden, P. L. (1986). Palaeomagnetic results from the Kromdraai and Sterkfontein hominid sites. *South African Journal of Science* **82**, 160–163.

Korkisch, J. and Hazan, I. (1965). Anion Exchange Separations in Hydrobromic Acid-Organic Solvent Media. *Analytical Chemistry* **37**, 707–710.

Kronfeld, J., Vogel, J. C. and Talma, A. S. (1994). A new explanation for extreme $^{234}U/^{238}U$ disequilibria in a dolomitic aquifer. *Earth and Planetary Science Letters* **123**, 81–93.

Ku, T.-L. (1976). The Uranium-series methods of age determination. *Annual Review of Earth and Planetary Sciences* **4**, 347–378.

Ku, T. L. (2000). Uranium-series methods. In J. S. Noller, J. M. Sowers and W. R. Lettis (Eds.), *Quaternary Geochronology.* AGU.

Latham, A. G., Herries, A., Quinney, P., Sinclair, A. and Kuykendall. K. (1999). The Makapansgat Australopithecine site from a speleological perspective. In A. M. Pollard (Ed.), *Geoarchaeology: exploration, environments, resources.* Number 165, pp. 61–77. The Geological Society of London.

Latham, A. G., Herries, A. I. R. and Kuykendall, K. (2003). The formation and sedimentary infilling of the Limeworks Cave, Makapansgat, South Africa. *Palaeontologia Africana* **39**, 69–82.

Latham, A. G. and Schwarcz, H. P. (1992). Carbonate and Sulphate precipitates. In M. Ivanovich and R. S. Harmon (Eds.), *Uranium-series Disequilibrium: Applications to Earth, Marine, and Environmental Sciences* (2nd ed.)., Chapter 12, pp. 423–459. Oxford Science.

Leakey, R. E. (1981). *The Making of Mankind.* Book Club Associates, London.

Ludwig, K. (1977). Effect of initial radioactive-daughter disequilibrium on U-Pb isotope apparent ages of young minerals. *Journal of Research, U.S. Geological Survey* **5**, 663–667.

Ludwig, K. R. (2003). ISOPLOT 3.00: A Geochronological Toolkit for Microsoft Excel.

Maguire, B. (1980). Further observations on the nature and provenance of the lithic artefacts from the Makapansgat Limeworks. *Palaeontologia Africana* **23**, 127–151.

Manhes, G. (1982). Développement de L'énsemble Chronométrique U-Th-Pb. Contribution à la Chronologie Initiale du Système Solaire. Thèse de doctorat d'état, Université de Paris VII.

Manhes, G., Minster, J. F. and Allègre, C. J. (1978). Comparative Uranium-Thorium-Lead and Rubidium-Strontium study of the Saint Sèverin amphoterite: consequences for early solar system chronology. *Earth and Planetary Science Letters* **39**, 14–24.

Marshall, D. J. (1988). *Cathodoluminescence of Geological Materials.* Unwin Hyman.

McFadden, P. L., Brock, A. and Partridge, T. C. (1979). Palaeomagnetism and the age of the Makapansgat hominid site. *Earth and Planetary Science Letters* **44**, 373–381.

McKee, J. K. (1991). Palaeo-ecology of the Sterkfontein Hominids: A review and synthesis. *Palaeontologia Africana* **28**, 41–51.

McKee, J. K. (1996). Faunal Evidence and Sterkfontein Member 2 Foot Bones of Early Hominid. *Science* **271**, 1301.

McKie, R. (2000). *Ape-man: The story of human evolution.* BBC Worldwide Ltd.

Moorbath, S., Taylor, P. N., Orpen, J. L., Treloar, P. and Wilson, J. F. (1987). First direct radiometric dating of Archean stromatolitic limestone. *Nature* **326**, 865–867.

Partridge, T. C. (1973). Geomorphological Dating of Cave Openings at Makapansgat, Sterkfontein, Swartkrans and Taung. *Nature* **246**, 75–79.

Partridge, T. C. (1978). Re-appraisal of lithostratigraphy of Sterkfontein hominid site. *Nature* **275**, 282–287.

Partridge, T. C. (1979). Re-appraisal of lithostratigraphy of Makapansgat Limeworks hominid site. *Nature* **279**, 484–488.

Partridge, T. C. (1982). Some preliminary observations on the stratigraphy and sedimentology of the Kromdraai B Hominid site. In J. A. Coetzee and E. M. Van Zinderen Bakker Sr (Eds.), *Palaeoecology of Africa and the Surrounding Islands*, Volume 15, pp. 3–12. SASQUA Proceedings of the VIth biennial Conference, Transvaal Museum, Pretoria, 26-29 May 1981. Edited by the SASQUA Editorial Committee: Vogel, J.C., Voigt, E.A. and Partridge, T.C.: A.A. Balkema.

Partridge, T. C. (1986). Palaeoecology of the Pliocene and Lower Pleistocene hominids of Southern Africa: how good is the chronological and palaeoenvironmental evidence? *South African Journal of Science* **82**, 80–83.

Partridge, T. C. (2000). Hominid-Bearing Cave and Tufa Deposits. In T. C. Partridge and R. R. Maud (Eds.), *The Cenozoic of Southern Africa*, Chapter 7, pp. 100–125. Oxford University Press.

Partridge, T. C., Granger, D. E., Caffee, M. W. and Clarke, R. J. (2003). Lower Pliocene Hominid remains from Sterkfontein. *Science* **300**, 607–612.

Partridge, T. C., Latham, A. G. and Heslop, D. (2000). Appendix on Magnetostratigraphy of Makapansgat, Sterkfontein, Taung and Swartkrans. In T. C. Partridge and R. R. Maud (Eds.), *The Cenozoic of Southern Africa*, Chapter 7, pp. 126–129. Oxford University Press.

Partridge, T. C., Shaw, J., Heslop, D. and Clarke, R. J. (1999). The new Hominid skeleton from Sterkfontein: Age and preliminary assessment. *Journal of Quaternary Science* **14**, 293–298.

Partridge, T. C. and Watt, I. B. (1991). The stratigraphy of the Sterkfontein Hominid Deposit and its relationship to the underground cave system. *Palaeontologia Africana* **28**, 35–40.

Pickering, R. (2004). The stratigraphy, chronology and palaeoenvironment of the Pleistocene cave fill, Gladysvale Cave, South Africa,. MSc thesis, University of the Witwatersrand.

Pickering, T. R., Clarke, R. J. and Heaton, J. L. (2004). The context of Stw 573, an early hominid skull and skeleton from Sterkrfontein Member 2: taphonomy and paleoenvironment. *Journal of Human Evolution* **46**, 277–295.

Pickford, M. (2004). Southern Africa: a cradle of evolution. *South African Journal of Science* **100**, 205–214.

Pike, A. W. G. and Pettitt, P. B. (2003). U-series dating and Human Evolution. In B. Bourdon, G. M. Henderson, C. C. Lundstrom and S. P. Turner (Eds.), *Reviews in Mineralogy & Geochemistry*, Volume 52; Uranium-series Geochemistry, pp. 607–629. Mineralogical Society of America.

Porcelli, D. and Swarzenski, P. W. (2003). The Behavior of U- and Th-series Nuclides in Groundwater. In B. Bourdon, G. M. Henderson, C. C. Lundstrom

and S. P. Turner (Eds.), *Reviews in Mineralogy & Geochemistry*, Volume 52: Uranium-series Geochemistry, pp. 317–361. Mineralogical Society of America.

Rasbury, E. T., Hanson, G. N., Meyers, W. J. and Saller, A. H. (1997). Dating of the time of sedimentation using U-Pb ages for paleosol calcite. *Geochimica et Cosmochimica Acta* **61**, 1525–1529.

Rehkämper, M. (1995). A highly sensitive HPLC method for the determination of Th and U concentrations in geological samples. *Chemical Geology* **119**, 1–12.

Richards, D. A., Bottrell, S. H., Cliff, R. A., Ströhle, K. and Rowe, P. J. (1998). U-Pb Dating of a speleothem of Quaternary age. *Geochimica et Cosmochimica Acta* **62**, 3683–3688.

Richards, D. A. and Dorale, J. A. (2003). Applications of Speleothems. In B. Bourdon, G. M. Henderson, C. C. Lundstrom and S. P. Turner (Eds.), *Reviews in Mineralogy & Geochemistry*, Volume 52; Uranium-series Geochemistry, pp. 407–460. Mineralogical Society of America.

Romer, R. L. (2001). Isotopically heterogeneous initial Pb and continuous ^{222}Rn loss in fossils: The U-Pb systematics of *Brachiosaurus brancai*. *Geochimica et Cosmochimica Acta* **65**, 4201–4213.

Schwarcz, H. P. and Blackwell, B. A. (1992). Archaeological Applications. In M. Ivanovich and R. S. Harmon (Eds.), *Uranium-series Disequilibrium: Applications to Earth, Marine, and Environmental Sciences* (2nd ed.)., Chapter 15, pp. 513–552. Oxford Science.

Schwarcz, H. P, Grün, R. and Tobias, P. V. (1994). ESR dating studies of the australopithecine site of Sterkfontein, South Africa. *Journal of Human Evolution* **26**, 175–181.

Schwarcz, H. P. and Lee, H. K. (2000). Electron Spin Resonance dating of fault rocks. In J. S. Noller, J. M. Sowers and W. R. Lettis (Eds.), *Quaternary Geochronology*, pp. 177–186. AGU.

Smith, P. E., Brand, U. and Farquhar, R. M. (1994). U-Pb systematics and alteration trends of Pennsylvanian-aged aragonite and calcite. *Geochimica et Cosmochimica Acta* **58**, 313–322.

Smith, P. E. and Farquhar, R. M. (1989). Direct dating of Phanerozoic sediments by the ^{238}U-^{206}Pb method. *Nature* **341**, 518–521.

Smith, P. E., Farquhar, R. M. and Hancock, R. G. (1991). Direct radiometric age determination of carbonate diagenesis using U-Pb in secondary calcite. *Earth and Planetary Science Letters* **105**, 474–491.

Steiger, R. H. and Jäger, E. (1977). Subcommission on Geochronology: Convention on the use of decay constants in geo- and cosmochronology. *Earth and Planetary Science Letters* **36**, 359–362.

Tankard, A. J., Jackson, M. P. A., Eriksson, K. A., Hobday, D. K., Hunter, D. R. and Minter, W. E. L. (1982). *Crustal Evolution of Southern Africa: 3.8 Billion Years of Earth History.* Springer-Verlag.

Thackeray, J. F., Kirschvink, J. L. and Raub, T. D. (2002). Palaeomagnetic analyses of calcified deposits from the Plio-Pleistocene hominid site of Kromdraai, South Africa. *South African Journal of Science* **98**, 537–539.

Thompson, G. M., Lumsden, D. N., Walker, R. L. and Carter, J. A. (1975a). Uranium series dating of stalagmites from Blanchard Springs Caverns, U.S.A. *Geochimica et Cosmochimica Acta* **39**, 1211–1218.

Thompson, P., Ford, D. C. and Schwarcz, H. P. (1975b). U^{234}/U^{238} Ratios in limestone cave seepage waters and speleothem from West Virginia. *Geochimica et Cosmochimica Acta* **39**, 661–669.

Tilton, G. R. (1973). Isotopic Lead ages of Chondritic Meteorites. *Earth and Planetary Science Letters* **19**, 321–329.

Tobias, P. V. (1973). Implications of the New Age Estimates of the Early South African Hominids. *Nature* **246**, 79–83.

Tobias, P. V. (2000). The Fossil Hominids. In T. C. Partridge and R. R. Maud (Eds.), *The Cenozoic of Southern Africa*, Chapter 17, pp. 252–276. Oxford University Press.

Turner, A. (1997). Further remains of carnivora (mammalia) from the Sterkfontein Hominid site. *Palaeontologia Africana* **34**, 115–126.

Verosub, K. L. (2000). Palaeomagnetic dating. In J. S. Noller. J. M. Sowers and W. R. Lettis (Eds.), *Quaternary Geochronology*, pp. 339–356. AGU.

Vrba, E. S. (1974). Chronological and ecological implications of the fossil Bovidae at the Sterkfontein Australopithecine site. *Nature* **250**, 19–23.

Vrba, E. S. (1975). Some evidence of chronology and palaeoecology of Sterkfontein, Swartkrans and Kromdraai from the fossil Bovidae. *Nature* **27**, 301–304.

Vrba, E. S. (1981). Palaeomagnetic results from the Kromdraai and Sterkfontein hominid sites. *South African Journal of Science* **82**, 160–163.

Vrba, E. S. (1982). Biostratigraphy and chronology, based particularly on Bovidae, of southern hominid-associated assemblages: Makapansgat, Sterkfontein, Taung, Kromdraai, Swartkrans; also Elandsfontein (Saldanha), Broken Hill (now Kabwe) and Cave of Hearths. In *Proc. Congres Internationale de Paleontologie Humaine*, Volume 2, pp. 707–752. Nice, Union Internationale des Sciences Prehistoriques et Protohistorique.

Vrba, E. S. (1985). Early Hominids in Southern Africa: updated observations on chronological and ecological background. In P. V. Tobias (Ed.), *Hominid Evolution: Past, Present and Future.* Alan R. Liss.

Wells, L. H. and Cooke, H. B. S. (1956). Fossil Bovidae fom the Limeworks Quarry, Makapansgat, Potgietersrus. *Palaeontologia Africana* **4**, 1–56.

Wendt, I. and Carl, C. (1985). U/Pb dating of discordant 0.1 Ma old secondary U minerals. *Earth and Planetary Science Letters* **73**, 278–284.

Wilkinson, M. J. (1973). Sterkfontein Cave System: Evolution of a Karst Form. MSc thesis, University of the Witwatersrand.

Winter, B. L. and Johnson, C. M. (1995). U-Pb dating of a carbonate subaerial exposure event. *Earth and Planetary Science Letters* **131**, 177–187.

Zhao, J. X., Hu, K., Collerson, K. D. and Xu, H. K. (2001). Thermal ionization mass spectrometry U-series dating of a homind site near Nanjing, China. *Geology* **29**, 27–30.

Appendices

Appendix A

Sampling Methodology

A.1 Sample screening by Scanning Electron Microscopy (S.E.M.) and Cathodoluminescence

Initial screening of LAB03 from the Limeworks and SK3[1] from Sterkfontein by S.E.M. showed very subtle differences between the samples and within individual samples. The images are shown in Figures (A.1), (A.2) and (A.3). Darker areas on the images are indicative of higher concentrations of magnesium. Banding which is easily visible to the naked eye was not translated on the S.E.M. image. In fact in LAB03 the lineations which can be seen in Figure (A.2) are perpendicular to those on the hand sample. There were no obvious inclusions apart from odd grains of fluorite. Cathodoluminescence revealed that the samples were extremely pure. Calcite normally fluoresces as a result of the trace elements present but these samples did not fluoresce at all, apart from the fragments of fluorite (Marshall, 1988).

[1]Sample analysed initially by B. Cliff to test suitability of speleothem for this technique.

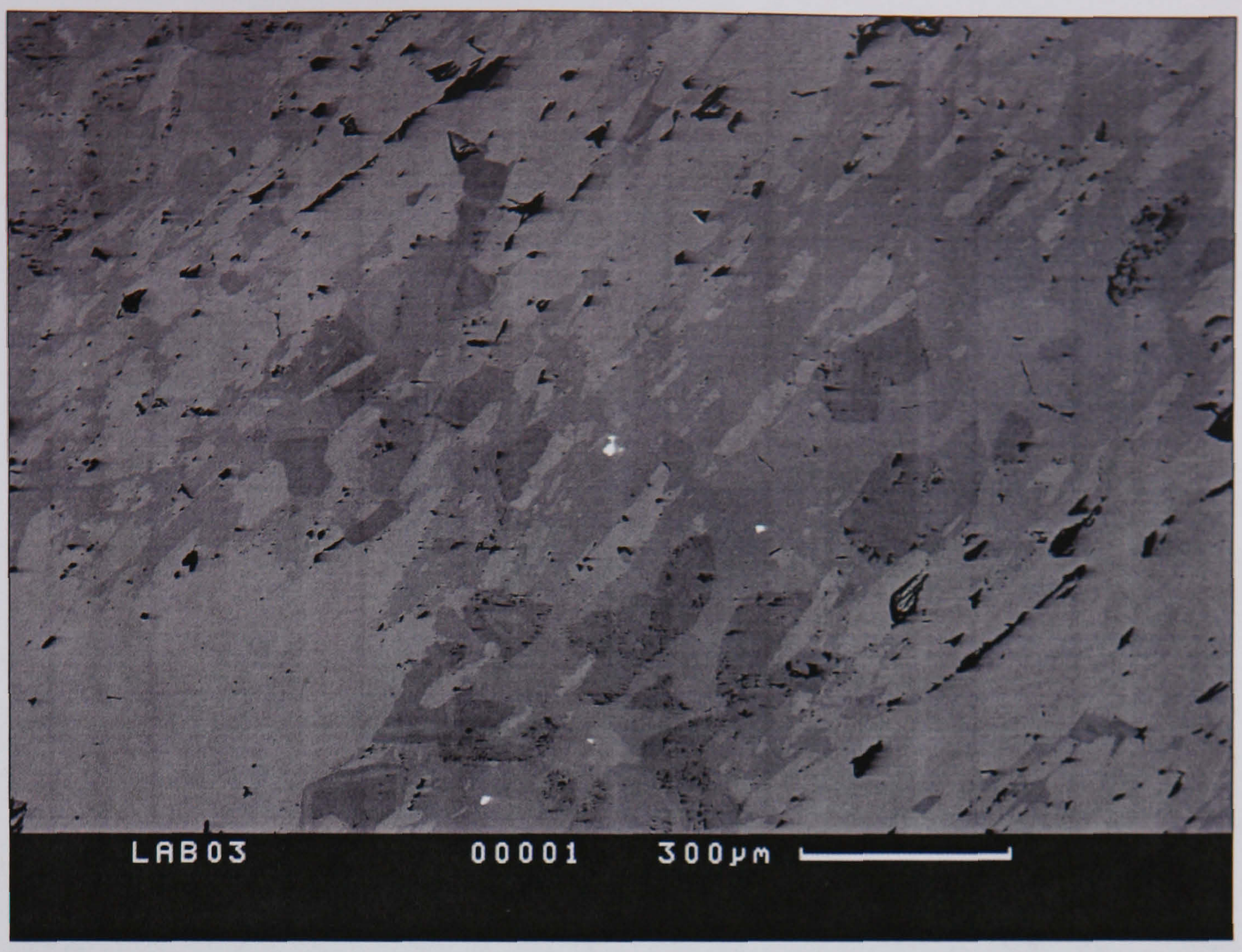

Figure A.1: S.E.M. image of sample LAB03 from the Limeworks. Scale bar represents 300μm

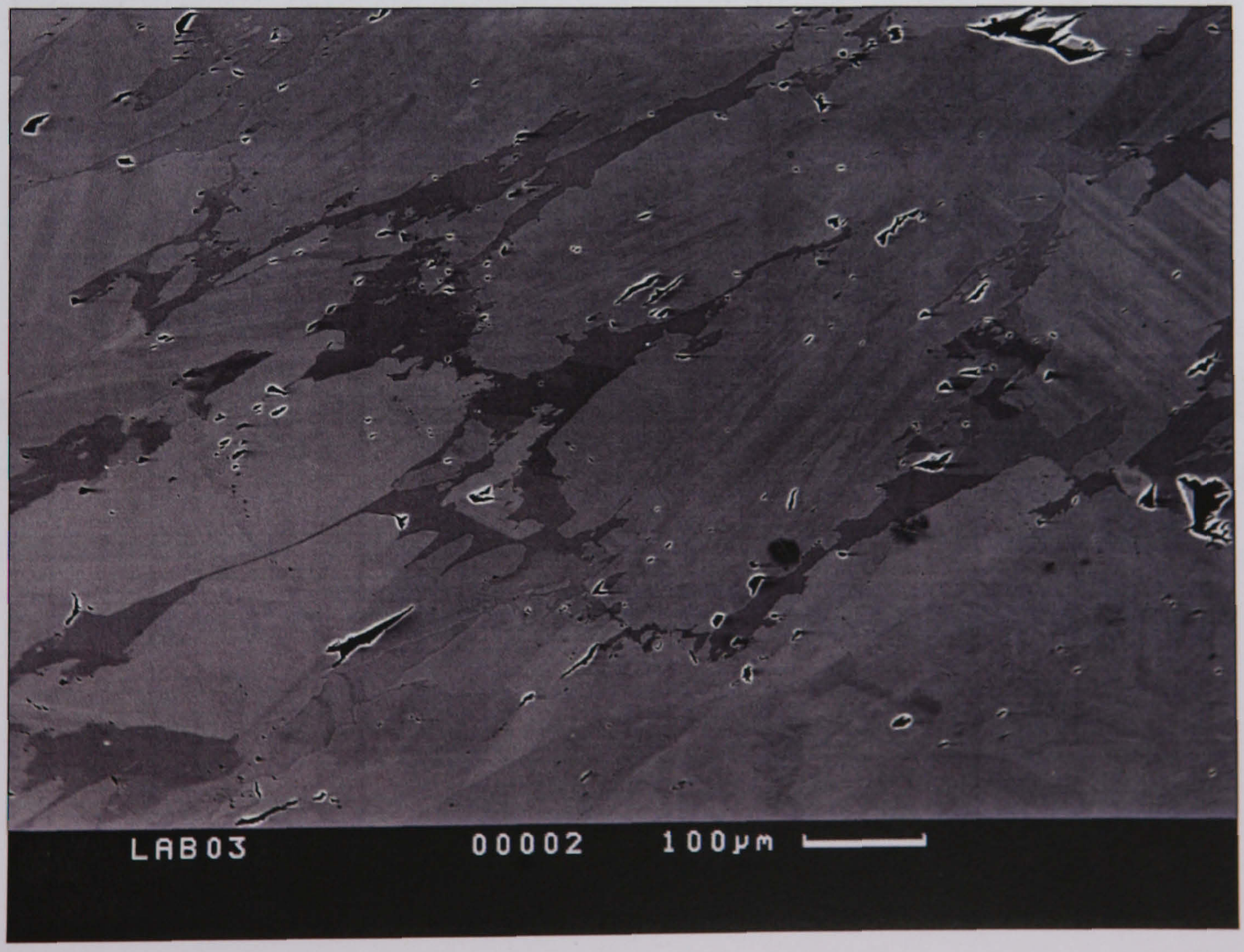

Figure A.2: S.E.M. image of sample LAB03 from the Limeworks. Scale bar represents 100μm. White outlined black marks are polishing pits.

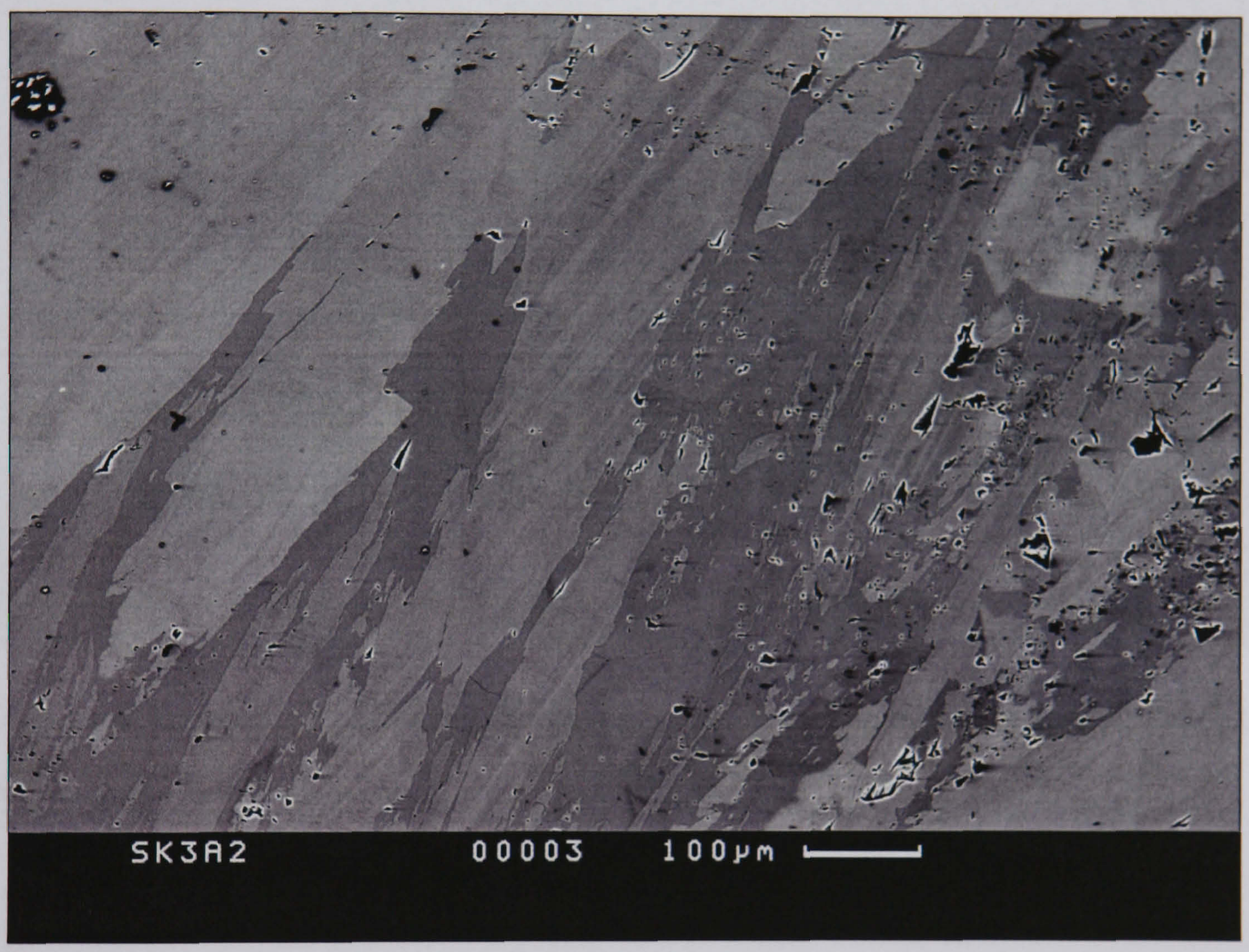

Figure A.3: S.E.M. image of sample SK3 from Sterkfontein. Scale bar represents 100μm. The white outlined black marks are polishing pits and are not features of the sample.

A.2 Sample Provenance

The following photographs provide additional provenance for all the hand-samples analysed.

A.2.1 Sterkfontein

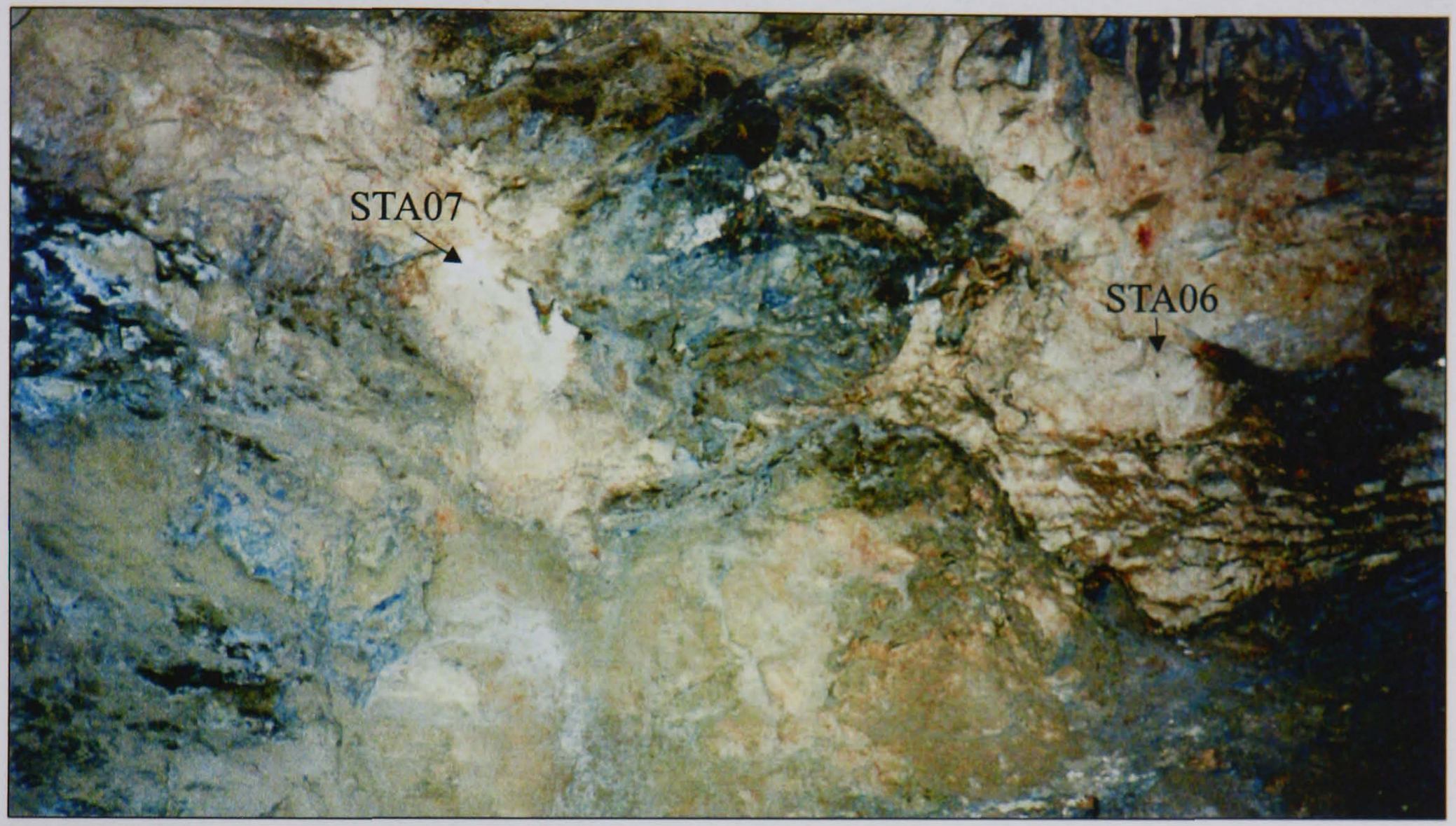

Figure A.4: Photograph of flowstone layer 2D showing where samples STA07-C and STA06 were removed.

Figure A.5: Photograph of flowstone layer 2D showing where samples STA03, STA04 and STA05 were removed.

Figure A.6: Photograph of sample STA04 in situ, after removal.

Figure A.7: Photograph of flowstone layer 2D showing where sample STA07-C was removed.

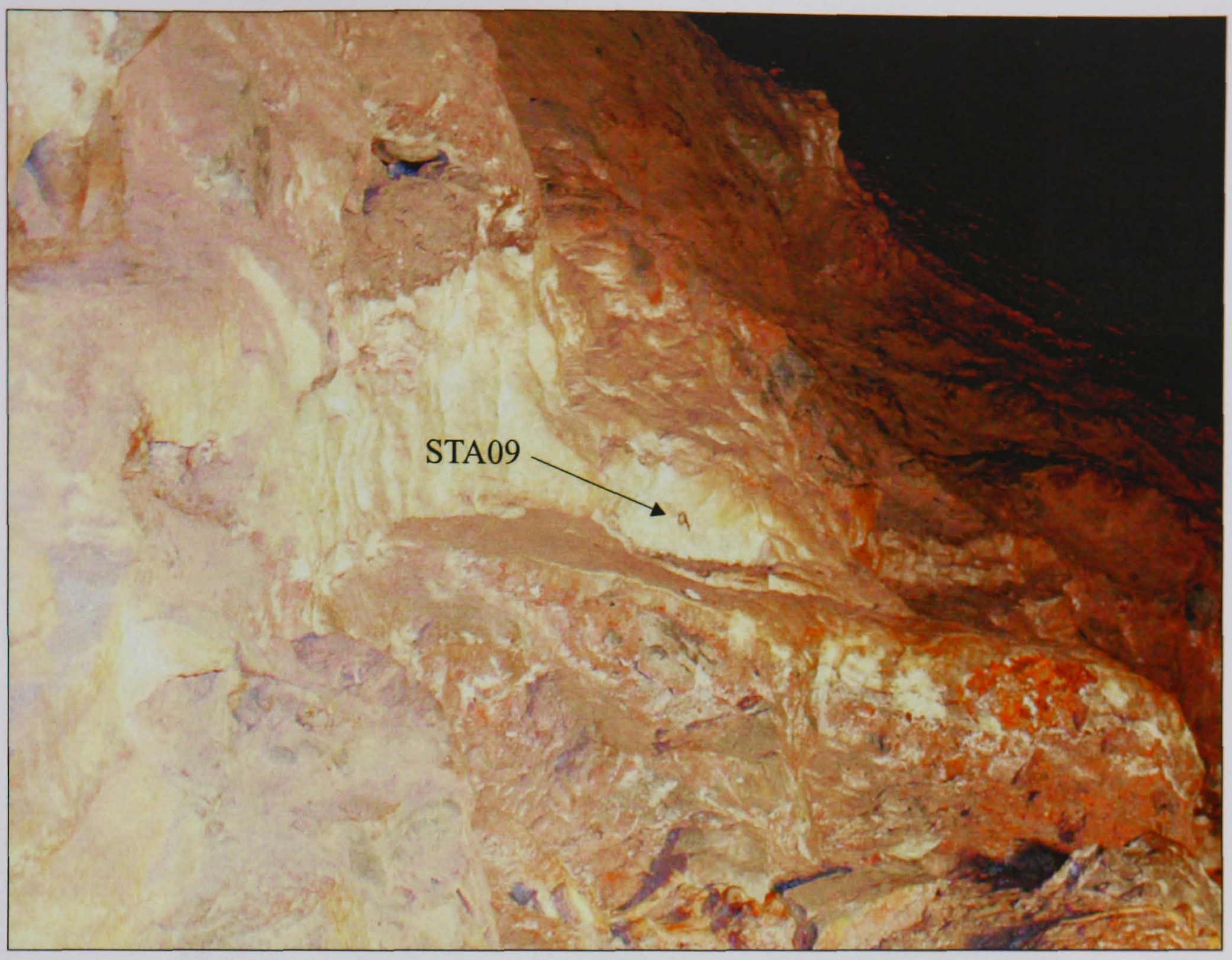

Figure A.8: Photograph of flowstone layer 2C showing where sample STA09 was removed from. This layer also yielded sample STA12. The hand bones of the hominid StW 573 can be seen at the very bottom of the picture in the centre.

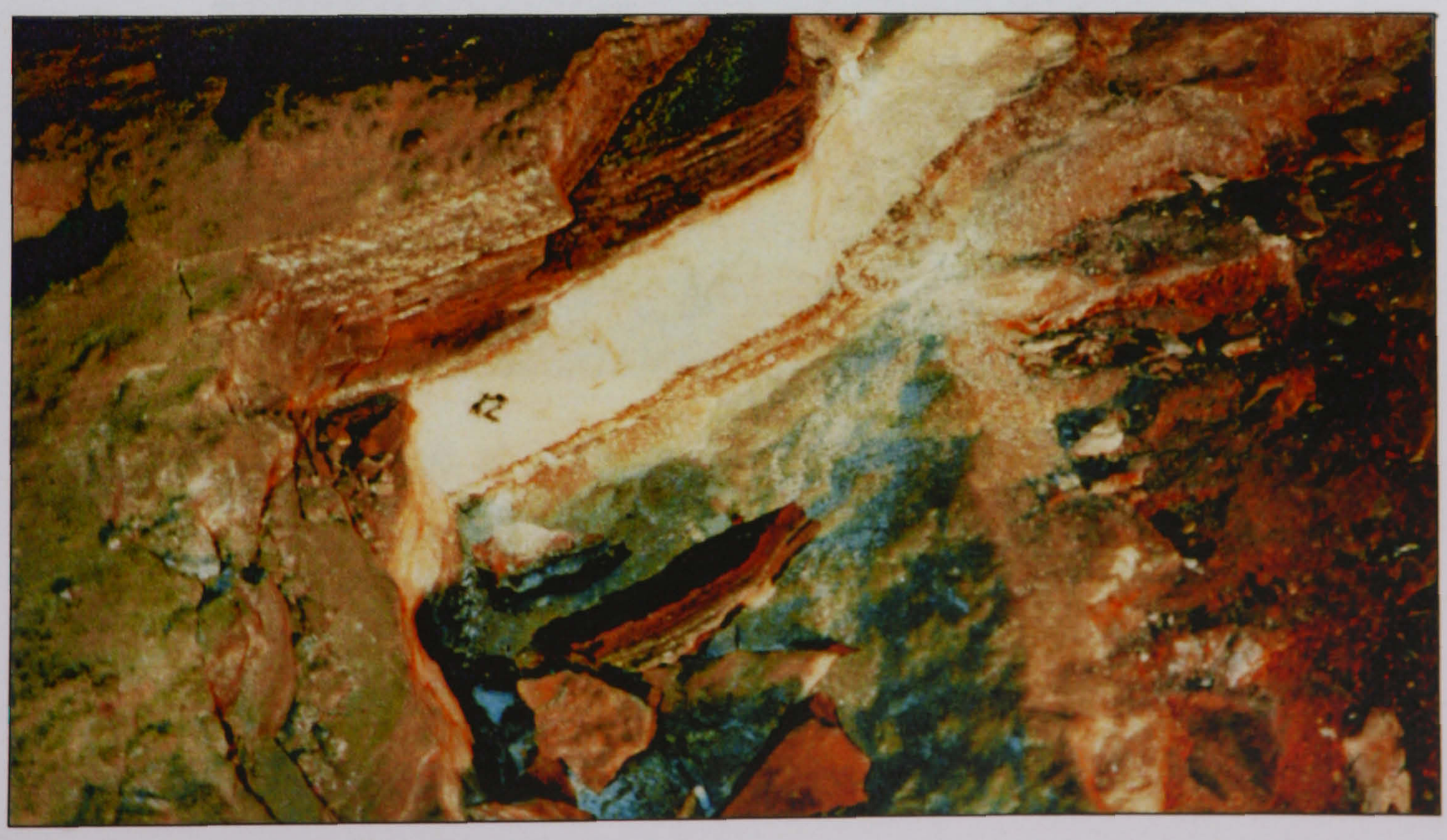

Figure A.9: Photograph of flowstone layer 2C showing where sample STA12 was removed from.

Figure A.10: Photograph of flowstone layer 2B showing where sample STA14 was removed from. This layer also yielded samples STA15 and STA16.

Figure A.11: Photograph of sample STA14 in situ, after removal.

Figure A.12: Photograph of sample STA15 in situ, after removal.

Figure A.13: Photograph of sample STA16 in situ, after removal.

A.2.2 Limeworks

Figure A.14: Photograph of sample LAB03 in situ in the OAE prior to removal.

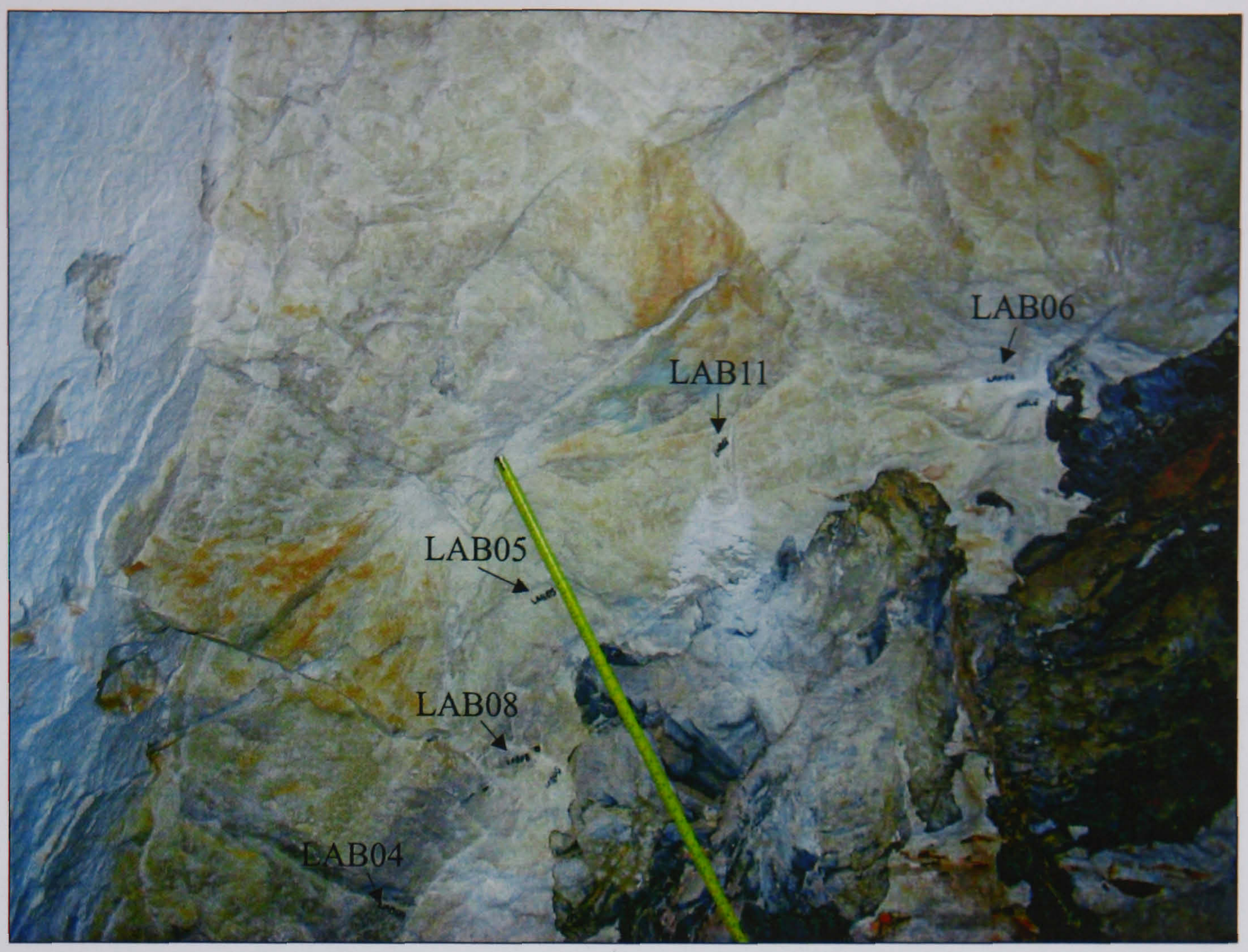

Figure A.15: Photograph showing where samples LAB04, LAB05, LAB06, LAB08 and LAB11 were removed from in the OAE.

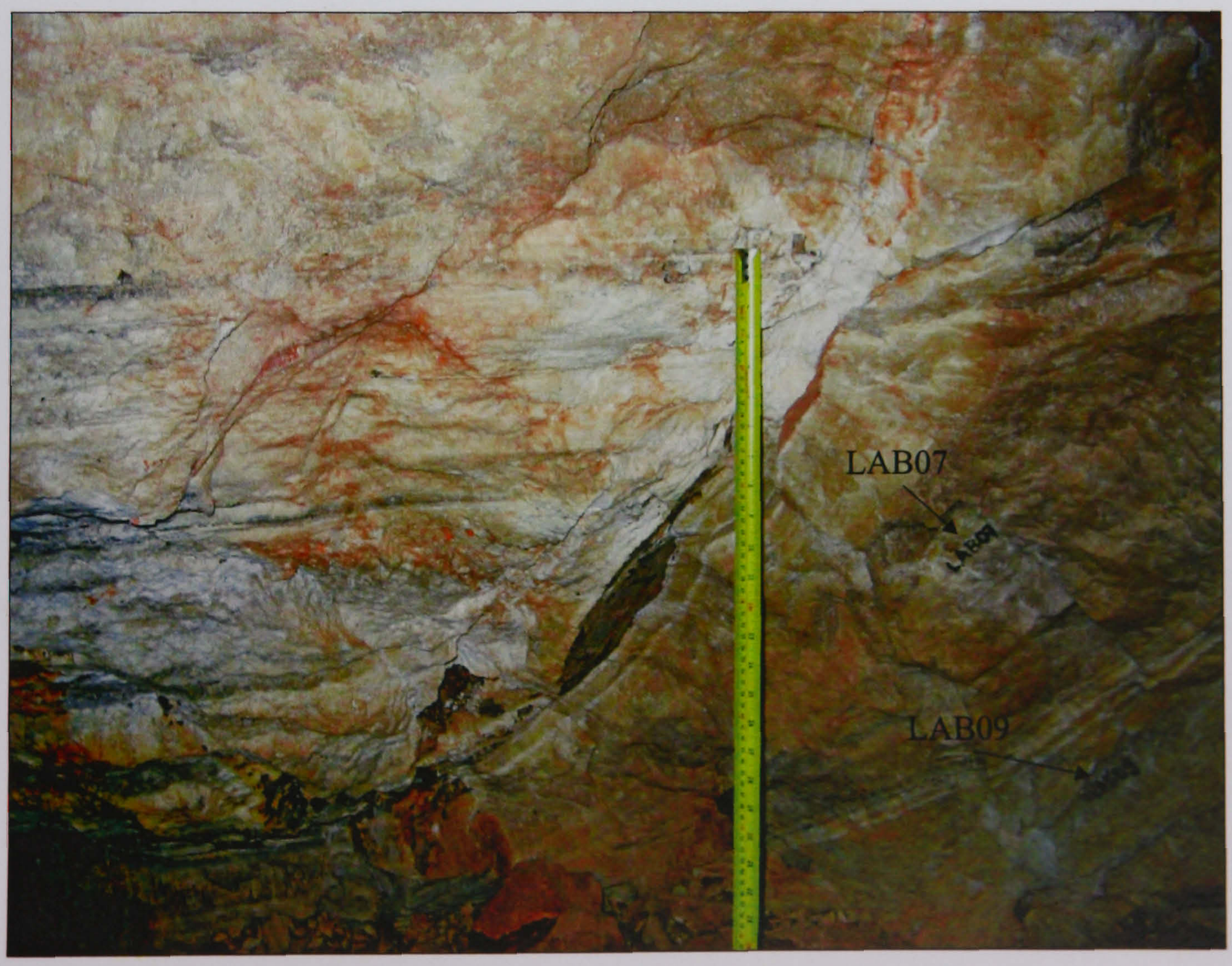

Figure A.16: Photograph showing where samples LAB07 and LAB09 were removed from in the OAE.

A.2.3 Kromdraai B

Figure A.17: Photograph of sample KBP03 in situ, after removal.

A.2.4 Swartkrans

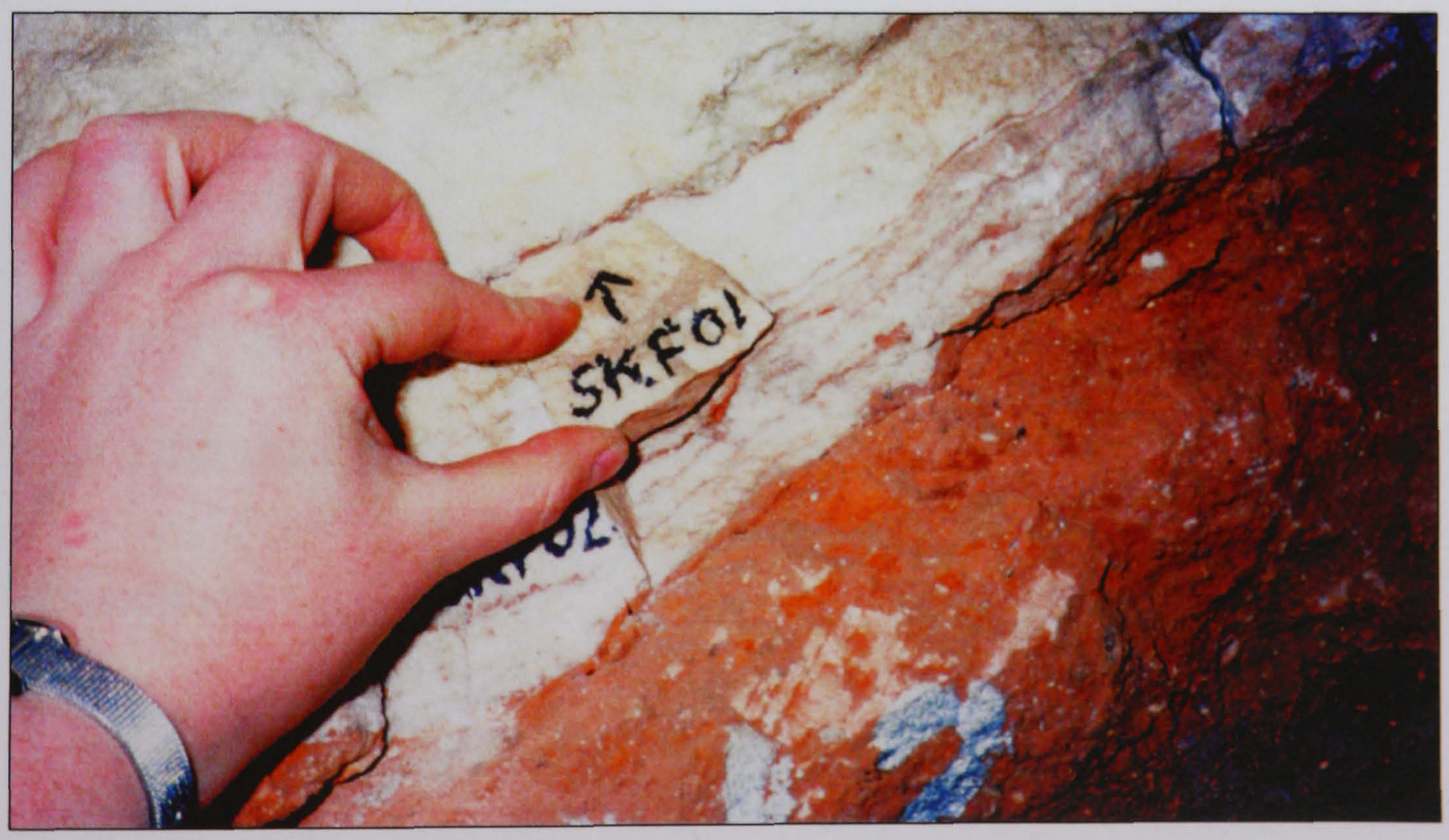

Figure A.18: Photograph of sample SKF01 in situ, after removal.

Appendix B

Chemistry Methodology

B.0.5 Lab Specifications

All separations were done in a Class 10 workstation - laminar flow workstation defined by Federal Standard 209E.

B.0.6 Spike data

The spike used was ^{202}Pb-^{233}U-^{236}U.

Concentration;

- 0.157 nM/g ^{202}Pb
- 1.772 nM/g ^{236}U

Composition;

- $^{208}Pb/^{206}Pb = 2.028$
- $^{207}Pb/^{206}Pb = 0.8303$
- $^{204}Pb/^{206}Pb = 0.06086$
- $^{202}Pb/^{206}Pb = 1210.7$

- $^{238}U/^{236}U = 0.001104$
- $^{235}U/^{236}U = 0.002032$
- $^{233}U/^{236}U = 0.38704$

The natural $^{238}U/^{235}U$ was assumed to be 137.88

B.0.7 Beaker Preparation

7ml and 15ml Savillex© vials were;

- Boiled for 20 minutes in 50% HCl then washed several times in deionised water.
- Filled with aqua regia of 8M HNO_3 and 6M HCl and left to stand on a warm hotplate for at least five days.
- Rinsed thoroughly in 18.2MΩ water and dried completely on a hotplate.

B.0.8 Resin Preparation

The resin used for both the U and Pb separation was Bio rad AG1x8, 200-400 mesh, in chloride form. This follows the work of Tilton (1973), Manhes (1982) and Chen and Wasserburg (1981). This was cleaned with several washes of 6M HCl and 18.2MΩ water and stored in 18.2MΩ water for Pb separations and in 0.25M HNO_3 for U separations.

B.0.9 Frit preparation

Frits were cut from sheets of polypropylene and stored in 6M HCl.

B.0.10 Preparation of Reagents

The HBr used in the Pb separation was prepared from UpA HBr. Immediately prior to a separation it was purified further on an anion exchange column of AG1x8

Reagent	U content (ppt)	Pb content (ppt)
HBr	< 1	< 20
HCl	< 0.1	< 1
HF	< 5	< 20
H_3PO_4	$\star$	$\star$
HNO_3	< 0.01	Not applicable

Table B.1: Table of contamination level in UpA reagents used. $\star$ = content was below the detection limits of 0.04ppm used for this reagent.

200-400 resin to further reduce possible contamination. The concentration of the CPHBr (column-passed) was always 0.5M.

The minor contamination which may be attributed to the UpA reagents is shown in Table (B.1).

B.0.11 Sample preparation

Samples of up to 3g were removed from the hand samples. The positions of these were recorded.

Cleaning

- Samples were placed in cleaned and weighed 15ml Savillex© vials.
- Samples and vials were weighed and sample weight calculated by subtracting original vial weight.
- Samples were not from a clean environment so were initially washed in 18.2MΩ water in an ultrasonic bath for 15 minutes. This was repeated using acetone. This removed any surface dirt (Manhes *et al.*, 1978).
- Samples were etched in 3M HCl for $\approx$ 30 seconds - larger samples were etched for longer - to remove the outer layer of the sample chip.
- After etching samples were rewashed in 18.2MΩ water and acetone, and dried on the hotplate.

- Samples were weighed again. This was the recorded weight of sample for calculation purposes.

Dissolution

Samples were dissolved in 1ml/g (of sample weight) of 18.2MΩ water and 2ml/g of concentrated HCl (Romil UpA) and were left overnight. Adding the water first limits the effervescence which results from this reaction.

Spiking and Aliquoting

- Six 7ml Savillex© vials were weighed, spiked and weighed again. The spike used was ^{202}Pb-^{233}U-^{236}U.

- Spike size was typically 30-40mg. Spike bottle was weighed before and after spiking of each vial. Weight difference was taken to be the spike weight. The weight changes in the vials were used as a cross check.

- The sample aliquots were added to five vials, the sixth one being a blank. Blanks were subjected to the same process as the samples.

- Aliquot volume was usually $\leq$ 1.3ml, which contained a sample of $\approx$ 0.43g. The amount analysed was restricted to this so that the sample-spike aliquot could be contained in a 1.8ml centrifuge tube for the fluoride precipitation step.

- Sample-spike mixture was left overnight on a warm hotplate to homogenise.

Fluoride precipitation

- For the columns to flow efficiently it was necessary to remove the calcium from the samples. This was done by putting the sample-spike aliquots into centrifuge tubes and adding 1ml/g (of sample) of HF. Fluorides of the major elements such as Ca and Mg are insoluble and form a white residue. Trace Pb and U, of which the fluorides are soluble, remain in solution (Smith *et al.*, 1991; Smith *et al.*, 1994).

- These were centrifuged at 3000rpm for 15 minutes.
- The supernate was transferred back to the original cleaned vials.
- The precipitate was processed a second time with 750ml of 0.5M CPHBr to ensure all Pb was removed.
- Supernates were dried down on the hotplate.

Conversion to bromide

To ensure the samples were converted to bromide they were dissolved in 250ml of CPHBr and dried down again.

B.0.12 Lead Separation

Column preparation

- Six columns made from four times shrinkfit Teflon tubing with a resin bed volume of 50μl were washed in 18.2MΩ water and fitted with a polyethylene frit.
- Columns were then washed with acetone, CPHBr, and 18.2MΩ water, respectively.
- AG1x8 resin was added to the columns, and this was cleaned with $\approx$ 1ml washes of 6M HCl, 18.2MΩ water, 6M HCl, 18.2MΩ water, 6M UpA HCl, and 18.2MΩ water.
- The resin was finally conditioned with 0.25ml of CPHBr.

Separation

- The separation was possible because of the complexation of Pb by bromide ions. Major elements, such as Al, Fe, Mg. Ca, Ba, K, Na, Ti, within the sample do not form these complexes. The Pb complexes were retained by the resin while the other elements pass through.

- A new set of vials to collect the U fraction were placed under the columns. U was not retained by the anionic exchange resin at this stage (Korkisch and Hazan, 1965).

- The samples were loaded onto the columns in 0.25ml of CPHBr and allowed to soak in.

- Samples were washed through with 0.25ml of CPHBr twice. This was changed to 0.5ml in one wash.

- To ensure all HBr was flushed out of the column, 0.125ml of 3M HCl was loaded.

- The cleaned original vials were placed beneath the columns and the Pb fraction was eluted with 0.5ml of 6M UpA HCl

- After the Pb samples were dried down they were dissolved in 0.1ml of CPHBr and put through the separation again to further purify the Pb, with the exception that no U fraction was collected as it was assumed it had all eluted in the first separation.

B.0.13 Uranium Separation

Column preparation

- Six columns made from four times shrinkfit Telfon tubing with a resin bed volume of 750μl and already containing AG1x8 resin were cleaned with 0.25M UpA HNO_3.

- Columns were then conditioned with 3ml 8M HNO_3.

- After each separation the columns were cleaned with and stored in 0.25M HNO_3. The resin was not replaced.

Sample preparation

The fluoride precipitates were reprocessed firstly in preparation for the U separation.

- Precipitates were mixed with 0.5ml 8M HNO_3, put in the ultrasonic bath for 15 minutes, and then centrifuged at 3000rpm for 15 minutes.

- The supernate was removed and added to the U fraction from the Pb separation. This was repeated and the collective solutions were dried down.

- Samples were converted to nitrate by dissolving in 100μl of concentrated HNO_3, and dried down. Caution was taken when adding concentrated HNO_3 as violent reactions could occur if the sample was not cooled sufficiently.

Separation

- Samples were loaded onto the columns in 0.25ml 8M HNO_3 and allowed to soak in. This results in the best distribution coefficient for U on AG1x8 (Carswell, 1957; Faris and Buchanan, 1964).

- Samples were rinsed in with 0.5ml 8M HNO_3, followed by 1.75ml 8M HNO_3 (equivalent to three times the resin bed volume). In these conditions most ions, apart from U, were not retained by the resin and were therefore eluted from the column at this stage.

- Following this U can be easily removed with water or a weak acid (Chen and Wasserburg, 1981). U was eluted in 3ml 0.25M HNO_3 into the cleaned vials.

- After drying down, samples were redissolved in 0.25ml 8M HNO_3 and the columns were reconditioned with 3ml 8M HNO_3. The separation was then repeated.

B.0.14 Loading

Filament Preparation

Preparation for both single and double filaments.

- Filament holders were stripped of old Re. Posts of filaments were buffed to get off any strongly welded fragments.

- Filament holders were cleaned with Al-oxide paste and then boiled in deionised water then 18.2MΩ water.
- New Re ribbon was welded on to the filament posts.
- Single filaments were outgassed at a maximum of 4.5A.
- Double filaments were outgassed at a maximum of 5.5A.

Sample Preparation

- Final drying of samples was done with a couple of drops of Aldrich 0.002M H_3PO_4 to prevent the samples drying down entirely and to make them more visible in the vials, which eased loading (Manhes *et al.*, 1978; Bourdon, 1992).
- A couple of drops of concentrated HNO_3 was then added to the samples and they were dried down again. This was intended to reduce the organic content of the sample that was a problem when loading.

Loading standards

- A Re filament was heated to $\approx$ 1A.
- Approximately 1μl of silica gel was loaded on to the filament and allowed to partially dry down.
- Approximately 1μl of the standard, SRM981, was loaded on top of the silica gel, and allowed to dry down.
- The filament was then heated to $\approx$ 2A until a white deposit formed, and then until it glowed briefly.

Loading lead samples

- A Re filament was heated to $\approx$ 1A.
- Approximately 1μl of silica gel was loaded on to the filament and allowed to partially dry down.

- The sample was dissolved in $\approx 1\mu$l of 18.2MΩ water and loaded on top of the silica gel. It was allowed to dry down.
- The filament was then heated to $\approx$ 2A until a white deposit formed, and then until it glowed briefly.

Loading uranium samples

- A Re filament was heated to ≈1A.
- The sample was dissolved in $\approx 1\mu$l of 18.2MΩ water and loaded onto the filament. It was allowed to dry down.
- The filament was gradually heated to $\approx$ 2A until a black deposit formed, and then until it glowed briefly.

Running techniques for lead samples and blanks

Pb samples were measured using a static method with the ^{204}Pb in the centre cup. ^{204}Pb signals that were below $\approx$ 2mV (0.02pA) were measured on the SEM and a yield calibration was performed in such cases. All other isotopes were measured on the faraday detector.

- Filament was gently heated until a temperature of $\approx$ 1200°C was achieved.
- The beam was focused and centred once the signal had stabilised.
- The signal was focused at the beginning, and a peak centre was done every 5 blocks.
- The sample signal was measured for 10 blocks of 15 cycles, totalling 150 measurements.

Pb blanks were run in the same way as samples, but the ^{204}Pb was always measured on the SEM. The signal was again recorded for 10 blocks of 15 cycles, with an automatic focus before the measuring began, and a peak centre every 4 blocks.

Running techniques for uranium samples and blanks

U samples were run using a multidynamic method.

- The ionisation filament of the double U filament was heated initially to ≈ 4600mA, or until a ^{187}Re beam of ≈ 6mV (0.06pA) was detected.
- The Re beam was focused, centred, and measured, to check yield.
- The evaporation filament was then ramped up to ≈ 700mA and the ionisation to 5000mA, or until the temperature had reached 1850 – 1900°C.
- The detector was then set to scan for U.
- When the signal had stabilised the beam was focused and centred.
- The signal was measured 50 times in 5 blocks of 10 cycles.

U blanks were measured using a dynamic method. The measurements were recorded in the same way as the U samples.

Lead Data

The Pb data was converted into a template in Excel that could be imported into the EP package. Raw data from the TIMS was streamlined by highlighting outliers using a macro. The macro accepted values within the following calculated value and highlighted those outside that value;

$$\text{Accept window} = \geq (\overline{x} + 2.6 \times \sigma) \text{ and } \leq (\overline{x} - 2.6 \times \sigma) \tag{B.1}$$

Where $\overline{x}$ = mean, and σ = absolute standard deviation.

Any highlighted values could then be removed at the discretion of the individual. The ratios that were imported and used in the EP package were ^{202}Pb/^{206}Pb, ^{204}Pb/^{206}Pb, ^{207}Pb/^{206}Pb and ^{208}Pb/^{206}Pb.

Uranium Data

The U data was imported into a template in Excel to convert the numbers into a template suitable for the EP package. The template used the raw data to make the following calculations;

- Φ (Phi) - the fractionation factor for U. This differs from the Pb fractionation factor in that it works on an exponential basis in terms of isotopic weight, unlike Pb fractionation which is a linear calculation. Phi was calculated thus;

$$\Phi = \frac{\ln\left([^{233}U/^{236}U]_s/[^{233}U/^{236}U]_m\right)}{\ln(233/236)} \tag{B.2}$$

  The $^{233}U/^{236}U$ ratio acts as an independent check as these isotopes were found only in the spike.

- Normalised ratios - the $^{236}U/^{238}U$ and $^{235}U/^{238}U$ measured ratios were corrected for fractionation by multiplying by the numerator mass to the power of Phi, and dividing by the denominator mass to the power of Phi.

$$[^{236}U/^{238}U]_n = \frac{[^{236}U/^{238}U]_m \times 236^{\Phi}}{238^{\Phi}} \tag{B.3}$$

- $^{238}U/^{235}U$ bias - the correction for yield variations between the faraday and the SEM. ^{238}U was the only isotope measured on the faraday so the $^{238}U/^{235}U$ ratio was used as a correction for bias by comparing the accepted value in nature with that measured. The bias was calculated by taking the normalised $^{238}U/^{235}U$ ratio, minus that which was in the spike;

$$[^{238}U/^{235}U]_{m-s} = \frac{(1/[^{236}U/^{238}U]_n) - [^{238}U/^{236}U]_s}{([^{235}U/^{238}U]_n/[^{236}U/^{238}U]_n) - [^{235}U/^{236}U]_s} \tag{B.4}$$

Then dividing by the accepted (minus one) ratio in nature;

$$[^{238}U/^{235}U]_b = \frac{[^{238}U/^{235}U]_{m-s}}{[^{238}U/^{235}U]_{nat}} - 1 \tag{B.5}$$

- Bias corrected ratios - the raw $^{236}U/^{238}U$ and $^{235}U/^{238}U$ ratios were corrected for the detector bias by multiplying the raw ratios by the bias (plus one) ratio;

$$[^{236}U/^{238}U]_c = [^{236}U/^{238}U]_m \times (1 + [^{238}U/^{235}U_b]) \quad \text{(B.6)}$$

- $^{236}U/^{238}U$ re-normalised - this ratio was normalised again as described previously, taking into account the correction for bias;

$$[^{236}U/^{238}U]_r = \frac{[^{236}U/^{238}U]_c \times 236^{\Phi}}{238^{\Phi}} \quad \text{(B.7)}$$

- $^{238}U/^{236}U$ final - having corrected for fractionation and detector bias the $^{238}U/^{236}U$ ratio was calculated from the reciprocal of the $^{236}U/^{238}U$ re-normalised ratio, minus the $^{238}U/^{236}U$ from the spike. This accounts for ^{238}U in the spike. This ratio was imported and used by the EP package;

$$[^{236}U/^{238}U]_f = \frac{1}{[^{236}U/^{238}U]_r} - [^{238}U/^{236}U]_s \quad \text{(B.8)}$$

B.0.15 Alternative Lead separation technique

A second separation technique was applied to repeats of certain samples to see if the Pb measurements could be improved. The samples and columns were prepared in exactly the same way but the columns were made up with AG-MP1 (macroporous) resin. The separation was as follows;

- Resin was cleaned with full column of 1M HNO_3, and half a column of 18.2MΩ water.
- Resin was conditioned with 270μl 1M HBr.
- New vial to collect U fraction was placed under column and sample was loaded in 1ml of 1M HBr.
- Sample was rinsed in with 270μl 1M HBr.

- Sample was rinsed in further and U eluted with two full columns of 0.5M HBr.
- Sample was eluted with 270μl 1M HNO_3.

As with the main separation technique this separation was done twice for each sample. The U separation was performed afterwards as standard. No improvement was detected with the Pb results so this technique was not pursued any further. Results bearing an 's' symbol on the end of the sample name represent samples which were separated by this technique.

Appendix C

Results

C.0.16 Rejected samples

The following tables contain the results from Sterkfontein and the Limeworks samples that were felt to be inaccurate. Subscripts in the tables denote the reasons for rejecting each result.

Sample	Date	U (ppm)	Pb (ppm)	Pb (ng)	$^{206}Pb/^{204}Pb$ before blank	$^{238}U/^{208}Pb$	Error (1σ)	$^{206}Pb/^{208}Pb$	Error (1σ)	$^{207}Pb/^{204}Pb$	Error (1σ)	$^{208}Pb/^{204}Pb$	Error (1σ)
STA07-C2[1]	09/08/04	1.247	0.0014	0.593	34.31	1849	96	0.914	0.022	17.09	0.09	41.39	0.23
STA09-A1-1[▲,2]	24/05/04	0.458	0.0009	0.112	33.66	1284	430	1.418	0.314	16.68	0.42	37.55	0.73
STA09-A1-2[Δ,2]	24/05/04	0.818	0.0007	0.162	49.78	4043	1215	2.25	0.53	18.46	0.88	38.74	0.7
STA09-A2-2[◎,2,3]	04/10/04	0.961	0.0016	0.076	27.44	1339	584	1.066	0.255	17.89	1.07	41.28	1.78
STA09-C2-1A[4]	15/10/03	0.689	0.0048	2.072	22.02	250.8	3.3	0.588	0.001	15.71	0.08	37.84	0.19
STA09-C2-1B[4]	27/01/04	1.142	0.0081	3.515	22.19	246.8	2.1	0.587	0.001	15.87	0.04	38.08	0.1
STA09-C2-1C[1,3]	15/10/03	1.341	0.0012	0.508	50.79	3239	354	1.79	0.11	15.65	0.46	33.65	1.05
STA09-C2-1C[4]	27/01/04	1.383	0.0061	2.62	24.37	415.6	4.6	0.658	0.002	15.77	0.06	37.51	0.15
STA09-C2-1D[3]	15/10/03	1.028	0.0037	1.609	25.59	512.6	9.3	0.705	0.005	15.82	1.72	37.03	4.06
STA12-A2[⊛,4]	04/10/04	0.541	0.0045	0.801	20.71	207.6	6.8	0.565	0.003	15.6	0.03	37.27	0.09
STA12-B3-A[4]	27/04/04	0.317	0.0035	1.516	20.66	155.6	2.7	0.548	0.001	15.77	0.02	38.05	0.04
STA15-05[1,3]	25/03/03	1.08	0.0022	0.912	34.35	1036	37	1.01	0.02	15.63	0.29	36.1	0.67
STA15-A2-E[3]	23/08/04	0.772	0.0021	0.913	31.26	729.4	24.2	0.873	0.013	15.39	0.11	37.76	0.19

Table C.1: Table of rejected Sterkfontein results. Sample weights were 430 ± 50mg apart from the following samples; ▲ - 127mg; Δ - 249mg; ◎ - 48.3mg; ⊛ - 177mg. Reason for rejection; 1. Variation from expected $^{208}Pb/^{204}Pb$; 2. Large blank correction; 3. Large mass spectrometry errors; 4. Apparent contamination.

Sample	Date	U (ppm)	Pb (ppm)	Pb (ng)	$^{206}Pb/^{204}Pb$ before blank	$^{238}U/^{208}Pb$	Error (1σ)	$^{206}Pb/^{208}Pb$	Error (1σ)	$^{207}Pb/^{204}Pb$	Error (1σ)	$^{208}Pb/^{204}Pb$	Error (1σ)
LAB03-2-2[1]	02/12/02	1.667	0.0084	3.5	35.99	420.5	3.9	0.9881	0.0043	16.04	0.04	37	0.11
LAB03-2-2[1,2]	06/11/02	1.306	0.0075	3.9	38.42	376.7	4.1	1.052	0.005	16.22	0.03	37.2	0.09
LAB03-2-4[1,2]	06/11/02	1.109	0.0055	2.48	54.16	523	8.7	1.506	0.016	16.68	0.03	37.4	0.09
LAB03-2-5[3]	18/06/03	0.412	0.0331	14.31	19.96	21.16	0.1	0.5281	0.0005	15.67	0.04	37.9	0.1
LAB03-2-8[2]	12/02/03	1.895	0.0089	3.84	37.20	462.3	5.7	1.053	0.005	15.56	0.18	35.9	0.4
LAB03-2-9[2,3]	12/02/03	0.473	0.0258	11.14	20.44	31.54	0.2	0.5469	0.0006	15.56	0.09	37.5	0.22

Table C.2: Table of rejected Limeworks results. Sample weights were 430 ± 50mg. Reason for rejection; 1. Variation in U concentration between repeats; 2. Large mass spectrometry errors; 3. Apparent contamination.

C.0.17 Rejected blanks

Rejected blank results are shown in Table (C.3) that follows.

C.0.18 Standards results

Standards results are shown in Table (C.4) that follows.

Blank	Date	Pb(ng)	Error(1σ)	206pM	Error(1σ)	$^{206}Pb/^{204}Pb$	Error(1σ)	$^{207}Pb/^{204}Pb$	Error(1σ)	$^{208}Pb/^{204}Pb$	Error(1σ)
423	17/02/2004	0.717	0.028	0.859	0.034	17.550	0.381	15.285	0.327	36.825	0.796
422	14/06/2004	2.059	0.080	2.510	0.100	18.526	0.006	15.707	0.007	38.134	0.019
448	28/07/2004	0.574	0.022	0.694	0.027	18.174	0.018	15.578	0.020	37.808	0.052

Table C.3: Rejected blank results. These were rejected because of the large amounts of Pb they contained. These amounts were likely to be anomalous and not representative of the samples analysed at the same time.

Standard	Date	$^{207}Pb/^{206}Pb$	Fractionation ‰	$^{208}Pb/^{206}Pb$	Fractionation ‰	$^{206}Pb/^{204}Pb$	Fractionation ‰	Average ‰ Fractionation	Average Fractionation
SRM981 1	04/12/02	0.9137	-0.92	2.1629	-0.95	16.9024	-0.98	-0.95	-0.00095
SRM981 2	29/01/03	0.9147	0.12	2.1670	-0.01	16.9400	0.13	0.08	0.00008
SRM981 3	29/01/03	0.9147	0.14	2.1670	0.00	16.9286	-0.21	-0.02	-0.00002
SRM981 4	25/03/03	0.9140	-0.60	2.1638	-0.74	16.9112	-0.72	-0.69	-0.00069
SRM981 5	27/03/03	0.9141	-0.50	2.1643	-0.61	16.9161	-0.58	-0.57	-0.00057
SRM981 6	25/07/03	0.9135	-1.19	2.1615	-1.28	16.8962	-1.16	-1.21	-0.00121
SRM981 7	16/07/03	0.9137	-1.00	2.1621	-1.14	16.8979	-1.11	-1.09	-0.00109
SRM981 8	17/07/03	0.9137	-0.93	2.1624	-1.07	16.8999	-1.05	-1.02	-0.00102
							Overall average	-0.68	-0.00068
							Standard deviation	0.49	0.00049

Standard	Date	$^{207}Pb/^{206}Pb$	Fractionation ‰	$^{208}Pb/^{206}Pb$	Fractionation ‰	$^{206}Pb/^{204}Pb$	Fractionation ‰	Average ‰ Fractionation	Average Fractionation
SRM981 9	25/07/03	0.9115	-3.38	2.1574	-2.21	16.9195	-0.48	-2.02	-0.00202
SRM981 10	14/10/03	0.9135	-1.14	2.1617	-1.22	16.8981	-1.11	-1.16	-0.00116
SRM981 11	14/10/03	0.9135	-1.24	2.1614	-1.31	16.8963	-1.16	-1.23	-0.00123
SRM981 12	04/12/03	0.9140	-0.69	2.1636	-0.78	16.9103	-0.75	-0.74	-0.00074
SRM981 13	04/12/03	0.9140	-0.67	2.1636	-0.78	16.9107	-0.73	-0.73	-0.00073
SRM981 14	08/12/03	0.9139	-0.75	2.1634	-0.83	16.9086	-0.80	-0.79	-0.00079
SRM981 15	08/12/03	0.9142	-0.37	2.1650	-0.47	16.9210	-0.43	-0.42	-0.00042
SRM981 16	12/12/03	0.9140	-0.62	2.1639	-0.72	16.9125	-0.68	-0.67	-0.00067
SRM981 17	12/12/03	0.9138	-0.90	2.1627	-0.99	16.9028	-0.97	-0.95	-0.00095
							Overall average	-0.84	-0.00084
							Standard deviation	0.27	0.00027

Standard	Date	$^{207}Pb/^{206}Pb$	Fractionation ‰	$^{208}Pb/^{206}Pb$	Fractionation ‰	$^{206}Pb/^{204}Pb$	Fractionation ‰	Average ‰ Fractionation	Average Fractionation
SRM981 18	29/01/04	0.9139	-0.75	2.1649	-0.49	16.9345	-0.03	-0.42	-0.00042
SRM981 19	29/01/04	0.9139	-0.78	2.1634	-0.84	16.9109	-0.73	-0.78	-0.00078
SRM981 20	03/02/04	0.9136	-1.02	2.1619	-1.17	16.8944	-1.22	-1.14	-0.00114
SRM981 21	04/02/04	0.9136	-1.05	2.1623	-1.09	16.8895	-1.36	-1.17	-0.00117
SRM981 22	06/02/04	0.9137	-1.01	2.1621	-1.14	16.8979	-1.11	-1.09	-0.00109
SRM981 23	04/02/04	0.9137	-0.95	2.1622	-1.11	16.9047	-0.91	-0.99	-0.00099
SRM981 24	04/02/04	0.9138	-0.84	2.1632	-0.88	16.9590	0.69	-0.35	-0.00035
SRM981 25	06/02/04	0.9136	-1.09	2.1624	-1.06	16.8711	-1.91	-1.35	-0.00135
SRM981 26	06/02/04	0.9140	-0.59	2.1629	-0.95	16.8610	-2.20	-1.25	-0.00125
							Overall average	-0.95	-0.00095
							Standard deviation	0.36	0.00036

Standard	Date	$^{207}Pb/^{206}Pb$	Fractionation ‰	$^{208}Pb/^{206}Pb$	Fractionation ‰	$^{206}Pb/^{204}Pb$	Fractionation ‰	Average ‰ Fractionation	Average Fractionation
SRM981 27	11/03/04	0.9143	-0.32	2.1647	-0.53	16.8875	-1.42	-0.76	-0.00076
SRM981 28	10/03/04	0.9139	-0.70	2.1635	-0.80	16.9095	-0.77	-0.76	-0.00076
SRM981 29	10/03/04	0.9140	-0.59	2.1639	-0.73	16.9116	-0.71	-0.67	-0.00067
SRM981 30	17/03/04	0.9135	-1.23	2.1610	-1.38	16.8920	-1.29	-1.30	-0.00130
SRM981 31	22/03/04	0.9138	-0.81	2.1629	-0.95	16.9041	-0.93	-0.89	-0.00089
SRM981 32	23/03/04	0.9145	-0.14	2.1658	-0.28	16.9276	-0.24	-0.22	-0.00022
SRM981 33	29/02/04	0.9147	0.09	2.1669	-0.03	16.9360	0.01	0.02	0.00002
							Overall average	-0.65	-0.00065
							Standard deviation	0.44	0.00044

Standard	Date	$^{207}Pb/^{206}Pb$	Fractionation ‰	$^{208}Pb/^{206}Pb$	Fractionation ‰	$^{206}Pb/^{204}Pb$	Fractionation ‰	Average ‰ Fractionation	Average Fractionation
SRM981 34	25/03/04	0.9140	-0.65	2.1636	-0.79	16.9099	-0.76	-0.73	-0.00073
SRM981 35	08/05/04	0.9139	-0.73	2.1633	-0.85	16.9062	-0.87	-0.82	-0.00082
SRM981 36	08/05/04	0.9141	-0.53	2.1642	-0.65	16.9146	-0.62	-0.60	-0.00060
SRM981 37	08/05/04	0.9142	-0.39	2.1647	-0.53	16.9189	-0.49	-0.47	-0.00047
SRM981 38	08/05/04	0.9142	-0.37	2.1648	-0.52	16.9183	-0.51	-0.47	-0.00047
							Overall average	-0.62	-0.00062
							Standard deviation	0.16	0.00016

Standard	Date	$^{207}Pb/^{206}Pb$	Fractionation ‰	$^{208}Pb/^{206}Pb$	Fractionation ‰	$^{206}Pb/^{204}Pb$	Fractionation ‰	Average ‰ Fractionation	Average Fractionation
SRM981 39	12/05/04	0.9139	-0.74	2.1633	-0.87	16.9063	-0.87	-0.82	-0.00082
SRM981 40	12/05/04	0.9136	-1.02	2.1620	-1.17	16.8961	-1.17	-1.12	-0.00112
SRM981 41	12/05/04	0.9138	-0.88	2.1627	-1.00	16.9018	-1.00	-0.96	-0.00096
SRM981 42	22/05/04	0.9139	-0.73	2.1634	-0.83	16.9081	-0.81	-0.79	-0.00079
SRM981 43	22/05/04	0.9139	-0.80	2.1630	-0.92	16.9054	-0.89	-0.87	-0.00087
SRM981 44	22/05/04	0.9138	-0.83	2.1629	-0.95	16.9043	-0.92	-0.90	-0.00090
SRM981 45	18/06/04	0.9139	-0.73	2.1632	-0.87	16.9074	-0.83	-0.81	-0.00081
							Overall average	-0.90	-0.00090
							Standard deviation	0.11	0.00011

Standard	Date	$^{207}Pb/^{206}Pb$	Fractionation ‰	$^{208}Pb/^{206}Pb$	Fractionation ‰	$^{206}Pb/^{204}Pb$	Fractionation ‰	Average ‰ Fractionation	Average Fractionation
SRM981 46	02/07/04	0.9141	-0.58	2.1640	-0.70	16.9124	-0.68	-0.65	-0.00065
SRM981 47	02/07/04	0.9139	-0.71	2.1634	-0.84	16.9088	-0.79	-0.78	-0.00078
SRM981 48	26/06/04	0.9142	-0.43	2.1648	-0.52	16.9194	-0.48	-0.47	-0.00047
SRM981 49	07/07/04	0.9137	-0.99	2.1621	-1.14	16.8976	-1.12	-1.08	-0.00108
SRM981 50	19/08/04	0.9142	-0.43	2.1647	-0.53	16.9190	-0.49	-0.48	-0.00048
SRM981 51	19/08/04	0.9145	-0.11	2.1662	-0.20	16.9358	0.01	-0.10	-0.00010
SRM981 52	19/08/04	0.9141	-0.56	2.1640	-0.69	16.9128	-0.67	-0.64	-0.00064
							Overall average	-0.60	-0.00060
							Standard deviation	0.30	0.00030

Standard	Date	$^{207}Pb/^{206}Pb$	Fractionation ‰	$^{208}Pb/^{206}Pb$	Fractionation ‰	$^{206}Pb/^{204}Pb$	Fractionation ‰	Average ‰ Fractionation	Average Fractionation
SRM981 53	23/08/04	0.9137	-0.92	2.1625	-1.05	16.8993	-1.07	-1.01	-0.00101
SRM981 54	15/09/04	0.9136	-1.03	2.1621	-1.13	16.8987	-1.09	-1.09	-0.00109
SRM981 55	15/09/04	0.9138	-0.88	2.1625	-1.03	16.8984	-1.10	-1.00	-0.00100
SRM981 56	06/10/04	0.9141	-0.50	2.1643	-0.62	16.9147	-0.62	-0.58	-0.00058
SRM981 57	06/10/04	0.9139	-0.79	2.1631	-0.89	16.9065	-0.86	-0.85	-0.00085
SRM981 58	11/10/04	0.9141	-0.49	2.1643	-0.62	16.9151	-0.61	-0.57	-0.00057
SRM981 59	11/10/04	0.9140	-0.64	2.1637	-0.77	16.9102	-0.75	-0.72	-0.00072
SRM981 60	25/10/04	0.9142	-0.48	2.1642	-0.66	16.9840	1.43	0.10	0.00010
SRM981 61	25/10/04	0.9137	-0.92	2.1625	-1.04	16.9009	-1.02	-0.99	-0.00099
							Overall average	-0.85	-0.00085
							Standard deviation	0.20	0.00020

Table C.4: Table of Standards results and fractionation factors. Overall ‰ average fractionation factors and standard deviation were values applied to samples. Also see **Table (5.1) in Methodology chapter**. Accepted values for standard SRM981; $^{207}Pb/^{206}Pb = 0.9146$; $^{208}Pb/^{206}Pb = 2.1670$ $^{206}Pb/^{204}Pb = 16.9356$.